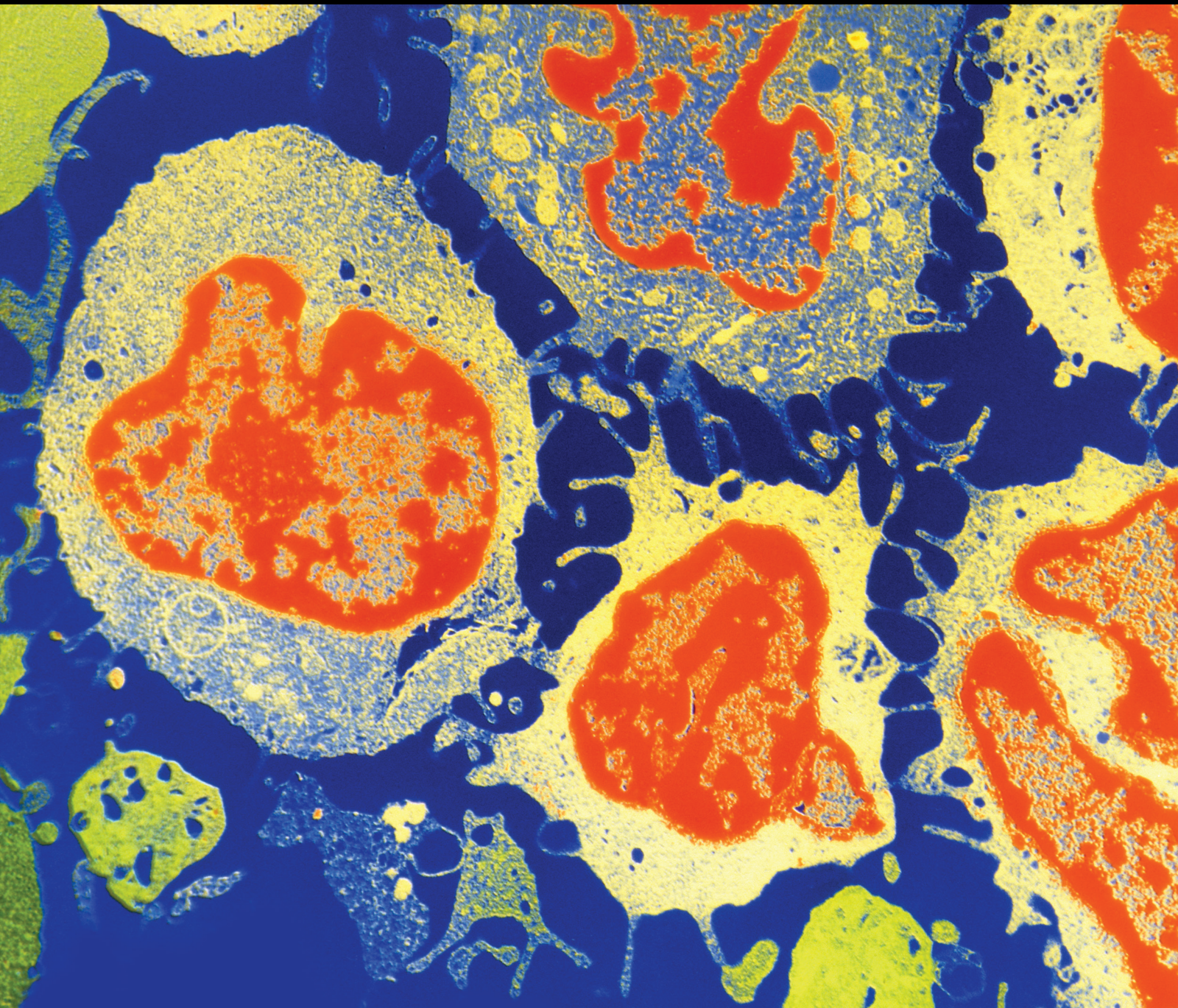


Colorectal Cancer: from Molecular Genetics to Diagnosis and Therapy

Lead Guest Editor: Simona Gurzu

Guest Editors: Zsolt Kovacs, Mark Slevin, and Ioan Jung





Colorectal Cancer: from Molecular Genetics to Diagnosis and Therapy

Journal of Oncology

Colorectal Cancer: from Molecular Genetics to Diagnosis and Therapy

Lead Guest Editor: Simona Gurzu

Guest Editors: Zsolt Kovacs, Mark Slevin, and Ioan Jung



Copyright © 2022 Hindawi Limited. All rights reserved.

This is a special issue published in "Journal of Oncology" All articles are open access articles distributed under the Creative Commons Attribution License, which permits unrestricted use, distribution, and reproduction in any medium, provided the original work is properly cited.

Chief Editor

Bruno Vincenzi, Italy

Academic Editors

Thomas E. Adrian, United Arab Emirates

Ruhai Bai , China

Jiaolin Bao, China


Rossana Berardi, Italy

Benedetta Bussolati, Italy


Sumanta Chatterjee, USA


Thomas R. Chauncey, USA

Gagan Chhabra, USA

Francesca De Felice , Italy

Giuseppe Di Lorenzo, Italy

Xiangya Ding , China

Peixin Dong , Japan

Xingrong Du, China

Elizabeth R. Dudnik , Israel

Pierfrancesco Franco , Italy

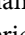
Ferdinand Frauscher , Austria

Rohit Gundamaraju, USA

Han Han , USA

Jitti Hanprasertpong , Thailand


Yongzhong Hou , China

Wan-Ming Hu , China


Jialiang Hui, China

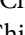
Akira Iyoda , Japan

Reza Izadpanah , USA

Kaiser Jamil , India

Shuang-zheng Jia , China

Ozkan Kanat , Turkey

Zhihua Kang , USA

Pashtoon M. Kasi , USA

Jorg Kleeff, United Kingdom

Jayaprakash Kolla, Czech Republic

Goo Lee , USA

Peter F. Lenehan, USA

Da Li , China

Rui Liao , China

Rengyun Liu , China

Alexander V. Louie, Canada

Weiren Luo , China


Cristina Magi-Galluzzi , USA

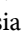
Kanjoormana A. Manu, Singapore


Riccardo Masetti , Italy

Ian E. McCutcheon , USA

Zubing Mei, China

Giuseppe Maria Milano , Italy

Nabiha Missaoui , Tunisia

Shinji Miwa , Japan

Sakthivel Muniyan , USA

Magesh Muthu , USA

Nandakumar Natarajan , USA


P. Neven, Belgium


Patrick Neven, Belgium

Marco Noventa, Italy

Liren Qian , China

Shuanglin Qin , China

Dongfeng Qu , USA

Amir Radfar , USA

Antonio Raffone , Italy


Achuthan Chathrattil Raghavamenon, India

Faisal Raza, China

Giandomenico Roviello , Italy

Subhadeep Roy , India


Prasannakumar Santhekadur , India

Chandra K. Singh , USA

Yingming Sun , China


Mohammad Tarique , USA

Federica Tomao , Italy


Vincenzo Tombolini , Italy

Maria S. Tretiakova, USA

Abhishek Tyagi , USA

Satoshi Wada , Japan


Chen Wang, China

Xiaosheng Wang , China

Guangzhen Wu , China

Haigang Wu , China


Yuan Seng Wu , Malaysia

Yingkun Xu , China

WU Xue-liang , China

ZENG JIE YE , China

Guan-Jun Yang , China




Junmin Zhang , China

Dan Zhao , USA

Dali Zheng , China


Contents

Identification of APC Mutation as a Potential Predictor for Immunotherapy in Colorectal Cancer

Fen Feng, Huake Sun, Zhikun Zhao, Chao Sun, Yongtian Zhao, Hanqing Lin, Jie Yang, Yajie Xiao , Wei Wang , and Dongfang Wu 

Research Article (9 pages), Article ID 6567998, Volume 2022 (2022)

Downregulation of LRRC19 Is Associated with Poor Prognosis in Colorectal Cancer

Ya-Juan Wang, Man Liu, Hui-Ying Jiang, and Yong-Wei Yu 

Research Article (13 pages), Article ID 5848823, Volume 2022 (2022)

Prognostic Utility of Platelet-to-Albumin Ratio among Critically Ill Patients with Colorectal Cancer: A Propensity Score Matching Study

Anshu Li , Zhiyong Wang , Qing Lv , and Yan Ling 


Research Article (12 pages), Article ID 6107997, Volume 2022 (2022)

Nonpolypous Hamartomas of the Gastrointestinal Tract: An Updated Review on Classification, Denominations, and Clinical Management

Simona Gurzu , Diana Burlacu , and Ioan Jung 







Review Article (9 pages), Article ID 6983460, Volume 2022 (2022)

Dissection of Immune Profiles in Microsatellite Stable and Low Microsatellite Instability Colon Adenocarcinoma by Multiomics Data Analysis

Tao Yang, Jiali Lei, Qiushi Feng, Dandan Song, and Xiaosheng Wang 

Research Article (20 pages), Article ID 8588164, Volume 2022 (2022)

Creation and Validation of a Survival Nomogram Based on Immune-Nutritional Indexes for Colorectal Cancer Patients

Yulan Liu , Yang Meng , Chenliang Zhou , Ya Liu, Shan Tian , Jiao Li , and Weiguo Dong 


Research Article (12 pages), Article ID 1854812, Volume 2022 (2022)

In-House Validated Map of Lymph Node Stations in a Prospective Cohort of Colorectal Cancer: A Tool for a Better Preoperative Staging

Patricia Simu , Ioan Jung , Laura Baniias , Zsolt Zoltan Fulop , Tivadar Bara , Iunius Simu , Sebastian Andone , Raluca Ioana Stefan-van Staden , Catalin Bogdan Satala , Ioana Halmaciu , and Simona Gurzu 

Research Article (10 pages), Article ID 1788004, Volume 2022 (2022)

Application of Prognostic Models Based on Psoas Muscle Index, Stage, Pathological Grade, and Preoperative Carcinoembryonic Antigen Level in Stage II-III Colorectal Cancer Patients Undergoing Adjuvant Chemotherapy

Li Shan, Tian Li , Wenhao Gu, Yuting Gao, Erdong Zuo, Huizhu Qiu, Rong Li, and Xu Cheng 

Research Article (12 pages), Article ID 6851900, Volume 2022 (2022)

Research Article

Identification of APC Mutation as a Potential Predictor for Immunotherapy in Colorectal Cancer

Fen Feng,¹ Huake Sun,² Zhikun Zhao,³ Chao Sun,³ Yongtian Zhao,³ Hanqing Lin,³ Jie Yang,³ Yajie Xiao ,³ Wei Wang ,¹ and Dongfang Wu ³

¹Cancer Center, The First People's Hospital of Foshan City, Foshan 518100, China

²Department of Geriatrics, Guangzhou First People's Hospital, Guangzhou 510180, China

³YuceBio Technology Co., Ltd., Shenzhen 518100, China

Correspondence should be addressed to Yajie Xiao; xiaoyajie@yucebio.com, Wei Wang; wangwei@fsyyy.com, and Dongfang Wu; wudf@yucebio.com

Received 28 February 2022; Accepted 13 June 2022; Published 13 July 2022

Academic Editor: Zsolt Kovacs

Copyright © 2022 Fen Feng et al. This is an open access article distributed under the Creative Commons Attribution License, which permits unrestricted use, distribution, and reproduction in any medium, provided the original work is properly cited.

To date, anticancer immunotherapy has presented some clinical benefits to most of advanced mismatch repair deficient (dMMR)/microsatellite instability-high (MSI-H) colorectal cancer (CRC) patients. In addition to MSI status, we aimed to reveal the potential predictive value of adenomatous polyposis coli (APC) gene mutations in CRC patients. A total of 238 Chinese CRC patients was retrospectively identified and analyzed for clinical features and gene alternations in APC-mutant type (MT) and APC-wild-type (WT) groups. Clinical responses were then evaluated from the public TCGA database and MSKCC immunotherapy database. Although programmed cell death ligand 1 (PD-L1) level, MSI status, loss of heterogeneity at the human leukocyte antigen (HLA LOH), and tumor neoantigen burden (TNB) level were not statistically different between the APC-MT group and APC-WT group, tumor mutation burden (TMB) level was significantly higher in APC-MT patients ($P < 0.05$). Furthermore, comutation analysis for APC mutations revealed co-occurring genomic alterations of PCDHB7 and exclusive mutations of CTNBN1, BRAF, AFF3, and SNX25 ($P < 0.05$). Besides, overall survival from MSKCC-CRC cohort was longer in the APC-WT group than in the APC-MT group (HR 2.26 (95% CI 1.05–4.88), $P < 0.05$). Furthermore, most of patients in the APC-WT group were detected as high-grade immune subtypes (C2–C4) comparing with those in the APC-MT group. In addition, the percentages of NK T cells, Treg cells, and fibroblasts cells were higher in APC-WT patients than in APC-MT patients ($P < 0.05$). In summary, APC mutations might be associated with poor outcomes for immunotherapy in CRC patients regardless of MSI status. This study suggested APC gene mutations might be a potential predictor for immunotherapy in CRC.

1. Introduction

Immune checkpoint inhibitors (ICIs) targeting at the programmed cell death ligand 1 (PD-L1) or cytotoxic T lymphocyte antigen 4 (CTLA-4) signaling pathway presented impressive success in different cancer types [1–4]. Unfortunately, the overall response rate to ICI therapy remains still limited. Subsequently, some biomarkers such as PD-L1 expression, microsatellite instability (MSI), and tumor mutation burden (TMB) have been established for predicting the efficacy of immunotherapy. However, still lots of patients have low values of these recommended

biomarkers. Therefore, novel diagnostic and prognostic biomarkers are expected for identifying more patients who can benefit from immunotherapy [5–7].

Colorectal cancer (CRC) ranks the third most common cancer and the second leading cause of cancer-related deaths worldwide [8]. Even though most of primary colorectal lesions are resectable, the 5-year survival rate for advanced CRC is still low. Generally, except for some patients with MSI-H/DNA mismatch repair-deficient (dMMR) tumors, CRC is supposed to be a low immune-reactive cancer with limited immune infiltrating cells or extensive infiltrating immunosuppressive T cells. In recent studies, MSI-H/

dMMR CRC patients have showed lasting clinical responses and improved survival outcomes to ICI therapy [9–11]. The pity is that immunotherapy provides few clinical benefits to most of advanced non-MSI-H/dMMR CRC patients.

Adenomatous polyposis coli (APC) gene on chromosome 5q21-q22 is known as a tumor suppressor gene and is highly mutated in CRC [12, 13]. Particularly, APC mutations have demonstrated to be related with familial adenomatous polyposis (FAP) which can lead to tumor progression in CRC development [14–17]. A recent study has presented that APC is a negative regulator in the wingless signaling transduction (WNT)/beta-catenin pathway [18]. Loss of functions at APC genes can aid in proteasomal destabilization, degradation, and nuclear accumulation of beta-catenin, leading to activation of T cell factor or lymphoid enhancer factor for initiating tumorigenesis [19–22].

In addition to MSI status, we aimed to reveal the latent predictive value of APC mutations in order to provide a potential biomarker for indicating therapeutic responses in CRC patients with immunotherapy.

2. Methods

2.1. Sample Collection and Preparation. Relevant clinical and sequencing data were collected from January 2019 to June 2020, respectively. General demographic data and pathological diagnostic information were checked with corresponding medical record for each patient. A certain amount of fresh tumor tissue or formalin-fixed paraffin-embedded (FFPE) tumor tissue after a biopsy or surgery were either taken for each patient to perform PD-L1 expression analysis and genomic profiling. The study was approved by the Ethic Committee of YuceBio Technology Co., Ltd., and each patient or family member signed an informed written consent.

Genomic DNAs were isolated from each tumor tissue, and its matched peripheral blood sample was extracted using the GeneRead DNA Kit and Qiagen DNA blood mini kit (Qiagen), respectively, and extracted DNAs were then amplified, purified, and analyzed using YuceOne™ Plus NGS panel (Yucebio, China) [23, 24]. FFPE sections were stained with anti-PD-L1 22C3 mouse monoclonal primary antibody on a Dako Autostainer Link 48 system.

2.2. Sequencing Data Processing. Sequencing reads were filtered at the condition of >10% N rate or >10% bases with quality score <20 using SOAPnuke (Version 1.5.6). The somatic single nucleotide variants (SNVs) together with insertions and deletions (Indels) were analyzed using VarScan (Version 2.4), and furthermore, the in-house method was implemented to distinguish the possible false positive mutations. Afterwards, SnpEff (Version 4.3) was used to perform functional annotation for detected mutations in the tumor samples.

Tumor mutation burden (TMB) was measured as the total number of nonsilent somatic mutations including coding base substitution and indels per megabase, while tumor neoantigen burden (TNB) was calculated as the total

number of all mutations which may generate neoantigens per megabase. HLA genotyping was assessed by OptiType [25] (Version 1.3.2), and the loss of heterogeneity (LOH) of HLA was detected as previously described [26, 27]. The levels of microsatellite instability (MSI) were calculated using the MSIsensor [28].

2.3. Data Acquisition and Immune Signature Analysis from Public Database. TCGA-CRC cohort data with somatic nucleotide mutations (SNVs), copy number variations (CNVs), mRNA expressions, clinical features, and survival information were downloaded from The Cancer Genome Atlas (TCGA) public database (<https://portal.gdc.cancer.gov/>). MSKCC pancancer or CRC immunotherapy cohort data with SNVs, clinical features, and survival information were downloaded from the cBioPortal (<https://www.cbioportal.org>) public database. Patients without follow-up information and survival data were excluded.

The immune subtypes were characterized into 6 immune subtypes of IFN- γ dominant, TGF- β dominant, inflammatory, lymphocyte depleted, wound healing, and immunologically quiet [29]. These subtypes were classified by macrophage or lymphocyte signature difference, Th1 cell/Th2 cell ratio, intratumoral heterogeneity level, aneuploidy, neoantigen load level, overall cell proliferation, immunomodulatory gene expression, and prognosis. Then, the proportions of infiltrating immune cells were calculated using the xCell method integrating gene set enrichment approaches with deconvolution approaches [30]. This method can provide gene signatures for 64 cell types generated from extensive expression profiles, including multiple adaptive and innate immunity cells, epithelial cells, hematopoietic progenitors, and extracellular matrix cells.

2.4. Statistical Analysis. Correlations between APC mutations and clinical parameters of CRC patients in this study were examined using Fisher's exact test for categorical variables. Kruskal–Wallis rank sum tests or Wilcoxon rank sum tests were used for comparisons of continuous variables among different groups. Survival analysis was performed from the public TCGA-CRC dataset, public MSKCC pancancer immunotherapy dataset, and MSKCC-CRC immunotherapy dataset using the Kaplan–Meier survival curve and log-rank test. $P < 0.05$ was regarded to be statistically significant. All statistical analyses in this study were performed with R statistical computing environment v3.6.1 software (<https://www.r-project.org>).

3. Results

3.1. Clinical Characteristics. As given in Table 1, a total of 238 Chinese CRC patients were identified in this study. The median age of the whole population was 59 and 58.4% (139/238) was male patients. The number of patients at grade IV was 112 (47.06%). Altogether, there were 36 patients lacking detailed information of cancer type. The number of patients with colon cancer was 113 (47.78%), while the number of patients with rectum cancer was 89 (37.39%). In general, the

TABLE 1: Clinical characteristics and biomarkers of CRC patients.

	Total (<i>n</i> = 238)	APC-MT group (<i>n</i> = 175)	APC-WT group (<i>n</i> = 63)	<i>P</i> value
Age	59 (26–89)	61 (52–68)	59 (49–66)	0.189
Gender				
Female	99	72	27	0.882
Male	139	103	36	
Stage [#]				
I–III	64	45	19	0.614
IV	112	87	29	
Type [#]				
Colon	113	82	31	0.186
Rectum	89	72	17	
MSI				
MSI-H	15	9	6	0.223
MSI-L	223	166	57	
HLA LOH				
Yes	39	32	7	0.235
No	199	143	56	
TMB	6.69 (4.69–8.71)	6.7 (4.69–8.73)	5.36 (3.59–7.64)	0.022*
TNB	2.62 (1.34–4.69)	2.68 (1.34–4.02)	2.55 (0.67–4.70)	0.766

TMB, tumor mutation burden; Mut/Mb, mutations per megabase; TNB, tumor neoantigen burden; Neo/Mb, neoantigens per megabase; HLA, human leukocyte antigen; LOH, loss of heterogeneity. **P* values <0.05. [#]Some data were missing.

number of the APC-mutant type (MT) and APC-wild-type (WT) patients with CRC was 175 (73.53%) and 63 (26.37%), respectively. Besides, 93.70% (223/238) was at MSI-L status, while 6.30% (15/238) was at MSI-H status. Furthermore, there were no significant differences of gender, tumor stage, and tumor subtype between the APC-MT group and the APC-WT group. Although PD-L1, MSI, HLA LOH, and TNB were not statistically different between the APC-MT and APC-WT groups (*P* > 0.05), TMB level was significantly higher in APC-MT patients (*P* < 0.05).

3.2. Mutational Landscape. The 20 most frequent genomic alternations in CRC patients are shown in Figure 1(a), including TP53, APC, KRAS, PIK3CA, SMAD4, FBXW7, TCF7L2, and FAT4 with a frequency more than 10%. Furthermore, comutation analysis in Figure 1(b) revealed co-occurring genomic alterations of PCDHB7 and exclusive mutations of CTNNB1, BRAF, AFF3, and SNX25 (*P* < 0.05) with APC genes. In TCGA cohort, shown in Supplementary Figure S1, mutations of AFF3 and SNX25 were not exclusive from APC mutations (*P* < 0.1), while those alternations of CTNNB1 and BRAF were positively exclusive (*P* < 0.05). In the MSKCC database, shown in Supplementary Figure S1, there was also an indistinct mutually exclusion of CTNNB1 and BRAF from APC mutations (*P* < 0.1). Additionally, hotspot in APC genes in NGS results (Figure 1(c)) were similar with MSKCC (Figure 1(d)) and TCGA public datasets (Figure 1(e)).

3.3. Biomarker Analysis. Next, we also performed further analyses between other immunotherapy biomarkers and APC mutations in this study (Figures 2(a) and 2(b)). In MSI-L CRC patients, TMB level was highly correlated with APC mutations (*P* < 0.05). Unfortunately, due to small sample size, the relationship with TMB level and APC mutations

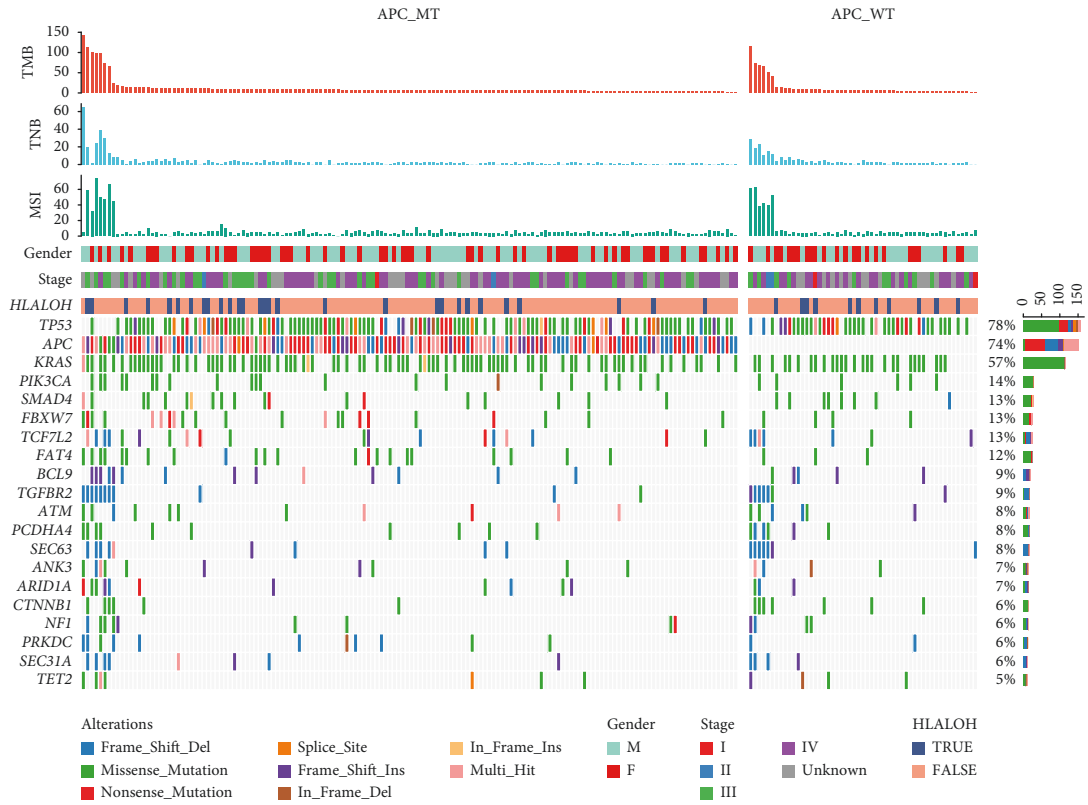
was not found in MSI-H CRC patients. Besides, APC mutations were independent factors from MSI status, PD-L1 expression, and HLA LOH in this study (Figures 2(c)–2(e)).

3.4. Survival Analysis. As shown in Figures 3(a) and 3(b), patients without APC mutations did not have prolonged overall survival from TCGA CRC cohort (HR 1.00 (95% CI 0.64–1.56), *P* > 0.05) and MSKCC pancancer immunotherapy cohort (HR 1.13 (95% CI 0.88–1.45), *P* > 0.05). Interestingly, overall survival from MSKCC-CRC immunotherapy cohort was longer in the APC-WT group than in the APC-MT group (HR 2.27 (95% CI 1.05–4.88), *P* < 0.05) (Figure 3(c)).

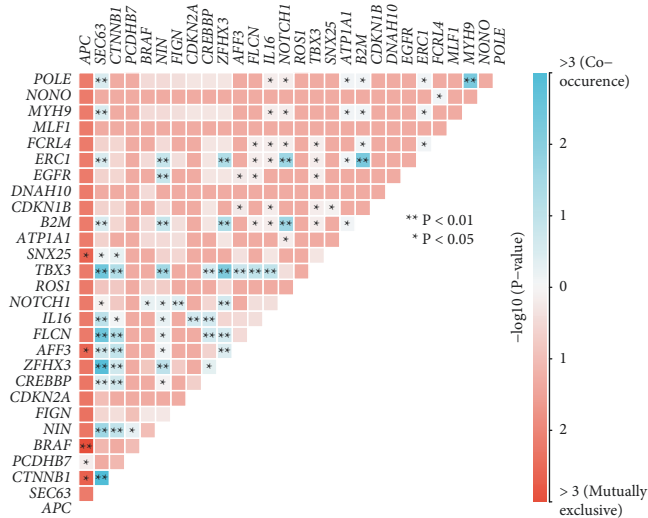
3.5. Immune Signatures. Furthermore, we primarily characterized immune signatures in CRC patients in the APC-WT group and APC-MT group in Figure 4. Most of patients in the APC-WT group were detected as high-grade immune subtypes (C2–C4) compared with the APC-MT group. In addition, the percentages of NK T cell, Treg cells, and fibroblasts cells were higher in APC-WT patients with non-MSI-H status than in APC-MT patients with non-MSI-H status (*P* < 0.05). But the statistical differences were not observed in patients with MSI-H status.

4. Discussion

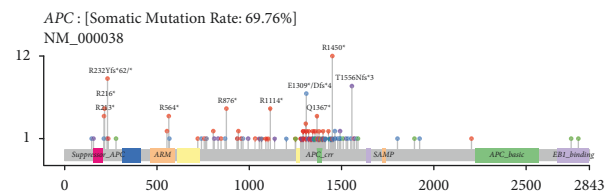
Instead of MSI status, we elucidated the predictive value of APC mutations for poor clinical responses to immunotherapy in CRC patients. Furthermore, we found that TMB was significantly higher in APC-MT patients than in APC-WT patients. In addition, we distinguished important co-occurring genomic alterations and exclusive mutations and illustrated immune signature for underlying potential mechanisms for its predictive role in CRC.



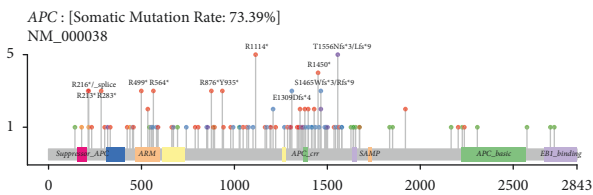
(a)



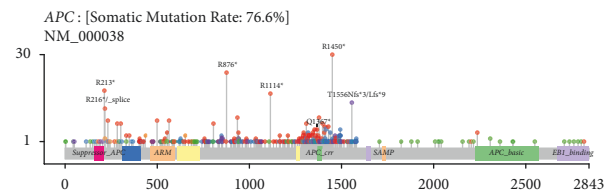
(b)



(c)



(d)



(e)

FIGURE 1: Distinct mutational patterns in Chinese CRC patients by APC gene mutation. (a) The mutational landscape of top mutated genes. (b) Co-occurring and exclusive mutations. (c) Hotspot in APC genes in NGS results. (d) Hotspot in APC genes in the public MSKCC-CRC dataset. (e) Hotspot in APC genes in the public TCGA-CRC dataset.

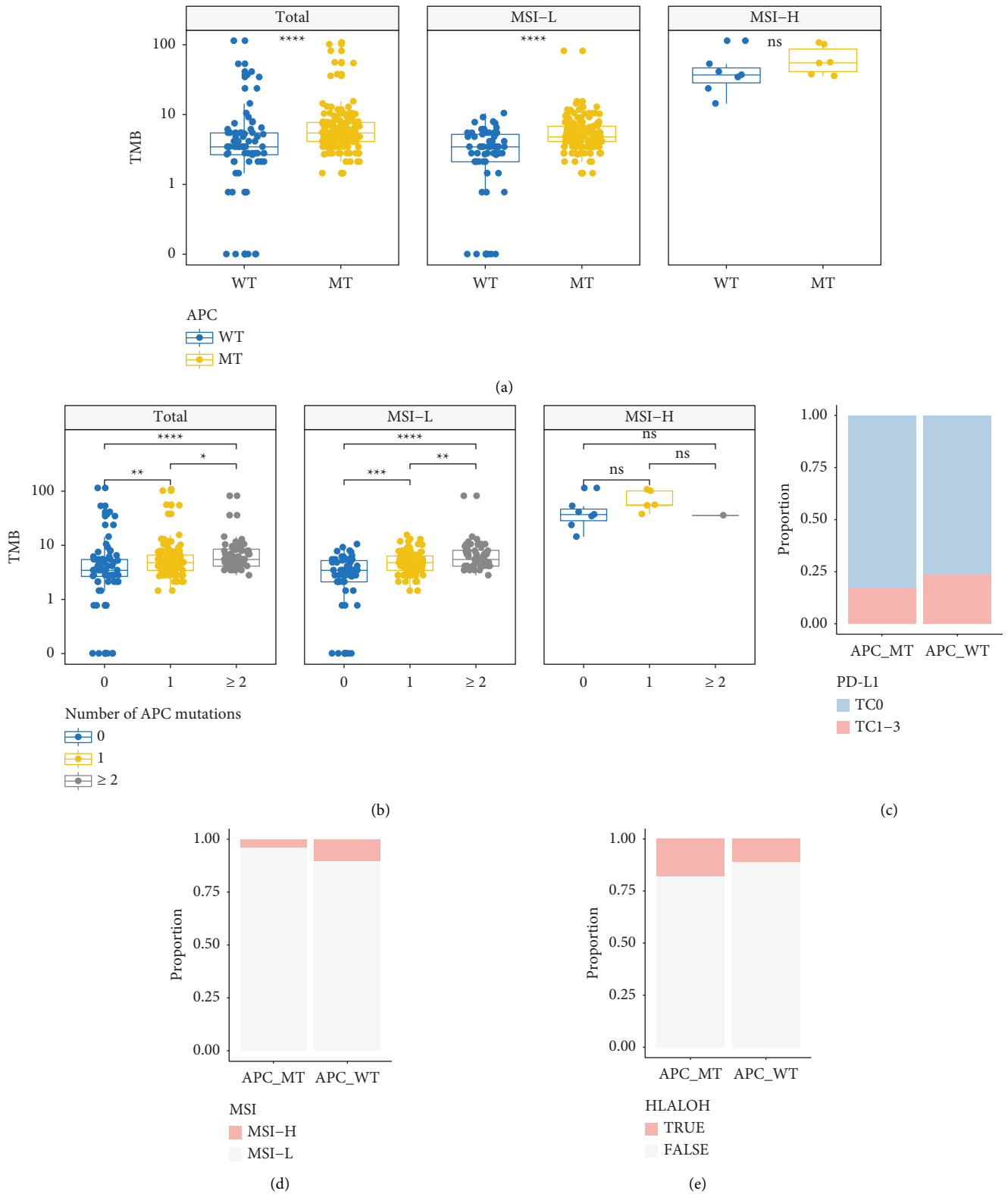


FIGURE 2: Correlation analysis in the groups with or without APC mutations. (a) TMB level with different MSI status. (b) TMB level with different MSI status and different APC mutated genes. (c) PD-L1 expression. (d) MSI status. (e) HLA LOH status. Comparisons were done by the Wilcoxon test or Fisher's test. N.S. was regarded to be nonstatistically significant.

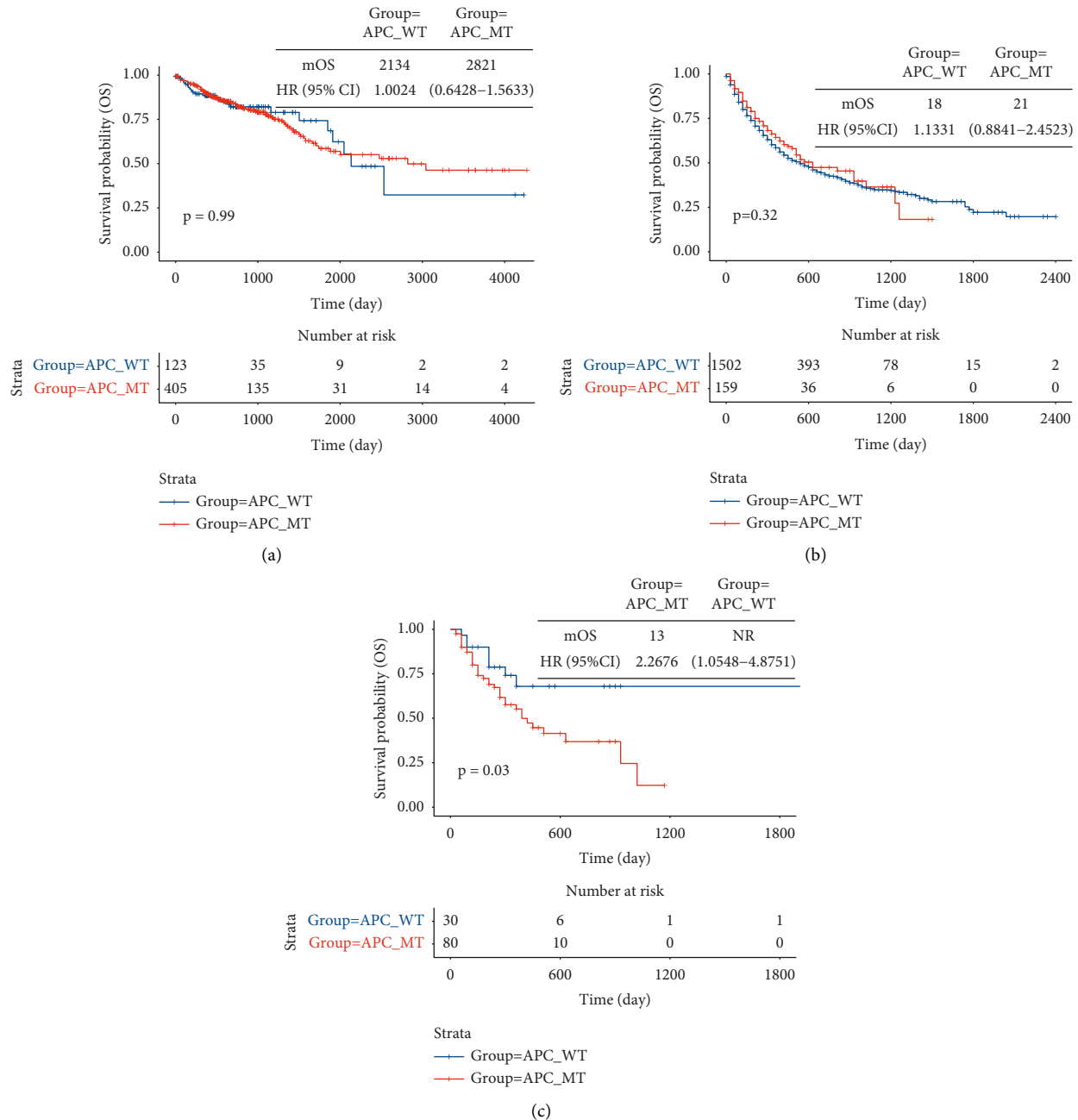


FIGURE 3: Survival analysis in the groups with or without APC mutations from public cohorts. (a) TCGA-CRC cohort. (b) MSKCC pancancer immunotherapy cohort. (c) MSKCC-CRC immunotherapy cohort.

Although PD-L1 expression is the gold biomarker for immunotherapy, broad inconsistency of this biomarker can be resulted from the variability of immunohistochemical staining antibodies and heterogeneous expression [31, 32]. Recently, TMB has emerged as an important biomarker in immunotherapy, especially for prognosis prediction [10, 33]. In clinical practice, TMB level in some cancer types such as lung cancers and melanoma have been demonstrated to be substantially related with the clinical outcomes of immunotherapy. Although there were some disagreements on the cutoff values, FDA approved pembrolizumab monotherapy

for adult and pediatric patients with unresectable or metastatic solid tumors of high TMB level ≥ 10 mut/Mb [32]. In this study, we found that TMB levels was higher in APC-MT patients than in APC-WT patients, in addition to MSI status. However, the overall TMB levels were around 5, which was much lower than those results in public CRC datasets. This inconstancy might be resulted from different sequencing methods or sequencing products. TCGA CRC cohort data were generated from whole exome sequencing, and MSKCC cohort data were generated from different targeted sequencing panels. Also, the cutoff values might be

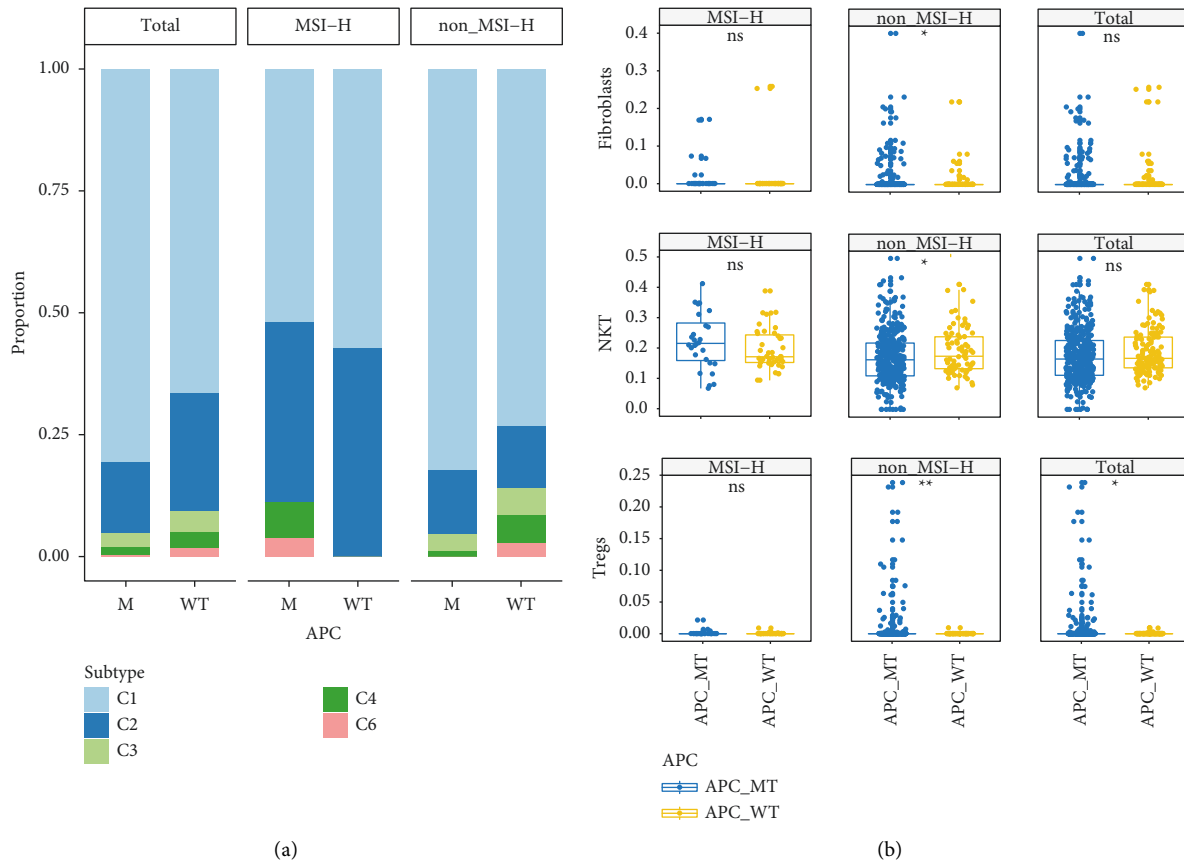


FIGURE 4: Immune signatures in the groups with or without APC mutations. (a) The percentages of immune subtypes. (b) The proportions of NK T cell, Treg cells, and fibroblasts cells. Comparisons were done by the Wilcox test or Fisher's test. N.S. was regarded to be non-statistically significant.

inconsistent between public datasets and our study. The definite relationship needed to be further studied.

Besides, this study also presented more alternations beyond TP53 and KRAS in APC-WT patients, which may drive tumor metastasis signaling in advanced cancers [34, 35]. As is known, APC genes can downregulate the WNT/beta-catenin pathway and consequently initiate tumorigenesis. CTNNB1, BRAF, AFF3, and SNX25 were enriched within the APC-WT CRC patients, suggesting a latent mechanism for activating WNT/beta-catenin. Prior studies indicated that CTNNB1 alternations were mutually exclusive with APC mutations, which may replace APC mutation to be the initiator genomic alteration in CRC development [36]. As an oncogenic gene for β -catenin mediated tumorigenesis, AFF3 can act on transcription and RNA splicing in some aggressive cancer [37]. On the other hand, mutations of PCDHB7 co-occurred in the APC-WT subgroup. Expression of the protocadherin genes such as PCDHB7 may reduce WNT signaling to β -catenin and protein expression of the stem cell marker [38]. These exclusive alternations to APC mutations might lead to more robust WNT activation and worse overall outcome.

To date, in-depth immunogenomic analyses with tumor-infiltrating lymphocytes in tumor microenvironments are proven to activate tumor immunogenicity. The enrichment

of several adverse prognostic gene mutations in the Wnt signaling pathway is ubiquitous in tumorigenesis and cancer development [18]. In turn, recruitment of tumor-infiltrating T cells is reduced for mediating immune escape [39]. In this study, we also observed lower percentage of NK T cell, Treg cells, and fibroblasts cells and more high-grade immune subtypes (C2–C4) in the APC-WT group at non-MSI-H status compared with the APC-MT group. No significant differences were observed with patients at MSI-H status.

Our study involved several limitations. First, most of the patients in our studies were MSI-L, which might cause some statistical bias. Second, some of clinical diagnostic data such as cancer stage and tumor subtype were lacking, which cannot give a more in-depth analysis on the differences of the clinical characteristics. Third, due to lack of sufficient PFS and OS data in our real-world practice, we used public TCGA or MSKCC datasets to evaluate the predictive role of APC mutations on clinical response.

In summary, APC mutations are associated with poor outcomes of immunotherapy in CRC patients regardless of MSI status. Compared with APC-MT CRC tumors, APC-WT tumors presented more genomic alterations for activating the WNT signaling pathway. Our data suggest APC gene mutations might be a potential predictor to identify CRC patients who can benefit from immunotherapy.

Data Availability

The datasets used and analyzed during the current study are available from the corresponding author upon request.

Ethical Approval

All the study procedures were approved by the Ethic Committee of YuceBio Technology Co., Ltd.

Consent

The study was conducted after the acquisition of written informed consent from the patients.

Conflicts of Interest

The authors declare that they have no conflicts of interest.

Authors' Contributions

FF, HS, ZZ, and CS contributed to research design, manuscript drafting, and methodology conceptualization; YZ, HL, and JY contributed to data analysis and interpretation; YX, WW, and DW contributed to study supervision and manuscript revision. All authors contributed to the article and approved the submitted version. Fen Feng, Huake Sun, Zhikun Zhao, and Chao Sun equally contributed to this work.

Acknowledgments

This study was funded by Self-Funded Science and Technology Project of Foshan City in 2019 (1920001002013).

Supplementary Materials

Supplementary Figure S1. Co-occurring and exclusive analysis with APC mutations from TCGA cohort (A) and MSKCC cohort. (*Supplementary Materials*)

References

- [1] D. B. Doroshow, M. F. Sanmamed, K. Hastings et al., "Immunotherapy in non-small cell lung cancer: facts and hopes," *Clinical Cancer Research*, vol. 25, pp. 4592–4602, 2019.
- [2] S. Sadanand, "Immunotherapy for esophageal cancer," *Nature Medicine*, 2021.
- [3] T. Yap, E. Parkes, W. Peng, J. Moyers, M. Curran, and H. Tawbi, "Development of immunotherapy combination strategies in cancer," *Cancer Discovery*, vol. 11, p. 1368, 2021.
- [4] T. Zhang and D. George, "Immunotherapy and targeted-therapy combinations mark a new era of kidney cancer treatment," *Nature Medicine*, vol. 27, pp. 586–588, 2021.
- [5] D. Camidge, R. Doebele, and K. Kerr, "Comparing and contrasting predictive biomarkers for immunotherapy and targeted therapy of NSCLC," *Nature Reviews Clinical Oncology*, vol. 16, pp. 341–355, 2019.
- [6] L. Emens, "Predictive biomarkers: progress on the road to personalized cancer immunotherapy," *Journal of the National Cancer Institute*, vol. 113, pp. 1601–1603, 2021.
- [7] T. Chan, M. Yarchoan, E. Jaffee et al., "Development of tumor mutation burden as an immunotherapy biomarker: utility for the oncology clinic," *Annals of Oncology*, vol. 30, pp. 44–56, 2019.
- [8] F. Bray, J. Ferlay, I. Soerjomataram, R. Siegel, L. Torre, and A. Jemal, "Global cancer statistics 2018: GLOBOCAN estimates of incidence and mortality worldwide for 36 cancers in 185 countries," *CA Cancer Journal of Clinicians*, vol. 68, pp. 394–424, 2018.
- [9] A. Ooki, E. Shinozaki, and K. Yamaguchi, "Immunotherapy in colorectal cancer: current and future strategies," *Journal of the Anus, Rectum and Colon*, vol. 5, pp. 11–24, 2021.
- [10] M. Duffy and J. Crown, "Biomarkers for predicting response to immunotherapy with immune checkpoint inhibitors in cancer patients," *Clinical Chemistry*, vol. 65, pp. 1228–1238, 2019.
- [11] J. Hindson, "PD1 blockade for advanced MSI-H CRC," *Nature Reviews Gastroenterology & Hepatology*, vol. 18, p. 82, 2021.
- [12] L. Zhang and J. Shay, "Multiple roles of APC and its therapeutic implications in colorectal cancer," *Journal of the National Cancer Institute*, vol. 109, 2017.
- [13] S. Seton-Rogers, "Colorectal cancer: APC restores order," *Nature Reviews Cancer*, vol. 15, p. 454, 2015.
- [14] M. B. Yurgelun, M. H. Kulke, C. S. Fuchs et al., "Cancer susceptibility gene mutations in individuals with colorectal cancer," *Journal of Clinical Oncology*, vol. 35, pp. 1086–1095, 2017.
- [15] P. Boland, M. Yurgelun, and C. Boland, "Recent progress in Lynch syndrome and other familial colorectal cancer syndromes," *CA Cancer Journal for Clinicians*, vol. 68, pp. 217–231, 2018.
- [16] R. Kariv, M. Caspi, N. Fliss-Isakov et al., "Resorting the function of the colorectal cancer gatekeeper adenomatous polyposis coli," *International Journal of Cancer*, vol. 146, pp. 1064–1074, 2020.
- [17] S. Gaujoux, S. Pinson, A. Gimenez-Roqueplo et al., "Inactivation of the APC gene is constant in adrenocortical tumors from patients with familial adenomatous polyposis but not frequent in sporadic adrenocortical cancers," *Clinical Cancer Research*, vol. 16, pp. 5133–5141, 2010.
- [18] B. MacDonald, K. Tamai, and X. He, "Wnt/beta-catenin signaling: components, mechanisms, and diseases," *Developmental Cell*, vol. 17, pp. 9–26, 2009.
- [19] W.-C. Ting, L.-M. Chen, J.-B. Pao et al., "Common genetic variants in Wnt signaling pathway genes as potential prognostic biomarkers for colorectal cancer," *PLoS One*, vol. 8, Article ID e56196, 2013.
- [20] M. Caspi, A. Wittenstein, M. Kazelnik, Y. Shor-Nareznay, and R. Rosin-Arbesfeld, "Therapeutic targeting of the oncogenic Wnt signaling pathway for treating colorectal cancer and other colonic disorders," *Advanced Drug Delivery Reviews*, vol. 169, pp. 118–136, 2021.
- [21] D. Flanagan, E. Vincan, and T. Pesse, "Wnt signaling in cancer: not a binary ON:OFF switch," *Cancer Research*, vol. 79, pp. 5901–5906, 2019.
- [22] W. Hankey, W. Frankel, and J. Groden, "Functions of the APC tumor suppressor protein dependent and independent of canonical WNT signaling: implications for therapeutic targeting," *Cancer Metastasis Reviews*, vol. 37, pp. 159–172, 2018.
- [23] K. Li, J. Liu, L. Wu et al., "Genomic correlates of programmed cell death ligand 1 (PD-L1) expression in Chinese lung

- adenocarcinoma patients,” *Cancer Cell International*, vol. 22, p. 138, 2022.
- [24] C. Zhou, T. Jiang, Y. Xiao et al., “Good tumor response to chemoradioimmunotherapy in dMMR/MSI-H advanced colorectal cancer: a case series,” *Frontiers in Immunology*, vol. 12, Article ID 784336, 2021.
- [25] A. Szolek, B. Schubert, C. Mohr, M. Sturm, M. Feldhahn, and O. Kohlbacher, “OptiType: precision HLA typing from next-generation sequencing data,” *Bioinformatics*, vol. 30, pp. 3310–3316, 2014.
- [26] N. McGranahan, R. Rosenthal, C. T. Hiley et al., “TRACERx Consortium Allele-specific HLA loss and immune escape in lung cancer evolution,” *Cell*, vol. 171, pp. 1259–1271, 2017.
- [27] J. Yi, L. Chen, Y. Xiao, Z. Zhao, and X. Su, “Investigations of sequencing data and sample type on HLA class Ia typing with different computational tools,” *Briefings in Bioinformatics*, vol. 22, 2021.
- [28] B. Niu, K. Ye, Q. Zhang et al., “MSIsensor: microsatellite instability detection using paired tumor-normal sequence data,” *Bioinformatics*, vol. 30, pp. 1015–1016, 2014.
- [29] V. Thorsson, D. L. Gibbs, S. D. Brown et al., “The immune landscape of cancer,” *Immunity*, vol. 48, pp. 812–830, 2018.
- [30] D. Aran, Z. Hu, and A. Butte, “xCell: digitally portraying the tissue cellular heterogeneity landscape,” *Genome Biology*, vol. 18, p. 220, 2017.
- [31] M. S. Tsao, K. M. Kerr, M. Kockx et al., “PD-L1 immunohistochemistry comparability study in real-life clinical samples: results of blueprint phase 2 project,” *Journal of Thoracic Oncology*, vol. 13, pp. 1302–1311, 2018.
- [32] M. Bassanelli, S. Sioletic, M. Martini et al., “Heterogeneity of PD-L1 expression and relationship with biology of NSCLC,” *Anticancer Research*, vol. 38, pp. 3789–3796, 2018.
- [33] Z. Zeng, B. Yang, and Z. Liao, “Biomarkers in immunotherapy-based precision treatments of digestive system tumors,” *Frontiers in Oncology*, vol. 11, Article ID 650481, 2021.
- [34] R. Pandey, N. Johnson, L. Cooke et al., “TP53 mutations as a driver of metastasis signaling in advanced cancer patients,” *Cancers*, vol. 13, 2021.
- [35] A. Yari, A. Samoudi, A. Afzali et al., “Mutation status and prognostic value of KRAS and BRAF in southeast Iranian colorectal cancer patients: first report from southeast of Iran,” *Journal of Gastrointestinal Cancer*, vol. 52, 2020.
- [36] A. Sparks, P. Morin, B. Vogelstein, and K. Kinzler, “Mutational analysis of the APC/beta-catenin/Tcf pathway in colorectal cancer,” *Cancer Research*, vol. 58, pp. 1130–1134, 1998.
- [37] L. Lefèvre, H. Omeiri, L. Drougat et al., “Combined transcriptome studies identify AFF3 as a mediator of the oncogenic effects of β -catenin in adrenocortical carcinoma,” *Oncogenesis*, vol. 4, p. e161, 2015.
- [38] C. C. Wong, J. Xu, X. Bian et al., “In colorectal cancer cells with mutant KRAS, SLC25A22-mediated glutaminolysis reduces DNA demethylation to increase WNT signaling, stemness, and drug resistance,” *Gastroenterology*, vol. 159, pp. 2163–2180, 2020.
- [39] S. Spranger and T. Gajewski, “Impact of oncogenic pathways on evasion of antitumour immune responses,” *Nature Reviews Cancer*, vol. 18, pp. 139–147, 2018.

Research Article

Downregulation of LRRC19 Is Associated with Poor Prognosis in Colorectal Cancer

Ya-Juan Wang,¹ Man Liu,² Hui-Ying Jiang,³ and Yong-Wei Yu ⁴

¹Department of Pathology, Shengzhou People's Hospital, Shengzhou Branch of the First Affiliated Hospital of Zhejiang University, Shengzhou, Zhejiang, China

²Department of Clinical Laboratory, Shengzhou People's Hospital, Shengzhou Branch of the First Affiliated Hospital of Zhejiang University, Shengzhou, Zhejiang, China

³Intensive Care Unit, Shengzhou People's Hospital, Shengzhou Branch of the First Affiliated Hospital of Zhejiang University, Shengzhou, Zhejiang, China

⁴Intensive Care Unit, The First Affiliated Hospital, Zhejiang University School of Medicine, Hangzhou, China

Correspondence should be addressed to Yong-Wei Yu; yuyongwei@zju.edu.cn

Received 8 April 2022; Accepted 25 May 2022; Published 26 June 2022

Academic Editor: Simona Gurzu

Copyright © 2022 Ya-Juan Wang et al. This is an open access article distributed under the Creative Commons Attribution License, which permits unrestricted use, distribution, and reproduction in any medium, provided the original work is properly cited.

Objective. Colorectal cancer (CRC) is globally one of the most often diagnosed cancers with high mortality rates. This study aimed to explore novel biomarkers for the diagnosis and prognosis of CRC. **Methods.** We collected 4 datasets about CRC in GEO and sought differentially expressed genes (DEGs) with GEO2R. Leucine-rich repeat-containing protein 19 (LRRC19) expression was assessed through the Oncomine and TIMER database analyses, which was further confirmed by qRT-PCR of CRC samples. We used online survival analysis tools (GEPIA, PrognoScan, and Kaplan–Meier plotter) to examine the prognostic value of LRRC19 in CRC and other malignancies. GO and KEGG enrichment analyses were employed to explore the biological functions of LRRC19. Finally, we conducted network prediction by STRING and further validation on the GEPIA to discover other molecules that might interact with LRRC19. **Results.** A total of 21 upregulated and 46 downregulated DEGs were identified from the 4 datasets. The TIMER and Oncomine online analyses showed lower mRNA of LRRC19 in CRC tissues compared with adjacent normal tissues, which was validated by qRT-PCR in CRC patient samples. The survival analysis through the GEPIA and PrognoScan websites revealed that low LRRC19 expression was significantly correlated with poor prognosis in CRC patients. The Kaplan–Meier plotter survival analysis indicated that low LRRC19 expression was significantly associated with the disease progression of patients with ovarian cancer, gastric cancer, breast cancer, and lung cancer. The enrichment analysis suggested that low expression of LRRC19 could be involved in the retinol metabolism and the zymogen granule membrane. Through STRING and GEPIA, it was found that LRRC19 is clearly associated with ZCCHC10, MOB3B, IMMP2L, and TRMT11. **Conclusion.** LRRC19 mRNA was prominently decreased in human CRC tissues and was significantly associated with shorter survival in CRC patients. LRRC19 might serve as a possible target for early diagnosis and prognosis assessment in CRC.

1. Introduction

Among the most commonly diagnosed cancers, colorectal cancer (CRC) ranked third in men and second in women, with an estimated 1.4 million cases and 693,900 deaths in 2012 worldwide [1]. Although investigators have tried hard to uncover the molecular mechanism of occurrence and progression of CRC, it has not been thoroughly illustrated. Therefore, it is necessary to further explore CRC-related

genes and pathways, which helps not only to unravel the molecular mechanism of the tumorigenesis and development of CRC but also to guide the development of hopeful diagnostic and prognostic biomarkers and optimal therapeutic strategies [2].

The past few years of research obtained increased tumor biomarkers related to the progression or prognosis of human cancers. A number of above-mentioned biomarkers have been assessed in CRC patients, such as BRAF, KRAS, NRAS,

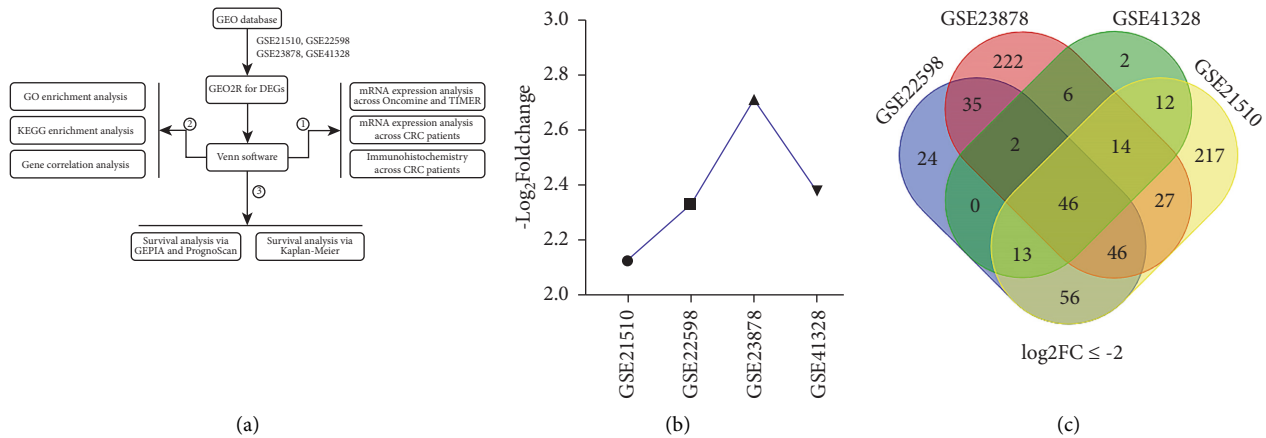


FIGURE 1: Flowchart and Venn diagram of DEGs. (a) Flowchart. (b) LRRC19 expression level in 4 GEO databases. (c) 46 DEGs downregulated in the four datasets ($\log_2FC \leq -2$). Different colors meant different datasets. The overlapped areas show the number of DEGs among GSE21510, GSE22598, GSE23878, and GSE41328.

and MMR [3–5]. The gene chip detection technique, which can recognize all genes within the same sample time-point expression information, is generally used to screen differentially expressed genes (DEGs). Publicly available databases, including the Gene Expression Omnibus (GEO) and The Cancer Genome Atlas (TCGA), have stored huge amounts of core microarray data about the relationship between genes and cancers at the gene level [6, 7]. Therefore, a mass of gene expression profiles and prognostic biomarkers have been accumulated regarding CRC. However, as a result of independent sample heterogeneity, the outcomes were different or limited. To address these deficiencies, our study used the method of integrated bioinformatics with expression profiling techniques to recognize steady biomarkers for CRC.

We employed four microarray datasets (GSE21510, GSE22598, GSE23878, and GSE41328) to screen DEGs in CRC tissues by virtue of the GEO2R tool and Venn diagram software [8–11]. As a result, we found that LRRC19 mRNA was significantly downregulated in CRC samples compared with adjacent normal tissues. Based on the microarray findings, qRT-PCR was performed for further expression validation and to explore the association between the expression level of LRRC19 and the clinicopathological features. Then, a combination of online databases (including GEPIA, UALCAN, and Kaplan–Meier plotter) was further performed to assess the correlation between LRRC19 expression and survival in CRC patients. Meanwhile, the analyses of Gene Ontology (GO) and Kyoto Encyclopedia of Gene and Genome (KEGG) enriched pathways were also conducted for annotation and visualization with LRRC19 potential function. Finally, a network of LRRC19 interactions with other molecules was predicated in the STRING and GEPIA databases (Figure 1(a)).

2. Materials and Methods

2.1. Data Resource and Description. Original data between CRC tumor and nontumor samples were downloaded from

the Gene Expression Omnibus (GEO; <https://www.ncbi.nlm.nih.gov/>) database, and four gene expression profiles (GSE21510, GSE22598, GSE23878, and GSE41328) were elected [12]. The array data of GSE21510 comprised 104 CRC and 44 adjacent normal tissues [8]. GSE22598 included 17 CRC and 17 adjacent normal tissue samples [9]. GSE23878 consisted of 35GC and 24 adjacent normal tissue samples [10]. Finally, GSE41328 contained 10 CRC and 10 adjacent normal tissue samples [11].

2.2. Data Preprocessing of DEGs. The GEO2R (<https://www.ncbi.nlm.nih.gov/geo/geo2r/>) online analysis tool was used to screen differentially expressed genes (DEGs) between CRC and adjacent normal tissues [7]. The adjusted P values were applied to correct the occurrence of false-positive results using the Benjamini and Hochberg false discovery rate method by default [13]. The fold change (FC) of LRRC19 was evaluated by log transformation. $|\log_2FC| > 1$ and adjusted $P < 0.01$ were regarded as the screened threshold. Subsequently, the Venn software was used online (<https://bioinformatics.psb.ugent.be/webtools/Venn/>) to recognize the original data among the four datasets and to reveal the commonly expressed DEGs.

2.3. LRRC19 mRNA Expression Analysis across OncoPrint and TIMER. The LRRC19 gene expression levels in various types of cancers were identified via the OncoPrint database and the TIMER database. The summarization of LRRC19 expression in different tumor samples and its specific expression in CRC specimens compared with adjacent normal tissues were analyzed via the OncoPrint portal (<https://www.oncoPrint.org/>) [14]. The cutoff values were a P value of 0.01, fold change of 1.5, top 10% gene ranking, and the data had to be from mRNA. The fold change in LRRC19 expression in various datasets is given in Table 1. We also analyzed LRRC19 expression in different types of cancer via the Tumor Immune Estimation Resource (TIMER) database (<https://timer.cistrome.org/>) [15].

TABLE 1: Oncomine analysis of LRRC19 mRNA expression in colorectal cancer.

Cohort no.	Cohort	Microarray	Sample (<i>n</i>)	Fold change	<i>P</i> value
1	Hong colorectal	mRNA	Colorectal carcinoma vs. normal	-12.606	1.87E-32
2	Skrzypczak colorectal 2	mRNA	Colon carcinoma epithelia vs. normal	-4.523	5.01E-11
		mRNA	Colon adenoma epithelia vs. normal	-3.598	5.64E-09
		mRNA	Colon carcinoma vs. normal	-5.626	1.02E-08
		mRNA	Colon adenoma vs. normal	-6.367	8.55E-07
3	Kaiser colon	mRNA	Colon mucinous adenocarcinoma vs. normal	-10.541	3.22E-08
		mRNA	Cecum adenocarcinoma vs. normal	-5.335	8.25E-08
		mRNA	Colon adenocarcinoma vs. normal	-4.466	5.5E-10
		mRNA	Rectal adenocarcinoma vs. normal	-5.807	0.0000303
		mRNA	Rectosigmoid adenocarcinoma vs. normal	-6.676	0.0000224
4	Gaedeke colorectal	mRNA	Rectal adenocarcinoma vs. normal	-7.798	3.04E-35
5	Skrzypczak colorectal	mRNA	Colorectal adenocarcinoma vs. normal	-2.757	3.71E-14
		mRNA	Colorectal carcinoma vs. normal	-4.481	1.74E-10
6	Sabates-Bellver colon	mRNA	Colon adenoma vs. normal	-2.58	5.24E-13
		mRNA	Rectal adenoma vs. normal	-2.955	0.000167
7	TCGA colorectal	mRNA	Colon mucinous adenocarcinoma vs. normal	-11.699	2.11E-13
		mRNA	Rectal adenocarcinoma vs. normal	-7.875	8.12E-15
		mRNA	Cecum adenocarcinoma vs. normal	-8.857	4.47E-10
		mRNA	Colon adenocarcinoma vs. normal	-6.529	3.42E-13

2.4. Patients and Tissue Specimens. Tumor tissues from 56 CRC cancer patients were collected between May 2020 and February 2021 at Shengzhou People's Hospital and subjected to quantitative reverse transcriptase PCR (qRT-PCR) analysis. Fifteen of these tissues had adjacent normal samples for control. Our experiments were in accordance with the ethical standards formulated in the Helsinki Declaration. This study was authorized by the Ethics Committee of Shengzhou People's Hospital Health Authority.

2.5. Quantitative Real-Time PCR (qRT-PCR). Total RNA was extracted from CRC tissues using TRIzol reagent (ThermoFisher Scientific, USA). Subsequently, the cDNA was amplified by a Reverse Transcriptional Kit (Promega, USA). The real-time PCR was performed using SYBR Premix Ex Taq II (Takara Bio Inc., Otsu, Japan) by an ABI 7500 Fast Real-Time PCR System (ThermoFisher Scientific, USA). GAPDH was employed as the internal reference to control, and the mRNA level was evaluated using a threshold cycle value, for which the formula was $2^{-\Delta\Delta CT}$, where $\Delta CT = (CT(\text{target gene}) - CT(\text{GAPDH}))$. The primers used were as follows: LRRC19: forward: 5'-ATGAAAGTCA-CAGGCATCACAATCC-3' and reverse: 5'-ATTTTCTT-CACATAATTCATGGATA-3'; and GAPDH: forward: 5'-TCGACAGTCAGCCGCATCTTCTTT-3' and reverse: 5'-ACCAAATCCGTTGACTCCGACCTT-3'.

2.6. Immunohistochemistry. Immunohistochemistry was performed as previously described [16]. Anti-LRRC19 antibody was used to detect protein expression in myocardial tissue. The Olympus microscope was used to capture images at 200 magnification, and 3 fields of view of each sample were randomly selected to quantify the relative intensity of protein staining.

2.7. Survival Analysis in CRC via GEPIA and PrognoScan. The PrognoScan database (<https://dna00.bio.kyutech.ac.jp/PrognoScan/index.html>) was utilized to analyze the correlation between LRRC19 expression and survival in various types of cancers [17]. Associations between gene expression and patient prognosis, such as overall survival (OS) and disease-free survival (DFS), were searched on the PrognoScan site. The threshold was defined as a Cox *P* value <0.05. Subsequently, the correlation between LRRC19 expression and overall survival of CRC patients was explored on the GEPIA website (<https://gepia.cancer-pku.cn/>) using COAD-TCGA and READ-TCGA. GEPIA is a Web-based tool to deliver fast and customizable functionalities based on TCGA and GTEx data [18].

2.8. Survival Analysis in Patients with Malignancies through the Kaplan-Meier Plotter. The Kaplan-Meier Plotter (<https://kmplot.com/analysis/>) is an online tool containing the survival information (including OS, RFS, PPS, DMPS, FP, or PFS) of patients with breast cancer, lung cancer, gastric cancer, or ovarian cancer. It can estimate the effect of 54,675 genes on survival using 10,461 cancer samples. We used the Kaplan-Meier plotter to analyze the relationship between LRRC19 expression and survival in breast, ovarian, lung, and gastric cancers [19]. The log-rank *P* value and hazard ratio (HR) with 95% confidence intervals were also calculated.

2.9. GO and KEGG Pathway Enrichment Analysis. The GO (<https://www.geneontology.org>) database can provide functional classification for genomic data, including biological process (BP), cellular component (CC), and molecular function (MF) [20]. It is a widely used annotating tool of genes and gene products. The Kyoto Encyclopedia of Genes and Genomes (KEGG, <https://www.genome.ad.jp/kegg/>)

TABLE 2: Detailed information of the four GEO datasets.

ID	Contributor(s), year	Tumor	Nontumor	Platform
GSE21510	Tsukamoto et al., 2010	104	44	Affymetrix Human Genome U133 Plus 2.0 Array
GSE22598	Okazaki et al., 2010	17	17	Affymetrix Human Genome U133 Plus 2.0 Array
GSE23878	Uddin et al., 2010	35	24	Affymetrix Human Genome U133 Plus 2.0 Array
GSE41328	Lin et al., 2012	10	10	Affymetrix Human Genome U133 Plus 2.0 Array

TABLE 3: All 67 commonly differentially expressed genes (DEGs).

DEGs	Total	Gene name
Upregulated	21	CDH3, MMP7, TRIB3, FOXQ1, MMP3, INHBA, NFE2L3, CEMIP, AZGP1, CLDN2, CXCL8, DPEP1, ASCL2, AJUBA, CLDN1, EPHX4, COL11A1, CTHRC1, MMP1, CRNDE, KRT23
Downregulated	46	LGALS2, NR3C2, SPIB, HSD17B2, ABCG2, ZG16, GUCA2B, CHP2, SCARA5, CLCA4, DHRS11, AKR1B10, ARL14, CA4, NXPE4, SCIN, TSPAN7, CA2, FCGBP, PKIB, ANPEP, CEACAM7, ABCA8, MUC2, BEST2, SLC51B, ADH1B, AQP8, GCG, CD177, MS4A12, PCK1, ADH1C, HEPACAM2, UGT2A3, GCNT2, LRRC19, SCNN1B, C2orf88, LAMA1, BEST4, CA1, SI, GUCA2A, DHRS9, CA7

database is a networked website designed for genic function analysis, annotation, and visualization [21]. In this study, GO enrichment analysis and KEGG pathway analysis were performed using the “enrichplot” package in R software (<https://www.R-project.org/>) to explore the biological functions of LRRC19. A P value <0.05 was considered statistically significant.

2.10. Gene Correlation Analysis of LRRC19. To identify other molecules that might have a relationship with LRRC19, protein-protein interaction analysis (PPI) was performed using the STRING database (<https://string-db.org/>). Then, we used the online database GEPIA for further gene expression correlation analysis, which was performed on The Cancer Genome Atlas (TCGA) expression data. Spearman’s correlation analysis was conducted, the nonlog scale was used for calculation, and the log-scale axis was used for visualization.

2.11. Statistical Analysis. All data were analyzed using the SPSS statistical package (version 17.0; SPSS Inc., Chicago, IL, USA). The associations between LRRC19 expression and clinicopathological characteristics were evaluated by the chi-square tests and Spearman’s correlation analysis. Student’s t -test was performed to compare the expression of LRRC19 between CRC and adjacent normal tissues. Data were analyzed by GraphPad Prism software and presented as mean \pm SD indicated in the figure legends. $P < 0.05$ was considered to denote a statistically significant difference.

3. Results

3.1. DEG Filtering. Four GSE datasets were obtained from the GEO database as follows: GSE21510, GSE22598, GSE23878, and GSE41328 (Table 2). Through analysis conducted using the GEO2R online tool with the cutoff criterion of adjusted $P < 0.05$ and $|\log_2FC| \geq 2$, the results

showed that GSE21510 consisted of 955 DEGs, GSE22598 included 342 DEGs, GSE23878 contained 481 DEGs, and GSE41328 contained 206 DEGs. Finally, the commonly expressed 67 DEGs, including 21 upregulated and 46 downregulated genes, were discovered in the CRC tissues compared with the paracarcinoma tissue by Venn software in the four datasets (Table 3, Figure 1(c), and Figures S1(A) and S1(B)). Of the above genes, we found that LRRC19 was one of the downregulated genes in CRC samples (Figure 1(b)) and its character in CRC was unclear. As a result, LRRC19 was ultimately selected for further study.

3.2. mRNA Expression Levels of LRRC19 in Different Types of Human Cancers. The OncoPrint database analysis proved that LRRC19 mRNA expression in CRC was reduced according to 19 of 23 analyses compared with the normal tissues (Figure 2(a) and Table 1). Additionally, LRRC19 mRNA expression was lower in breast cancer, cervical cancer, kidney cancer, and pancreatic cancer. Meanwhile, higher expression levels were observed in esophageal cancer, leukemia, and lymphoma in some datasets.

To further assess LRRC19 expression in human cancers, we detected LRRC19 expression using the TIMER database (Figure 2(b)). The discriminate expression between the tumor and adjacent normal tissues for LRRC19 across most tumors is shown in Figure 2(b). LRRC19 expression was obviously lower in colon adenocarcinoma (COAD), kidney chromophobe (KICH), kidney renal clear cell carcinoma (KIRC), kidney renal papillary cell carcinoma (KIRP), liver hepatocellular carcinoma (LIHC), lung adenocarcinoma (LUAD), lung squamous cell carcinoma (LUSC), and rectum adenocarcinoma (READ) compared with adjacent normal tissues. Nevertheless, LRRC19 expression was obviously higher in esophageal carcinoma (ESCA), head and neck cancer (HNSC), and stomach adenocarcinoma (STAD) compared with adjacent normal tissues.

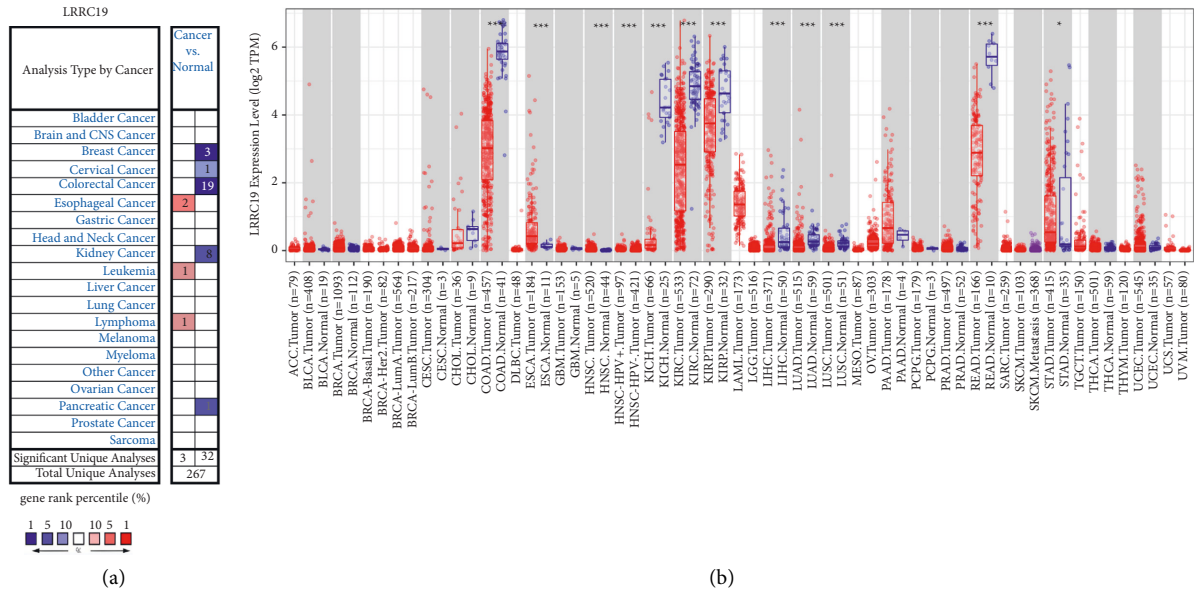


FIGURE 2: LRRC19 expression levels in different types of human cancers. (a) Increased or decreased LRRC19 in datasets of different cancers compared with normal tissues in the Oncomine database. (b) Human LRRC19 expression levels in different tumor types from the TCGA database determined by TIMER (* $P < 0.05$, ** $P < 0.01$, *** $P < 0.001$).

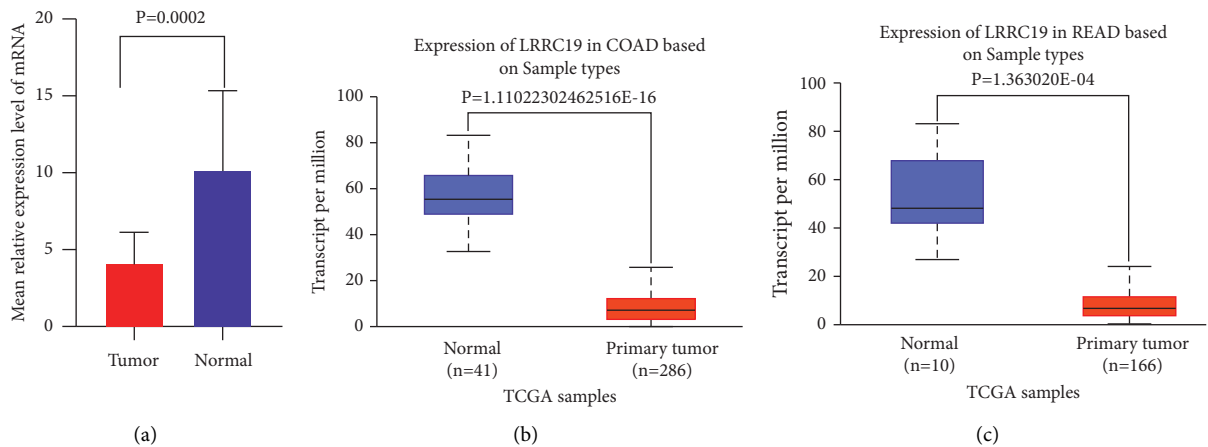


FIGURE 3: LRRC19 expression was decreased in colorectal cancer specimens at mRNA. (a) The average LRRC19 expression \pm SD for all studied tumors and their corresponding normal tissues ($P < 0.001$). Y-axis, the mean relative expression level of LRRC19 expression normalized to normal tissues, GAPDH as an internal control. (b)-(c) The mRNA expression of LRRC19 analyzed using TCGA-COAD and TCGA-READ datasets through UALCAN website.

3.3. Validation of the mRNA Expression Pattern of LRRC19 in CRC Clinical Samples. The aforementioned pancancer analysis of LRRC19 expression showed that it was significantly lower in CRC tissues compared with adjacent normal tissues. To further confirm the distinguishing LRRC19 mRNA expression in patients after radical resection for CRC, we performed qRT-PCR on 15 paired CRC and noncancerous colorectal tissues (Figure S1(C)). The results further confirmed the significantly lower expression of LRRC19 mRNA in CRC, compared with adjacent normal tissues ($P < 0.001$, Figure 3(a)). The result of qRT-PCR was further confirmed through the UALCAN website (Figures 3(b) and 3(c)) (for subtype analysis, Figure S2), which is an interactive Web portal for

analyzing cancer transcriptome data based on the TCGA gene expression data [22].

3.4. Validation of the Immunohistochemistry of LRRC19 in CRC Clinical Samples. Furthermore, we collected tumor samples from patients with colorectal cancer and normal tissues adjacent to the tumor for pathological sections and used immunohistochemistry to evaluate the expression of LRRC19 in colorectal cancer. As a result, as shown in Figure 4, we could establish that LRRC19 expression was also significantly reduced in CRC samples compared with adjacent normal control tissues. This indicated that LRRC19 was also significantly decreased in human CRC tissue at the protein function level.

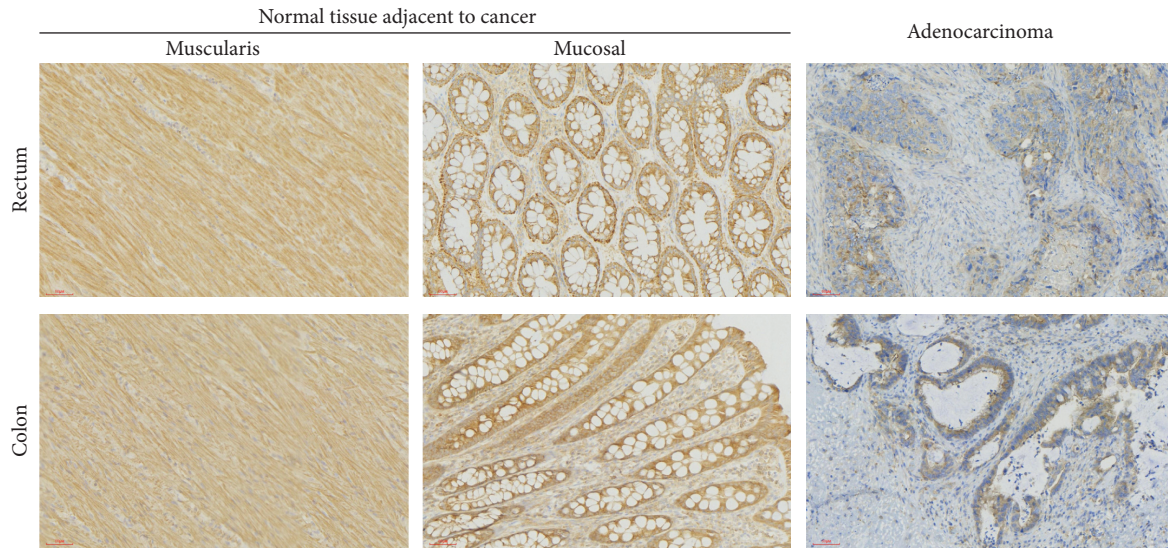


FIGURE 4: LRRC19 expression decreased in colorectal cancer specimens at protein. Expression levels of LRRC19 protein in adenocarcinoma samples from patients with colorectal cancer (rectum, $n = 9$) and colorectal cancer (colon, $n = 9$) and in adjacent normal tissues (muscularis, mucosal) (200x).

TABLE 4: Association between LRRC19 mRNA and clinicopathological factors in CRC patients.

Characteristics	Total ($N = 56$)	LRRC19 mRNA		P value
		Low ($n = 26$)	High ($n = 30$)	
Age				0.589
≤ 65	22	9	13	
> 65	34	17	17	
Gender				0.278
Male	33	13	20	
Female	23	13	10	
Tumor location				0.399
Colon	19	7	12	
Rectum	37	19	18	
Pathology stage				0.104
I	0	0	0	
II	29	9	20	
III	27	15	12	
T stage				0.038
T1	1	0	1	
T2	9	2	7	
T3	31	13	18	
T4	15	11	4	
N stage				0.047
N0	34	12	22	
N1	12	6	6	
N2	10	8	2	
M stage				0.211
M0	54	24	30	
M1	2	2	0	

3.5. *Correlation of LRRC19 Expression with the Clinicopathological Factors of CRC.* The LRRC19 mRNA levels in 56 CRC tissues were further correlated with the clinicopathological characteristics of CRC (Table 4). Based on the average value of LRRC19 mRNA level, there were 30 patients

with high LRRC19 expression and 26 patients with low LRRC19 expression. LRRC19 expression was negatively associated with T stage ($P = 0.038$) and N stage ($P = 0.047$). Meanwhile, no important correlation was discovered between LRRC19 expression and other clinicopathological features, including age ($P = 0.589$), gender ($P = 0.278$), tumor location ($P = 0.399$), pathology stage ($P = 0.104$), and M stage ($P = 0.211$).

3.6. *Association of Lower LRRC19 Expression with the Shorter Survival of CRC Patients.* We used the TCGA database through the GEIPA website to study the correlation between LRRC19 mRNA expression and the survival of patients with CRC (data based on COAD and READ modules). The results showed that low levels of LRRC19 mRNA expression in CRC tissues were significantly correlated with poorer overall survival (OS) ($P < 0.059$) among patients with CRC (Figures 5(a) and 5(b)). Subsequently, LRRC19 expression was assessed by means of the PrognScan website and was remarkably found to significantly affect the prognosis of CRC patients. Two cohorts (GSE17536 and GSE14333) (30, 31) containing 226 specimens at different stages of CRC proved that low LRRC19 expression was markedly related to poorer prognosis (OS HR = 0.84, 95% CI = 0.72 to 0.98, Cox $P = 0.025916$; DFS HR = 0.75, 95% CI = 0.61 to 0.92, Cox $P = 0.005594$; DSS HR = 0.80, 95% CI = 0.68 to 0.95, Cox $P = 0.011420$; DFS HR = 0.78, 95% CI = 0.68 to 0.89, Cox $P = 0.000287$) (Figures 5(c)–5(f)). Thereby, it can be conjectured that low LRRC19 expression is an independent risk factor and indicates poor prognosis in CRC patients. The lower the expression of LRRC19, the worse the shorter survival of CRC patients.

3.7. *Lower LRRC19 Expression Displays Poorer Prognosis of Patients with Malignancies.* To further evaluate the prognostic potential of LRRC19 in different cancers, we used the

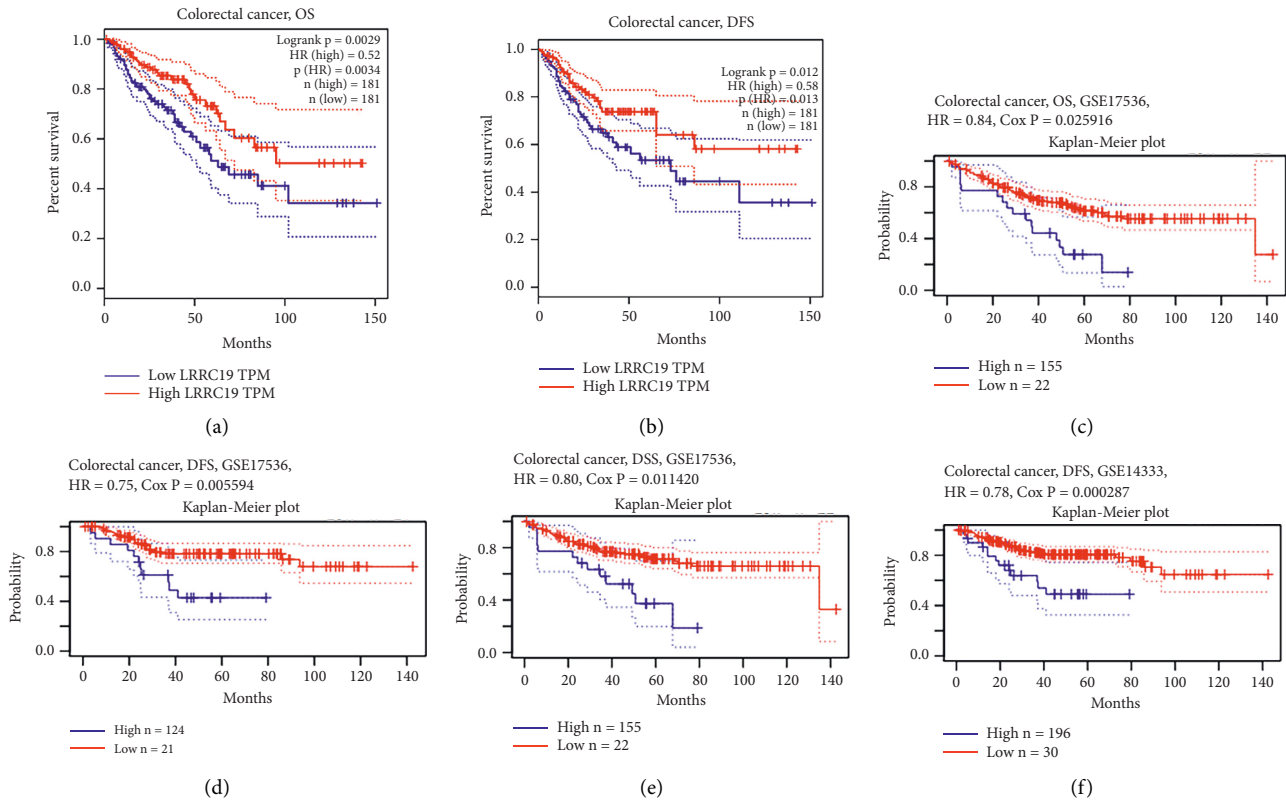


FIGURE 5: Correlation between LRR19 expression and survival of CRC patients. (a)–(b) Survival curves of OS and DFS in the database of TCGA through GEIPA website. (c)–(f) Kaplan–Meier survival curves of OS, DSS, and DFS compared the high and low expressions of LRR19 in two colorectal cancer cohorts (GSE17536 ($n = 177$) and GSE14333 ($n = 226$)) on the Prognoscan website. OS, overall survival; DFS, disease-free survival; DSS, disease-specific survival.

Kaplan–Meier plotter database to evaluate the LRR19 prognostic significance in four types of cancer, including breast cancer, ovarian cancer, lung cancer, and gastric cancer (Figure 6). Interestingly, poor prognosis in ovarian cancer (OS HR = 0.77, 95% CI = 0.68 to 0.88, $P = 0.00013$; PFS HR = 0.75, 95% CI = 0.66 to 0.87, $P = 8.3e - 05$) and gastric cancer (OS HR = 0.72, 95% CI = 0.59 to 0.88, $P = 0.0013$; FP HR = 0.72, 95% CI = 0.57 to 0.9, $P = 0.0036$) was shown to correlate with lower LRR19 expression (Figures 6(a)–6(d)). Meanwhile, low LRR19 expression was correlated with poor prognosis of RFS in BRCA and had less influence on OS (Figures 6(e) and 6(f)). However, low LRR19 expression was correlated with a better prognosis of FP in lung cancer (Figures 6(g) and 6(h)). These results revealed that lower LRR19 was significantly associated with the prognosis of patients with malignancies, including breast cancer, lung cancer, gastric cancer, and ovarian cancer. In addition, increased or decreased LRR19 expression has different prognostic effects according to the cancer type.

3.8. Gene Ontology Function Enrichment Analysis of LRR19 in CRC. To identify the biological significance and function of LRR19, we performed an enrichment analysis for LRR19 (Figure 7). The GO enrichment analysis showed the functional roles of LRR19 in three ways, including biological process (BP), cellular components (CC), and

molecular function (MF). For biological processes, our results revealed that LRR19 was largely involved in antimicrobial humoral response, chloride transmembrane transport, chloride transport, inorganic anion transmembrane transport, and inorganic anion transport in COAD. Meanwhile, in READ, LRR19 mainly took part in immune response-activating cell surface receptor signaling pathway, immune response-activating signal transduction, humoral immune response, complement activation, classical pathway, humoral immune response mediated by circulating immunoglobulin, complement activation, immunoglobulin-mediated immune response, B-cell-mediated immunity, and lymphocyte-mediated immunity. For cellular components, both COAD and READ revealed that downregulated LRR19 was associated with apical part of cell, apical plasma membrane, anchored component of membrane, zymogen granule, NADPH oxidase complex, and zymogen granule membrane. For molecular function, downregulated LRR19 was principally enriched in chloride transmembrane transporter activity, inorganic anion transmembrane transporter activity, protein serine/threonine phosphatase inhibitor activity, superoxide-generating NAD(P)H oxidase activity, and intracellular calcium-activated chloride channel activity in COAD. At the same time, LRR19 was mainly enriched in antigen binding, immunoglobulin receptor binding, chloride transmembrane transporter activity, superoxide-generating NAD(P)H oxidase activity, and

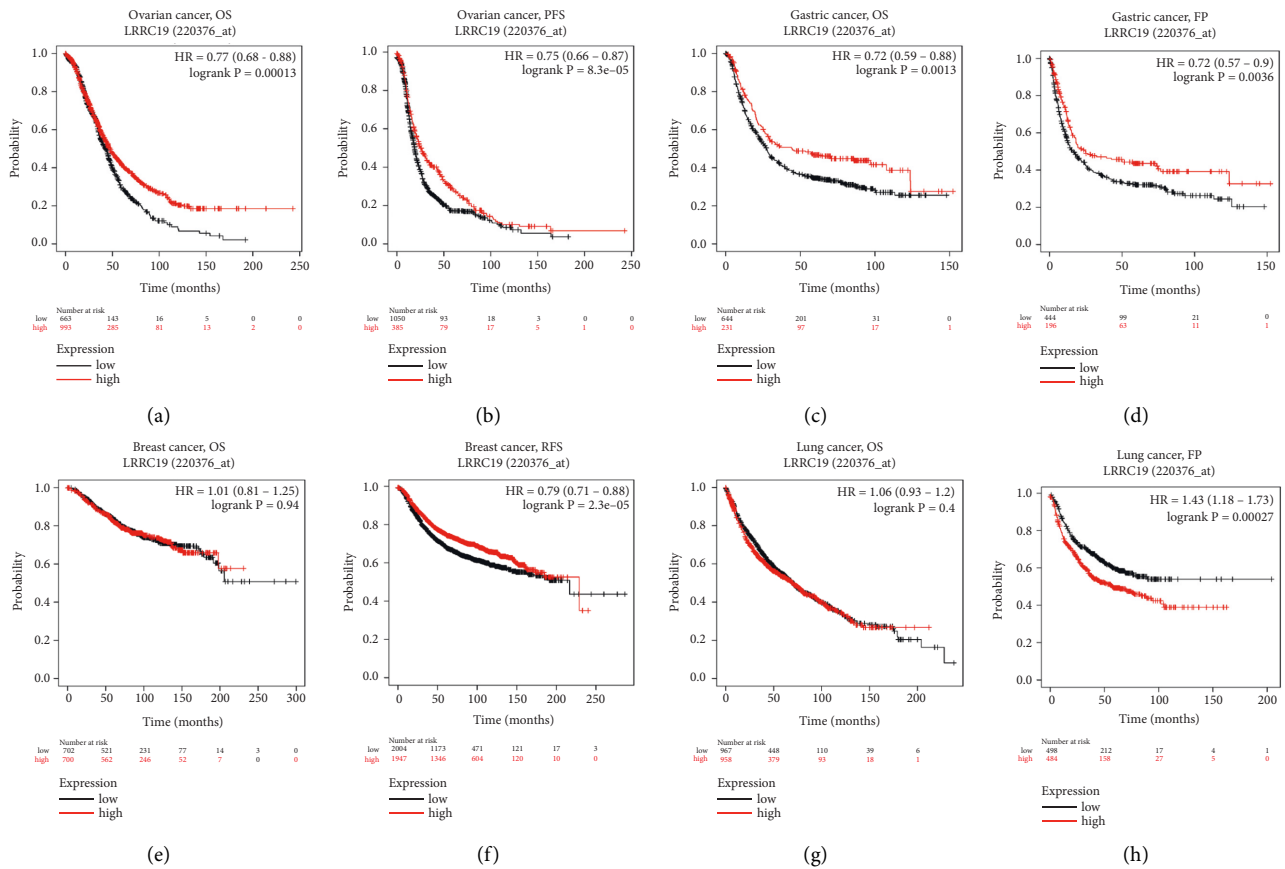


FIGURE 6: Kaplan–Meier survival curves comparing the high and low expressions of LRRC19 in different types of cancer in the Kaplan–Meier plotter databases. (a)-(b) OS and PFS survival curves of ovarian cancer ($n = 1,657$, $n = 1,436$). (c)-(d) OS and FP survival curves of gastric cancer ($n = 881$, $n = 645$). (e)-(f) OS and RFS survival curves of breast cancer ($n = 1,402$, $n = 3,955$). (g)-(h) OS and FP survival curves of lung cancer ($n = 1,927$, $n = 982$). OS, overall survival; PFS, progression-free survival; FP, first progression; RFS, relapse-free survival.

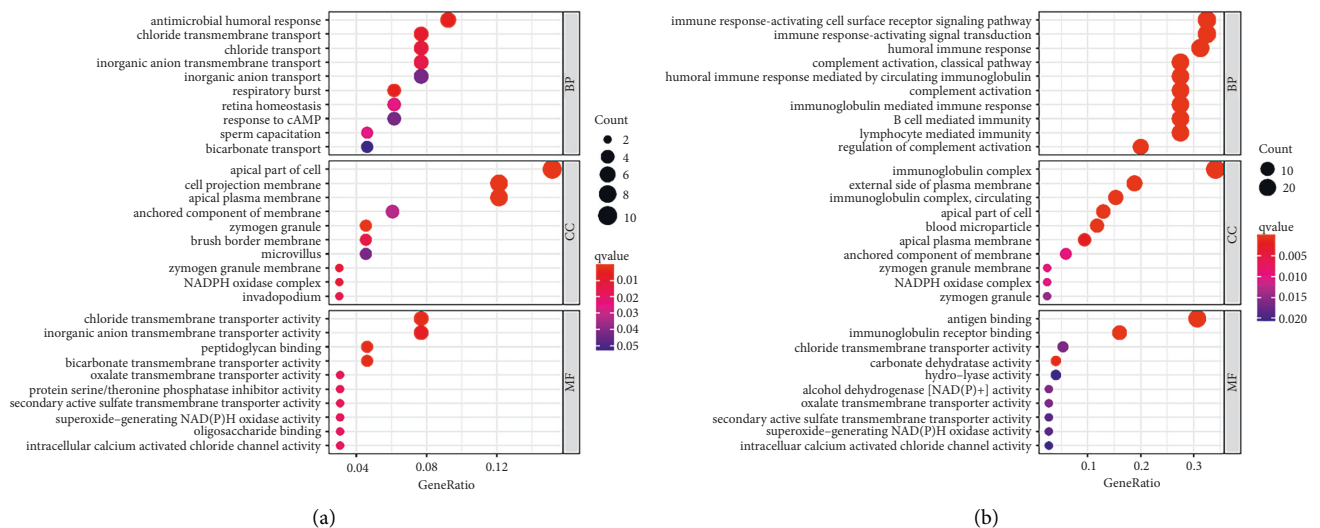


FIGURE 7: Top 10 GO term enrichment analysis of LRRC19 in CRC. (a) LRRC19-related BP, CC, and MF analyses in COAD. (b) LRRC19-related BP, CC, and MF analyses in READ. GO, Gene Ontology; BP, biological process; CC, cellular component; MF, molecular function.

intracellular calcium-activated chloride channel activity in READ (for immune subtype, Figure S3).

3.9. KEGG Pathway Enrichment Analysis of LRRC19 in CRC. The KEGG pathway analysis revealed that LRRC19 was enriched in pancreatic secretion, bile secretion, pentose and glucuronate interconversions, drug metabolism-cytochrome P450, retinol metabolism, metabolism of xenobiotics by cytochrome P450, and chemical carcinogenesis in COAD (Figure 8(a)). In READ, we revealed that LRRC19 was enriched in pancreatic secretion, nitrogen metabolism, retinol metabolism, bile secretion, and proximal tubule bicarbonate reclamation (Figure 8(b)). Remarkably, our data support that LRRC19 plays an important role by regulating the above cancer-related signaling pathways.

3.10. Forecast and Explanation of Associations between LRRC19 and Other Molecular Networks. To determine the other molecules that might have an association with LRRC19, we applied an interaction network prediction using the STRING database (<https://string-db.org>) and further evaluation in the GEPIA database to increase the authenticity of the result (Figure 9). According to the results, a total of 7 candidate proteins (ARMCX3, IMMP2L, MOB3B, TRMT11, TUSC1, ZCCHC10, and TMEM214) might have an interaction with LRRC19 in this study (Figure 9(a)). Afterwards, we sought for the relationship between LRRC19 and 7 molecules in the GEPIA database. We used the non-log scale for calculation and the log-scale axis for visualization. The results indicated that the estimates for both database sites were partially congruent (Figures 9(b)–9(h)). We found that ZCCHC10 and MOB3B were positively correlated with LRRC19 (Pearson's correlation coefficient: $R > 0.3$; Figures 9(b) and 9(d)), whereas IMMP2L and TRMT11 were negatively correlated with LRRC19 (Pearson's correlation coefficient $R < -0.3$; Figures 9(e) and 9(h)), but there is no obvious linear relationship between TUSC1, ARMCX3, and TMEM214 with LRRC19 based on the current data ($-0.3 \leq R \leq 0.3$; Figures 9(c), 9(f), and 9(g)).

4. Discussion

During the past several decades, dietary, lifestyle, inflammatory infection, medication risk factors, and genetics have been confirmed to be involved in the generation and progression of CRC; however, the detailed molecular mechanism remains unclear [23]. Even though important advancements have been made in terms of looking into the underlying mechanisms associated with the diagnosis, treatment, and prognosis estimation of CRC, more optimal and new CRC biomarkers are yet in urgent need. Thus, in our study, we utilized bioinformatic tools to analyze four GEO datasets to screen more effective proto-oncogenes or tumor suppressors. We picked out LRRC19 as a potential tumor suppressor gene for its significant downregulation of mRNA levels in CRC tissues, as well as its largely unknown status in most of the tumors including CRC. More importantly, compared with previous studies, we further

screened potential hub genes [24] that play important biological functions in CRC by adding an important dataset (GSE21510, which has the most CRC samples).

LRRC19, a functional transmembrane receptor, belongs to the mammalian protein subgroup of singleton LRR-only group within the LRR family [25, 26]. Except for LRRC19, the mammalian protein subgroup also contains 14 kinds of leucine-rich repeat (LRR) proteins, such as LRRC17, LRRC25, and Lrg1. In postmenopausal women, the low plasma level of LRRC17 was considered as an independent risk factor for osteoporotic fractures [27]. In addition, in ovarian cancer, LRRC17 also acts as a prognostic gene as it regulates cancer cell viability via the p53 pathway [28]. Hoffman et al. proposed that LRRC25 might increase the risk of breast cancer, given that elevated LRRC25 leads to an enhanced inflammatory response [29]. Zhang and colleagues found that overexpressed LRG1 could induce the EMT process and angiogenesis in colorectal cancer [30]. However, only few studies have been conducted on the LRRC19 in human tumors. This study showed that the LRRC19 protein appears to be specifically expressed in the kidney, spleen, and intestine [31]. Liu et al. reported that the reduced expression of LRRC19 was an independent risk factor for OS and LRRC19 could serve as a novel biomarker for prognosis and adjuvant treatment of selenium [32]. Chai et al. proposed that LRRC19 can activate NF- κ B and induce the expression of pro-inflammatory cytokines and is involved in the response to local inflammation [31]. Cao et al. reported that LRRC19 is associated with enteritis, colitis, and colitis-associated tumorigenesis in *Lrrc19* KO mice [33]. LRRC19 was also mentioned for its therapeutic potential in pressure ulcers, by promoting NF- κ B-dependent pro-inflammatory response [34]. The latest research demonstrated that LRRC19 can increase the permeability of the gut epithelial barrier by degrading PKC to reduce the expression of ZO-1, ZO-3, and occludin [35].

In our study, we first evaluated LRRC19 mRNA expression in human CRC using data from the TIMER and OncoPrint online tools. The results displayed that LRRC19 mRNA expression was dramatically reduced in CRC tissues compared with adjacent normal tissues, which was further verified by the qPCR result for paired clinical samples. The above results of LRRC19 differential expression were immediately confirmed by the UALCAN website. These findings revealed that the expression of LRRC19 mRNA was significantly decreased in CRC tissues, which might be necessary for the occurrence and progression of CRC. Subsequently, we also investigated the association between LRRC19 mRNA with the clinicopathological characteristics in CRC patients. LRRC19 expression was negatively related to *T* stage ($P = 0.038$) and *N* stage ($P = 0.047$) and showed no significant difference in age, gender, tumor location, pathology stage, and *M* stage between the two groups. In addition, we adopted the GEPIA and Prognoscan websites to assess the prognostic value of LRRC19 expression. Our research revealed that reduced LRRC19 expression was markedly associated with shorter OS, DFS, or DSS in CRC patients. These data remind us that downregulated LRRC19 might be a general event in CRC and a beneficial biomarker

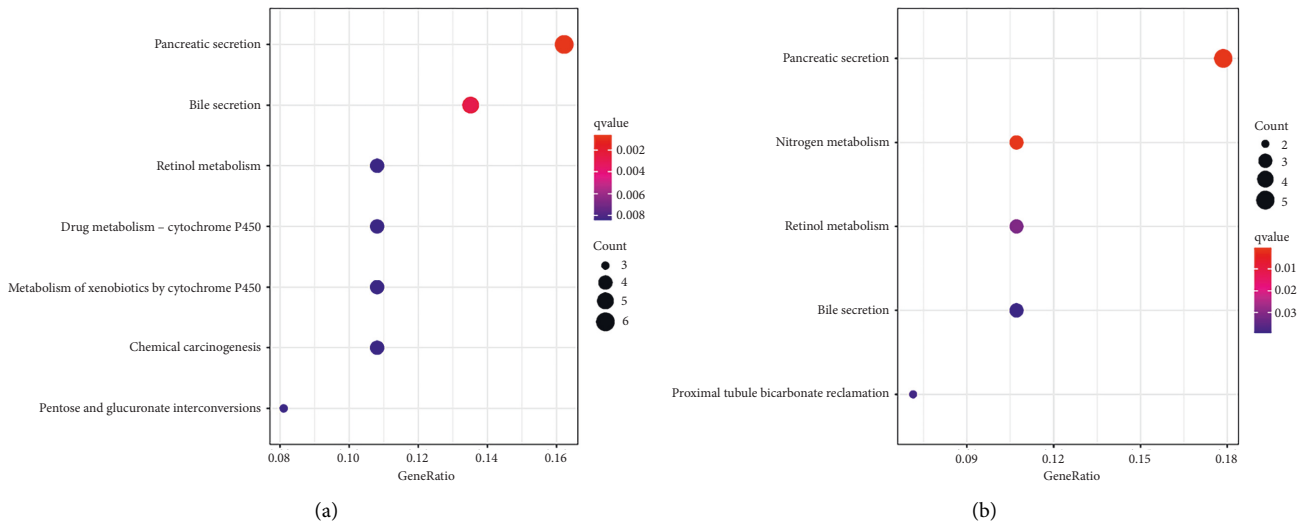


FIGURE 8: KEGG pathway enrichment analysis of LRRC19 in CRC. (a) LRRC19-related pathways in COAD. (b) LRRC19-related pathways in READ. KEGG, Kyoto Encyclopedia of Genes and Genomes.

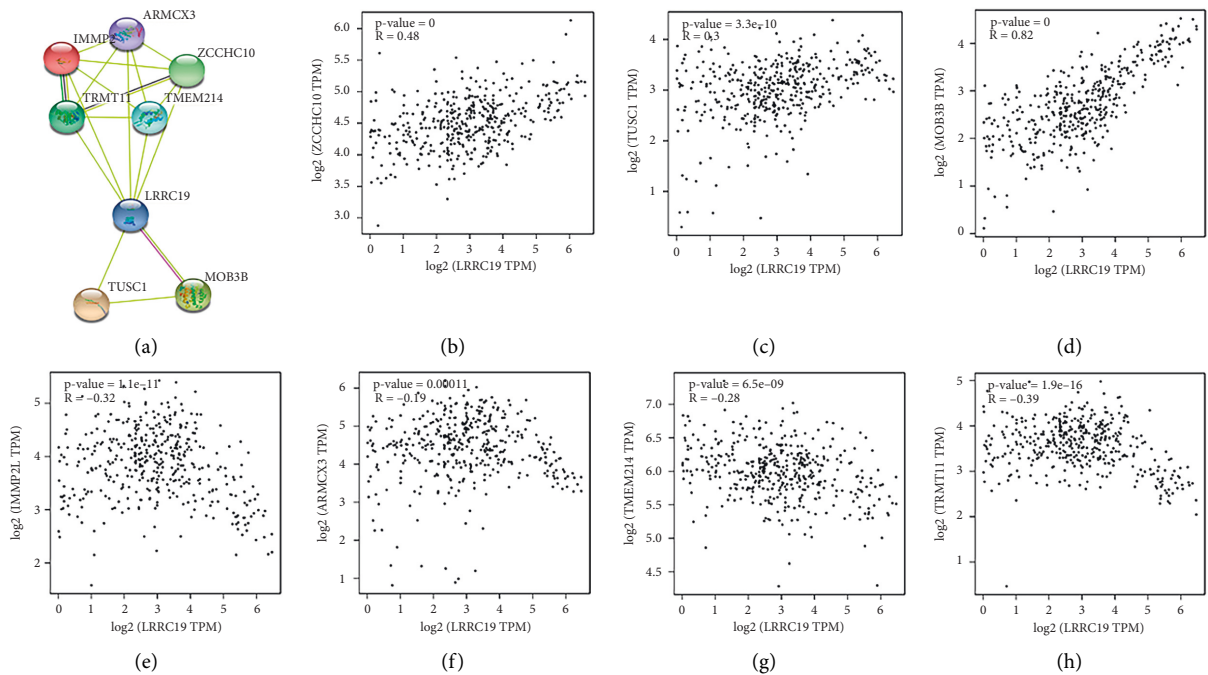


FIGURE 9: Network prediction and annotation of LRRC19 with other molecules. (a) Seven candidate molecules might have an interaction with LRRC19. (b)–(h) The GEPIA database showed that the above candidate molecules might be associated with LRRC19. (b)–(d) Positive relation ($R > 0$). (e)–(h) Negative relation ($R < 0$).

for the prognosis of CRC patients. Further survival analysis in four human common cancers (including breast cancer, lung cancer, gastric cancer, and ovarian cancer) inferred that lower LRRC19 expression significantly correlates with poorer progression (including OS, RFS, PPS, DMPs, FP, or PFS) in patients, suggesting the potential value of lower LRRC19 expression on prognostic prediction.

To further clarify the biological functions of LRRC19 in CRC, GO and KEGG pathway analyses were carried out (Figures 7 and 8). Overall, our analysis suggested that low

expression of LRRC19 could be mainly involved in the transmembrane transport, immune response, NADPH oxidase complex, zymogen granule membrane, and retinol metabolism, leading to the tumorigenesis and progression of CRC. Among the identified pathways, retinol metabolism pathway took part in CRC occurrence, and the incidence of CRC was associated with lower serum levels of retinol [36]. Of the screened biological processes, the immune response has also been found to be implicated in colorectal cancer [37, 38], which offers us a new research direction of

anticancer therapeutic approach via immune checkpoint inhibition. Chai et al. also verified that LRRC19 can be involved in the response to local inflammation [31]. For cellular components, NADPH oxidase and zymogen granule have long been recognized as essential factors in colorectal carcinogenesis and development. For instance, upregulated NOX4 predicts poor prognosis and facilitates tumor progression in CRC [39]. Meng et al. proved that zymogen granule protein 16 (ZG16) regulates PD-L1 expression and immune response in CRC [40]. Furthermore, LRRC19 is involved in a number of molecular functions related to tumor progression, such as protein serine/threonine phosphatase inhibitor activity and superoxide-generating NAD(P)H oxidase activity. The above study indicates that LRRC19 participates in many biological processes involving tumorigenesis and progression.

However, through GO and KEGG enrichment analyses, we also found some interesting points. It can be seen that in terms of BP and MF in the GO enrichment analysis, in COAD, the function of LRRC19 is more closely related to some ion transport; in READ, the relationship between LRRC19 and immune activation is stronger. However, in the CC plate, the functions performed by LRRC19 are relatively close. We speculate that, at the functional level, LRRC19 has different biases in COAD and READ, which may be related to their specific locations, but LRRC19, as a functional transmembrane receptor, naturally has greater similarities in cellular components. However, when several types of molecules with different functional tendencies are enriched in the KEGG pathway, it can be seen that their main functions are similar in COAD and READ, which is also in line with the characteristics of LRRC19 transmembrane transporter, which is related to the secretion of various substances, metabolic hooks.

Finally, to discern the other molecules that might interact with LRRC19, we carried out a network prediction of LRRC19 with other molecules in the STRING database along with further validation on the GEPIA website. We found that LRRC19 might interact with ZCCHC10, MOB3B, IMMP2L, and TRMT11. Some of these known or predicted interacted genes had been reported to be oncogenes or tumor suppressor genes. For example, for zinc finger CCHC-type-containing 10 (ZCCHC10), acting as a direct target of miR-410-3p in CRC, miR-410-3p-mediated ZCCHC10 suppression can facilitate the EMT process, cell migration, and invasion of CRC cells by means of regulating NF- κ B activation [41]. ZCCHC10 can also inhibit lung cancer progression and cisplatin resistance through reducing MDM2-mediated p53 ubiquitination and degradation [42]. These shreds of evidence underline that ZCCHC10 plays its role as a tumor suppressor gene in CRC and lung cancer.

Meanwhile, ZCCHC10, which may have a positive linear relationship with LRRC19, can reduce the ubiquitination and degradation of p53 and inhibit EMT and cell migration. MASPIN, which is also closely related to p53 in CRC, can also inhibit tumor proliferation and has antiangiogenic and proapoptotic properties. Coincidentally, MASPIN is a useful tool for identifying tumor buds and, through examining the subcellular localization of its staining, for evaluating EMT in

CRC. Cytoplasmic MASPIN positivity is associated with the best prognosis, but nuclear MASPIN positivity is associated with the shortest survival time and high invasion [43, 44]. Therefore, we speculate that there may be a connection between LRRC19 and MASPIN, and this connection may make LRRC19 assist MASPIN in the molecular classification of CRC. However, the biological function and detailed molecular mechanism of LRRC19 in CRC should be further handled in future studies.

All in all, our research has certain novel and exciting findings, which may help other researchers in the field or scholars interested in this direction. For example, the low expression of LRRC19 may be mainly involved in biological processes such as transmembrane transport and immune response, which can provide the possibility of in-depth research for the majority of scholars. Second, we screened several molecular markers that may be directly related to LRRC19 by combining STRING and GEPIA databases, which also provide a bridge for further exploration of the detailed molecular mechanism of LRRC19.

5. Conclusion

Overall, this study is the first to demonstrate that LRRC19 prominently decreases in human CRC. Moreover, reduced LRRC19 expression was significantly associated with shorter survival in CRC patients. The results of the functional enrichment pathway and PPI analyses suggest that LRRC19 might be a tumor suppressor gene. Additional research will be needed to seek the detailed mechanisms of LRRC19 function and its possible clinical value in CRC.

Data Availability

The data used to support this study are mainly based on public databases and are available after the remaining part of the experimental data is verified.

Ethical Approval

This study was approved by the Ethics Committee of Shengzhou People's Hospital Health Authority.

Consent

Written informed consent was obtained from all participants included in the study.

Conflicts of Interest

The authors declare that they have no conflicts of interest.

Authors' Contributions

Yong-Wei Yu guided the idea of the manuscript; Ya-Juan Wang completed database processing, data export, and manuscript writing; Man Liu completed paraffin embedding, immunostaining, and photography of CRC samples; and Hui-Ying Jiang was responsible for the final compilation of pictures and tables.

Supplementary Materials

Figure S1: (A) Venn diagram reveals all 67 DEGs in the four datasets ($|\log_2FC| \geq 2$). (B) 21 DEGs upregulated in the four datasets ($\log_2FC \geq 2$). (C) LRR19 mRNA expression in 15 pairs of CRC tissues and noncancerous colorectal tissues measured by qPCR analysis. Figure S2: mRNA expression of LRR19 analyzed using TCGA-COAD and TCGA-READ datasets through UALCAN website and a full TCGA subtype analysis. Figure S3: correlation between LRR19 gene expression and TILs in COAD and READ and MESO by the TIMER database. (*Supplementary Materials*)

References

- [1] Q. Qin, L. Yang, Y. K. Sun et al., "Comparison of 627 patients with right- and left-sided colon cancer in China: differences in clinicopathology, recurrence, and survival," *Chronic Diseases and Translational Medicine*, vol. 3, no. 1, pp. 51–59, 2017.
- [2] L. A. Torre, F. Bray, R. L. Siegel, J. Ferlay, J. L. Tieulent, and A. Jemal, "Global cancer statistics, 2012," *CA: A Cancer Journal for Clinicians*, vol. 65, no. 2, pp. 87–108, 2012.
- [3] X.-N. Chang, F.-M. Shang, H.-Y. Jiang et al., "Clinicopathological features and prognostic value of kras/nras/braf mutations in colorectal cancer patients of central China," *Current Medical Science*, vol. 41, no. 1, pp. 118–126, 2021.
- [4] A. Bourhis, C. De Luca, M. Cariou et al., "Evaluation of kras, nras and braf mutational status and microsatellite instability in early colorectal carcinomas invading the submucosa (pt1): towards an in-house molecular prognostication for pathologists?" *Journal of Clinical Pathology*, vol. 73, no. 11, pp. 741–747, 2020.
- [5] A. K. Siraj, S. K. Parvathareddy, P. Annaiyappanaidu et al., "Pd-11 expression is associated with deficient mismatch repair and poor prognosis in middle eastern colorectal cancers," *Journal of Personalized Medicine*, vol. 11, no. 2, p. 73, 2021.
- [6] R. Petryszak, T. Burdett, B. Fiorelli et al., "Expression Atlas update—a database of gene and transcript expression from microarray- and sequencing-based functional genomics experiments," *Nucleic Acids Research*, vol. 42, no. D1, pp. D926–D932, 2014.
- [7] T. Barrett, S. E. Wilhite, P. Ledoux et al., "NCBI GEO: archive for functional genomics data sets—update," *Nucleic Acids Research*, vol. 41, no. D1, pp. D991–D995, 2013.
- [8] S. Tsukamoto, T. Ishikawa, S. Iida et al., "Clinical significance of osteoprotegerin expression in human colorectal cancer," *Clinical Cancer Research*, vol. 17, no. 8, pp. 2444–2450, 2011.
- [9] S. Okazaki, T. Ishikawa, S. Iida et al., "Clinical significance of unc5b expression in colorectal cancer," *International Journal of Oncology*, vol. 40, pp. 209–216, 2012.
- [10] S. Uddin, M. Ahmed, A. Hussain et al., "Genome-wide expression analysis of middle eastern colorectal cancer reveals foxm1 as a novel target for cancer therapy," *American Journal Of Pathology*, vol. 178, no. 2, pp. 537–547, 2011.
- [11] G. Lin, X. He, H. Ji, L. Shi, R. W. Davis, and S. Zhong, "Reproducibility probability score-incorporating measurement variability across laboratories for gene selection," *Nature Biotechnology*, vol. 24, no. 12, pp. 1476–1477, 2006.
- [12] R. Edgar, M. Domrachev, and A. E. Lash, "Gene expression omnibus: ncbi gene expression and hybridization array data repository," *Nucleic Acids Research*, vol. 30, no. 1, pp. 207–210, 2002.
- [13] R. Søkilde, B. Kaczkowski, A. Podolska et al., "Global microRNA analysis of the nci-60 cancer cell panel," *Molecular Cancer Therapeutics*, vol. 10, no. 3, pp. 375–384, 2011.
- [14] D. R. Rhodes, S. K. Sundaram, V. Mahavisno et al., "OncoPrint 3.0: genes, pathways, and networks in a collection of 18,000 cancer gene expression profiles," *Neoplasia*, vol. 9, no. 2, pp. 166–180, 2007.
- [15] T. Li, J. Fu, Z. Zeng et al., "TIMER2.0 for analysis of tumor-infiltrating immune cells," *Nucleic Acids Research*, vol. 48, no. W1, pp. W509–W514, 2020.
- [16] K.-Y. Huang, Y.-W. Yu, S. Liu et al., "A single, acute astragaloside iv therapy protects cardiomyocyte through attenuating superoxide anion-mediated accumulation of autophagosomes in myocardial ischemia-reperfusion injury," *Frontiers in Pharmacology*, vol. 12, Article ID 642925, 2021.
- [17] H. Mizuno, K. Kitada, K. Nakai, and A. Sarai, "Prognoscan: a new database for meta-analysis of the prognostic value of genes," *BMC Medical Genomics*, vol. 2, no. 1, p. 18, 2009.
- [18] Z. Tang, C. Li, B. Kang, G. Gao, C. Li, and Z. Zhang, "Gepia: a web server for cancer and normal gene expression profiling and interactive analyses," *Nucleic Acids Research*, vol. 45, no. W1, pp. W98–W102, 2017.
- [19] B. Györfy, A. Lanczky, A. C. Eklund et al., "An online survival analysis tool to rapidly assess the effect of 22,277 genes on breast cancer prognosis using microarray data of 1,809 patients," *Breast Cancer Research and Treatment*, vol. 123, no. 3, pp. 725–731, 2010.
- [20] L. Cheng, H. Lin, Y. Hu, J. Wang, and Z. Yang, "Gene function prediction based on the gene ontology hierarchical structure," *PLoS One*, vol. 9, no. 9, Article ID e107187, 2014.
- [21] M. Tanabe and M. Kanehisa, "Using the Kegg database resource," *Current Protocols in Bioinformatics*, 2012.
- [22] D. S. Chandrashekar, B. Bashel, S. A. H. Balasubramanya et al., "Ualcan: a portal for facilitating tumor subgroup gene expression and survival analyses," *Neoplasia*, vol. 19, no. 8, pp. 649–658, 2017.
- [23] A. T. Chan, S. Ogino, E. L. Giovannucci, and C. S. Fuchs, "Inflammatory markers are associated with risk of colorectal cancer and chemopreventive response to anti-inflammatory drugs," *Gastroenterology*, vol. 140, no. 3, pp. 799–808, 2011.
- [24] H. Yang, Y. Lu, W. Lan, B. Huang, and J. Lin, "Down-regulated solute carrier family 4 member 4 predicts poor progression in colorectal cancer," *Journal of Cancer*, vol. 11, no. 12, pp. 3675–3684, 2020.
- [25] A. P. West, A. A. Koblansky, and S. Ghosh, "Recognition and signaling by toll-like receptors," *Annual Review of Cell and Developmental Biology*, vol. 22, no. 1, pp. 409–437, 2006.
- [26] J. Dolan, K. Walshe, S. Alsbury et al., "The extracellular leucine-rich repeat superfamily; a comparative survey and analysis of evolutionary relationships and expression patterns," *BMC Genomics*, vol. 8, no. 1, p. 320, 2007.
- [27] N. Hong, B.-J. Kim, C. H. Kim et al., "Low plasma level of leucine-rich repeat-containing 17 (lrrc17) is an independent and additive risk factor for osteoporotic fractures in postmenopausal women," *Journal of Bone and Mineral Research*, vol. 31, no. 12, pp. 2106–2114, 2016.
- [28] C.-K. Oh, J. J. Park, M. Ha et al., "Lrrc17 is linked to prognosis of ovarian cancer through a p53-dependent anti-apoptotic function," *Anticancer Research*, vol. 40, no. 10, pp. 5601–5609, 2020.
- [29] J. D. Hoffman, R. E. Graff, N. C. Emami et al., "Cis-eqtl-based trans-ethnic meta-analysis reveals novel genes associated with breast cancer risk," *PLoS Genetics*, vol. 13, no. 3, Article ID e1006690, 2017.

- [30] J. Zhang, L. Zhu, J. Fang, Z. Ge, and X. Li, "LRG1 modulates epithelial-mesenchymal transition and angiogenesis in colorectal cancer via HIF-1 α activation," *Journal of Experimental & Clinical Cancer Research*, vol. 35, no. 1, p. 29, 2016.
- [31] L. Chai, L. Dai, Y. Che et al., "LRRC19, a novel member of the leucine-rich repeat protein family, activates NF- κ B and induces expression of proinflammatory cytokines," *Biochemical and Biophysical Research Communications*, vol. 388, no. 3, pp. 543–548, 2009.
- [32] Y. Zhang, J. Wang, and X. Liu, "Lrrc19-a bridge between selenium adjuvant therapy and renal clear cell carcinoma: a study based on datamining," *Genes*, vol. 11, no. 4, p. 440, 2020.
- [33] S. Cao, X. Su, B. Zeng et al., "The gut epithelial receptor lrrc19 promotes the recruitment of immune cells and gut inflammation," *Cell Reports*, vol. 14, no. 4, pp. 695–707, 2016.
- [34] J. Sun, Z. Wang, and X. Wang, "Suppression of lrrc19 promotes cutaneous wound healing in pressure ulcers in mice," *Organogenesis*, vol. 14, no. 1, pp. 13–24, 2018.
- [35] X. Su, J. Wei, H. Qi et al., "LRRC19 promotes permeability of the gut epithelial barrier through degrading PKC- ζ and PKC/ λ to reduce expression of ZO1, ZO3, and occludin," *Inflammatory Bowel Diseases*, vol. 27, no. 8, pp. 1302–1315, 2021.
- [36] H. Luo, Y.-J. Fang, M.-S. Lu et al., "Dietary and serum vitamins a and e and colorectal cancer risk in Chinese population: a case-control study," *European Journal of Cancer Prevention*, vol. 28, no. 4, pp. 268–277, 2019.
- [37] S. Sakimura, S. Nagayama, M. Fukunaga et al., "Impaired tumor immune response in metastatic tumors is a selective pressure for neutral evolution in crc cases," *PLoS Genetics*, vol. 17, no. 1, Article ID e1009113, 2021.
- [38] S. M. Toor, V. S. Nair, K. Murshed, M. A. Nada, and E. Elkord, "Tumor-infiltrating lymphoid cells in colorectal cancer patients with varying disease stages and microsatellite instability-high/stable tumors," *Vaccines*, vol. 9, no. 1, p. 64, 2021.
- [39] X.-L. Lin, L. Yang, S.-W. Fu et al., "Overexpression of nox4 predicts poor prognosis and promotes tumor progression in human colorectal cancer," *Oncotarget*, vol. 8, no. 20, Article ID 33600, 2017.
- [40] H. Meng, Y. Ding, E. Liu, W. Li, and L. Wang, "Zg16 regulates pd-1l expression and promotes local immunity in colon cancer," *Translational oncology*, vol. 14, no. 2, Article ID 101003, 2021.
- [41] Z.-H. Ma, P.-D. Shi, and B.-S. Wan, "MiR-410-3p activates the NF- κ B pathway by targeting ZCCHC10 to promote migration, invasion and EMT of colorectal cancer," *Cytokine*, vol. 140, Article ID 155433, 2021.
- [42] Y. Ning, N. Hui, B. Qing et al., "Zcchc10 suppresses lung cancer progression and cisplatin resistance by attenuating mdm2-mediated p53 ubiquitination and degradation," *Cell Death & Disease*, vol. 10, no. 6, p. 414, 2019.
- [43] L. Baniias, I. Jung, T. Bara et al., "Immunohistochemical-based molecular subtyping of colorectal carcinoma using maspin and markers of epithelial-mesenchymal transition," *Oncology Letters*, vol. 19, pp. 1487–1495, 2020.
- [44] S. Gurzu, Z. Szentirmay, and I. Jung, "Molecular classification of colorectal cancer: a dream that can become a reality," *Romanian journal of morphology and embryology*, vol. 54, pp. 241–245, 2013.

Research Article

Prognostic Utility of Platelet-to-Albumin Ratio among Critically Ill Patients with Colorectal Cancer: A Propensity Score Matching Study

Anshu Li ¹, Zhiyong Wang ¹, Qing Lv ¹, and Yan Ling ²

¹Department of Gastrointestinal Surgery, Union Hospital, Tongji Medical College, Huazhong University of Science and Technology, 430022 Wuhan, China

²Health Management Center, Union Hospital, Tongji Medical College, Huazhong University of Science and Technology, 430022 Wuhan, China

Correspondence should be addressed to Qing Lv; lvq11111@aliyun.com and Yan Ling; 2011xh0836@hust.edu.cn

Anshu Li and Zhiyong Wang contributed equally to this work.

Received 4 April 2022; Revised 4 May 2022; Accepted 7 May 2022; Published 26 May 2022

Academic Editor: Simona Gurzu

Copyright © 2022 Anshu Li et al. This is an open access article distributed under the Creative Commons Attribution License, which permits unrestricted use, distribution, and reproduction in any medium, provided the original work is properly cited.

The platelet-to-albumin ratio (PAR) was developed to evaluate inflammatory and nutritional status among patients. The primary goal of the current study was to gain insight into the prognostic role of PAR in critically ill patients with colorectal cancer (CRC). The secondary aim was to develop and verify a clinical model including PAR for the prediction of 28-day mortality. This observational, multicenter study used data from the Medical Information Mart for Intensive Care (MIMIC) IV, e-ICU databases, and Union cohort. Data from 776 critically ill patients with CRC were from the e-ICU database, 219 from the MIMIC-IV database, and 135 from the Wuhan Union Hospital. Propensity score matching (PSM) analysis, along with inverse probability treatment weighting, was used to control the influence of confounding factors. Support vector machine (SVM) and LASSO Cox models were then applied to identify significant metrics associated with 28-day mortality in the test cohort. Receiver operating curve (ROC) analysis, along with sensitivity and specificity, was measured to assess the predictive performances of PAR and the survival nomogram. The threshold value for PAR was 8.6, and patients with high PAR (≥ 8.6) experienced higher 28-day mortality compared to those with low PAR (< 8.6). ROC curve analyses revealed that the discriminative ability of PAR was better than platelet count and albumin alone. LASSO Cox regression along with SVM identified six significant metrics associated with 28-day mortality in critically ill patients with CRC, including PAR. The C-index of the critically ill CRC nomogram was 0.802 (0.744–0.859) in the e-ICU training cohort, 0.839 (0.779–0.899) in the e-ICU validation cohort, 0.787 (0.695–0.879) in the MIMIC-IV cohort, and 0.767 (0.703–0.831) in the Union cohort. PAR is a simple score that combines inflammatory and nutritional status. PAR was a reliable index to predict short-term survival outcome of critically ill patients with CRC. Moreover, a clinical nomogram incorporating PAR exhibited satisfactory performance for predicting 28-day mortality of critically ill patients with CRC.

1. Introduction

Colorectal cancer (CRC) is reported to be the third most common cancer in terms of incidence and the second leading cause of cancer-related death globally [1]. Despite major advances in CRC healthcare, the worldwide incidence and mortality rates of CRC continue to increase, with >2.2 million newly diagnosed cases and 1.1 million deaths

projected by 2030 [2]. Major progress has been achieved in the treatment of CRC in past decades, especially in the field of molecular targeted therapy and immunotherapy. Nevertheless, a vast number of CRC patients with advanced stage disease do not benefit from these therapies, and their long-term survival outcomes remain unsatisfactory [3].

Most recent research has focused on biomarkers for the early diagnosis of CRC and the assessment of long-term

survival outcomes of individuals with CRC. However, few studies have specifically devoted attention to critically ill patients with CRC. Advances in anticancer treatment and survival evaluation are closely linked to the increased number of patients with CRC requiring intensive care [4]. CRC patients in advanced stages of disease are especially vulnerable to complications with severe infection, acute respiratory failure, cardiovascular events, and neurological disorders; thus these individuals commonly require intensive care [5]. Recently, mortality rates of CRC patients have decreased with the wide application of advanced organ support techniques. Because early organ support is related to improved survival for critically ill CRC patients, identification of novel biomarkers with adequate predictive accuracy is crucial for accurate risk stratification to avoid delayed organ support for individuals with CRC at high risk for death.

Inflammation and malnutrition are the important factors responsible for disease progression among patients with CRC [6]. The inflammatory response drives the progression of malnutrition, and continued malnutrition status may, in turn, induce severe and systemic inflammatory responses, which results in a vicious cycle [7]. In recent years, many oncologists have preferred to focus on clinical metrics combining malnutrition and inflammation. Sugimachi et al [8] investigated the significance of the immunonutritional index in evaluating the risk associated with the elderly patients undergoing pancreatectomy and found that immunonutritional status was remarkably impaired. Hayama et al [9] developed a nutrition inflammation status model based on cholesterol, serum albumin, neutrophil count, C-reactive protein (CRP), and platelet count for the prediction of overall survival among individuals with CRC. Liu et al. [10] also created a survival nomogram based on several immunonutritional indexes, and this immunonutritional model demonstrated good accuracy for the prediction of survival outcomes among CRC patients. Matsubara et al. [11] identified CRP-to-albumin ratio as the most significant prognostic biomarker among immunonutritional indexes among patients with non-small cell lung cancer. However, these studies were all based on well-established indexes, and no additional novel biomarkers were explored.

Platelet-to-albumin ratio (PAR), a combined indicator of nutritional and inflammatory status, has been indicated as a potent survival biomarker in peritoneal dialysis and various cancer. We hypothesized that PAR is correlated with the short-term mortality of critically ill patients with CRC. Therefore, we performed this clinical study to determine whether PAR could be a prognostic metric for critically ill patients with CRC in intensive care unit (ICU) through a propensity score matching (PSM) analysis. Then, we will design and validate a clinical model consisting of PAR for the prediction of short-term mortality of critically ill patients with CRC.

2. Materials and Methods

2.1. Study Design. This is a retrospective and observational study based on data from two large critical databases (e-ICU and MIMIC-IV). The two databases mainly contain

participants who are critically ill, but also contain individuals with cancer. E-ICU database was mined to design and internally verify the prognostic significance of PAR and survival nomogram, and MIMIC-IV database was searched to externally validate the significance of PAR and survival nomogram. Finally, we also collected the clinical data of 135 CRC patients who were admitted to ICU from Wuhan Union Hospital. Our study design was strictly in line with the Declaration of Helsinki, and our research plan was approved by the clinical ethics committee of Wuhan Union Hospital.

2.2. Data Collection. Data from critically ill patients with CRC were collected from two critical care databases; however, potentially eligible participants were excluded for the following reasons: complicated with other malignant tumors; lost or absent critical clinical information, such as platelet count, albumin, or survival data; and age <18 years. Ultimately, data from 776 critically ill patients with CRC were collected from the e-ICU database and 219 from the Medical Information Mart for Intensive Care (MIMIC) IV database. The main outcome of this retrospective analysis was 28-day, all-cause mortality of critically ill patients with CRC. The optimal cut-off value for PAR was determined using X-tile version 3.6.1 based on 28-day mortality. X-tile is an easy-to-use tool for the selection of survival outcome-based cut-point [12]. The X-tile software for grouping uses each number between the range of the removed PAR counts as the cut-off value. Subsequently, the X^2 score and P value are measured using the number as the cut-off value. The final number with the maximum X^2 score and the minimum P value was identified as the optimal cut-off value [13].

2.3. Statistical Analysis. Propensity score matching (PSM) and propensity score-based inverse probability of treatment weighting (IPTW) were also used to adjust the covariates to ensure robustness of the results. One-to-one nearest neighbor matching, with a caliper width of 0.05, was applied in the current study. An IPTW model was constructed using the estimated propensity scores as weights. Standardized mean differences were calculated to evaluate the effectiveness of the PSM and IPTW models. Continuous metrics are summarized as mean and standard deviation, and categorical indexes are expressed as frequency with percentage. Differences in clinical features between the high and low PAR groups were detected using the chi-squared test or Student's t -test according to the data type. Because machine learning methods could help to handle nonlinear and high-order terms automatically and improve the predictive performance of clinical model [14, 15], the support vector machine algorithm, along with LASSO Cox regression, was then applied to identify significant metrics associated with 28-day mortality in the test cohort, and only informative metrics with $P < 0.05$ were finally included in the construction of the survival nomogram. Receiver operating curve (ROC) along with sensitivity and specificity was measured to assess the predictive performances of PAR and survival nomogram. The Kaplan-Meier curves along with

log-rank test were utilized to estimate the prognostic role of PAR and survival nomogram in critically ill patients with CRC. Sensitive analyses were conducted to enhance the robustness of our conclusions. All the statistical works were finished via SPSS software (version 25.0) and R software (4.1.0). *P* value no more than 0.05 implicates statistical significance.

3. Results

3.1. Description of Baseline Features. Based on the inclusion criteria, data from 776 critically ill patients with CRC from e-ICU database, 219 from the MIMIC-IV database, and 135 from the Union cohort were included. For the purpose of model construction and verification, subjects were randomly divided into an e-ICU cohort, a training cohort ($N=547$), and an internal validation cohort ($N=229$). Both the MIMIC-IV cohort ($N=219$) and Union cohort ($N=135$) served as external validation cohorts. As listed in Table S1, the mean age of the critically ill patients with CRC was 69.2 years in the e-IUC training cohort, 69.9 years in the e-ICU validation cohort, 69.4 years in MIMIC-IV cohort, and 57.5 years in Union cohort, indicating that older CRC patients were more likely to progress to critically ill status, probably due to underlying diseases or advanced tumor stage. The proportion of males was 57.0%, 63.3%, 57.5%, and 48.9% in the e-ICU training cohort, e-ICU validation cohort, MIMIC-IV cohort, and Union cohort, respectively. Regarding 28-day in-hospital mortality, there were no statistical differences among the four cohorts (13.3% in the e-ICU training cohort, 14.8% in the e-ICU validation cohort, 17.4% in the MIMIC-IV cohort, and 14.8% in the Union cohort).

Using 28-day in-hospital mortality as the final outcome, X-tile software was used to ascertain the threshold value of PAR. As shown in Figure 1, PAR demonstrated the most significant association with 28-day in-hospital mortality at a PAR value of 8.6. Subsequently, critically ill patients with CRC were divided into low and high PAR groups based on the PAR threshold value. In the e-ICU training cohort, there was a higher proportion of female CRC patients, use of mechanical ventilation, and higher Overall Anxiety Severity and Impairment Scale (OASIS) and Acute Physiology Score (APS) III scores in the high PAR group. Due to differences in several clinical metrics between the low and high PAR groups, PSM was applied to balance the distribution of common features. In total, 202 individuals with low PAR were matched with 202 exhibiting high PAR. To further reduce the imbalance between the low and high PAR groups, IPTW was also performed (Figure 2). As shown in Table 1, all clinical metrics were deemed to be well balanced in the weighted cohort. Receiver operating characteristic (ROC) curve analysis was used to compare the predictive performance of PAR, platelet count, and albumin level for 28-day mortality in critically ill patients with CRC. As shown in Table S2, PAR showed the highest predictive performance, not only in the e-ICU cohort (area under the ROC curve [AUC] 0.789), but also in the MIMIC-IV cohort (AUC 0.75).

3.2. Survival Analysis and Sensitivity Analysis of PAR. Kaplan-Meier curves comparing 28-day mortality of critically ill patients according to the cut-off for PAR are shown in Figure 3. CRC patients admitted to the ICU with high PAR demonstrated higher 28-day mortality compared to those with low PAR in the original cohort (hazard ratio [HR] 2.66 [95% confidence interval (CI) 1.80–3.94]; $P < 0.0001$) (Figure 3(a)). After balancing several confounding risk metrics, the strong correlation between 28-day mortality and high levels of PAR existed not only in the PSM cohort (HR 2.2 [95% CI 1.29–3.73]; $P = 0.003$) (Figure 3(b)), but also in weighted cohort (HR 2.51 [95% CI 1.58–3.99]; $P < 0.0001$) (Figure 3(c)). Interestingly, when this survival correlation of PAR was validated using the same threshold value, CRC patients admitted to the ICU with high PAR experienced higher 28-day mortality compared to those with low PAR in the MIMIC-IV cohort (HR 3.88 [95% CI 1.99–7.35]; $P < 0.0001$) (Figure 3(d)). Regarding the sensitivity analysis, a univariate Cox model was constructed in the original, PSM, weighted, and validation cohorts to assess the predictive value of PAR for 28-day mortality. Some potential covariates were also adjusted in the three models, and the results demonstrated a similar tendency ($P < 0.01$) (Table 2).

3.3. Clinical Model for the Survival Prediction of Critically Ill Patients with CRC. The LASSO Cox model (Figure 4(a)), along with the SVM algorithm (Figure 4(a)), was used to identify clinical metrics closely associated with 28-day mortality of critically ill CRC individuals in the e-ICU training set. Final result (Figure 4(c)) revealed that the optimal survival model had four potential predictors (PAR, acute kidney injury, vasopressor, and international normalized ratio). Subsequently, the clinical nomogram was constructed for the prediction of 28-day mortality of critically ill patients with CRC based on the four potent risk factors (Figure 5). The four-factor clinical model was considered to be the critically ill CRC nomogram, and this clinical model achieved satisfactory predictive performance for the prediction of 28-day mortality in critically ill individuals with CRC. The C-index for the critically ill CRC nomogram was 0.873 (0.829–0.916) in the primary cohort, 0.896 (0.851–0.941) in the e-ICU validation cohort, 0.827 (0.743–0.912) in the MIMIC-IV cohort, and 0.767 (0.703–0.831) in the Union cohort.

3.4. Evaluation of the Clinical Model and Risk Stratification. Calibration curves were used to precisely measure the goodness of fit of the critically ill CRC nomogram. The critically ill CRC nomogram demonstrated an encouraging goodness of fit between the predicted and actual 28-day mortality among critically ill patients with CRC, not only in the e-ICU training (Figure 6(a)) and internal validation cohorts (Figure 6(b)), but also in the MIMIC-IV (Figure 6(c)) and Union (Figure 6(d)) cohorts. Decision curve analysis (DCA) was also implemented to assess the clinical utility of the critically ill CRC nomogram. As listed in Figures 6(e)–6(h), if the risk threshold of a critically ill CRC patient was 0.2, the critical ill CRC nomogram gained more

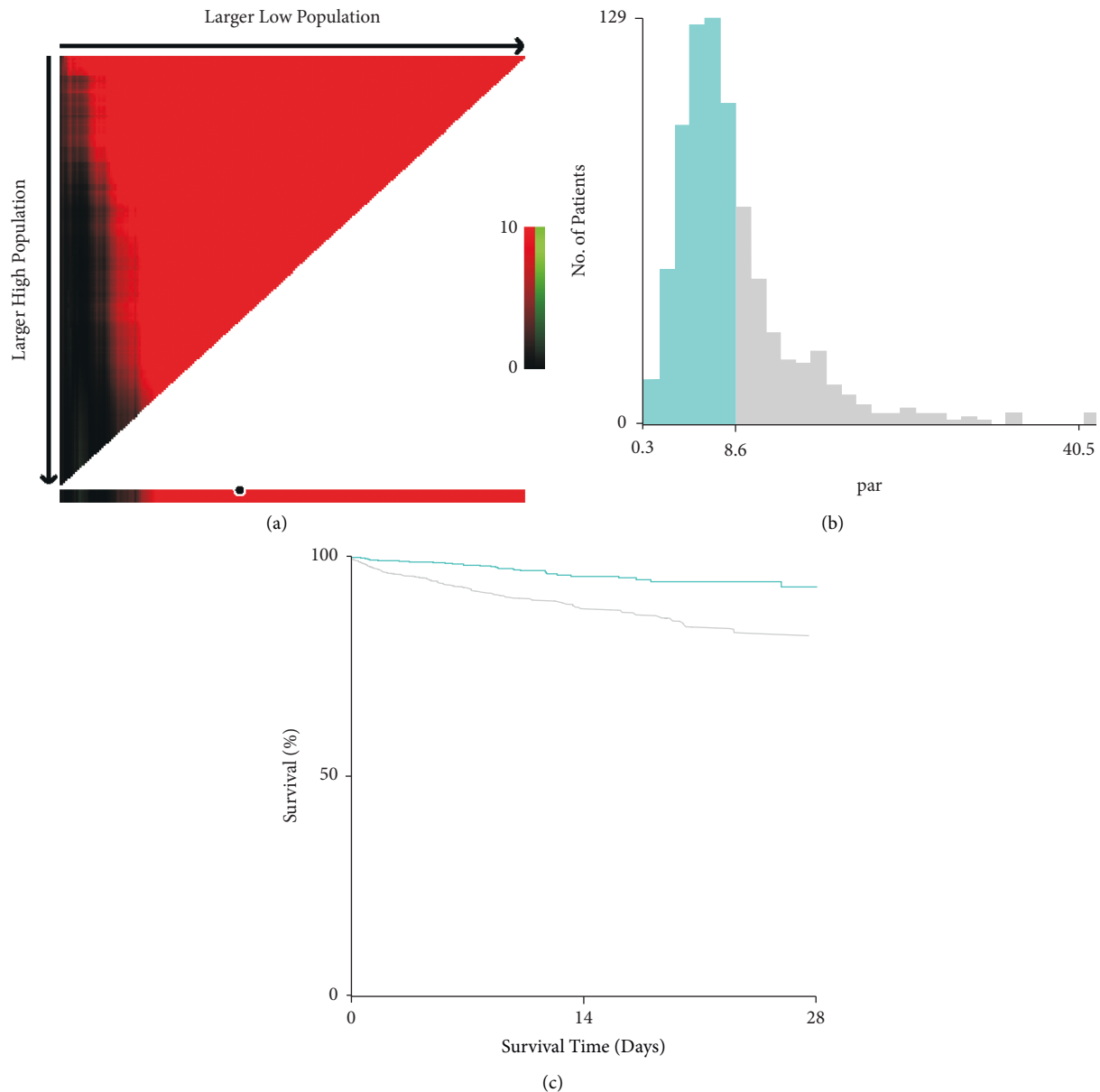


FIGURE 1: X-tile analyses of PAR values in e-ICU database. X-tile plots for critically ill patients with CRC (a). Black circles refers to the optimal threshold value of PAR (b). Kaplan-Meier curve of critically ill patients with CRC divided by PAR (c).

clinical benefit than either treat-all regimen or treat-none scheme, suggesting that the survival nomogram was competent for the prediction of 28-day mortality among critically ill CRC patients in clinical practice.

Finally, we divided critically ill CRC patients into the low risk and high risk subgroups based on the median value of the nomogram. A remarkably statistical difference in 28-day mortality between the low risk and high risk subgroups was revealed by Kaplan-Meier curve in the e-ICU training cohort (HR = 13.42, 95% CI: 4.88–36.91, $P < 0.0001$, Figure 7(a)), the e-ICU validation cohort (HR = 29.24, 95% CI: 3.7–59.24, $P = 0.004$, Figure 7(b)), MIMIC-IV cohort (HR = 4.06, 95% CI: 1.68–9.77, $P = 0.002$, Figure 7(c)), and Union cohort (HR = 13.96, 95% CI: 1.75–60.46, $P = 0.024$, Figure 7(d)). Hence, the survival analyses revealed that the critically ill

CRC nomogram could be used for risk stratification among critically ill CRC patients, and critically ill CRC patients with high risk might receive earlier and radical treatment.

4. Discussion

To our knowledge, the present investigation was the first clinical study based on two large cohorts to explore the association between PAR and survival outcome among critically ill patients with CRC and also confirmed the relationship with our own cohort. We found that higher PAR was correlated with an increased risk for 28-day mortality among critically ill patients with CRC, and PAR was a potent prognostic biomarker of short-term mortality after the adjustment for confounding variables. After PSM, we found

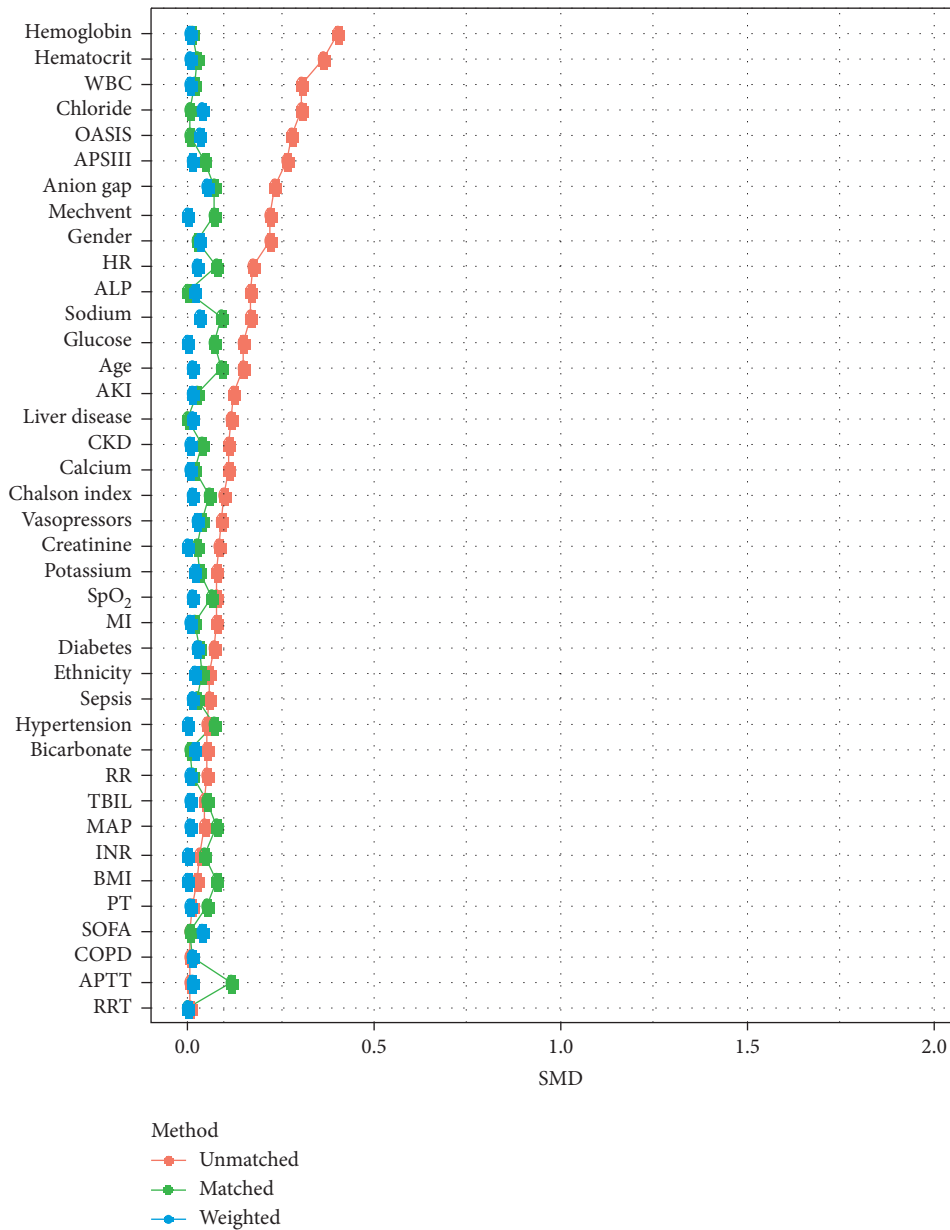


FIGURE 2: Standardized mean difference (SMD) of clinical metrics before and after propensity score matching and weighting in the e-ICU cohort.

the prognostic value of PAR for the prediction of 28-day mortality in critically ill patients with CRC was much higher compared to that before PSM. Moreover, we designed the first survival nomogram for the prediction of 28-day mortality in critically ill patients with CRC. This predictive model demonstrated good predictive performance not only in the e-ICU test and internal cohorts, but also in the MIMIC-IV and the Union cohorts, which are totally different from e-ICU database.

In past decades, platelet count was regarded to be a key factor in hemostasis and thrombosis in past decades. However, accumulating evidence has shown that platelets could contribute to tumorigenesis and invasion through complex crosstalk between platelets and tumor cells [16]. In

the microenvironment of CRC, platelets can promote growth and metastasis of tumor cells via releasing transforming growth factor-beta and vascular epidermal growth factor. A recent study [17] reported that platelet count was positively correlated with serum levels of CRP and a variety of cytokines and highlighted the close correlation between platelets and inflammation status in CRC. Moreover, cytokines secreted by platelets can, in turn, promote cancer-associated inflammation [18].

On the other hand, albumin is an acute-phase protein used in clinical practice and decreases in response to inflammatory reactions and responses. Moreover, low levels of albumin generally signify malnutrition and can exert negative effects on survival outcomes among patients with CRC

TABLE 1: Comparison of baseline metrics between the low and high PAR groups.

Baseline metrics	Original cohort			Matched cohort			Validation cohort		
	Low PAR	High PAR	<i>P</i>	Low PAR	High PAR	<i>P</i>	Low PAR	High PAR	<i>p</i>
Number	511	265	—	202	202	—	154	65	—
Age, years	70.1 (13.4)	68.1(13.6)	0.051	68.6 (14.1)	69.5 (12.8)	0.472	69.7 (12.0)	68.7 (15.2)	0.620
Gender, male, <i>n</i> (%)	320 (62.6)	137 (51.7)	0.004	113 (55.9)	107 (53.0)	0.617	98 (63.6)	28 (43.1)	0.008
BMI, kg/m ²	27.7 (7.9)	28.0 (8.3)	0.590	28.2 (8.4)	28.1 (8.3)	0.885	29.2 (8.4)	27.5 (8.3)	0.186
<i>Ethnicity, n (%)</i>			0.568			0.479			0.087
White	400 (78.3)	199 (75.1)		155 (76.7)	154 (76.2)		110 (71.4)	40 (61.5)	
Black	66 (12.9)	41 (15.5)		33 (16.3)	28 (13.9)		19 (12.3)	6 (9.2)	
Other	45 (8.8)	25 (9.4)		14 (6.9)	20 (9.9)		25 (16.2)	19 (29.2)	
<i>Interventions, n (%)</i>									
MV use	136 (26.6)	99 (37.4)	0.003	77 (38.1)	66 (32.7)	0.298	49 (31.8)	29 (44.6)	0.098
RRT use	6 (1.2)	3 (1.1)	1.000	1 (0.5)	1 (0.5)	1.000	7 (4.5)	0 (0.0)	0.185
Vasopressor use	75 (14.7)	48 (18.1)	0.093	33 (16.3)	32 (15.8)	1.000	57 (37.0)	23 (35.4)	0.940
<i>Score system, points</i>									
SOFA	3.5 (1.0)	3.4 (1.1)	0.909	3.6 (1.2)	3.4 (1.2)	0.592	4.8 (1.5)	5.4 (1.4)	0.282
OASIS	23.6 (10.2)	26.7 (10.4)	0.001	26.1 (10.9)	26.7 (10.1)	0.716	31.9 (8.7)	35.2 (9.8)	0.013
APSIH	43.5 (12.5)	50.0 (24.1)	0.001	48.6 (14.6)	47.7 (14.8)	0.725	47.8 (21.1)	56.1 (25.0)	0.021
<i>Comorbidities, n (%)</i>									
Hypertension	75 (14.7)	34 (12.8)	0.553	30 (14.9)	26 (12.9)	0.666	64 (41.6)	19 (29.2)	0.117
Diabetes	131 (25.6)	60 (22.6)	0.406	47 (23.3)	50 (24.8)	0.816	46 (29.9)	9 (13.8)	0.020
CKD	57 (11.2)	21 (7.9)	0.196	16 (7.9)	15 (7.4)	1.000	21 (13.6)	7 (10.8)	0.720
Myocardial infarct	41 (8.0)	16 (6.0)	0.390	16 (7.9)	16 (7.9)	1.000	25 (16.2)	6 (9.2)	0.252
CHF	64 (12.5)	20 (7.5)	0.046	24 (11.9)	15 (7.4)	0.178	35 (22.7)	11 (16.9)	0.434
COPD	63 (12.3)	32 (12.1)	1.000	22 (10.9)	23 (11.4)	1.000	30 (19.5)	18 (27.7)	0.245
Liver disease	11 (2.2)	2 (0.8)	0.253	1 (0.5)	1 (0.5)	1.000	16 (10.4)	4 (6.2)	0.461
CCI, points	5.7 (2.3)	5.4 (1.5)	0.191	5.5 (2.3)	5.5 (2.5)	0.965	8.9 (2.6)	9.0 (2.9)	0.670
<i>Complications, n (%)</i>									
AKI	119 (23.3)	81 (30.6)	0.168	54 (26.7)	49 (24.3)	0.347	43 (27.9)	20 (30.8)	0.793
Sepsis	76 (14.9)	45 (17.0)	0.507	29 (14.4)	28 (13.9)	1.000	73 (47.4)	29 (44.6)	0.818
<i>Vital signs</i>									
MAP, mmHg	87.1 (16.1)	87.9 (17.4)	0.548	88.9 (16.0)	87.7 (17.0)	0.464	83.0 (19.6)	81.6 (16.7)	0.623
Heart rate, bpm	89.2 (21.0)	93.9 (21.7)	0.004	92.4 (22.1)	92.2 (22.4)	0.934	96.5 (24.3)	100.6 (23.2)	0.248
RR, bpm	19.1 (5.0)	19.3 (5.4)	0.504	19.6 (5.7)	19.6 (5.4)	0.943	19.9 (5.4)	20.8 (6.3)	0.252
SpO ₂ , %	96.9 (3.2)	96.6 (4.7)	0.080	96.6 (4.0)	96.7 (3.4)	0.687	95.8 (5.7)	97.0 (4.7)	0.137
<i>Laboratory results</i>									
WBC, ×10 ⁹ /L	10.5 (4.0)	13.5 (5.8)	0.001	12.3 (4.8)	12.1 (4.7)	0.817	11.2 (4.3)	13.4 (4.8)	0.123
HGB, g/dL	11.2 (2.3)	10.1 (2.3)	0.001	10.4 (2.3)	10.4 (2.2)	0.898	10.4 (1.9)	9.8 (2.2)	0.033
PLT, ×10 ⁹ /L	186.7 (70.9)	388.2 (95.7)	0.001	195.1 (77.8)	370.9 (97.6)	<0.001	189.0 (64.3)	346.9 (94.9)	<0.001
HCT, %	34.1 (6.7)	31.5 (6.6)	0.001	32.3 (6.9)	32.3 (6.2)	0.973	32.5 (5.6)	31.0 (5.9)	0.070
Albumin, g/dL	3.5 (0.7)	2.9 (0.6)	0.001	3.5 (0.7)	2.9 (0.7)	<0.001	3.5 (0.6)	2.7 (0.7)	<0.001
PAR	5.4 (1.9)	14.0 (5.0)	0.001	5.6 (1.9)	13.4 (5.5)	<0.001	5.5 (1.8)	13.0 (4.0)	<0.001
ALP, U/L	138.5(64.9)	174.3 (72.7)	0.018	169.5 (65.4)	154.8(61.5)	0.501	132.7(68.90)	132.1(67.2)	0.965
Bilirubin, mmol/L	1.2 (0.5)	1.3 (0.6)	0.504	1.3 (0.5)	1.2 (0.5)	0.612	1.6 (0.6)	1.1 (0.5)	0.217
Anion gap, mEq/L	10.8 (4.0)	12.0 (4.9)	0.001	11.5 (4.6)	11.2 (4.3)	0.445	14.7 (4.2)	15.5 (4.7)	0.221
Bicarbonate, mEq/L	24.0 (4.5)	24.2 (4.6)	0.504	24.2 (4.6)	24.4 (4.2)	0.569	22.8 (4.6)	22.6 (5.4)	0.783
BUN, mg/dL	22.9 (8.2)	24.9 (9.9)	0.166	24.1 (9.4)	23.1 (8.4)	0.593	24.2 (10.8)	25.6 (12.6)	0.662
Creatinine, mg/dL	1.3 (0.5)	1.4 (0.6)	0.254	1.4 (0.5)	1.4 (0.5)	0.628	1.3 (0.6)	1.2 (0.5)	0.572
Glucose, mg/dL	141.0(63.2)	131.4(50.2)	0.032	140.0(67.3)	133.1 (52.2)	0.249	144.9 (59.3)	133.5 (56.0)	0.189
Potassium, mmol/L	4.1 (0.7)	4.2 (0.9)	0.269	4.1 (0.9)	4.2 (0.8)	0.521	4.2 (0.9)	4.2 (0.7)	0.796
Sodium, mmol/L	137.2 (5.3)	136.2 (5.9)	0.022	136.2(6.2)	136.4(5.6)	0.783	137.4 (5.2)	137.8 (4.1)	0.579
Calcium, mg/dL	8.5 (1.1)	8.6 (0.9)	0.160	8.6 (1.0)	8.6 (0.9)	0.812	8.4 (0.7)	8.2 (0.6)	0.216
Chloride, mmol/L	103.3 (6.3)	101.4 (6.8)	0.001	101.8 (7.0)	102.1 (6.3)	0.725	102.7 (7.1)	102.3 (5.4)	0.704
PT, s	16.6 (7.8)	16.8 (7.3)	0.851	17.2 (7.3)	16.5 (7.4)	0.480	15.7 (5.3)	16.2 (5.7)	0.484
APTT, s	34.9 (10.7)	35.0 (8.0)	0.933	35.7 (11.6)	34.8 (7.8)	0.480	36.4 (10.8)	36.7 (11.7)	0.903
INR	1.5 (0.5)	1.5 (0.5)	0.686	1.5 (0.6)	1.5 (0.5)	0.577	1.4 (0.5)	1.5 (0.5)	0.526
<i>Clinical outcome</i>									
LOS, days	10.9 (4.6)	12.2 (5.2)	0.109	12.2 (5.4)	12.0 (5.4)	0.838	11.7 (5.6)	10.9 (5.3)	0.606
Death, <i>n</i> (%)	42 (8.2)	65 (24.5)	0.001	20 (9.9)	55 (22.3)	0.001	15 (9.7)	23 (35.4)	<0.001

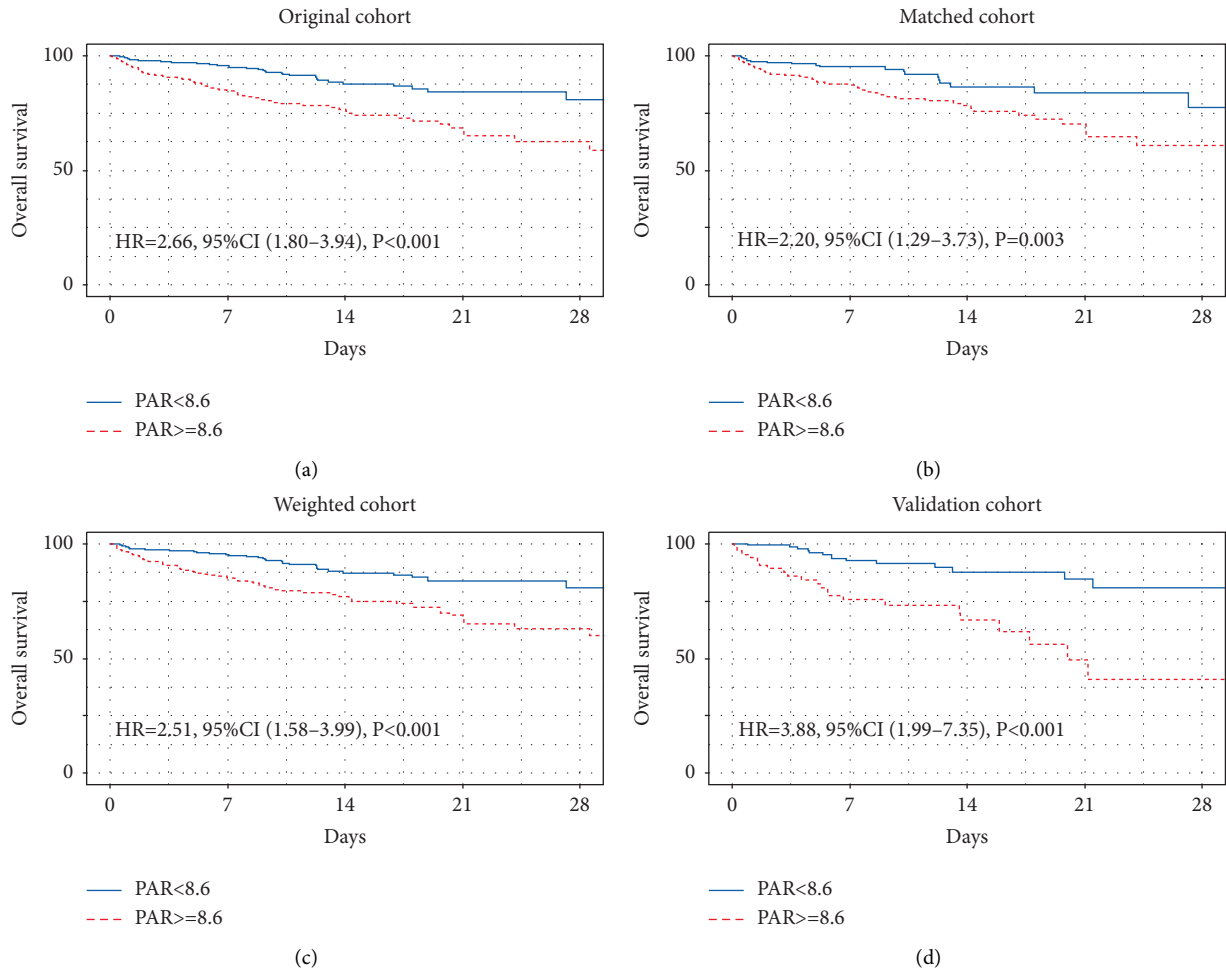


FIGURE 3: Kaplan-Meier curves for critically ill CRC patients stratified by PAR in the original cohort (a), in the matched cohort (b), in the weighted cohort (c), and in the validation cohort (d).

TABLE 2: Summary of results of 28-day mortality and sensitivity analysis.

	Original cohort		Matched cohort		Weighted cohort		Validation cohort	
	HR (95% CI)	P value	HR (95% CI)	P value	HR (95% CI)	P value	HR (95% CI)	P value
Unadjusted	2.66 (1.80-3.94)	<0.001	2.20 (1.29-3.73)	0.003	2.51 (1.58-3.99)	<0.001	3.82 (1.99-7.35)	<0.001
Model 1	2.74 (1.85-4.08)	<0.001	2.24 (1.31-3.84)	0.007	2.54 (1.57-4.11)	<0.001	3.77 (1.86-7.64)	<0.001
Model 2	3.07 (2.03-4.64)	<0.001	2.81 (1.59-4.97)	<0.001	2.79 (1.71-4.55)	<0.001	4.59 (2.04-10.34)	<0.001
Model 3	3.44 (2.15-5.49)	<0.001	3.81 (1.98-7.35)	<0.001	3.73 (2.02-6.90)	<0.001	6.79 (2.58-17.87)	<0.001

Model 1 adjusted for age, gender, BMI, ethnicity. Model 2 adjusted for model 1 plus comorbidities and Charlson comorbidity index. Model 3 adjusted for model 2 plus score system, interventions, complications.

[19]. PAR, derived from platelet count and albumin levels, represents an entirely different index, combining both nutritional and inflammatory status. It is quite significant in simultaneously evaluating inflammatory and nutritional status in critically ill patients with CRC. High levels of PAR represent higher platelet counts with inflammatory response, and lower levels of albumin with malnutrition, eventually resulting in inferior short-term clinical outcomes of critically ill patients with CRC. ROC curve analysis revealed that PAR demonstrated better accuracy than platelet count or albumin in the prediction of 28-day mortality among critically ill patients with CRC. In addition,

our analysis also demonstrated that ill patients with high PAR experienced higher 28-day mortality than those with low PAR.

Several clinical investigations have gained insight into the prognostic value of PAR. Yang et al. [20] performed a single-center study with 405 peritoneal dialysis patients and reported that PAR was a risk factor associated with mortality. Moreover, PAR not only contributed to critical illness but was also implicated in the risk assessment of a list of malignant tumors. Huang et al. [21] concluded that PAR was a potent risk factor for lymph node metastasis of gastric cancer and also constructed a clinical model including PAR

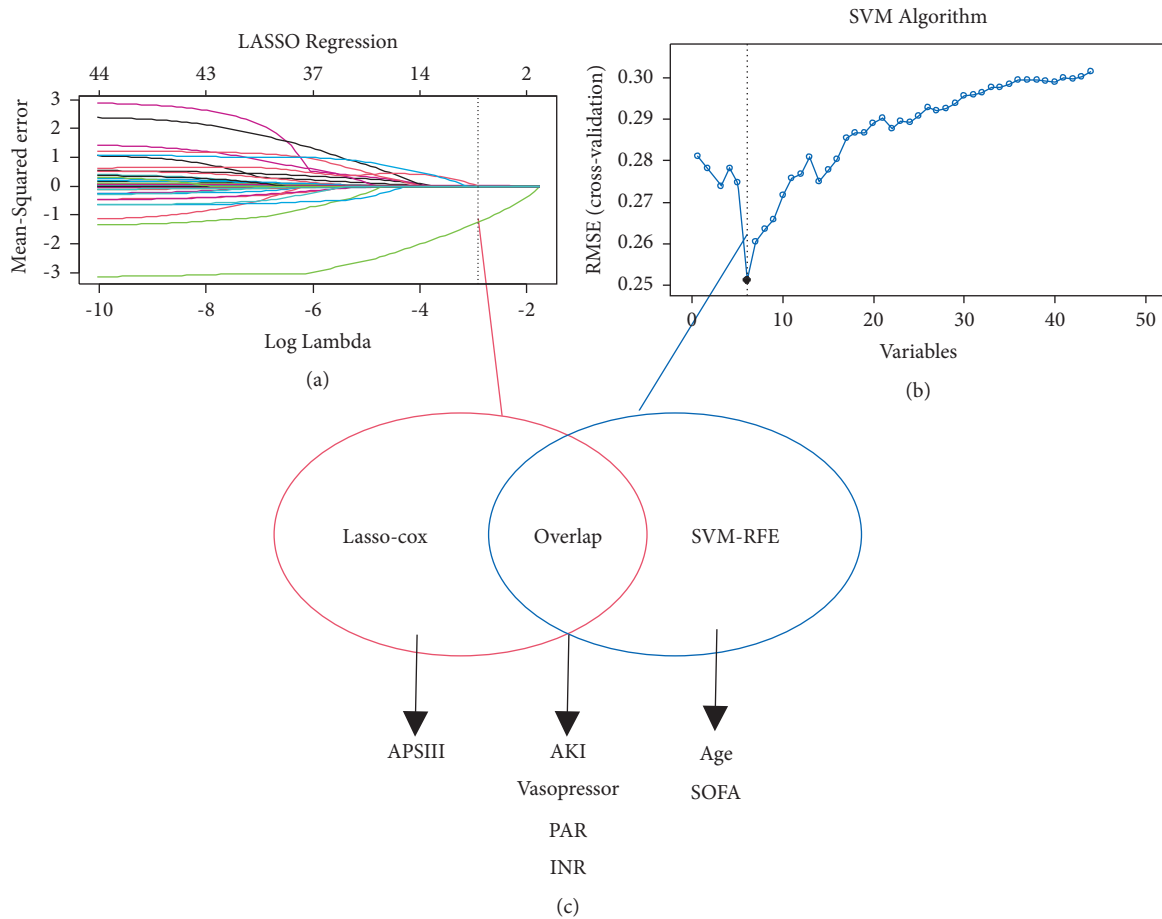


FIGURE 4: Selection of informative factors associated with 28-day mortality using the LASSO Cox regression model and SVM algorithm. (a) LASSO coefficient profiles of 44 clinical features. (b) Selection process of SVM algorithm. (c) Four significant indexes were selected by LASSO Cox regression model and SVM algorithm.

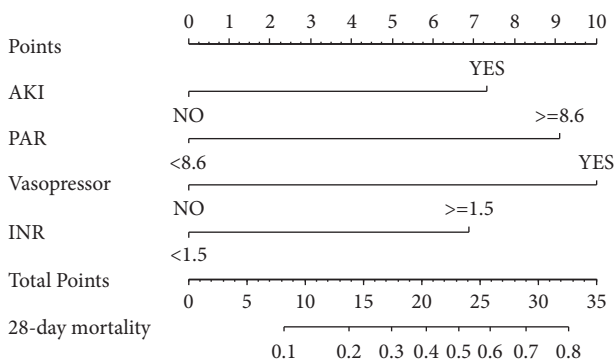


FIGURE 5: A clinical nomogram for the prediction of 28-day mortality among critically ill individuals with colorectal cancer.

for risk assessment of lymph node metastasis among individuals with gastric cancer. A recent study [22] involving 198 individuals with lung cancer revealed that high PAR was correlated with less unfavorable overall survival, while subsequent multivariate Cox analyses identified PAR as a potent risk indicator for worse overall survival. Saito et al. [23] assessed the prognostic role of PAR in cholangiocarcinoma and found that preoperative

PAR was inversely associated with overall and disease-free survival in cholangiocarcinoma patients who underwent primary resection. Li et al. [24] reported that individuals with hepatocellular carcinoma with high preoperative PAR exhibited a lower long-term survival rate and higher recurrent risk than hepatocellular carcinoma patients with low PAR. However, no study has addressed the clinical association between PAR and mortality among critically ill patients with CRC. Consistent with the results from other cancers, survival analysis also demonstrated that critically ill CRC patients with high PAR exhibited a risk ratio of 2.66 for mortality compared with the low PAR group in the primary cohort; this ratio was increased to 3.88 in the validation cohort.

Our analysis had three primary limitations. First, we could not assess the relationship between PAR and long-term survival outcomes of critically ill individuals with CRC, such as six-month and one-year mortality due to technical reasons. Subsequently, we only abstracted baseline PAR on admission and did not have information about time variations in PAR. Finally, because the two databases only included data from critically ill patients, some important inflammatory and nutritional indexes were missing, such as prognostic nutritional index, CRP, and lactate

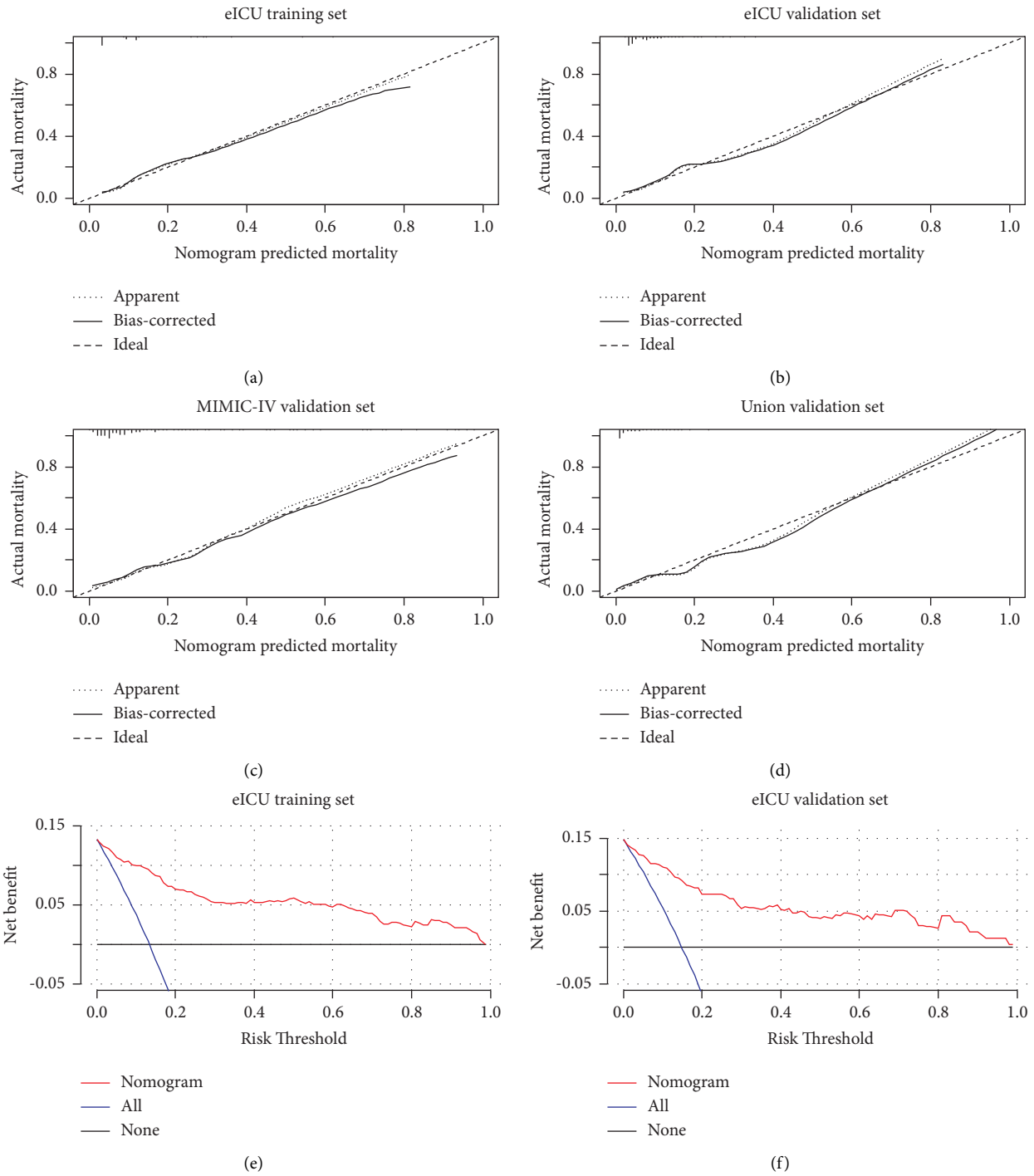


FIGURE 6: Continued.

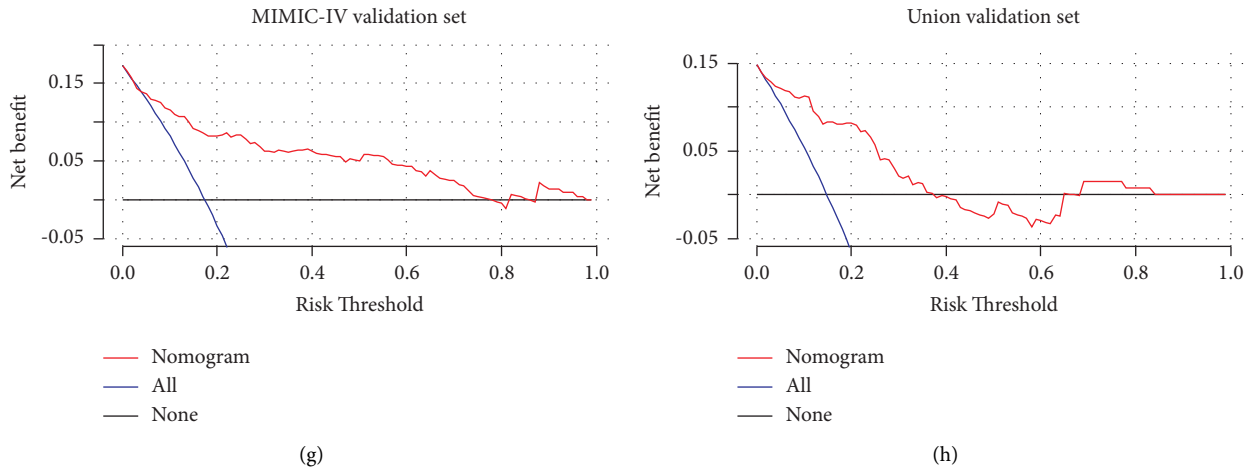


FIGURE 6: Calibration curves for in-hospital mortality in critically ill CRC patients in e-ICU training cohort (a), in e-ICU validation cohort (b), in MIMIC-IV cohort (c), and in the Union cohort (d). Decision curve analysis for 28-day mortality in CRC patients in ICU to detect its clinical usefulness in e-ICU training cohort (e), in e-ICU validation cohort (f), in MIMIC-IV cohort (g), and in the Union cohort (h).

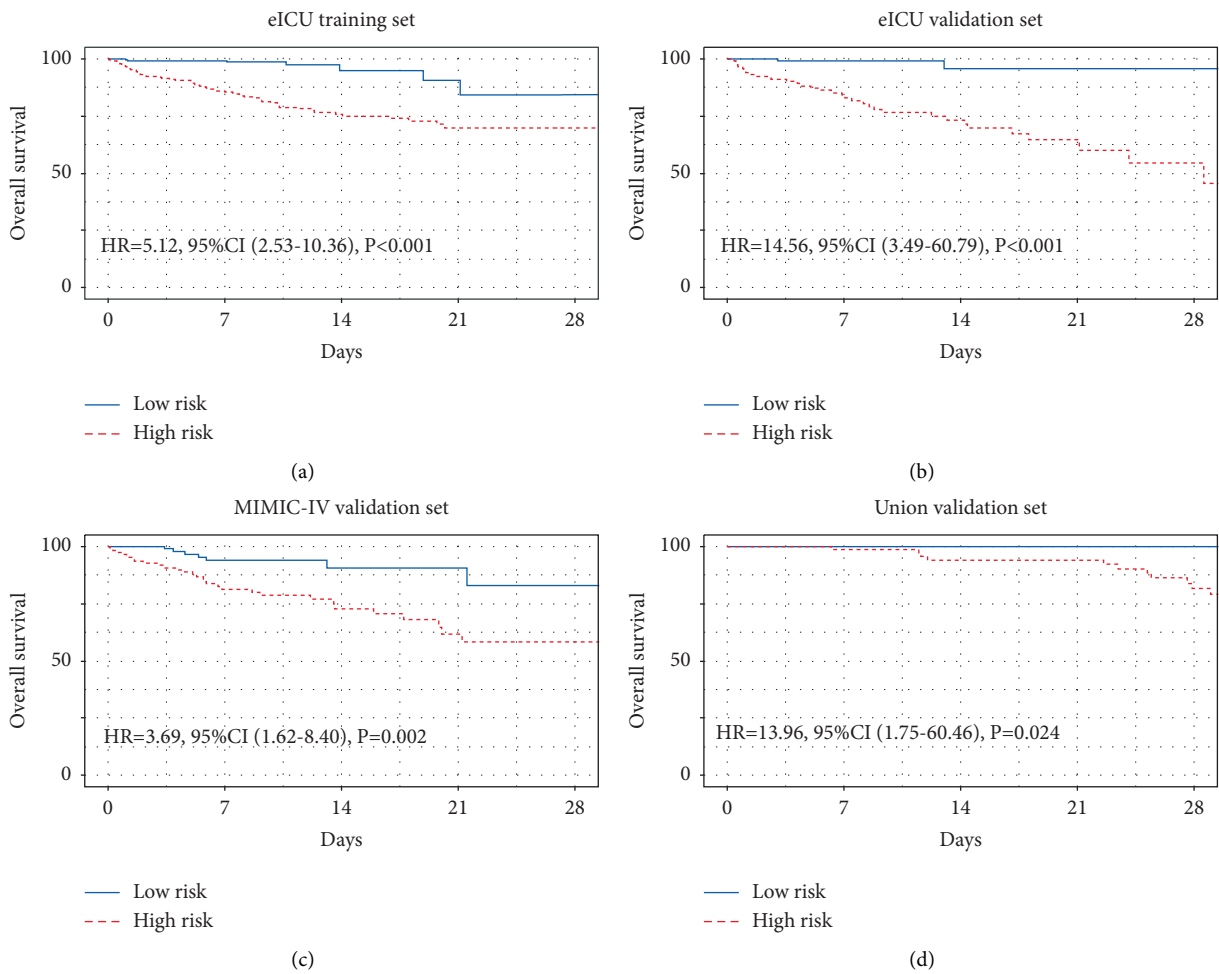


FIGURE 7: Kaplan-Meier curves of 28-day mortality for CRC patients stratified by the mean point predicted by the nomogram in e-ICU training cohort (a), in e-ICU validation cohort (b), in MIMIC-IV cohort (c), and in the Union cohort (d).

dehydrogenase; as such, we could not appraise the relationship between PAR and these well-established inflammatory and nutritional indexes. Hence, multicenter trials including more established indexes and longer follow-up are needed to further validate the prognostic role of PAR in critically ill patients with CRC.

5. Conclusion

This was the first clinical analysis to investigate the prognostic role of PAR among critically ill patients with CRC. PAR is a simple score that combines inflammatory and nutritional status. PAR can be applied to predict short-term survival outcome of critically ill patients with CRC. Moreover, a survival nomogram incorporating PAR demonstrated satisfactory performance for predicting 28-day mortality in critically ill patients with CRC.

Abbreviation

CRC:	Colorectal cancer
PAR:	Platelet-to-albumin ratio
BMI:	Body mass index
MV:	Mechanical ventilation
RRT:	Renal replacement therapy
SOFA:	Sequential organ failure assessment
OASIS:	Oxford acute severity of illness score
APSI:	Acute physiology score III
CKD:	Chronic kidney disease
CHF:	Congestive heart failure
COPD:	Chronic obstructive pulmonary disease
CCI:	Charlson comorbidity index
AKI:	Acute kidney injury
MAP:	Mean arterial pressure
RR:	Respiratory rate
WBC:	White blood cell
HGB:	Hemoglobin
PLT:	Platelet
HCT:	Hematocrit
ALP:	Alkaline phosphatase
BUN:	Blood urea nitrogen
PT:	Prothrombin time
APTT:	Activated partial thromboplastin time
INR:	International normalized ratio
LOS:	Length of hospital
SVM:	Support vector machine
PTW:	Probability of treatment weighing
PSM:	Propensity score matching.

Data Availability

The datasets used during the current study are available from the corresponding author on reasonable request.

Ethical Approval

Our research plan was approved by the clinical ethics committee of Wuhan Union Hospital.

Conflicts of Interest

All authors declared no conflicts of interest in this research.

Authors' Contributions

Ling Y and Lv Q conceived the research; Wang ZY collected the clinical data; Li AS completed the statistical analysis; Li AS and Wang ZY wrote the manuscript; Ling Y and Lv Q revised this manuscript. Anshu Li and Zhiyong Wang contributed equally to this article.

Supplementary Materials

Table S1. Comparisons of baseline characteristics among three cohorts. Table S2. ROC analysis of PAR, platelet count, and albumin. (*Supplementary Materials*)

References

- [1] H. Sung, J. Ferlay, R. L. Siegel et al., "Global cancer statistics 2020: GLOBOCAN estimates of incidence and mortality worldwide for 36 cancers in 185 countries," *CA: A Cancer Journal for Clinicians*, vol. 71, no. 3, pp. 209–249, 2021.
- [2] M. Arnold, M. S. Sierra, M. Laversanne, I. Soerjomataram, A. Jemal, and F. Bray, "Global patterns and trends in colorectal cancer incidence and mortality," *Gut*, vol. 66, no. 4, pp. 683–691, 2017.
- [3] F. Catalano, R. Borea, S. Puglisi et al., "Targeting the DNA damage response pathway as a novel therapeutic strategy in colorectal cancer," *Cancers*, vol. 14, no. 6, p. 1388, 2022.
- [4] A. O. Soubani, "Critical care prognosis and outcomes in patients with cancer," *Clinics in Chest Medicine*, vol. 38, no. 2, pp. 333–353, 2017.
- [5] F. D. Martos-Benitez, C. D. D. Soler-Morejón, K. X. Lara-Ponce et al., "Critically ill patients with cancer: a clinical perspective," *World Journal of Clinical Oncology*, vol. 11, no. 10, pp. 809–835, 2020.
- [6] G. Wu, J. Liu, H. Liu et al., "An applicable inflammation-joined and nutrition-related prognostic indicator in patients with colorectal cancer," *Frontiers in Oncology*, vol. 11, Article ID 644670, 2021.
- [7] T. He, X. An, H. P. Mao et al., "Malnutrition-inflammation score predicts long-term mortality in Chinese PD patients," *Clinical Nephrology*, vol. 79, no. 6, pp. 477–483, 2013.
- [8] K. Sugimachi, T. Iguchi, Y. Mano et al., "The impact of immunonutritional and physical status on surgical outcome after pancreaticoduodenectomy in elderly patients," *Anti-cancer Research*, vol. 39, no. 11, pp. 6347–6353, 2019.
- [9] T. Hayama, T. Ozawa, M. Tsukamoto et al., "Predicting overall survival using preoperative nutritional and inflammation status for colorectal cancer," *In Vivo*, vol. 36, no. 1, pp. 450–457, 2022.
- [10] Y. Liu, Y. Meng, C. Zhou et al., "Creation and validation of a survival nomogram based on immune-nutritional indexes for CRC patients," *Journal of Oncology*, vol. 2022, Article ID 1854812, 12 pages, 2022.
- [11] T. Matsubara, S. Takamori, N. Haratake et al., "Identification of the best prognostic marker among immunonutritional parameters using serum C-reactive protein and albumin in non-small cell lung cancer," *Annals of Surgical Oncology*, vol. 28, no. 6, pp. 3046–3054, 2021.

- [12] R. L. Camp, M. Dolled-Filhart, and D. L. Rimm, "X-tile: a new bio-informatics tool for biomarker assessment and outcome-based cut-point optimization," *Clinical Cancer Research*, vol. 10, no. 21, pp. 7252–7259, 2004.
- [13] W. Zhuang, J. Chen, Y. Li, and W. Liu, "Valuation of lymph node dissection in localized high-risk renal cell cancer using X-tile software," *International Urology and Nephrology*, vol. 52, no. 2, pp. 253–262, 2020.
- [14] Z. Zhang, L. Chen, P. Xu, and Y. Hong, "Predictive analytics with ensemble modeling in laparoscopic surgery: A technical note," *Laparoscopic, Endoscopic and Robotic Surgery*, vol. 5, no. 1, pp. 25–34, 2022.
- [15] D. Gustafson, M. Ngai, R. Wu et al., "Cardiovascular signatures of COVID-19 predict mortality and identify barrier stabilizing therapies," *EBioMedicine*, vol. 78, Article ID 103982, 2022.
- [16] X. R. Xu, G. M. Yousef, and H. Ni, "Cancer and platelet crosstalk: opportunities and challenges for aspirin and other antiplatelet agents," *Blood*, vol. 131, no. 16, pp. 1777–1789, 2018.
- [17] J. P. Vayrynen, S. A. Vayrynen, P. Sirnio et al., "Platelet count, aspirin use, and characteristics of host inflammatory responses in colorectal cancer," *Journal of Translational Medicine*, vol. 17, no. 1, p. 199, 2019.
- [18] T. Yamamoto, K. Kawada, and K. Obama, "Inflammation-related biomarkers for the prediction of prognosis in colorectal cancer patients," *International Journal of Molecular Sciences*, vol. 22, no. 15, p. 8002, 2021.
- [19] O. Yalav, U. Topal, A. G. Unal, and I. C. Eray, "Prognostic significance of preoperative hemoglobin and albumin levels and lymphocyte and platelet counts (HALP) in patients undergoing curative resection for colorectal cancer," *Annali Italiani di Chirurgia*, vol. 92, pp. 283–292, 2021.
- [20] Y. Yang, J. Yuan, L. Liu, S. Qie, L. Yang, and Z. Yan, "Platelet-to-albumin ratio: a risk factor associated with technique failure and mortality in peritoneal dialysis patients," *Renal Failure*, vol. 43, no. 1, pp. 1359–1367, 2021.
- [21] C. Huang, Y. Q. Xia, L. Xiao, J. Huang, and Z. M. Zhu, "Combining the platelet-to-albumin ratio with serum and pathologic variables to establish a risk assessment model for lymph node metastasis of gastric cancer," *Journal of Biological Regulators & Homeostatic Agents*, vol. 35, no. 2, pp. 811–817, 2021.
- [22] M. Guo, T. Sun, Z. Zhao, and L. Ming, "Preoperative platelet to albumin ratio predicts outcome of patients with non-small-cell lung cancer," *Annals of Thoracic and Cardiovascular Surgery*, vol. 27, no. 2, pp. 84–90, 2021.
- [23] N. Saito, Y. Shirai, T. Horiuchi et al., "Preoperative platelet to albumin ratio predicts outcome of patients with cholangiocarcinoma," *Anticancer Research*, vol. 38, no. 2, pp. 987–992, 2018.
- [24] C. Li, W. Peng, X. Y. Zhang, T. F. Wen, and L. P. Chen, "The preoperative platelet to albumin ratio predicts the prognosis of hepatocellular carcinoma patients without portal hypertension after liver resection," *Medicine*, vol. 98, no. 45, Article ID e17920, 2019.

Review Article

Nonpolypous Hamartomas of the Gastrointestinal Tract: An Updated Review on Classification, Denominations, and Clinical Management

Simona Gurzu ^{1,2,3}, Diana Burlacu ³, and Ioan Jung ¹

¹Department of Pathology, George Emil Palade University of Medicine, Pharmacy, Sciences and Technology, Targu Mures, Romania

²Research Center of Oncopathology and Transdisciplinary Research (CCOMT), George Emil Palade University of Medicine, Pharmacy, Sciences and Technology, Targu Mures, Romania

³Department of Pathology, Clinical County Emergency Hospital, Targu Mures, Romania

Correspondence should be addressed to Simona Gurzu; simonagurzu@yahoo.com

Received 23 March 2022; Accepted 22 April 2022; Published 9 May 2022

Academic Editor: Faisal Raza

Copyright © 2022 Simona Gurzu et al. This is an open access article distributed under the Creative Commons Attribution License, which permits unrestricted use, distribution, and reproduction in any medium, provided the original work is properly cited.

Purpose. To perform the first systematic report about histological subtypes of nonpolypous hamartomas of the gastrointestinal (GI) tract, from esophagus to anal canal. *Design.* From over 19,000 studies about hamartomas, most of them published as case series or case presentations, we have selected the most representative ones for the GI tract, excluding polyposis syndromes. To have a whole picture of these hamartomas, all of the data were combined with the personal experience of the authors who are GI pathologists. *Results.* The examined articles showed predominance of vascular and combined vascular and mesenchymal hamartomas. Arteriovenous hamartomas or Brunner gland hamartomas are mainly diagnosed in the small intestine, with preponderance for duodenum. Other malformations such cavernous hamartomas are more specific for the colorectal segments, whereas chondromatous hamartomas or those derived from the neural ectoderm were mostly reported in the esophagus. As newly recognized entities were admitted in the last years, misdiagnosis is frequent, and the best therapeutic approach is far to be known. *Conclusion.* Even rare, hamartomas of the GI tract need to be differentiated from tumors and familial polyposis syndromes. Knowing their proper denominations and possible complications is valuable for gastroenterologists, pathologists, and surgeons, to be aware in the differential diagnosis.

1. Introduction

Hamartomas are rare developmental aberrations that occur in 1 of 3000-4000 live births [1]. The term derives from the Greek word “hamartia” meaning error or failure. Albrecht defined these “tumor-like malformations” in 1904 as being composed by normal cells and tissue components, like the organ in which they occur, which show a disorganized architecture and a predominance of one component [2, 3]. As the diagnosis is frequently difficult, improper nomenclature and misdiagnoses can prolong the diagnosis time, and therapeutic approach requires a multidisciplinary team [4].

In gastrointestinal (GI) tract, hamartomas are uncommon and usually affect children and young adults. They can occur anywhere in the submucosa and rare in the mucosa of the

GI segments, from esophagus to the anal canal. At diagnosis, it is necessary to take into account that a GI tract hamartoma can frequently associate other malformations of the GI tract, pancreas, vertebrae, or other organs [1].

The two main groups of GI hamartomas are the hamartomatous familial gastrointestinal polyposis [5] and vascular hamartomas [4, 6–8]. The other uncommon subtypes include mesenchymal [3] and heterotopic hamartomas (e.g., ectopic pancreas or gastric mucosa, gastric duplication, and duplication cysts) [9–11].

The aim of this review is to synthesize the literature data regarding classification, evolution, therapeutic approaches, and incidence of these lesions. Only one previous similar review was published this year (2022) which refers to symptomatic polypoid hamartomas of the jejunum and ileum of

39 adults and 10 children [12]. As most of the gastrointestinal hamartomas reports are limited to single cases or case series, this is the first review addressing the histological subtypes of nonpolypous GI hamartomas, from esophagus to anal canal.

2. Methodology

To elaborate this review, a systematic search of the literature was undertaken to identify those representative papers which show classic and particular features of GI hamartomas. It was focused on the whole clinical data, from incidence to therapeutic approaches.

To enrich the above-mentioned aim, we have performed a systematic review of papers indexed in Medline (PubMed) and Web of Science databases. All data available till March 2022 were included. The following search terms were used as combined with hamartoma: “gastrointestinal” “esophagus”, “stomach”, “intestine”, “duodenum”, “jejunum”, “ileum”, “ileo-cecal”, “diverticul”, “colon”, “cecum”, “rectum”, and “anal canal”. The other searched MeSH terms and text words were “angiodysplasia”, “vascular malformation and gastrointestinal”, “neuromuscular and vascular hamartoma”, “caliber persistent artery”, “Dieulafoy lesion”, “duplication cyst and gastrointestinal”, “tailgut cyst”, “Brunner gland hamartoma”, “hemangioma and gastrointestinal”, and “lymphangioma and gastrointestinal”. Data assessment was conducted independently by two of the three authors (GS, BD, and JI) using predefined terms.

From the research, we have eliminated the hamartomatous familial gastrointestinal polyposis syndromes which include Cowden syndrome, juvenile polyposis, Peutz-Jeghers syndrome, Bannayan-Riley-Ruvalcaba syndrome, hereditary mixed polyposis syndrome, Gorlin syndrome, Birt-Hogg-Dube syndrome, neurofibromatosis type I, and multiple endocrine neoplasia syndrome 2B [5] (Figure 1).

3. Vascular Hamartomas

In 1996, the International Society for the Study of Vascular Anomalies (ISSVA) firstly classified vascular aberrations into vascular malformations and proliferative vascular lesions (tumors). This classification was updated in 2014 and grouped them in simple and combined vascular malformations [4]. Simple malformations include capillary-, venous-, arteriovenous-, and lymphatic malformations, same as arteriovenous fistula, whereas combination between vessels (more than two vascular malformations in the same lesion) is considered a combined malformation [4].

In GI tract, vascular hamartomas are rather not diagnosed than rare and are mostly arteriovenous type [4, 6]. Denominations such as “caliber-persistence” or “caliber-persistent artery”, “submucosal aneurysm,” “large submucosal arteries,” “angiodysplasia,” “submucosal arteriole malformation,” “vascular malformation,” and “gastric arteriosclerosis” are used in daily practice [6]. In the French literature, the “caliber persistence” is also known as “Dieulafoy’s lesion” [6, 13]. Although the 2014 updated ISSVA classification includes hemangiomas and lymphangiomas in the group of tumors,

the World Health Organization considers them as malformative lesions of the GI tract [4].

3.1. Arteriovenous Hamartomas. They are developed in GI submucosa and consist of proliferation of malformed capillaries and large arterial and venous structures, some of them with sinuous aspect [4, 14]. A characteristic feature is protrusion of the large vessels from submucosa, through muscularis mucosae, in mucosa, predisposing to occult or fulminant and even lethal hemorrhage [6, 15, 16]. Arteriovenous communications and shunting might coexist [4].

First description of Dieulafoy’s lesion was provided by Gallard in 1884 who called it as “millier aneurysm of stomach” [6]. The French pathologist Paul Georges Dieulafoy described it in 1897 as “exulceratio simplex” [6, 7]. The term was then changed by Voth in German literature in 1962 and firstly used by Krasznai in English literature in 1968 as “caliber persistence” [15, 16]. Nowadays, it is defined as a small erosion of the GI mucosa, due to a large caliber and persistent submucosal arteriole, and is the cause of 0.5%-14% of upper GI bleeding in adults [13]. In children and young people, this syndrome is rare (only 27 reported cases till 2019) but can be represented by multiple GI erosions and be part of PHACE syndrome (posterior fossa brain malformations, hemangiomas, arterial lesions, cardiac, and eye abnormalities) [13].

In English literature, Moore et al. firstly performed a classification of arteriovenous malformations of the GI tract in 1976, based on angiographic examination [17]. They split them in three groups: type 1: solitary lesions, more frequent in the proximal colon; type 2: large malformations, frequently flat, commonly located in the small intestine; and type 3: punctate angiomas associated or not to hereditary hemorrhagic telangiectasia (Rendu-Osler-Weber syndrome) [17]. Type 1 are acquired lesions of elderly people, whereas types 2 and 3 are rather malformative and affect younger ones [14].

Arteriovenous malformations are more frequent (up to 75%) in the proximal stomach, involving branches of the right gastric artery, followed by the small intestine [6, 13] but are uncommon in the inferior mesenteric artery region [18]. The acquired vascular disorders of the submucosal layer can be differentiated at angiography, from congenital vascular malformations (hamartomas), based on the intense and persistent vein opacification in the venous phase, as result of a rapid venous filling [14].

In some cases, these hamartomas can associate carcinomas that are usually diagnosed in early stage, especially in the stomach [8]. In other cases, congenital malformations such as Meckel’s diverticulum may serve as a place of development of an arteriovenous malformation [14]. Treatment consists in vascular embolization but, as this therapeutic approach can induce intestinal ischemia, surgical resection is recommended in selected patients. In children, antiangiogenic prolonged (3 years) therapy with rapamycin or other substances was proved effective to reduce GI bleeding and inhibit angio- and lymphangiogenesis [13].

3.2. Venous Hamartomas/Cavernous Hemangiomas. These rare malformations of distal colon and rectum were described in 1839 by Philips and only 351 cases were reported in Medline

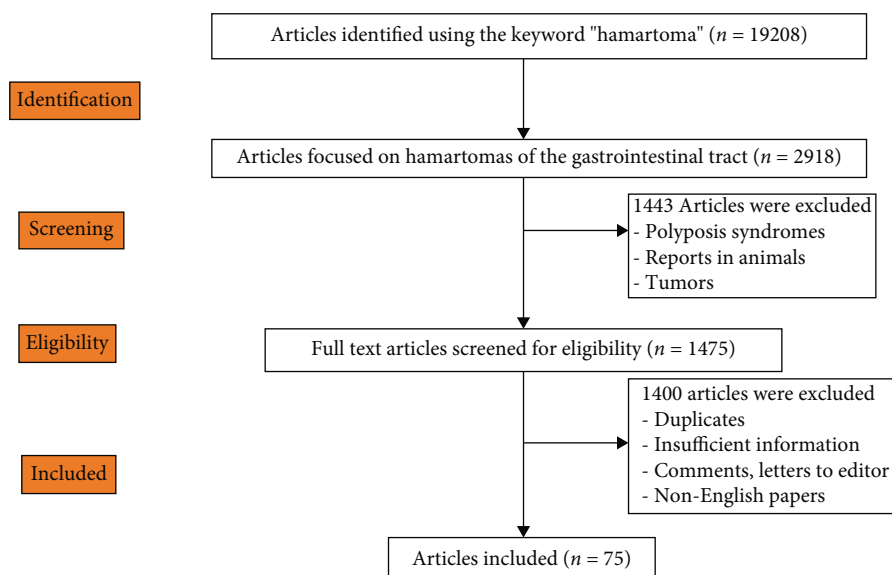


FIGURE 1: Preferred reported items for systematic reviews and meta-analyses (PRISMA) flow diagram for searching the PubMed and Web of Science databases between 2000 and 2022.

database till 2021 [19, 20]. In patients with anemia and occult, minimal, or fulminant rectal bleeding, the endoscopy can reveal unspecific lesions, from purple mucosa, submucosal petechiae, or fluid-filled cystic structures, which induce prolonged bleeding, after biopsy, till circumferential thickening of the GI wall and formation of phleboliths in 29-50% of the cases [19, 20]. Differential diagnosis includes hemorrhoids, pneumatosis or melanosis coli, ulcerative colitis, proctitis, and carcinoma [19, 20].

3.3. Lymphangiomas. They are composed by dilated lymphatic channels or cysts that are lined by podoplanin (D2-40) or LYVE-1 positive-endothelial cells and predominantly occur in the small intestine [4, 21]. Based on the size of the dilated vessels, lymphangiomas are classified in capillary, cavernous and cystic lymphangiomas [4, 21]. If capillary and cavernous lymphangiomas are mainly developed in the submucosa of the GI tract, cystic lymphangioma is rather a mesenteric lesion developed as result of the mTOR pathway activation, which is therapeutically inhibited by everolimus [21, 22].

3.4. Hemolymphangioma. It is a rare variant of lymphangioma, with venous and lymphatic component, which estimated incidence is 1.2 to 2.8 per 1000 newborn infants [21]. Only 8 cases were reported in adults, all of them in the small intestine [21]. Endoscopic or open surgery removal, along with endoscopic sclerotherapy, was used in the reported cases, as the therapy of choice [21].

Lymphangiomatosis, which is a multisystem presence of lymphangiomas, can involve the GI tract along with other organs such as the liver, spleen, or kidney [23]. GI lymphangiomatosis might associate occult anemia, spontaneous bleeding, and abdominal pain and can be complicated by protein-losing enteropathy [23]. In such cases, besides removal of the

lesion, when necessary, systemic therapy with rapamycin or thalidomide is recommended [23].

3.5. Multifocal Lymphoendotheliomatosis. It is a cutaneous-visceral lesion consisting on association of GI vascular hamartomas, which are characterized by distinct endothelial proliferation marked immunohistochemically by the lymphatic vessel endothelial LYVE-1 or hyaluronan receptor 1, with diffuse congenital vascular lesions of the skin, lung, spleen, choroid plexus, bones, etc. [24–26]. It might be complicated with thrombocytopenia refractory to blood cell transfusions and life-threatening bleeding, with a subsequent mortality rate of 65% in newborns [24, 27]. As this is a newly recognized entity, which was firstly described by North et al., there is no consensus on the proper therapy [25, 28]. The rapamycin inhibitors such as sirolimus, combination of vincristine and prednisolone, and association of aminocaproic acid, octreotide drip, and corticosteroids were used in the cases reported in literature [25–28]. In refractory cases, the antiangiogenic therapy with bevacizumab was suggested to be used [27].

4. Combined Vascular and Mesenchymal Hamartomas

4.1. Neuromuscular and Vascular Hamartoma. Neuromuscular and vascular hamartoma (NMVH), which is also known as fibrovascular hamartoma, represents a variant of vascular hamartomas in which the proliferated vessels are relatively small and mesenchymal components are associated [29]. Macroscopically, NMVH is a localized lesion of the submucosa of the small intestine, usually hemorrhagic, which is covered by normal or ulcerated mucosa and can protrude in the intestinal lumen [29, 30]. Uni- and multifocal thickening of the submucosa, with stenosis of the intestinal lumen, were also described [30, 31]. Small intestine

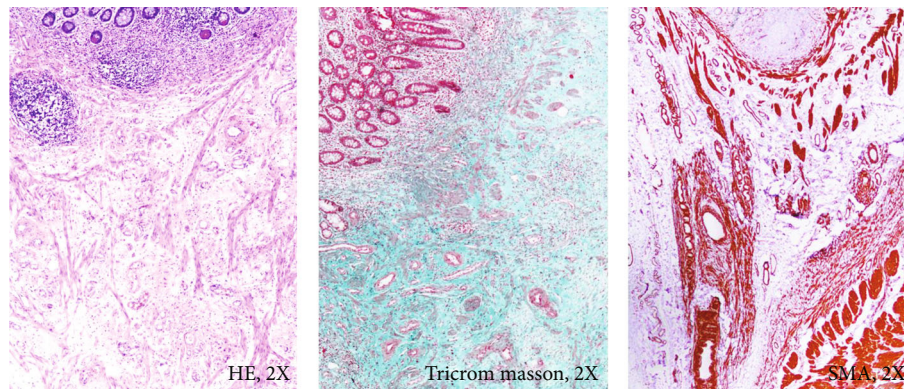


FIGURE 2: Microscopic and immunohistochemical features of neuromuscular and vascular hamartoma: enlarged submucosa with proliferation of small vessels marked by smooth muscle actin (SMA), embedded in a collagenous stroma.

contrast-enhanced ultrasonography is considered as the optimal imagistic method for diagnosis of NMVH [29].

Under light microscope, the overlying mucosa is intact or ulcerated, the muscularis mucosae appears disorganized, and submucosa is enlarged and encompasses fascicles of smooth muscle derived from the muscularis mucosae admixed, in a collagenous stroma, with hemangiomatic and lymphatic vessels, neural fibers, and ganglion-like cells with or without adipose tissue or other mesenchymal structures [30–33]. Amyloidosis and presence of inflammatory cells or lymphoid follicles at the upper edge of NMVH and focal duplication of the muscularis propria were also described [29, 31]. The proliferated vessels are small, with thin walls, or mature and positive to CD31/CD105 and smooth muscle actin (SMA) [34] and can show vasculitis, venopathic changes (“vessel-in-vessel” appearance of the veins, myointimal hump, concentric venous myohypertrophy, obliterative venopathy, etc.), or arteriopathies (concentric arterial medial hypertrophy, elastotic degeneration and crumpling of arterial elastic lamina, etc.) [31].

Fernando and McGovern described first two cases of NMVH, one in ileum and the other one in jejunum of two females (30 and 36 years) in 1982 [30]. Other 27 cases of the small intestine, located in jejunum or ileum of patients aged between 12 and 76 years, with a median age of 53.7 years and a male to female ratio of 1:1.5, were described till 2021 [29–33, 35]. Except the small intestine, NMVH can also involve the cecum, with two reported cases, one in a 76-year-old female [36] and one in a 13-year-old boy [37]. Sasaki et al. described one in the appendix of a 60-year-old male in 2020 [32]. One case of NMVH that was developed in a Meckel diverticulum was also reported in 2009 [38].

The clinical symptoms are nonspecific and consist of intermittent abdominal pain, vomiting, loss of weight and appetite, obstructive symptoms, diarrhea, occult hemorrhages, anemia, etc. [31–33]. In cecum, they can induce intussusception [37] and in appendix they can mimic an appendicitis [32].

Differential diagnosis of muscularization of the submucosa includes “burn-out phase” of Crohn’s disease, ischemic colitis with hyperplasia of muscularis mucosae, radiation enteritis, cryptogenic multifocal ulcerous stenosing enteritis (CMUSE), and other chronic inflammatory bowel diseases (IBDs) [30–32, 35, 39]. In chronic inflammatory lesions, NMVH-like

aspect can be induced by the mesenchymal morphologic response to inflammation [31] which is also known as type 2 epithelial to mesenchymal transition/mesenchymal metaplasia/neomuscularization responsible by tissue repair/fibrogenesis [31, 40, 41]. A similar lesion can be induced by consumption of nonsteroidal anti-inflammatory drugs (NSAIDs) and, because it is like a diaphragm-like annular stricture of the intestine, it was called “diaphragm disease” [29, 31]. In hamartomas with prominent neural proliferation, neurinomatous hyperplastic lesions such as paragangliomas, ganglioneuromas, glomus tumors, and neurofibromatosis need to be excluded [30].

4.2. Neuromesenchymal and Vascular Hamartoma. It is similar with NMVH but the mesenchymal components like adipose tissue and fibrous tissue are better represented [33]. In one of our cases, a similar lesion was found in the cecum of a 79-year-old female, without personal history of IBD or other significant diseases. This patient presented with obstructive symptoms and endoscopy was not successful, due to obstruction of the lumen. The abdominal contrasting computed tomography (CT) revealed the suspicion of an unusual cecal lipoma in which the contrast substance was absorbed in the upper edge of the lesion. Histopathological diagnosis revealed a well-defined lipomatous lesion covered by normal mucosa with submucosal proliferation of small podoplanin-positive lymphatic vessels, along with arterial and venous structures marked by CD31 and CD34, some of them enlarged or protruding into the mucosa. They were embedded in a collagenous stroma and in submucosa, muscularis mucosa was disorganized, and smooth muscle fiber bundles were scattered between the proliferated vessels (Figure 2). After surgical removal of hamartomatous lesion, no recurrences or other complications were reported after 13-month follow-up.

5. Mesenchymal Hamartomas

5.1. Mucosal Schwann Cell Hamartoma. It is an uncommon sessile lesion of the GI tract mucosa characterized by ill-defined proliferation of Schwann cells in the lamina propria, without whorls, palisading, fasciculation, or necrosis [34, 42]. These S100-positive elongated spindle cells have tapering small nuclei and well-defined eosinophilic cytoplasm and are

usually negative for neurofilament protein (NFP) [34, 43, 44]. In the past, these lesions were known as neuroma [45].

Gibson and Hornick described the first 26 cases of mucosal Schwann cell hamartomas of the colon presented as mucosal polyps [43]. Between 2008 and 2021, other 60 cases were reported. The 86 cases of the appendix ($n = 3$), proximal colon ($n = 16$), distal colon ($n = 57$), and rectum ($n = 10$) occurred in males and females with a median age of 60.2 years [43, 44]. Although Schwann cell hamartoma was considered as exclusively occurring in the colon, a series of 6 cases of gastroesophageal junction was published in 2020 by Li et al. [45].

As mucosal Schwann cell hamartomas can be multiple (4/86 cases), differential diagnosis includes von Recklinghausen's (type 1) neurofibromatosis, in which the mucosal crypts are not affected, and multiple neuromas from patients with multiple endocrine neoplasia type 2B (MEN 2B) [42–44]. As opposite, schwannoma is well circumscribed but not capsulated, is surrounded by a lymphoid peripheral cuff and is usually a solitary tumor [42, 43]. Schwannoma is more frequent in the distal colon followed by stomach and gastroesophageal junction [42–44]. Solitary ganglioneuroma, neurofibroma (ganglion cells are positive for CD34), leiomyoma (positive for smooth muscle actin), gastrointestinal stromal tumor (GIST), and perineuroma (formerly known as “benign fibroblastic polyp”) should also be excluded [34, 41, 45].

5.2. Neural Ectoderm-Derived Hamartomas. Systematized epidermal nevi of the esophagus are considered hamartomatous lesions originated from the neural ectoderm. This multisystemic syndrome mostly involves the brain, head and neck area, arms, and trunk. Oyesanya et al. reported the first case of verrucous epidermal naevi of the esophagus [46].

5.3. Rhabdomyomatous Mesenchymal Hamartoma. Hendrick et al. first described this “striated muscle hamartoma” in 1986 [47]. It is also known as “congenital midline hamartoma,” “hamartoma of cutaneous adnexa and mesenchyme,” and “skin tag hamartoma” [48, 49]. The commonest location is the deep dermis and the subcutaneous adipose tissue of the head and neck area of children (34 out of 46 cases reported up to 2016 and 88% of those published till 2019) but can also affect the jaw and rarely the tongue, orbit, back, appendages of the sacrum, digits, and even Eustachian tube [47–49]. Only four cases were reported in the perianal region [48, 49]. Rhabdomyomatous mesenchymal hamartomas are diagnosed as single or multiple papules or pedunculated or sessile polypoid lesions and are microscopically composed by randomly arranged disorganized desmin or myogenin-positive mature skeletal muscle fibers and myofibroblasts [48, 49]. Cleft lip/palate is commonly associated [49]. Differential diagnosis includes smooth muscle hamartoma, fetal rhabdomyoma/sarcoma, nevus lipomatous superficialis, infantile myofibromatosis, benign triton tumor (showing CTNNB1 mutation), and Langerhans-cell histiocytosis [47, 49]. In some cases, rhabdomyomatous mesenchymal hamartoma was described as part of the amnion band syndrome or Delleman (oculocerebrocutaneous) syn-

drome, which is characterized by absence of corpus callosum associated with colobomas, orbital cysts, cerebral cysts, skin tags, etc. [49].

5.4. Chondroma-Like Hamartomas. Chondromatous hamartoma is an uncommon intramural lesion of the esophagus composed by hyaline cartilage, spindle cells, and glandular structures [50]. It represents <7% of all benign polypoid lesions of the esophagus and are mainly located between muscle and mucosal layer and can be endoscopically resected [3, 50]. Differential diagnosis should firstly include low-grade chondrosarcoma, choristoma, and teratoma [50, 51].

Osteochondromatous hamartoma is a variant of chondromatous hamartoma in which cartilage proliferation is accompanied by bone, fat, and fibrous tissue [3]. Dysphagia, dry cough, vocal cord paralysis, vomiting, and infrequent weight loss can accompany these intramural lesions [50].

Chondroid hamartoma is composed by chondroid, adipose, and fibrous connective tissue [51].

Chondromesenchymal, angiomatous, lipomatous, and leiomyomatous hamartomas are other described variants [51]. Only 19 cases of esophageal hamartomas were reported to date, from which 8 involved the upper segment [50, 51]. Leiomyomatosis-like lymphangioleiomyomatosis was reported in three case reports, as a manifestation of tuberous sclerosis in colon and ileocecal segments. The epithelioid component can express melanoma markers such HMB-45 but is negative for C-kit, CD34, and DOG-1, which are characteristic for GISTs [52].

6. Heterotopic Hamartomas

6.1. Ectopic Pancreas. It is defined as abnormal presence of pancreatic tissue in anatomical areas which do not have continuity with the pancreas [9, 53]. It can be a solid or cystic lesion which mostly involves the stomach and small intestine but can be also developed in a Meckel's diverticulum, cystic duplication or other GI hamartomas [9, 53]. In 1909, von Heinrich classified the ectopic pancreas in two main groups, the classification being still available. It is about identification of ectopic tissue comprising ducts, acini, and Langerhans islands (type 1), presence of ducts and acini (type 2), or cystically dilated ducts only, without acini or endocrine component (Heinrich's type 3) [9, 54]. The main complications are hamartomatous chronic pancreatitis with pseudocyst formation, gastric outlet obstruction, and malignization [55].

6.2. Myoepithelial/Myoglandular Hamartoma. This hamartoma, which is also known as adenomyosis or ademyomata, is a variant of Heinrich's type 2 ectopic pancreas which appears as a submucosal mass of the GI tract [11, 55–58]. As it is especially located in the gastric antrum (85%) and pylorus (15%), Magnus-Alsleben called it in 1903 “adenoma of the pylorus” [56] being later called adenomyoma [57]. Only 58 cases were reported till 2019 in the stomach and 7 cases in the ampulla of Vater [11, 57, 59]. Under microscope, it is composed by smooth muscle bands admixed with glandular structures, some

of them cystically dilated, Brunner or pyloric glands, and trypsin-positive pancreatic acini [11, 57]. It can coexist with other malformations such as annular pancreas, gastric duplication, and duodenal adenomas [57]. In newborns, it can mimic the infantile hypertrophic pyloric stenosis [58]. Endoscopic submucosal resection can be the therapy of choice and the malignization rate is <2% [57].

6.3. Brunner's Gland Hamartoma. While Brunner described in 1688 the glands with the same name, Cruveilhier described first case of Brunner gland hamartoma in 1835 [60]. Then, the described lesion was separated in three entities: diffuse hyperplasia, localized hyperplasia, and hamartoma or adenoma which was recently denominated as benign glandular hyperplasia [10, 60–63]. It is about nodular or pedunculated uncommon submucosal masses of the duodenum diagnosed in adults [10, 60, 61]. About 70% of the cases involved the pylorus and duodenal bulb [64]. Only one pediatric pyloric localization was reported in literature [62, 63].

According to the Armed Forces Institute of Pathology, solitary or multiple masses below 5 mm in size, composed by excessive Brunner glands separated by fibrous septa, is indicated to be called “hyperplasia” [61, 64]. The term “hamartoma” is reserved to nonencapsulated solitary and larger than 5 mm, even giant masses, composed by sheets of Brunner glands along with acini and ducts, some being dilated, mesenchymal (smooth muscle bundles and adipose tissue), and lymphoid tissue, which are infrequently admixed with heterotopic pancreas [10, 61, 63]. Differentiation from an adenoma (Brunneroma) is not clearly defined in literature, and the two lesions are usually considered similar and were reported in patients between 24 and 76 years [59, 61, 63]. As incidence, 5–10% of duodenal benign lesions are thought to be Brunner's gland hamartomas [63].

Similar to other GI tract hamartomas, patients can be asymptomatic or present nonspecific symptoms such as abdominal pain, nausea, bilious vomiting, anemia, and intussusception [10, 61–63]. Treatment consists of endoscopic mucosal resection or surgical excision [10, 60], respectively, longitudinal pyloromyotomy with transverse pyloroplasty [62]. The main complications are intussusception and ileus. Although it was long-time known that malignization is not a complication of Brunner gland hyperplasia/hamartoma, recent data showed dysplasia in 2.1% and associated Brunner glands adenocarcinoma in 0.3% of cases [60, 64, 65].

The Brunner gland hyperplasia needs to be differentiated by polyposis syndromes, pancreatic heterotopia, pyloric/duodenal duplication cysts, nodular lymphoid hyperplasia or duodenitis, and tumors such as neuroendocrine neoplasm, lipoma, and leiomyoma [60, 62, 64].

6.4. Heterotopic Gastric Mucosa. It is an uncommon hamartoma of the cervical esophagus which is discovered incidentally in 1–10% of adults during screening endoscopies. It is predominantly composed by fundic-gland type (24%) followed by cardiac-gland type mucosa (15%), but most of the cases (61%) include both types [66]. Other segments of the GI tract, such as duodenum, jejunum, ileum, or Meckel's

diverticulum, can be infrequently involved. Although endoscopic resection is indicated, malignization was not reported.

7. Other Cystic Hamartomas

7.1. Duplication Cyst. The estimated incidence of GI tract duplications is 1:4500 live births [1]. Although 60% of the subepithelial lesions of the GI tract is supposed to be duplications [67], few cases can be found in English literature [68]. These enteric cysts are especially found in the ileum (33%), esophagus (20%), jejunum (10%), colon (13%), and stomach (2–9%) [1]. The appendix and duodenum are infrequently involved [1, 68–70]. A number of 50 cases were also reported as anal canal duplications [71].

First, jejunal duplication cyst was described in 1950 by Oyama [69] and, as it shares the mesenteric vascularization [67], was called “chyliferous cyst of the mesentery” [69]. Other 30 jejunal duplication cysts were reported till 2016 [9]. In the stomach, the lesion is also known as “double stomach” [68]. Distal greater curvature is mostly involved being followed by the posterior wall, the lesser curvature, the anterior wall, and pylorus [1, 68].

The patients can be asymptomatic, but if they are diagnosed in the first year of life or early childhood, mostly before the age of 12, abdominal pain, vomiting, weight loss, and even a palpable abdominal mass can be revealed [1, 68]. In adults, iron deficiency anemia, bleeding episodes, abdominal pain, nausea, vomiting, pancreatitis, and cholestasis might be the symptoms [68, 70].

These tubular or spheric malformative structures are attached by the adjacent GI segment and can communicate with the GI lumen or with the appendix or major duodenal papilla [9, 67, 70]. However, communication is not a condition for diagnosis and is not present in up to 80% of the cases [1, 9, 67]. To be diagnosed as a duplication cyst, the presence of a separate cyst-lining mucosa but a common muscular wall with the GI segment sharing a common blood supply is necessary to be proved [1]. Under microscope, the gastric or intestinal mucosa-lined cyst is surrounded by a well-defined smooth muscle coat, without a cleavage plane between the cyst and muscularis propria of the involved GI segment, making it contiguous with the GI wall [1, 9, 68]. In the anal canal duplication, the cyst is lined by squamous or transitional epithelium [71].

Inside the cyst, clear fluid is usually found, but bile and enteroliths were observed in duodenal cysts [70, 72]. The cystic wall might also incorporate an ectopic pancreas [9]. Depending on the localization, diameter, associated complications, and the experience of the surgical team, therapy consists of endoscopic removal or marsupialization, excision of the common wall, bypass, or surgical removal of the affected GI segment through laparotomy or laparoscopic methods [1, 9, 68, 70].

In some cases, they mimicked a neoplasm such as GIST or a neuroendocrine tumor [68]. In 11 cases reported in literature till 2018, gastric duplication cyst was reported as a premalignant lesion which predisposed to further development of carcinomas, especially adenocarcinomas or squamous cell carcinomas, but neuroendocrine tumors can also be developed [1]. In such

cases, elevated serum levels of carcinoembryonic antigen (CEA) or CA 19-9 can be found [1]. Although only one case of malignization a duplication of the anal canal was reported [71], the risk of malignization does not depend on the localization [70]. Elevated CEA can be found in patients with duplication cysts before malignization and can serve for identification of associated carcinomas in early stages [1].

7.2. Tailgut Cyst or Retrorectal Cystic Hamartoma. It is a duplication cyst located in the retrorectal-presacral space [73, 74]. It derives from a postnatal remnant of the hindgut and can show enteric or neuroenteric components. It is differentiated by the rectal cystic duplication by the absence of the smooth muscle coats. The male to female ratio is 1 : 5. The lesion varies from asymptomatic cyst to cystic structures which prolapses through the anal canal and can mimic hemorrhoids or dermoid cysts [73]. As development of neuroendocrine tumors, adenocarcinomas, and transitional or squamous cell carcinoma was reported in 24 cases [73, 74], the surgically resected specimens need to be attentively evaluated.

8. Summary and Future Perspectives

In GI tract, nonpolypous hamartomas proved to be more frequently incidentally diagnosed. Although rarely reported, their incidence seems to not be low, and more attention need to be paid to these mimickers. In some cases, neoplasms might be missed, and fatal hemorrhage or intestinal ileus can be the first symptoms, especially for hamartomas of the small intestine. In other cases, they can be premalignant lesions which evolve to transformation in carcinomas or neuroendocrine tumors. Large cohorts need to be examined to check the real incidence of nonpolypous GI hamartomas, at endoscopy or autopsy. As CEA level might be elevated in serum of patients with GI duplication cysts, this serum marker should not be used as an indicator of presence of a malignant tumor but should raise concerns about presence of a malformative lesion with risk for malignant transformation.

Data Availability

The literature data used to support the findings of this study are available from the corresponding author upon request. This is a systematic review of literature.

Conflicts of Interest

The authors have no conflict of interest to report.

Authors' Contributions

SG drafted the paper and contributed to the study design; DB contributed to the histopathological assessment and literature data assessment; IJ supervised the literature search process, contributed to the study design, and give the final consent for publication.

Acknowledgments

This work was supported by a grant of the Romanian National Authority for Scientific Research, CNCS – UEFISCDI, project number 20 PCCF/2018, code: PN-III-P4-ID-PCCF-2016-0006.

References

- [1] H. Tessely, A. Montanier, and E. Chasse, "Gastric duplication cyst with elevated CEA level: a case report," *Journal of Surgical Case Reports*, vol. 2018, no. 5, 2018.
- [2] E. Albrecht, "Ueber hamartome," *Verhandlungen der Deutschen Gesellschaft für Pathologie*, vol. 7, pp. 153–157, 1904.
- [3] J. Rasanen, I. Ilonen, A. Ristimäki, J. A. Salo, and A. A. Makitie, "A hamartoma presenting as an intramural upper oesophageal tumour," *Journal of Thoracic Disease*, vol. 9, no. 8, pp. E698–E701, 2017.
- [4] M. Wassef, F. Blei, D. Adams et al., "Vascular anomalies classification: recommendations from the International Society for the Study of Vascular Anomalies," *Pediatrics*, vol. 136, no. 1, pp. e203–e214, 2015.
- [5] I. Jung, S. Gurzu, and G. S. Turdean, "Current status of familial gastrointestinal polyposis syndromes," *World Journal of Gastrointestinal Oncology*, vol. 7, no. 11, pp. 347–355, 2015.
- [6] S. Gurzu, C. Copotoiu, C. Molnar, L. Azamfirei, and I. Jung, "Lethal gastric hemorrhage from a caliber-persistent artery of the antrum - a branch of the right gastric artery," *Hippokratia*, vol. 18, no. 2, pp. 172–176, 2014.
- [7] J. L. Senger and R. Kanthan, "The evolution of Dieulafoy's lesion since 1897: then and now-a journey through the lens of a pediatric lesion with literature review," *Gastroenterology Research and Practice*, vol. 2012, Article ID 432517, 2012.
- [8] S. Gurzu, C. Copotoiu, L. Azamfirei, and I. Jung, "A caliber persistent artery (Dieulafoy's lesion) which is associated with an early-stage gastric stump cancer following a distal gastrectomy," *Journal of Clinical and Diagnostic Research*, vol. 7, no. 8, pp. 1717–1719, 2013.
- [9] S. Gurzu, T. Bara Jr., T. Bara, A. Fetyko, and I. Jung, "Cystic jejunal duplication with Heinrich's type I ectopic pancreas, incidentally discovered in a patient with pancreatic tail neoplasm," *World Journal of Clinical Cases*, vol. 4, no. 9, pp. 281–284, 2016.
- [10] M. Maruo, T. Tahara, F. Inoue et al., "A giant Brunner gland hamartoma successfully treated by endoscopic excision followed by transanal retrieval: a case report," *Medicine (Baltimore)*, vol. 100, no. 14, article e25048, 2021.
- [11] T. Tanaka, K. Nishida, M. Iwamuro, S. Kikuchi, and T. Yoshino, "A case of myoepithelial hamartoma: morphological variation supported by OCT4 expression," *Case Reports in Gastrointestinal Medicine*, vol. 2021, Article ID 6617370, 2021.
- [12] N. Farkas, M. Conroy, and M. Baig, "A systematic review of symptomatic hamartomas of the jejunum and ileum," *Annals of the Royal College of Surgeons of England*, vol. 104, no. 1, pp. 18–23, 2022.
- [13] L. Kieswetter, T. D. Walters, I. Lara-Corrales, M. D. Carcao, B. Ngan, and E. Pope, "Dieulafoy lesions and PHACE syndrome," *Pediatric Dermatology*, vol. 36, no. 6, pp. 902–905, 2019.

- [14] S. Fataar, P. Morton, and A. Schulman, "Arteriovenous malformations of the gastrointestinal tract," *Clinical Radiology*, vol. 32, no. 6, pp. 623–628, 1981.
- [15] D. Voth, "Das architektonische Prinzip der magearterien in seiner Bedeutung für die Magenblutung," *Zentralblatt für allgemeine Pathologies und Pathologische Anatomie*, vol. 103, pp. 553–554, 1962.
- [16] G. Krasznai and V. Szokoly, "Congenital vascular malformation ("calibre-persistence") as a pathogenic factor of lethal gastric haemorrhage," *Acta Chirurgica Academiae Scientiarum Hungaricae*, vol. 9, no. 2, pp. 137–142, 1968.
- [17] J. D. Moore, N. W. Thompson, H. D. Appelman, and D. Foley, "Arteriovenous malformations of the gastrointestinal tract," *Archives of Surgery*, vol. 111, no. 4, pp. 381–389, 1976.
- [18] A. Türkvtan, P. Ozdemir Akdur, M. Akdoğan, T. Cumhuri, T. Ölçer, and E. Parlak, "Inferior mesenteric arteriovenous fistula with ischemic colitis: multidetector computed tomographic angiography for diagnosis," *The Turkish Journal of Gastroenterology*, vol. 20, no. 1, pp. 67–70, 2009.
- [19] S. Ganesanathan, J. Barlow, D. Durai, and A. B. Hawthorne, "Multiple venous malformations in the left colon and rectum: a long-standing case managed conservatively and an update of current literature," *BML Case Reports*, vol. 12, no. 3, article e227700, 2019.
- [20] A. R. Hermosa, J. Zorrilla-Ortuzar, and E. D. Valle-Hernández, "Diffuse cavernous hemangioma of the rectum," *Cirugia y Cirujanos*, vol. 89, no. 6, pp. 818–821, 2021.
- [21] S. X. Yang, Y. H. Zhou, J. Zhang et al., "Haemorrhagic ileal haemolymphangioma: a case report and review of the literature," *The Journal of International Medical Research*, vol. 49, no. 2, 2021.
- [22] S. El Zein, N. Gruel, S. Bonvalot, O. Mir, and S. Watson, "Neoadjuvant Everolimus for adult giant mesenteric cystic lymphangioma with mTOR pathway activation," *The Oncologist*, vol. 26, no. 7, pp. 554–557, 2021.
- [23] X. L. Ding, X. Y. Yin, Y. N. Yu, Y. Q. Chen, W. W. Fu, and H. Liu, "Lymphangiomatosis associated with protein losing enteropathy: a case report," *World Journal of Clinical Cases*, vol. 9, no. 15, pp. 3758–3764, 2021.
- [24] L. Pena Merino, R. Lopez Almaraz, A. Fernandez de Larrinoa, M. Rubio Lombrana, and M. R. Gonzalez-Hermosa, "Multifocal lymphangiendotheliomatosis without thrombocytopenia or clinical signs of systemic bleeding," *Pediatric Dermatology*, vol. 36, no. 6, pp. 965–966, 2019.
- [25] J. Manor, K. Patel, I. Iacobas, J. F. Margolin, and P. Mahajan, "Clinical variability in multifocal lymphangiendotheliomatosis with thrombocytopenia: a review of the literature," *Pediatric Hematology and Oncology*, vol. 38, no. 4, pp. 367–377, 2021.
- [26] R. M. Kline and L. M. Buck, "Bevacizumab treatment in multifocal lymphangiendotheliomatosis with thrombocytopenia," *Pediatric Blood & Cancer*, vol. 52, no. 4, pp. 534–536, 2009.
- [27] A. K. Shakir, Z. Yu, and M. A. Altaf, "Long-term complications and management of gastrointestinal bleeding in multifocal lymphangiendotheliomatosis," *Journal of Pediatric Hematology/Oncology*, vol. 41, no. 8, pp. e534–e537, 2019.
- [28] P. E. North, T. Kahn, R. M. Cordisco, S. S. Dadras, M. Detmar, and I. J. Frieden, "Multifocal lymphangiendotheliomatosis with thrombocytopenia: a newly recognized clinicopathological entity," *Archives of Dermatology*, vol. 140, no. 5, pp. 599–606, 2004.
- [29] J. Liu, Y. Liu, and Z. Ji, "Intestinal submucous fibrovascular hamartoma: a case report," *Radiology Case Reports*, vol. 16, no. 7, pp. 1857–1861, 2021.
- [30] S. S. Fernando and V. J. McGovern, "Neuromuscular and vascular hamartoma of small bowel," *Gut*, vol. 23, no. 11, pp. 1008–1012, 1982.
- [31] P. Ayyanar, S. Purkait, T. S. Mishra, S. Patra, and S. Mitra, "Histopathologic spectrum of neuromuscular and vascular hamartoma with special reference to the vasculopathic phenomenon," *International Journal of Surgical Pathology*, vol. 28, no. 4, pp. 382–392, 2020.
- [32] T. Sasaki, T. Furuhashi, M. Nishimura et al., "An extremely rare case of neuromuscular and vascular hamartoma of the appendix," *Surgical Case Reports*, vol. 6, no. 1, p. 216, 2020.
- [33] C. E. Smith, M. I. Filipe, and W. J. Owen, "Neuromuscular and vascular hamartoma of small bowel presenting as inflammatory bowel disease," *Gut*, vol. 27, no. 8, pp. 964–969, 1986.
- [34] C. Simsek, M. Uner, F. Ozkara et al., "Comprehensive clinicopathologic characteristics of intraabdominal neurogenic tumors: single institution experience," *World Journal of Clinical Cases*, vol. 9, no. 10, pp. 2218–2227, 2021.
- [35] S. Dhruv, S. Anwar, M. Kashi, and I. Mukherjee, "Neuromuscular and vascular hamartoma: starting point in Crohn's disease?," *Journal of Medical Cases*, vol. 12, no. 8, pp. 332–337, 2021.
- [36] T. Shiomi, K. Kameyama, Y. Kawano, Y. Shimizu, T. Takabayashi, and Y. Okada, "Neuromuscular and vascular hamartoma of the cecum," *Virchows Archiv*, vol. 440, no. 3, pp. 338–340, 2002.
- [37] Y. L. Chen, C. Y. Yu, C. H. Liu, D. H. Yang, G. S. Huang, and W. C. Chang, "Cecorectal intussusception induced by a cecal hamartoma," *Abdominal Imaging*, vol. 36, no. 1, pp. 46–49, 2011.
- [38] C. T. Hemmings, "Neuromuscular and vascular hamartoma arising in a Meckel's diverticulum," *Pathology*, vol. 38, no. 2, pp. 173–174, 2006.
- [39] L. Setaffy, M. J. M. Osuna, W. Plieschnegger, M. D. P. F. Rial, K. Geboes, and C. Langner, "Cryptogenic multifocal ulcerous stenosing enteritis (CMUSE), and neuromuscular and vascular hamartoma (NMVH): two sides of the same coin?," *Endoscopy*, vol. 47, no. 4, pp. 345–348, 2015.
- [40] S. Gurzu, L. Kobori, D. Fodor, and I. Jung, "Epithelial mesenchymal and endothelial mesenchymal transitions in hepatocellular carcinoma: a review," *BioMed Research International*, vol. 2019, Article ID 2962580, 2019.
- [41] S. Gurzu, S. Turdean, A. Kovacs, A. O. Contac, and I. Jung, "Epithelial-mesenchymal, mesenchymal-epithelial, and endothelial-mesenchymal transitions in malignant tumors: an update," *World Journal of Clinical Cases*, vol. 3, no. 5, pp. 393–404, 2015.
- [42] P. Pasquini, A. Baiocchi, L. Falasca et al., "Mucosal Schwann cell "hamartoma": a new entity?," *World Journal of Gastroenterology*, vol. 15, no. 18, pp. 2287–2289, 2009.
- [43] J. A. Gibson and J. L. Hornick, "Mucosal Schwann cell "hamartoma": clinicopathologic study of 26 neural colorectal polyps distinct from neurofibromas and mucosal neuromas," *The American Journal of Surgical Pathology*, vol. 33, no. 5, pp. 781–787, 2008.
- [44] T. Okamoto, T. Yoshimoto, and K. Fukuda, "Multiple non-polypoid mucosal Schwann cell hamartomas presenting as edematous and submucosal tumor-like lesions: a case report," *BMC Gastroenterology*, vol. 21, no. 1, p. 29, 2021.

- [45] Y. Li, P. Beizai, J. W. Russell, L. Westbrook, A. Nowain, and H. L. Wang, "Mucosal Schwann cell hamartoma of the gastroesophageal junction: a series of 6 cases and comparison with colorectal counterpart," *Annals of Diagnostic Pathology*, vol. 47, article 151531, 2020.
- [46] T. Oyesanya, E. Boozalis, S. G. Kwatra, and B. A. Cohen, "Oesophageal epidermal naevi as a feature of systematised epidermal naevus syndrome," *The Australasian Journal of Dermatology*, vol. 59, no. 2, pp. 128–130, 2018.
- [47] S. J. Hendrick, R. L. Sanchez, S. J. Blackwell, and S. S. Raimer, "Striated muscle hamartoma: description of two cases," *Pediatric Dermatology*, vol. 3, no. 2, pp. 153–157, 1986.
- [48] A. Sayan, G. Diniz, M. Mert, Z. Yildirim Ekin, and G. Koyluoglu, "Rhabdomyomatous mesenchymal hamartoma developed at an unexpected location," *Archivos Argentinos de Pediatría*, vol. 117, no. 5, pp. e519–e522, 2019.
- [49] K. Sampat, E. Cheesman, and S. Siminas, "Perianal rhabdomyomatous mesenchymal hamartoma," *Annals of the Royal College of Surgeons of England*, vol. 99, no. 6, pp. e193–e195, 2017.
- [50] C. Zhang, J. Xu, Z. Wang, Z. He, H. Yang, and J. Hu, "Chondromatous hamartoma of cervical esophagus: a case report and literature review," *Journal of Thoracic Disease*, vol. 9, no. 3, pp. E236–E244, 2017.
- [51] S. Hou, J. Wei, W. Lu, L. Wang, H. Liu, and Q. Zhang, "Intramural chondroid hamartoma in the distal esophagus in an adult: a case report and review of the literature," *Molecular and Clinical Oncology*, vol. 6, no. 1, pp. 19–22, 2017.
- [52] E. Erginoz, H. E. Taskin, G. H. Cavus, and A. K. Zengin, "Leiomyomatosis-like lymphangiomyomatosis: a case report of the colonic manifestation of tuberous sclerosis," *Medicine (Baltimore)*, vol. 100, no. 50, article e27723, 2021.
- [53] S. Hirasaki, M. Kubo, A. Inoue, Y. Miyake, and H. Oshiro, "Jejunal small ectopic pancreas developing into jejunojejunal intussusception: a rare cause of ileus," *World Journal of Gastroenterology*, vol. 15, no. 31, pp. 3954–3956, 2009.
- [54] H. von Heinrich, "Ein Beitrag zur Histologie des sogen: Akzesorischen Pankreas," *Virchows Archiv für Pathologische Anatomie und Physiologie und für Klinische Medizin*, vol. 198, no. 3, pp. 392–401, 1909.
- [55] C. F. Eisenberger, A. Kropp, T. E. Langwieler, A. Gocht, J. R. Izbicki, and W. T. Knoefel, "Heterotopic pancreatitis: gastric outlet obstruction due to an intramural pseudocyst and hamartoma," *Zeitschrift für Gastroenterologie*, vol. 40, no. 4, pp. 259–262, 2002.
- [56] E. Magnus-Alsleben, "Adenomyome des pylorus," *Virchows Archiv für Pathologische Anatomie und Physiologie und für Klinische Medizin*, vol. 173, no. 1, pp. 137–155, 1903.
- [57] S. Anand, A. K. Dhua, V. Bhatnagar, S. Agarwala, D. Kandasamy, and A. Kakkar, "Gastric adenomyosis: a rare cause of pyloric mass in children," *Journal of Indian Association of Pediatric Surgeons*, vol. 25, no. 3, pp. 172–174, 2020.
- [58] A. Aljadhali, A. Oviedo, and G. K. Blair, "Gastric hamartoma of the pylorus in an infant," *Journal of Pediatric Surgery*, vol. 47, no. 7, pp. E29–E31, 2012.
- [59] T. Tomoda, H. Kato, and H. Okada, "Myoepithelial hamartoma in the ampulla of Vater," *Clinical Gastroenterology and Hepatology*, vol. 17, no. 6, pp. e56–e57, 2019.
- [60] R. Rana, R. Sapkota, B. Kc, A. Hirachan, and B. Limbu, "Giant Brunner's gland adenoma presenting as upper gastrointestinal bleeding in 76 years old male: a case report," *JNMA; Journal of the Nepal Medical Association*, vol. 57, no. 215, pp. 50–52, 2019.
- [61] N. D. Patel, A. D. Levy, A. K. Mehrotra, and L. H. Sobin, "Brunner's gland hyperplasia and hamartoma: imaging features with clinicopathologic correlation," *AJR. American Journal of Roentgenology*, vol. 187, no. 3, pp. 715–722, 2006.
- [62] N. Petrasova, J. Snajdauf, O. Petru et al., "Gastric tumors in children: single-center study with emphasis on treatment of repeated recurrence," *Pediatric Surgery International*, vol. 36, no. 8, pp. 917–924, 2020.
- [63] A. Dhali, S. Ray, T. S. Mandal et al., "Surgical outcome of Brunner's gland hamartoma: a single-centre experience," *The Surgery Journal*, vol. 8, no. 1, pp. e14–e18, 2022.
- [64] S. Naito, M. Fukuzawa, S. Nakamura, S. Kono, J. Matsubayashi, and T. Itoi, "Giant Brunner's gland hamartoma diagnosed via endoscopic mucosal resection: a case report," *DEN Open*, vol. 2, no. 1, article e65, 2022.
- [65] T. Sakurai, H. Sakashita, G. Honjo, I. Kasyu, and T. Manabe, "Gastric foveolar metaplasia with dysplastic changes in Brunner gland hyperplasia: possible precursor lesions for Brunner gland adenocarcinoma," *The American Journal of Surgical Pathology*, vol. 29, no. 11, pp. 1442–1448, 2005.
- [66] K. Kishimoto, K. Shibagaki, S. Nonomura et al., "Heterotopic gastric mucosa in middle esophagus complicated with esophageal ulcers," *Internal Medicine*, 2022.
- [67] H. Ogino, T. Ochiai, N. Nakamura et al., "Duplication cyst of the small intestine found by double-balloon endoscopy: a case report," *World Journal of Gastroenterology*, vol. 14, no. 24, pp. 3924–3926, 2008.
- [68] M. Deesomsak, P. Aswakul, P. Junyangdikul, and V. Prachayakul, "Rare adult gastric duplication cyst mimicking a gastrointestinal stromal tumor," *World Journal of Gastroenterology*, vol. 19, no. 45, pp. 8445–8448, 2013.
- [69] V. E. Oyama, "Obstruction of the jejunum by a chyloferous cyst of the mesentery," *Revista Médica de Chile*, vol. 78, no. 4, pp. 280–281, 1950.
- [70] J. C. Ardengh, M. O. Brunaldi, R. Kemp, and J. S. D. Santos, "Duodenal duplication cyst with enteroliths diagnosed by echoendoscopy and treated by endoscopic marsupialization," *Arquivos de Gastroenterologia*, vol. 57, no. 1, pp. 110–111, 2020.
- [71] F. Akova, S. Altinay, and E. Aydin, "The controversy of surgical intervention for anal canal duplication in children," *Pakistan Journal of Medical Sciences*, vol. 36, no. 6, pp. 1330–1333, 2020.
- [72] A. K. Leite, A. I. David, and L. A. Szutan, "Duodenal duplication cyst filled with enteroliths: a case report," *Acta Gastroenterologica Latinoamericana*, vol. 39, no. 2, pp. 125–128, 2009.
- [73] M. Haydar and K. Griepentrog, "Tailgut cyst: a case report and literature review," *International Journal of Surgery Case Reports*, vol. 10, pp. 166–168, 2015.
- [74] M. Baverez, E. Thibaudeau, V. Libois, O. Kerdraon, H. Senellart, and J. L. Raoul, "Retrorectal mucinous adenocarcinoma arising from a tailgut cyst: a case report," *Case Reports in Oncology*, vol. 14, no. 1, pp. 147–151, 2021.

Research Article

Dissection of Immune Profiles in Microsatellite Stable and Low Microsatellite Instability Colon Adenocarcinoma by Multiomics Data Analysis

Tao Yang,^{1,2,3} Jiali Lei,^{1,2,3} Qiushi Feng,^{1,2,3} Dandan Song,^{1,2,3} and Xiaosheng Wang^{1,2,3} 

¹Biomedical Informatics Research Lab, School of Basic Medicine and Clinical Pharmacy, China Pharmaceutical University, Nanjing 211198, China

²Cancer Genomics Research Center, School of Basic Medicine and Clinical Pharmacy, China Pharmaceutical University, Nanjing 211198, China

³Big Data Research Institute, China Pharmaceutical University, Nanjing 211198, China

Correspondence should be addressed to Xiaosheng Wang; xiaosheng.wang@cpu.edu.cn

Received 23 December 2021; Revised 4 March 2022; Accepted 28 March 2022; Published 15 April 2022

Academic Editor: Simona Gurzu

Copyright © 2022 Tao Yang et al. This is an open access article distributed under the Creative Commons Attribution License, which permits unrestricted use, distribution, and reproduction in any medium, provided the original work is properly cited.

Background. Although microsatellite instability (MSI) is an indicator for active immunotherapy response, only 15% of colon adenocarcinoma (COAD) patients are with MSI. An investigation into the immune profiles in low MSI (MSI-L) and microsatellite stable (MSS) COAD remains lacking, whereas such exploration may provide new insights into COAD immunity. **Methods.** We hierarchically clustered MSI-L/MSS COAD based on the enrichment levels of 28 immune signatures to identify its immune-specific subtypes. We also comprehensively compared molecular and clinicopathologic profiles among these subtypes. **Results.** We identified three immune subtypes of MSI-L/MSS COAD (IM-H, IM-M, and IM-L), which had high, medium, and low immune signature scores, respectively. We demonstrated that this subtyping method was reproducible and predictable by analyzing five different datasets, including four bulk tumor datasets and one single-cell dataset. IM-H was characterized by high immunity, high stemness, strong potential of proliferation, invasion and metastasis, epithelial-mesenchymal transition, elevated expression of oncogenic pathways, low tumor purity, low intratumor heterogeneity (ITH), genomic instability, inferior response to chemotherapy, and unfavorable prognosis. IM-M was characterized by the highest ratio of immunostimulatory to immunosuppressive signatures, the best response to chemotherapy, and favorable prognosis. IM-L was characterized by low immunity, high tumor purity, high ITH, and genomic stability. **Conclusion.** The immune-specific subtyping of MSI-L/MSS COAD may provide new insights into the tumor immunity as well as clinical implications for immunotherapy of the COAD patients who lack MSI.

1. Introduction

Colorectal cancer (CRC), including colon cancer and rectal cancer, is the third most common cancer and the fourth leading cause of cancer deaths worldwide [1]. Although early-stage CRCs are often curative by surgical resection alone, late-stage CRCs have a poor prognosis due to recurrence or metastasis [2]. In CRC, colon cancer or colon adenocarcinoma (COAD) is more common than rectal cancer [3]. Previous studies have shown that COAD is highly heterogeneous in molecular profiles [4, 5]. For example, the

TCGA Research Network identified three molecular subtypes of COAD, including chromosomal instability (CIN), microsatellite instability (MSI), and CpG island methylator phenotype (CIMP) [6]. MSI, resulting from inactivation of the mismatch repair (MMR) system by either MMR gene mutations or hypermethylation of the MLH1 promoter, occurs in around 15% of colon cancers [7]. Based on the MSI status, COAD can be divided into three subgroups: MSI-H (high-frequency microsatellite instability), MSI-L (low-frequency microsatellite instability), and MSS (microsatellite stable). Major clinicopathologic and molecular

features show no significant difference between MSI-L and MSS tumors, although they are significantly different between MSI-H and MSI-L/MSS tumors [8]. MSI-H tumors are characterized by the strong lymphocyte infiltration, high tumor mutation burden (TMB), and high expression of immune checkpoint molecules, e.g., PD-L1 [9], and are thus more responsive to immunotherapies. As a result, MSI-H COAD patients have a more favorable prognosis than MSI-L/MSS patients [10].

Antitumor immunotherapies have recently been shown to be effective in treating various cancers [11]. Particularly, immune checkpoint inhibitors (ICIs) targeting cytotoxic T lymphocyte-associated antigen 4 (CTLA-4) and the programmed cell death protein 1 pathway (PD-1/PD-L1) have demonstrated successes in treatment of many refractory malignancies [12]. Nevertheless, currently, only a subset of cancer patients respond to ICIs [13]. To improve the response rate to ICIs in cancer patients, certain biomarkers have been identified, including *PD-L1* expression [14], TMB [15], and DNA damage repair deficiency or MSI [16]. In fact, besides its predictive value in the response to classic therapy with 5-FU [17], MSI is an indicator for the active response to immunotherapy [16]. Notably, the US Food and Drug Administration (FDA) have approved ICIs for treating solid tumors with high MSI [18]. Nevertheless, the immunotherapeutic efficiency for the majority of colon cancers, which are MSI-L/MSS, remains unclear or unexplored. Therefore, it is crucial to stratify MSI-L/MSS COAD patients responsive to immunotherapies.

It has been shown that the tumor immune microenvironment (TIME) plays a critical role in mediating antitumor immune response and immunotherapeutic response [19]. Thus, classification of MSI-L/MSS COADs based on the TIME may identify their subtypes responsive to immunotherapies. To this end, we aimed to identify subtypes of MSI-L/MSS COADs on the basis of the enrichment levels of 28 immune cells. We further analyzed molecular and clinicopathologic features of these subtypes, including pathway enrichment, genomic features, tumor phenotypes, and clinical outcomes. The identification of immune-specific subtypes may provide new insights into the pathogenesis of MSI-L/MSS COAD and potential clinical implications for immunotherapy of this disease.

2. Materials and Methods

2.1. Data Acquisition and Processing. We downloaded The Cancer Genome Atlas Colon Adenocarcinoma (TCGA-COAD) dataset, including RNA-Seq gene expression profiles (RSEM normalized), somatic mutation profiles (“maf” file), somatic copy number alterations (SCNAs) (“SNP6” files), protein expression profiles (Reverse Phase Protein Array (RPPA), normalized), pathological slides data, and clinical data, from the genomic data commons (GDC) data portal (<https://portal.gdc.cancer.gov/>). We obtained other COAD transcriptomic datasets (GSE39582, GSE41258, and GSE143985) from the NCBI gene expression omnibus (GEO) (<https://www.ncbi.nlm.nih.gov/geo/>). We also downloaded a single-cell RNA sequencing (scRNA-seq) dataset

(GSE132465 [20]) for COAD from the NCBI GEO. A summary of these datasets is shown in Supplementary Table S1.

2.2. Single-Sample Gene Set Enrichment Analysis. Based on gene expression profiles, the single-sample gene set enrichment analysis (ssGSEA) [21] calculates the enrichment score of a gene set in a sample, which represents the degree to which the genes in the gene set are coordinately up- or downregulated in the sample. We used the ssGSEA to evaluate the enrichment of immune cells, biological processes, and pathways in tumors based on the expression profiles of their marker or pathway genes. The marker or pathway genes are presented in Supplementary Table S2. We performed the ssGSEA with the R package “GSVA.”

2.3. Clustering Analysis. We hierarchically clustered MSI-L/MSS COAD to uncover its immune subtypes based on the enrichment scores of 28 immune cell types. These cell types included CD56-bright natural killer (NK) cells, effector memory CD4 T cells, eosinophil, CD56-dim NK cells, type 17 T helper cells, activated B cells, monocytes, memory B cells, activated CD4 T cells, type 2 T helper cells, plasmacytoid dendritic cells, neutrophils, macrophages, effector memory CD8 T cells, myeloid-derived suppressor cell (MDSC), immature B cells, T follicular helper cells, NK cells, immature dendritic cells, mast cells, type 1 T helper cells, activated dendritic cells, central memory CD4 T cells, gamma delta T cells, central memory CD8 T cells, regulatory T cells, activated CD8 T cells, and natural killer T cells [22]. The enrichment score of an immune cell type in a tumor was the ssGSEA score of its marker gene set in the tumor. Before clustering, we normalized the ssGSEA scores by *z*-score and transformed them into distance matrices by the R function “dist” with the parameter method = “Euclidean.” We performed hierarchical clustering using the function “hclust” in the R package “Stats” with the parameters method = “ward.D2” and members = NULL.

2.4. Class Prediction. To predict the immune subtypes of MSI-L/MSS COAD by the immune cell types, we first normalized attribute values (ssGSEA scores of immune cell types) by *z*-score. We used the random forest (RF) algorithm to perform the class prediction. In the RF, the number of trees was set to 100, and the attributes included all 28 immune cell types. We reported the accuracy and weighted *F*-score as the prediction performance. We implemented the class prediction by Weka (version 3.8.5) [23].

2.5. Survival Analysis. We used the Kaplan-Meier (K-M) model [24] to compare overall survival (OS) and disease-free survival (DFS) time among different groups of cancer patients. K-M curves were used to display the survival time differences, and log-rank tests were utilized to evaluate the significance of survival time differences. We performed survival analyses in TCGA-COAD and GSE39582 in which related data were available.

2.6. Evaluation of TMB, SCNA, ITH, Immune Scores, and Tumor Purity in Tumors. TMB was defined as the total count of somatic mutations in the tumor. We used GISTIC2

[25] to calculate G -scores in tumors with the input of “SNP6” files. The G -score indicates the amplitude of the SCNA and the frequency of its occurrence across a group of samples [25]. We used the DITHER algorithm [26] to evaluate ITH levels, which scores ITH at the DNA level. We utilized ESTIMATE [27] to evaluate immune scores and tumor purity for bulk tumors. The immune score indicates the tumor immune infiltration level and tumor purity the proportion of tumor cells in a bulk tumor.

2.7. Pathway and Gene Ontology (GO) Analysis. To identify pathways highly enriched in one class versus another class, we first identified upregulated genes in the class relative to another class using Student’s t test with a threshold of false discovery rate (FDR) < 0.05 and fold change (FC) > 2 . By inputting the upregulated genes into the GSEA web tool [28], we obtained highly enriched KEGG [29] pathways with a threshold of FDR < 0.05 . In addition, we used the weighted gene coexpression network analysis (WGCNA) [30] to identify the gene modules of coexpressed genes. Based on the expression correlations between the hub genes in gene modules, we identified the GO terms having significant correlations with specific traits. We performed the WGCNA analysis with the R package “WGCNA” (version 1.68).

2.8. scRNA-Seq Data Analysis. We analyzed a scRNA-seq dataset (GSE132465 [20]) for MSS COAD. The gene expression values have been normalized by natural log transformation of transcripts per million (TPM). We utilized the single-cell consensus clustering (SC3) method [31] to perform unsupervised clustering of cancer cells in each immune subtype. We used the inferCNV algorithm [32] to infer large-scale DNA copy number variations (CNVs) in cancer cells versus normal cells. We normalized the CNV values of cells output by inferCNV by subtracting the average of the maximum and minimum values in the matrix of CNV values to make the “0” representing the copy number in normal cells. We defined the CNV score of each cell as the average of quadratic sum of the CNV values for all genes.

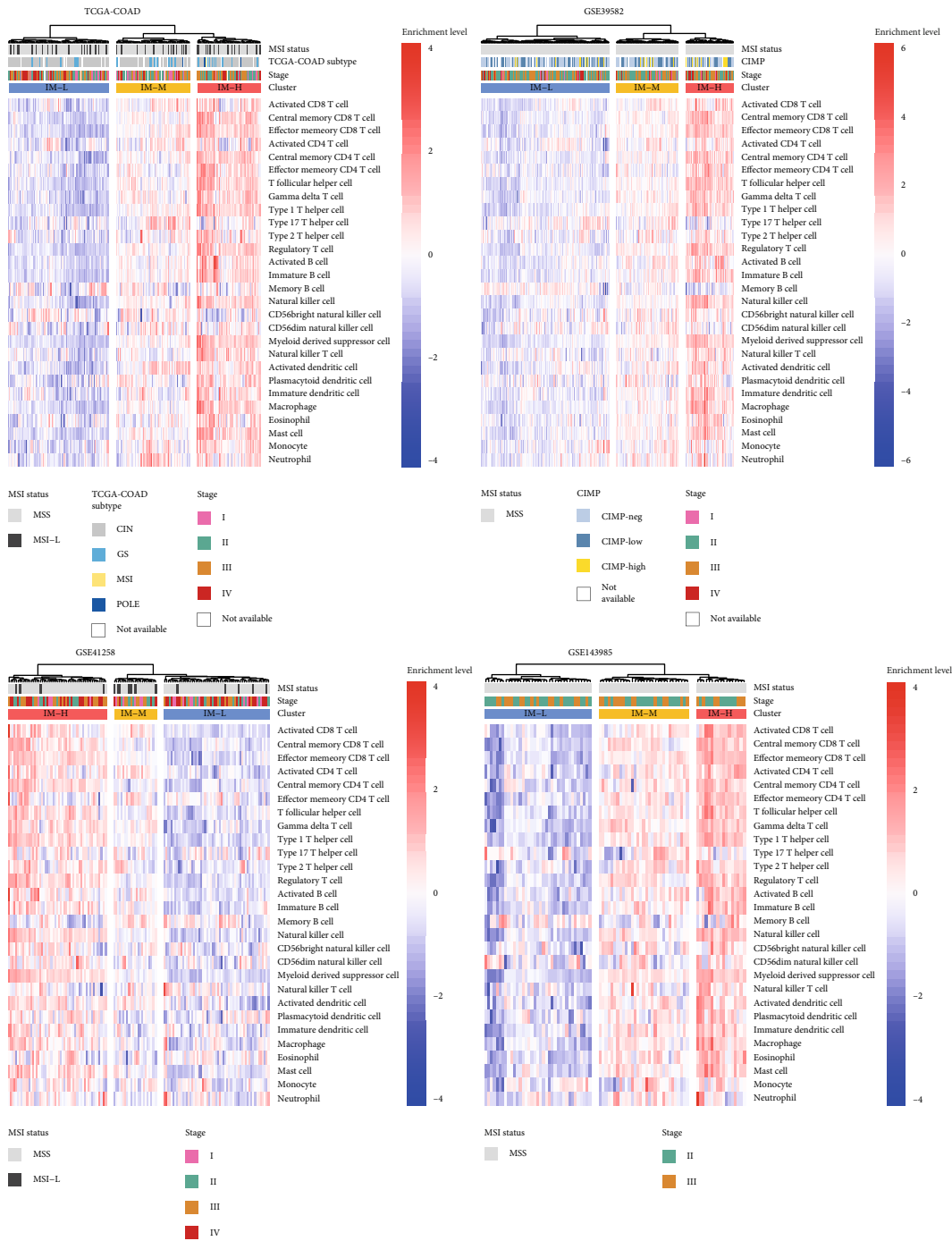
2.9. Statistical Analysis. We used Student’s t test (two-tailed) to compare two classes of normally distributed data, including gene expression levels, protein expression levels, and the ratios of two different immune signatures. The ratios were the log₂-transformed values of the average expression levels of all marker genes in an immune signature divided by those of all marker genes in another immune signature. In comparisons of two classes of nonnormally distributed data, such as ssGSEA scores of gene sets, TMB, ITH, immune scores, and tumor purity, we used the Mann–Whitney U test (one-tailed). We utilized the Spearman method to evaluate the correlation between pathway activities (ssGSEA scores) and immune scores. The Fisher’s exact test was used to analyze contingency tables. To adjust for P values in multiple tests, we calculated FDR with the Benjamini and Hochberg method [33]. We performed all statistical analyses with the R programming language (version 3.6.0).

3. Results

3.1. Clustering Analysis Identifies Three Immune Subtypes of MSI-L/MSS COAD. Based on the enrichment scores of 28 immune cell types, we identified three subtypes of MSI-L/MSS COAD by hierarchical clustering, consistently in the four bulk transcriptome datasets (TCGA-COAD, GSE39582, GSE41258, and GSE143985) (Figure 1). The three subtypes had high, medium, and low enrichment scores of the immune cells, termed IM-H, IM-M, and IM-L, respectively. The consistent clustering results demonstrate the reproducibility of this classification method. Furthermore, to explore whether this classification is predictable, we used the TCGA-COAD dataset as the training set and the other three datasets as test sets. The 10-fold cross-validation (CV) accuracy in the training set was 89.52%. The prediction accuracies were 82.88%, 72.93%, and 87.06% in GSE39582, GSE41258, and GSE143985, respectively (Figure 1(b)). The weighted F -scores in these predictions were 89.60%, 83.40%, 75.00%, and 87.30% for TCGA-COAD, GSE39582, GSE41258, and GSE143985, respectively (Figure 1(b)). Overall, these results demonstrate that the immunological classification of MSI-L/MSS COAD is reproducible and predictable.

Notably, both immunostimulatory signatures (such as M1 macrophages, activated CD8 T cells, and NK cells) and immunosuppressive signatures (such as M2 macrophages, regulatory T cells, MDSCs, and *PD-L1*) showed the highest enrichment scores in IM-H and the lowest enrichment scores in IM-L (one-tailed Mann–Whitney U test or two-tailed Student’s t test, $P < 0.001$) (Figure 2(a)). However, the ratios of immunostimulatory to immunosuppressive signatures (M1/M2 macrophages) were the highest in IM-M among the three subtypes (two-tailed Student’s t test, $P < 0.05$) in TCGA-COAD (Figure 2(b)). We further compared the percentages of tumor-infiltrating lymphocytes (TILs) among the three subtypes provided by the pathology slide data in TCGA-COAD. As expected, the percentages of TILs were significantly higher in IM-H than in IM-M and IM-L ($P < 0.001$) (Figure 2(c)). Taken together, these results confirmed that IM-H and IM-L had the highest and lowest enrichment of immune signatures, respectively.

We compared OS and DFS rates among the immune subtypes of MSI-L/MSS COAD in TCGA-COAD and GSE39582, in which related data were available. Survival analyses showed that IM-M had better DFS than IM-H and IM-L (log-rank test, $P < 0.05$) in TCGA-COAD, while there was no significant difference of DFS between IM-H and IM-L in this cohort ($P = 0.49$) (Figure 2(d)). Moreover, IM-M displayed better OS than IM-L in TCGA-COAD ($P < 0.05$) (Figure 2(d)). In GSE39582, IM-M showed better OS than IM-H ($P = 0.01$), and IM-L had better DFS than IM-H ($P < 0.05$) (Figure 2(d)). Taken together, these results indicate that IM-M and IM-H likely have the best and worst survival, respectively. In addition, we compared the response rate to chemotherapy among the three immune subtypes in TCGA-COAD. We found that the response (complete or partial response) rate to chemotherapy followed the pattern IM-M (77.78%) $>$ IM-L (70.59%) $>$ IM-H (50.00%) (Figure 2(e)), supporting the results of prognostic analysis.



(a)

FIGURE 1: Continued.

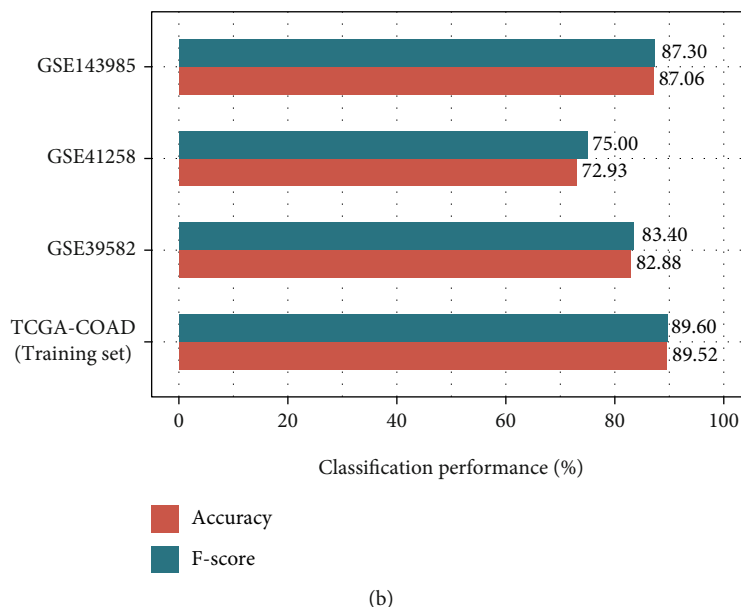


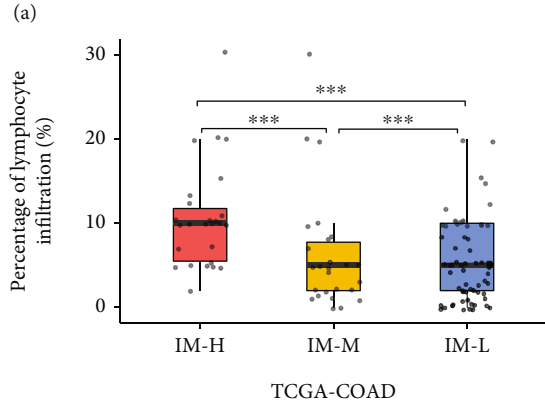
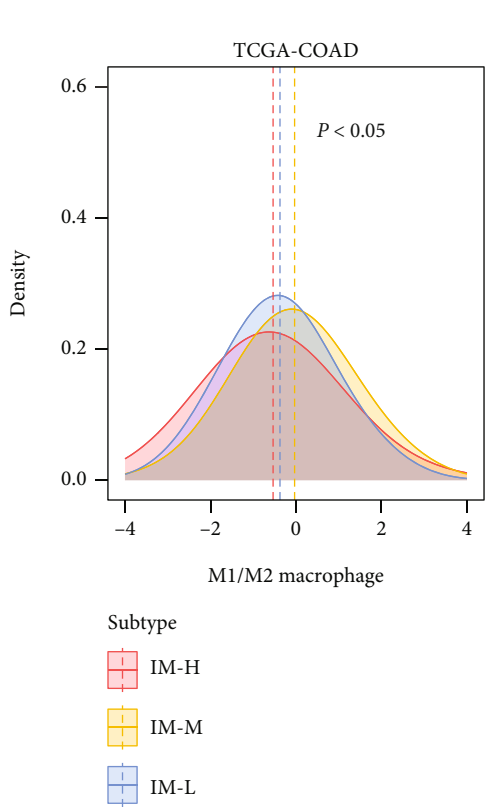
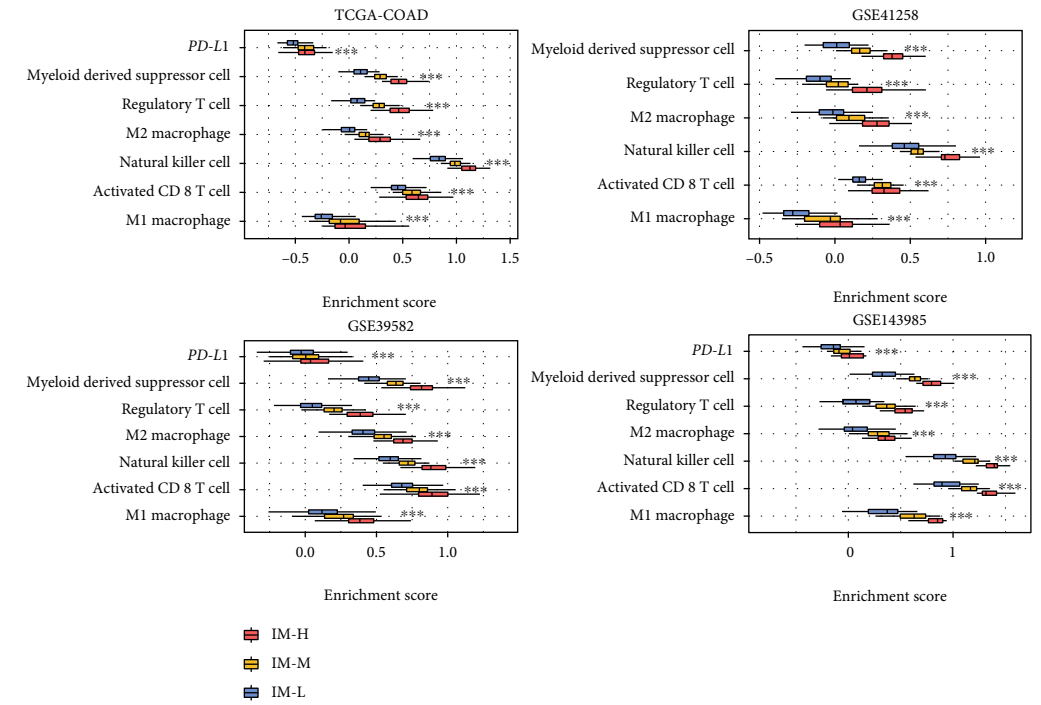
FIGURE 1: Hierarchical clustering of MSI-L/MSS COAD bulk tumors based on the enrichment of 28 immune cell types. (a) Clustering analyses uncovering three immune subtypes of MSI-L/MSS COAD, IM-H, IM-M, and IM-L, which have high, medium, and low immune cell enrichment scores, respectively, consistently in four datasets. (b) Prediction of the three immune subtypes of MSI-L/MSS COAD by random forest based on the enrichment scores of 28 immune cell types. TCGA-COAD dataset as the training set and the other three datasets as test sets. The 10-fold cross-validation results in the training set and prediction results in the other datasets are shown.

3.2. The Immune Subtypes of MSI-L/MSS COAD Have Significantly Different Phenotypic and Molecular Features. We observed that the phenotypic or molecular features indicative of tumor progression, such as stemness, epithelial-mesenchymal transition (EMT), proliferation, invasion, and metastasis, were significantly more enriched in IM-H compared to IM-M and IM-L ($P < 0.05$) (Figure 3(a)). Furthermore, numerous oncogenic pathways displayed significantly higher enrichment in IM-H versus IM-M and IM-L ($P < 0.001$), including the pathways of PI3K-Akt, VEGF, JAK-STAT, RAS, HIF-1, and MAPK signaling (Figure 3(b)). In contrast, tumor purity was significantly lower in IM-H than in IM-M and IM-L ($P < 0.001$) (Figure 3(c)); ITH scores followed the pattern IM-H < IM-M < IM-L ($P < 0.05$) (Figure 3(d)).

There was no significant difference of TMB among the three immune subtypes of MSI-L/MSS COAD (Kruskal-Wallis test, $P = 0.568$). However, tumor aneuploidy, namely, copy number alteration (CNA), showed significant difference among the subtypes, as evidenced by that the G -scores of copy number amplifications and deletions were the highest in IM-L and the lowest in IM-H (Figure 3(e)). Since the G -score represents the amplitude of CNA and the frequency of its occurrence across a group of samples [25], it indicated that IM-L and IM-H had the highest and lowest CNA, respectively. This result is in agreement with the previous studies showing that tumor aneuploidy correlates with reduced antitumor immune response [34]. Furthermore, we compared the enrichment scores of nine major DNA damage repair (DDR) pathways among the subtypes. These pathways included mismatch repair, base excision repair, nucleotide excision repair, the Fanconi anemia

(FA) pathway, homology-dependent recombination, nonhomologous DNA end joining, direct damage reversal/repair, translesion DNA synthesis, and damage sensor [35]. Notably, the enrichment scores of nine DDR pathways followed the pattern IM-L > IM-M > IM-H ($P < 0.05$) (Figure 3(f)). Together, these results indicated that IM-L and IM-H had the highest and lowest genomic instability, respectively.

We found 14 genes more frequently mutated in IM-H than in IM-L (Fisher's exact test, $P < 0.05$; odds ratio (OR) > 3). These genes included *USH2A*, *HMCN1*, *PTPRT*, *ADAMTSL3*, *TDRD6*, *TRO*, *TCHH*, *ATP8A2*, *CCDC9*, *DCDC5*, *FADS3*, *LRRC7*, *NOTCH3*, and *SPG20*. Notably, the mutations in each of these genes were correlated with significantly higher immune scores in MSI-L/MSS COAD ($P < 0.05$) (Supplementary Table S3). On the contrary, seven genes showed a significantly higher mutation rate in IM-L than in IM-H ($P < 0.04$; OR > 7), including *APC*, *CHD5*, *DCLK1*, *FBXL7*, *COL6A6*, *KRTAP10-10*, and *PCDHGA5*. *APC* is a tumor suppressor gene involved in the regulation of WNT signaling, whose mutations are prevalent in nonhypermutated tumors [36]. The *APC* mutations in IM-L were mainly truncating mutations (Figure 3(g)), which may initiate chromosome instability [37, 38]. This could partially explain why IM-L had higher genomic instability than IM-H. Furthermore, we compared gene mutation profiles between IM-M and IM-H/L. Notably, IM-H/L displayed a significantly higher frequency of *CUBN* mutations than IM-M ($P = 0.037$; OR = 7.15). A previous study has demonstrated that *CUBN* mutations might promote the malignancy of CRC [39]. There were 28 genes showing a significantly higher mutation rate in IM-M than in IM-H/L ($P < 0.05$; OR > 2). Noticeably, the



(b)

(c)

FIGURE 2: Continued.

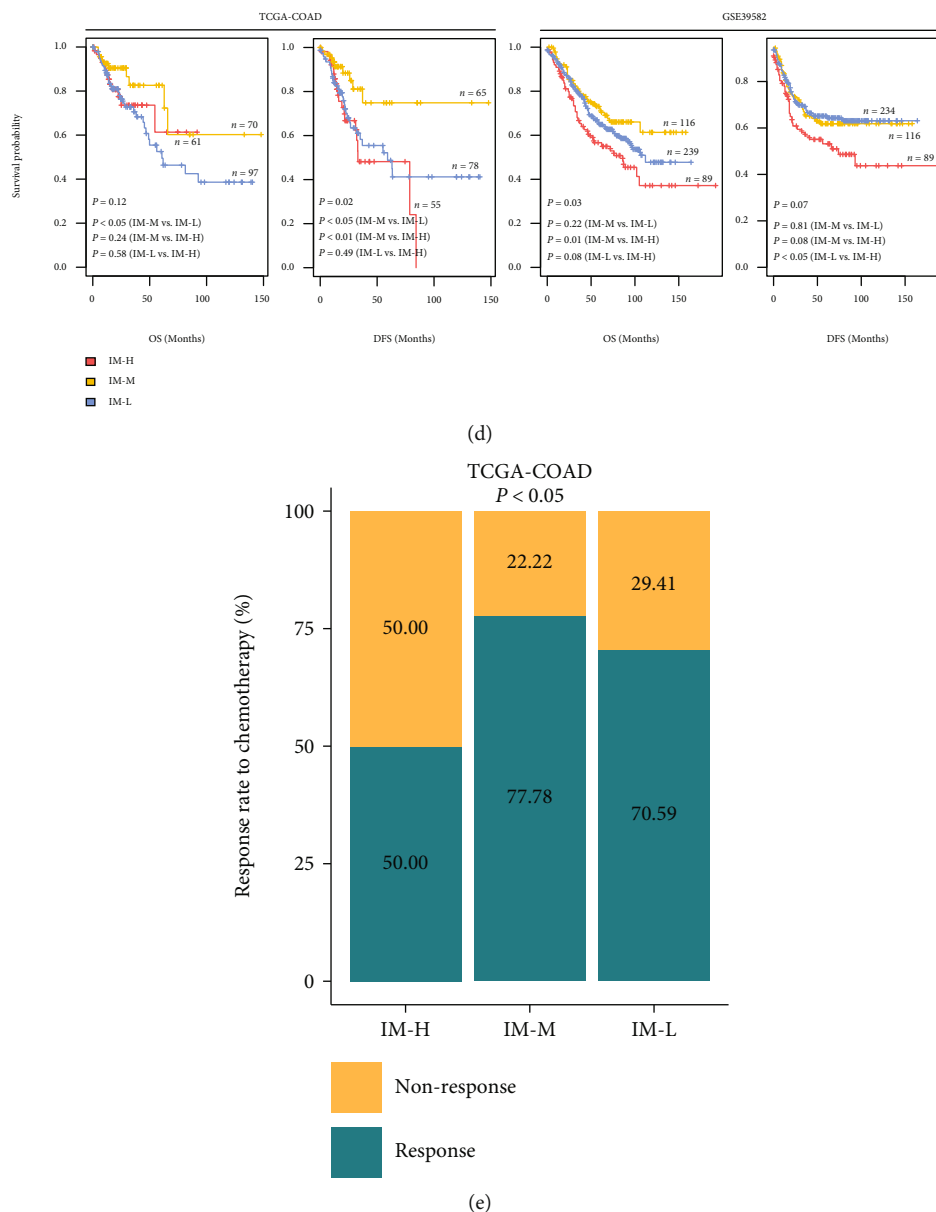


FIGURE 2: Comparisons of immune signature enrichment and clinical outcomes among the three immune subtypes. Comparisons of the enrichment scores of immunostimulatory signatures (M1 macrophages, activated CD8 T cells, and NK cells) and immunosuppressive signatures (M2 macrophages, regulatory T cells, myeloid-derived suppressor cells (MDSCs), and *PD-L1*) (a), ratios of immunostimulatory to immunosuppressive signatures (M1/M2 macrophages) (b), and the percentage of tumor-infiltrating lymphocytes (TILs) (c) among the three immune subtypes. The Kruskal–Wallis test (a), one-way ANOVA (b), and one-tailed Mann–Whitney *U* test (c). *P* values are shown. * $P < 0.05$, ** $P < 0.01$, *** $P < 0.001$, and ^{ns} $P \geq 0.05$. It also applies to the following figures. (d) Comparisons of overall survival (OS) and disease-free survival (DFS) rates among the immune subtypes by the Kaplan–Meier curves. The log-rank test *P* values are shown. (e) Comparisons of the response (complete or partial response) rates to chemotherapy among the three immune subtypes in TCGA-COAD. The chi-square test *P* value is shown.

mutation frequency of *NOTCH3* was significantly higher in IM-M than in IM-H/L ($P = 0.011$; OR = 5.16), and its mutation was associated with a higher OS rate in MSI-L/MSS COAD ($P = 0.033$) (Figure 3(h)).

We compared the expression of 226 proteins among the subtypes. We found 45 proteins significantly upregulated in IM-H relative to IM-L (two-tailed Student's *t* test, FDR < 0.05) (Figure 3(i) and Supplementary Table S4). Many of these proteins were protein kinases involved in signal

transduction, such as p38_MAPK, MEK1, MAPK_pT202_Y204, and Lck. Several cluster of differentiation CD molecules were also in the list of the 45 proteins, such as CD20, CD26, and CD31, supporting the higher tumor immunity in IM-H versus IM-L. The 45 proteins also included some molecules involved in immune regulation, such as ETS1 [40], Annexin-1 [41, 42], and Lck [43]. In contrast, 48 proteins showed significantly higher expression levels in IM-L than in IM-H (Figure 3(i) and

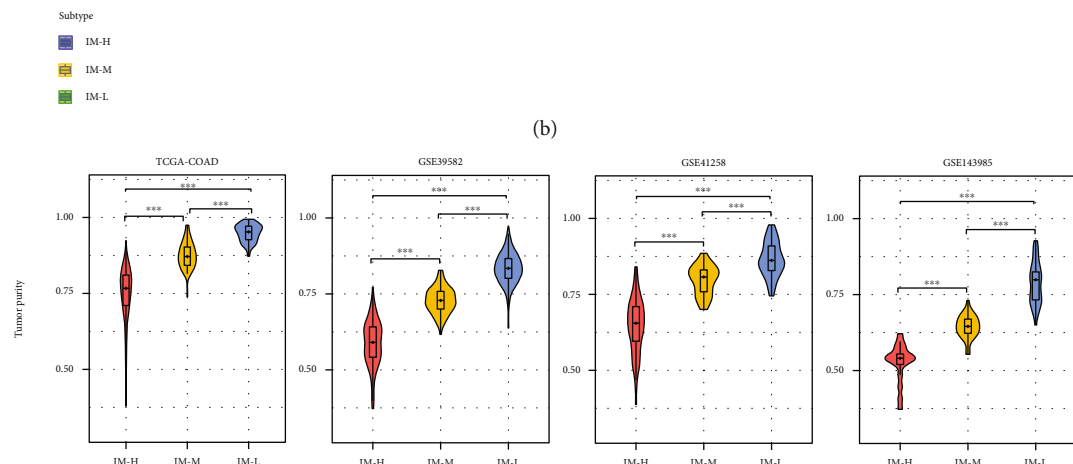
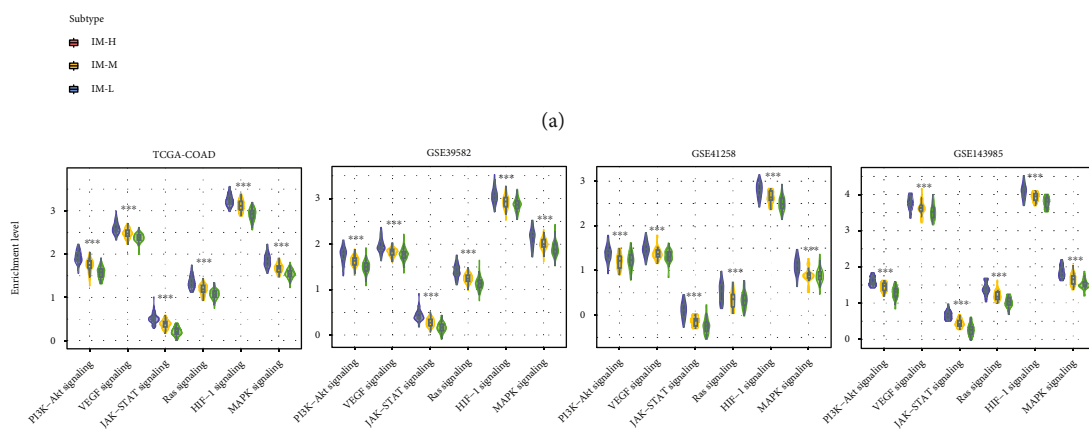
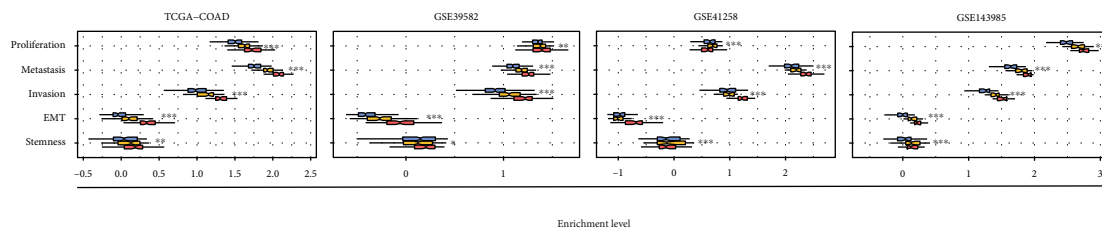
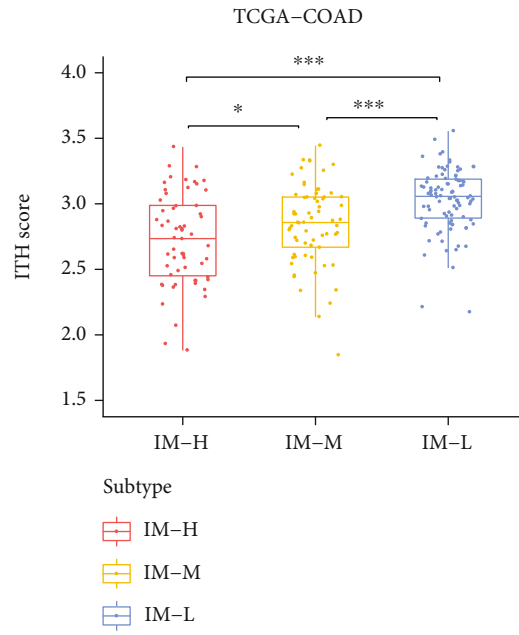
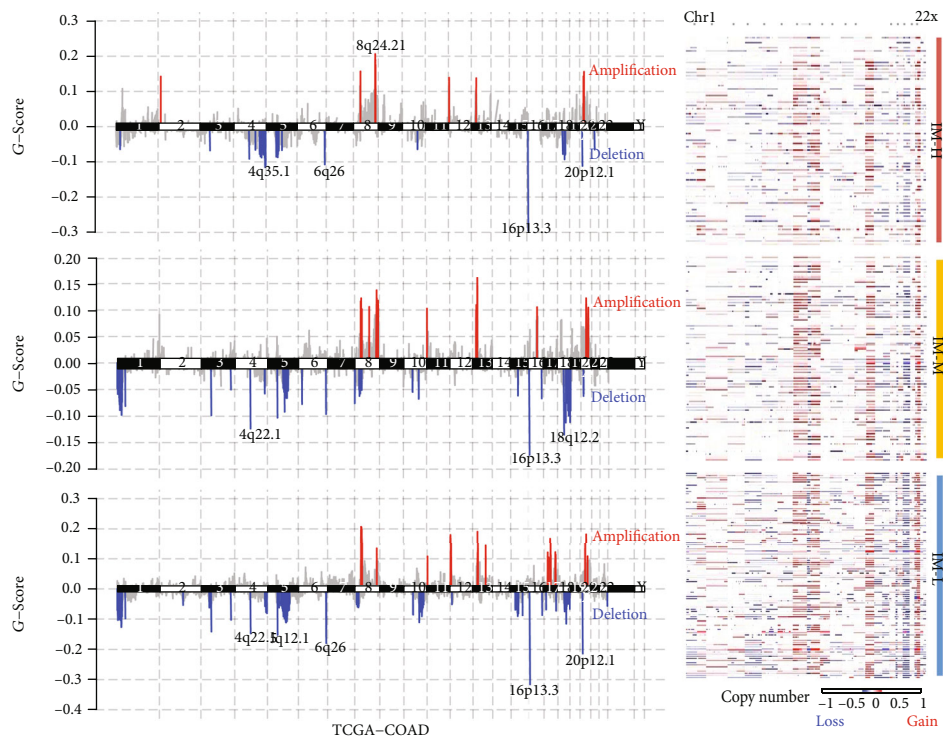


FIGURE 3: Continued.



(d)



(e)

FIGURE 3: Continued.

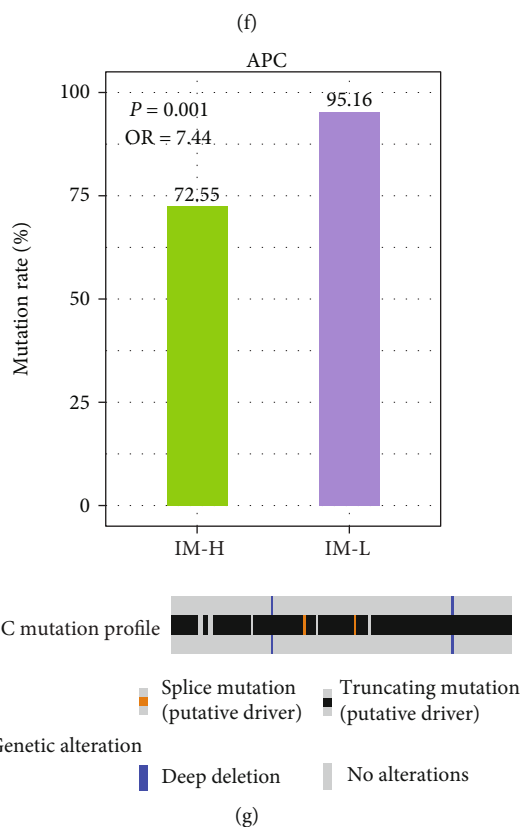
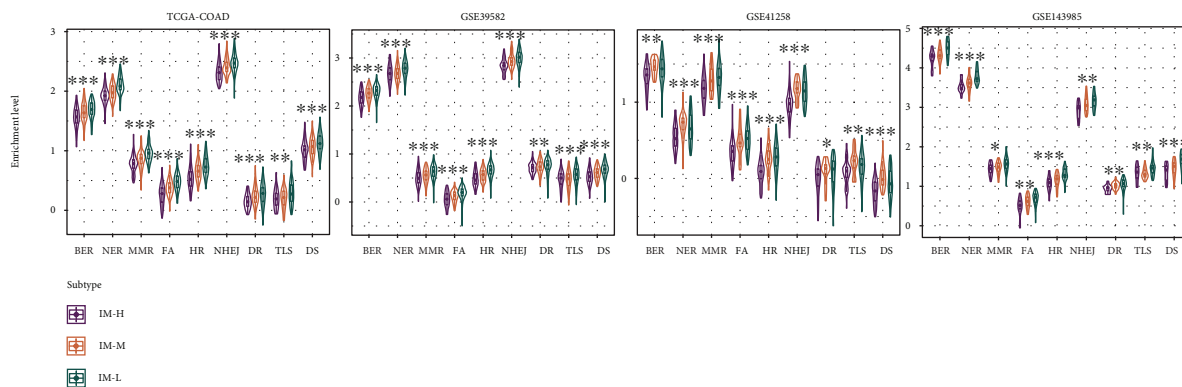
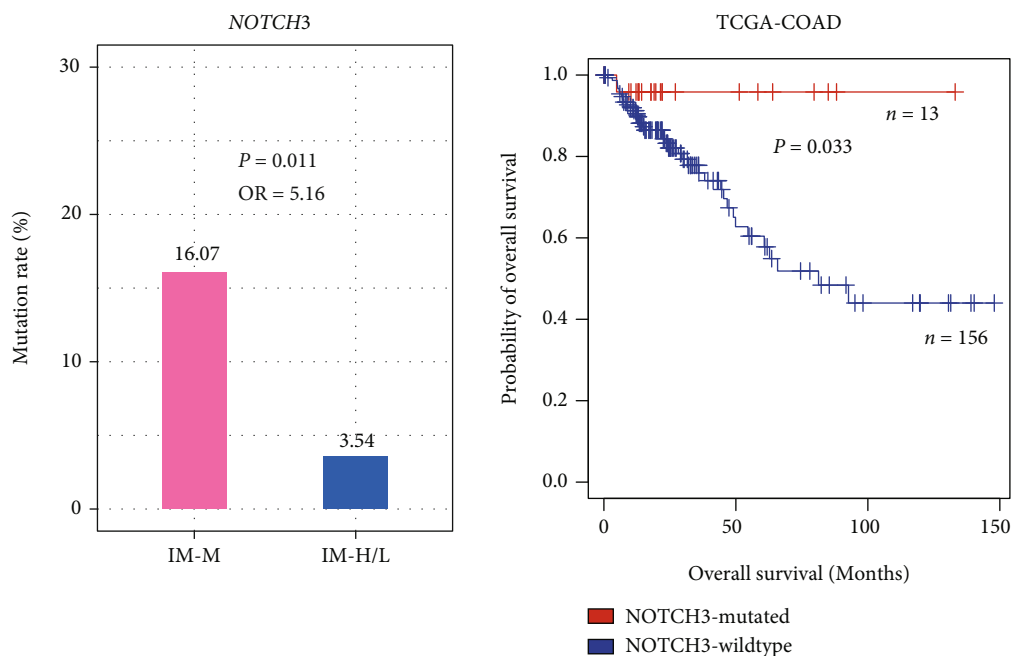
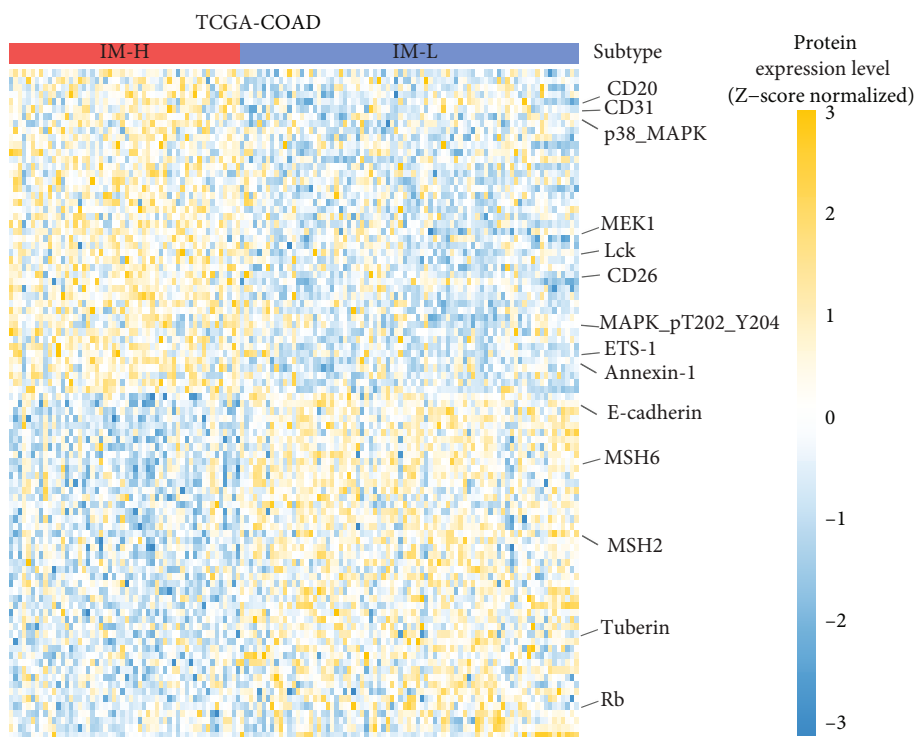


FIGURE 3: Continued.



(h)



(i)

FIGURE 3: Comparisons of phenotypic and molecular features among the immune subtypes. Comparisons of the tumor progressive phenotypic or molecular features (a), oncogenic pathways (b), tumor purity (c), intratumor heterogeneity (ITH) (d), copy number alteration (G-scores) (e), and DNA damage repair (DDR) pathways (f) among the three immune subtypes. The Kruskal–Wallis test (a and b) and one-tailed Mann–Whitney U test (c, d, and f) P values are shown. (g) Comparisons of *APC* mutation rate between the high (IM-H) and low (IM-L) immune subtypes and showing *APC* mutation profiles in IM-L. (h) Comparisons of *NOTCH3* mutation rate between the medium (IM-M) and the other two (IM-H/L) immune subtypes and overall survival rate between *NOTCH3*-mutated and *NOTCH3*-wild-type MSI-L/MSS COAD in TCGA-COAD. The Fisher’s exact test P values are shown in (g and h). (i) Heatmap showing the proteins with significant expression differences between IM-H and IM-L in TCGA-COAD (two-tailed Student’s t test, FDR < 0.05).

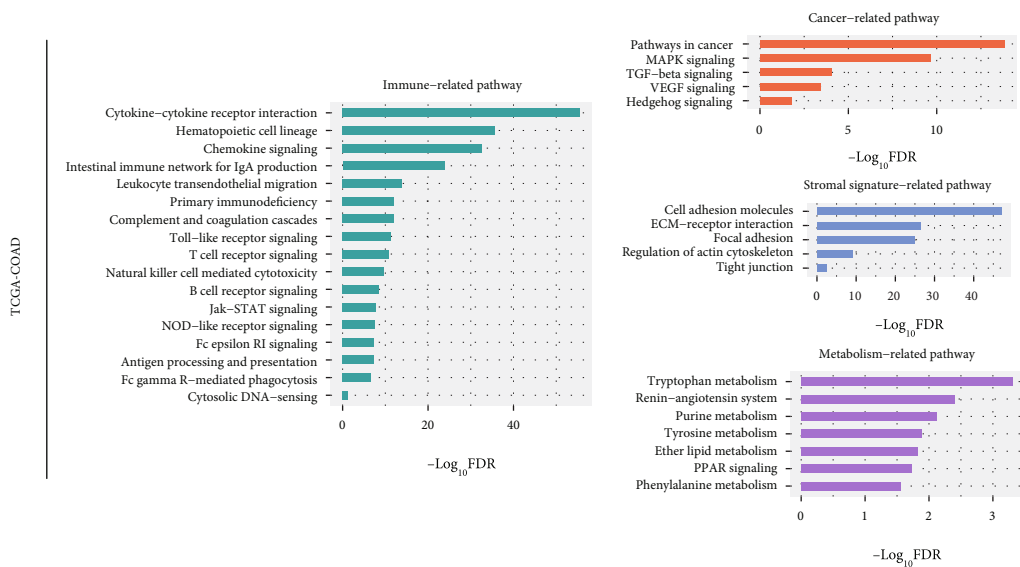
Supplementary Table S4). Notably, two DNA mismatch repair proteins (MSH2 and MSH6) were in the list of the 48 proteins. In addition, several tumor suppressors, such as Rb, tuberlin, and E-cadherin, were upregulated in IM-L relative to IM-H. The higher enrichment of these tumor suppressors in IM-L could explain why IM-L had a better relapse-free survival rate than IM-H.

3.3. Identification of Pathways and GO Highly Enriched in the Immune Subtypes of MSI-L/MSS COAD. Pathway analysis by GSEA [28] identified numerous KEGG pathways highly enriched in IM-H versus IM-L in TCGA-COAD. These pathways were mainly involved in immune, stromal, oncogenic, and metabolic signatures (Figure 4(a)). The immune-related pathways included cytokine-cytokine receptor interaction, hematopoietic cell lineage, chemokine signaling, intestinal immune network for IgA production, leukocyte transendothelial migration, complement and coagulation cascades, primary immunodeficiency, Toll-like receptor signaling, T cell receptor signaling, natural killer cell mediated cytotoxicity, B cell receptor signaling, Jak-STAT signaling pathway, NOD-like receptor signaling, Fc epsilon RI signaling, antigen processing and presentation, Fc gamma R-mediated phagocytosis, and cytosolic DNA-sensing pathway. It confirmed that IM-H had higher immune activity than IM-L. The stromal signature-related pathways included cell adhesion molecules, ECM-receptor interaction, focal adhesion, regulation of actin cytoskeleton, and tight junction. The cancer-related pathways included pathways in cancer, MAPK, TGF- β , VEGF, and Hedgehog signaling. The metabolism-related pathways included tryptophan metabolism, renin-angiotensin system, purine metabolism, tyrosine metabolism, ether lipid metabolism, PPAR signaling, and phenylalanine metabolism. As expected, in addition to the immune-related pathways, most of the other pathways showed significantly positive correlations of their enrichment scores with immune scores in MSI-L/MSS COAD (Spearman's correlation, $P < 0.05$) (Figure 4(b)).

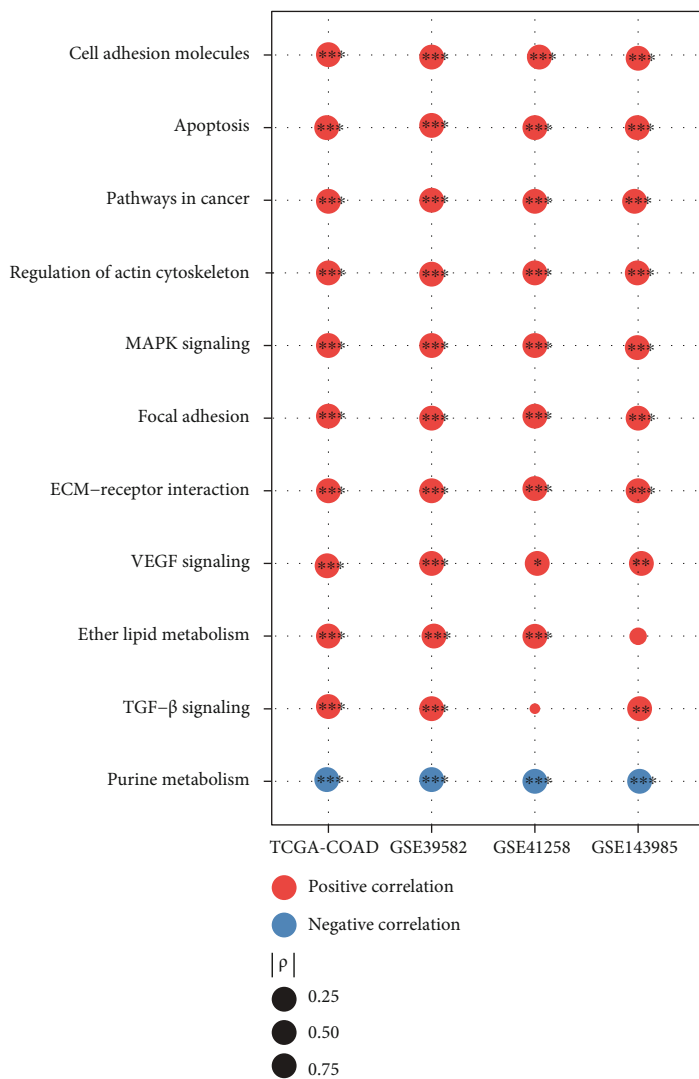
WGCNA [30] identified seven gene modules significantly differentiating MSI-L/MSS COAD by the subtypes and survival prognosis in TCGA-COAD (Figure 4(c)). Notably, six gene modules (highlighted in blue, yellow, brown, turquoise, black, and green, respectively) were significantly upregulated in IM-H, while they were downregulated in IM-L ($P < 0.001$). Interestingly, these gene modules' enrichment was consistently and negatively correlated with OS and/or DFS time ($P < 0.05$) (Figure 4(c)). The representative GO terms for these gene modules included innate immune response, adaptive immune response, binding, extracellular matrix, neuron part, and muscle system process (Figure 4(c)). It is in agreement with the previous results that immune and stromal pathways are upregulated in IM-H relative to IM-L. Besides, there was a gene module (highlighted in red) significantly upregulated in IM-M but downregulated in IM-L ($P < 0.01$). The representative GO term for this gene module was UDP-glycosyltransferase activity. UDP-glycosyltransferase activity accelerates metabolic inactivation of drug therapies

to produce drug resistance and affects cancer progression [44, 45]. That is, patients in the IM-L subtype are more likely to benefit from drug treatment because of low drug resistance.

3.4. Clustering Analysis Identifies Three Immune Subtypes of MSI-L/MSS COAD Single Cells. We performed a similar clustering analysis of MSI-L/MSS COAD single cells using a scRNA-seq dataset (GSE132465). This dataset involved gene expression profiles in 12,484 cancer cells from 16 MSS COAD patients. We hierarchically clustered these cancer cells based on the enrichment scores of four immune-related pathways, including antigen processing and presentation, apoptosis, JAK-STAT signaling, and PD-L1 expression pathway in cancer. We used these pathways instead of the previous 28 immune cell types in clustering single cells because these pathways are likely expressed in cancer cells themselves. Likewise, we identified three clusters of these cancer single cells (IM-H, IM-M, and IM-L), which had high, medium, and low enrichment scores of these pathways (Figure 5(a)). As expected, *PD-L1* expression levels were the highest in IM-H and the lowest in IM-L ($P < 0.001$) (Figure 5(b)). We further performed unsupervised clustering of each subtype of these single cells by SC3 [31] and identified 37, 29, and 41 cell clusters in IM-H, IM-M, and IM-L, respectively (Figure 5(c)). It indicated that IM-L and IM-M had the highest and lowest heterogeneity of cancer cells. Furthermore, we observed that the inferred CNVs by inferCNV [32] followed the pattern IM-L > IM-M > IM-H ($P < 0.001$) (Figure 5(d)). These results were consistent with those obtained in bulk tumors, supporting that IM-L and IM-H had the highest and lowest genomic instability, respectively, at the single-cell level. Based on the cell clustering results, we calculated the proportions of cancer cells of each patient in each subtype of IM-H, IM-M, and IM-L and assigned each patient into the subtype which involved the highest proportion of cancer cells of that patient. We further compared the enrichment levels of several T cell subpopulations among IM-H, IM-M, and IM-L patients, including CD4+ FOXP3 for regulatory CD4+ T cells, CD4+ IL7R for resting CD4+ T cells, CD4+ CXCL13 for activated CD4+ T cells, and CD8+ GZMB T cells. The enrichment levels of these T cell subpopulations were the average expression levels of their marker genes (Supplementary Table S2). Interestingly, the CD4+ FOXP3 T cell enrichment was the highest in IM-H and the lowest in IM-M ($P < 0.05$) (Figure 5(e)). However, the CD4+ CXCL13 T cell enrichment followed an opposite pattern: IM-H < IM-L < IM-M ($P < 0.001$). In addition, the CD4+ IL7R T cell enrichment was the highest in IM-L and the lowest in IM-M ($P < 0.001$), while the CD8+ GZMB T cell enrichment followed an opposite pattern: IM-L < IM-H < IM-M ($P < 0.001$). These results indicated that immunostimulatory signatures were the most enriched in IM-M, while immunosuppressive signatures were the least enriched in this subtype. It is consistent with the finding of the highest ratios of immunostimulatory to immunosuppressive signatures in IM-M among the three subtypes in bulk tumors.



(a)



(b)

FIGURE 4: Continued.

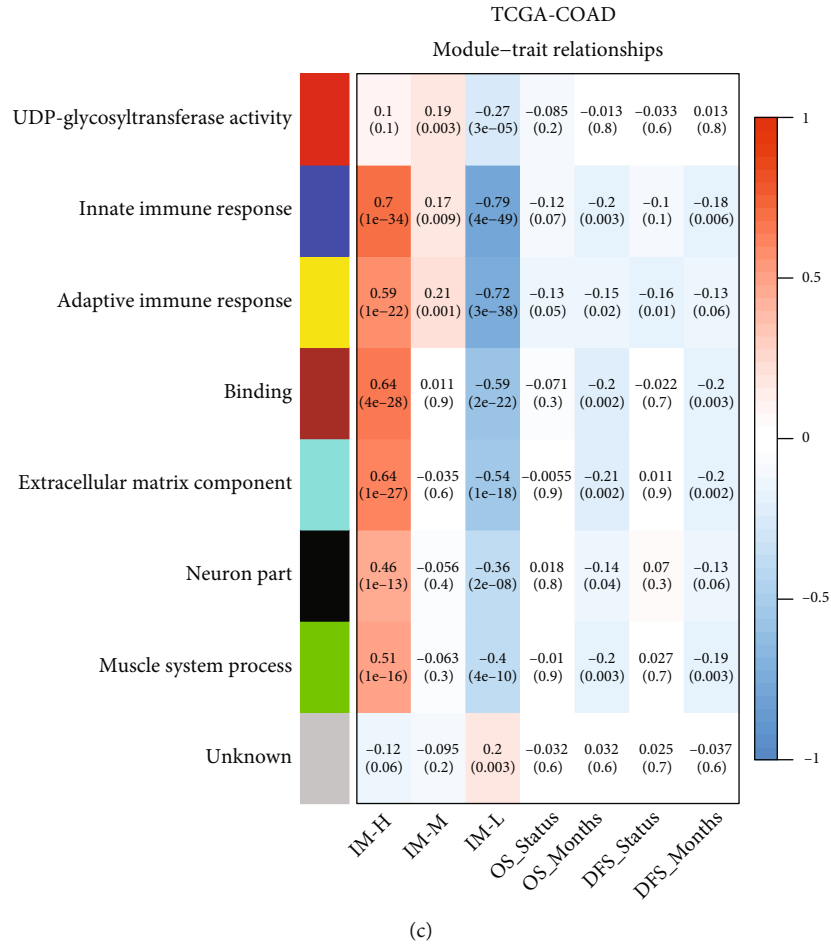
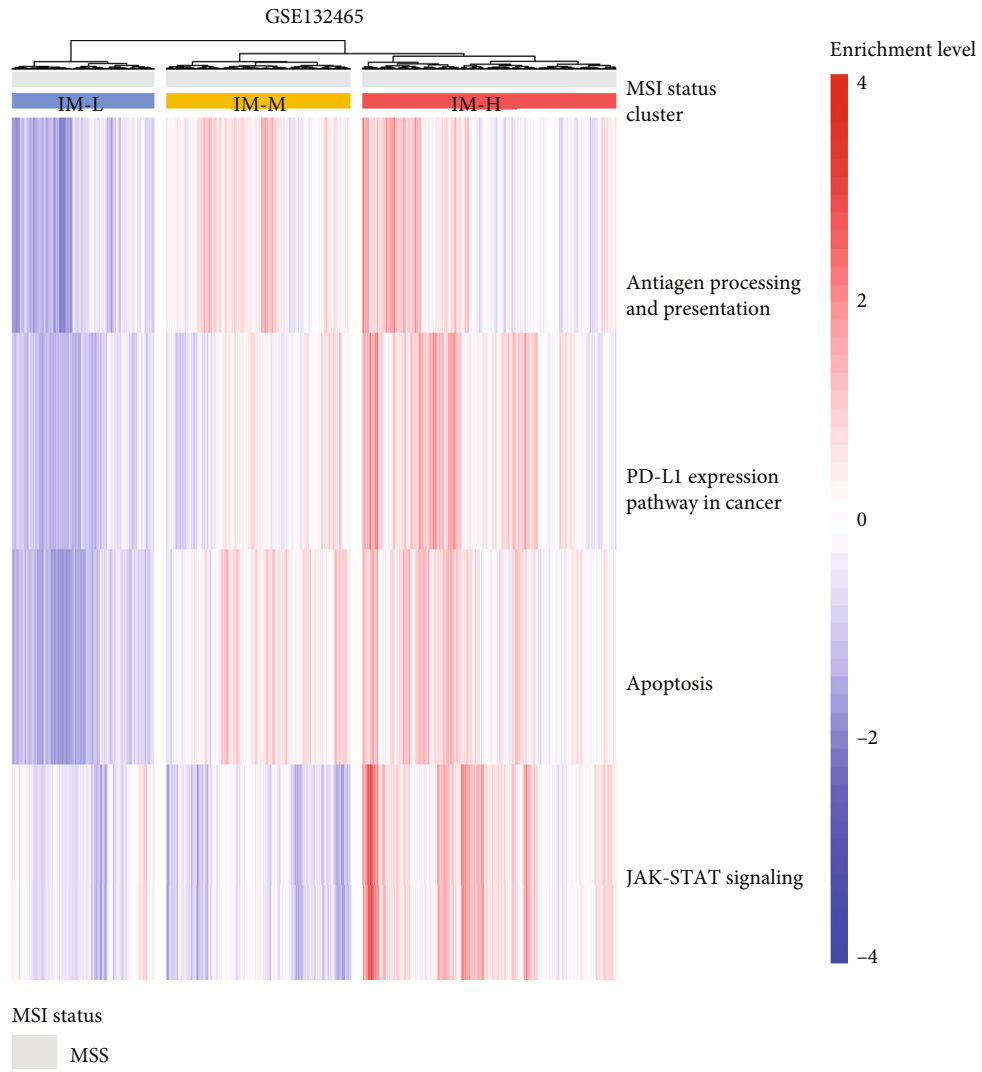


FIGURE 4: Pathways and Gene Ontology (GO) enriched in the immune subtypes. (a) The KEGG pathways upregulated in IM-H versus IM-L in TCGA-COAD. (b) Spearman’s correlations between the enrichment scores of pathways upregulated in IM-H and immune scores in MSI-L/MSS COAD. The correlation coefficients (ρ) and P values are shown. (c) The gene modules and their representative GO terms significantly differentiating MSI-L/MSS COAD by the immune subtypes and survival prognosis in TCGA-COAD.

4. Discussion

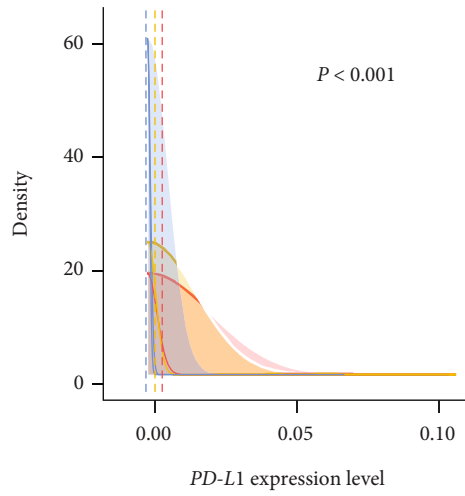
Although MSI has been identified as an indicator for antitumor immune response and immunotherapy response, only 15% of COAD patients are endowed with this feature. This study focused on MSI-L/MSS COAD and identified its immune subtypes based on the immune features displayed in the TIME. We identified three immune subtypes of MSI-L/MSS COAD (IM-H, IM-M, and IM-L), which had high, medium, and low immune signature scores, respectively. We demonstrated that this subtyping method was reproducible and predictable by analyzing five different datasets, including four bulk tumor datasets and one single cell dataset. IM-H was characterized by high immunity, high stemness, strong potential of proliferation, invasion and metastasis, EMT, high expression of oncogenic pathways, low tumor purity, low ITH, genomic instability, inferior response to chemotherapy, and unfavorable survival prognosis (Figure 6). IM-M was characterized by the highest ratio of immunostimulatory to immunosuppressive signatures, the best response to chemotherapy as well as survival prognosis. IM-L was characterized by low immunity, high

tumor purity, high ITH, and genomic stability. It is interesting to observe that IM-H has the worst survival among these subtypes, although this subtype displays the “hottest” TIME. The inverse association between tumor immune infiltration levels and clinical outcomes has also been observed in some other cancer types, such as glioma [46] and prostate cancer [47]. The main reason for the inverse association between tumor immune infiltration levels and clinical outcomes could be that the strong immune infiltration leads to tumor progression-promoting inflammation [48]. Our data indicate that this inflammation is in fact antitumor immunosuppression as IM-H displays the highest expression of various immunosuppressive signatures, including M2 macrophages, regulatory T cells, MDSCs, and *PD-L1*. Another interesting finding is that IM-M instead of IM-L has the best survival prognosis. A possible explanation for the best prognosis in IM-M could be that the immune-mediated tumor killing is the strongest in this subtype, as evidenced by the highest ratio of immunostimulatory to immunosuppressive signatures in bulk tumors, as well as the highest enrichment of immunostimulatory signatures (such as activated CD4+ T cells and CD8+ GZMB T cells) and the lowest enrichment



(a)

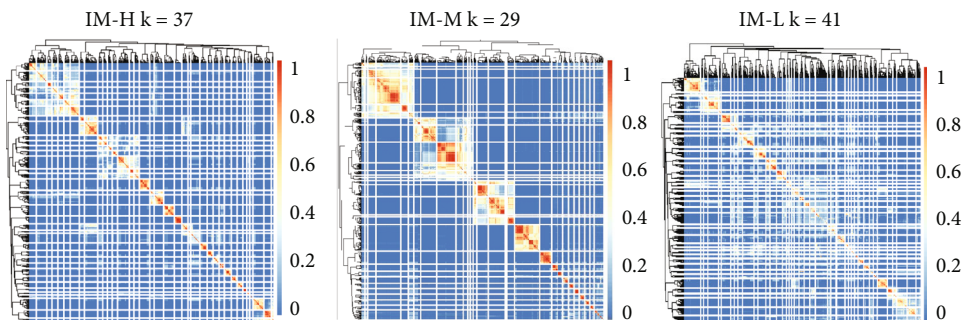
FIGURE 5: Continued.



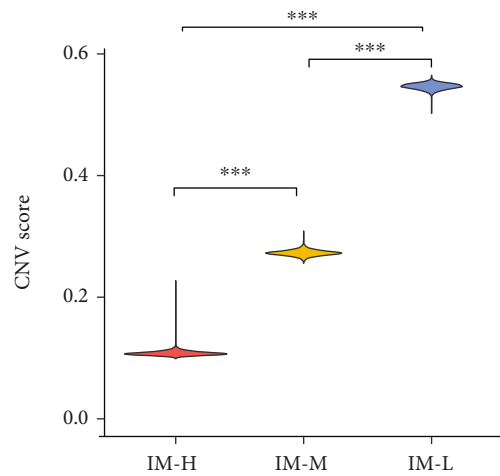
Subtype

- IM-H
- IM-M
- IM-L

(b)



(c)



(d)

FIGURE 5: Continued.

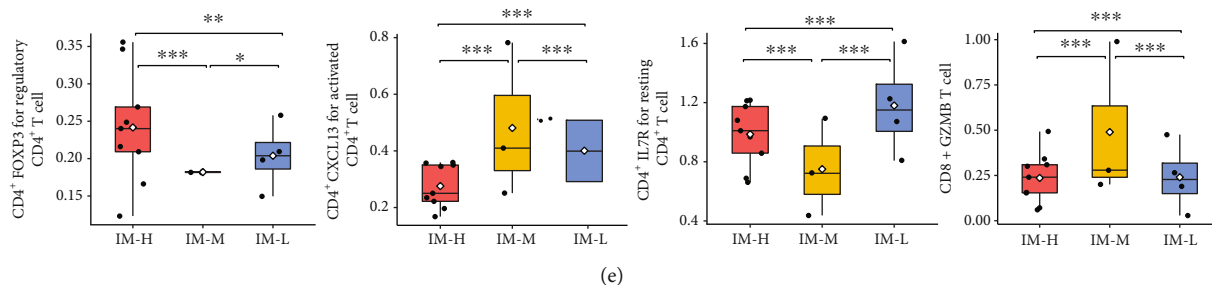


FIGURE 5: Validation of the immune signature enrichment-based subtyping method in MSS COAD single cells. (a) Hierarchical clustering of 12484 cancer cells from 16 MSS COAD patients based on the enrichment scores of four immune-related pathways identifying three subtypes. (b) Comparisons of *PD-L1* expression levels among the subtypes of cancer cells. The one-way ANOVA test *P* value is shown. (c) Unsupervised clustering of each subtype of single cells by SC3 [31] identifying 37, 29, and 41 clusters in IM-H, IM-M, and IM-L, respectively. (d) Comparisons of the inferred copy number variations (CNVs) by inferCNV [32] among the three immune subtypes of single cells. The one-tailed Mann–Whitney *U* test *P* values are shown. (e) Comparisons of the enrichment of T cell subpopulations among the immune subtypes. The two-tailed Student’s *t* test *P* values are shown.

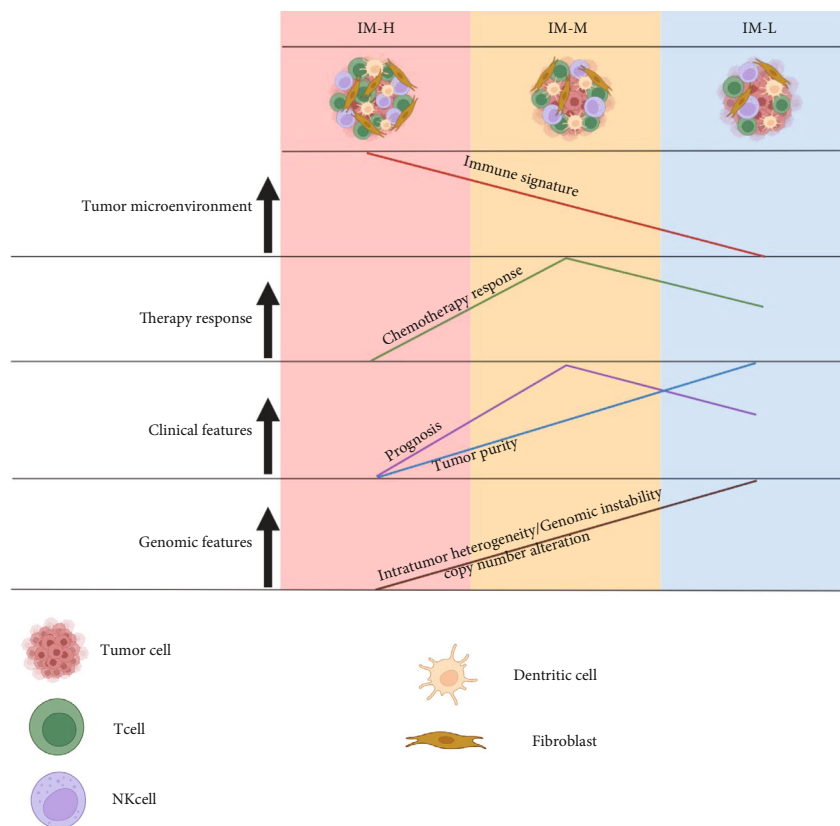


FIGURE 6: A summary of molecular and clinical characteristics of the three immune subtypes. The figure was created with <http://BioRender.com>.

of immunosuppressive signatures (such as regulatory CD4⁺ T cells and resting CD4⁺ T cells) in single cells in IM-M. In addition, previous studies [49, 50] have demonstrated that relative proportions of M1 macrophages and M2 macrophages correlates positively with survival prognosis in COAD. It is in line with the highest ratio of M1/M2 macrophages in IM-M. Nevertheless, by contrast, the association between tumor immune infiltration levels and clinical outcomes is positive in many other cancer types, such as gastric

cancer [51], head and neck squamous cell cancer [52], and triple-negative breast cancer [53]. Hence, the association between the TIME and malignancy is complex and cancer type dependent.

Among the three subtypes of COAD defined by TCGA (MSI, GS, and CIN) [54], MSI-L/MSS constituted around 82% of CIN. Notably, IM-L harbored the highest proportion of CIN cases (47.93% in IM-L versus 25.44% in IM-H and 26.63% in IM-M) (Fisher’s exact test, *P* < 0.05). CIN is

characterized by marked aneuploidy that is consistent with the highest CNA exhibited in IM-L. Furthermore, it conforms to the previous findings that aneuploidy correlates with reduced antitumor immune response [34]. Another previous study [55] identified four consensus subtypes of CRC (CMS1, CMS2, CMS3, and CMS4), by integrating six different classification systems. We found that 71.43% of IM-H cases were included in CMS4, compared to 23.81% of IM-M and 4.76% of IM-L in CMS4 (Fisher's exact test, $P < 0.001$). In fact, there were common features between CMS4 and IM-H, including EMT upregulation, TGF- β signaling pathway activation, stromal invasion, and worse prognosis. Meanwhile, 66.23% of IM-L cases were involved in CMS2, compared to 2.60% of IM-H and 31.17% of IM-M in CMS2. Again, CMS2 shared several prominent characteristics with IM-L, including high CIN, low immunogenicity, and decreased relapse rates. A previous study [56] molecularly classified CRC based on the expression levels of EMT-associated markers and identified three subtypes: epithelial, mesenchymal, and hybrid. Among the MSI-L/MSS COAD immune subtypes we identified, IM-H should have the highest overlaps with the mesenchymal subtype for its highest EMT scores, while IM-L should have the highest overlaps with the epithelial subtype for its lowest EMT scores; IM-M likely has the highest overlaps with the hybrid subtypes. That study [56] indicated that the EMT-based classification of CRCs could identify the most aggressive subtype showing a mesenchymal phenotype, consistent with our results showing that IM-H has the worst clinical outcomes among the three immune subtypes of MSI-L/MSS COAD.

MSI-H is an established indicator for immunotherapy response for its high TMB, *PD-L1* expression, and TIL level. However, we found that IM-H COADs likely had significantly higher TIL levels than MSI-H COADs ($P < 0.05$). Moreover, *PD-L1* expression levels showed no significant difference between MSI-H and IM-H COADs in two of the three datasets ($P > 0.35$). These data indicate that a proportion of non-MSI-H tumors could also be propitious to immunotherapy. Thus, the immune signature enrichment-based subtyping of MSI-L/MSS COAD may identify non-MSI-H patients responding well to immunotherapy. In fact, the immunotherapy of MSI-L/MSS COAD has been under investigation by clinical trials [57]. In addition, the combination of immunotherapy with other therapies could be a promising direction in treating MSI-L/MSS COADs.

This study has several limitations. First, the results presented in this study were obtained by bioinformatics analyses but lack experimental validation. Our next step is to validate the results by *in vitro* and *in vivo* experiments. Second, although our classification has potential value in stratifying COAD patients responsive to immunotherapies, it needs to be verified with clinical data with immunotherapy information. It is also an objective of our future research.

5. Conclusions

Based on the enrichment scores of immune signatures, MSI-L/MSS COAD can be classified into three subtypes with

high, medium, and low enrichment of immune signatures in the TIME. The immune-specific subtypes have significantly different TIME, tumor purity, stemness, tumor progression phenotypes, ITH, genomic features, response to chemotherapy, and survival prognosis. This study may provide new insights into COAD immunity, as well as identify non-MSI patients responsive to immunotherapy.

Data Availability

The data used to support the findings of this study were presented in Supplementary Tables and from public databases: the genomic data commons (GDC) data portal (<https://portal.gdc.cancer.gov/>) and the NCBI gene expression omnibus (GEO) (<https://www.ncbi.nlm.nih.gov/geo/>).

Conflicts of Interest

The authors declare that they have no competing interests.

Authors' Contributions

Tao Yang was responsible for the software, validation, formal analysis, investigation, data curation, and visualization, wrote the original draft, and wrote, reviewed, and edited the manuscript. Jiali Lei was responsible for the software, formal analysis, investigation, and visualization. Qiushi Feng was responsible for the software, investigation, and funding acquisition. Dandan Song was responsible for the software and investigation. Xiaosheng Wang was responsible for the conceptualization, methodology, resources, investigation, supervision, project administration, and funding acquisition, wrote the original draft, and wrote, reviewed, and edited the manuscript.

Acknowledgments

This work was supported by the China Pharmaceutical University (grant number 3150120001 to XW) and the Jiangsu Province Graduate Research and Innovation Program Project (grant number KYCX21_0664 to Qiushi Feng).

Supplementary Materials

Table S1: a summary of the datasets analyzed. Table S2: the gene sets representing immune cells, pathways, and biological processes. Table S3: genes with significantly different mutation rates between the immune subtypes of MSI-L/MSS COAD in TCGA-COAD. Table S4: 93 proteins differentially expressed between IM-H and IM-L in TCGA-COAD. (*Supplementary Materials*)

References

- [1] J. Weitz, M. Koch, J. Debus, T. Höhler, P. R. Galle, and M. W. Büchler, "Colorectal cancer," *The Lancet*, vol. 365, no. 9454, pp. 153–165, 2005.
- [2] D. I. Obrand and P. H. Gordon, "Incidence and patterns of recurrence following curative resection for colorectal

- carcinoma," *Diseases of the Colon & Rectum*, vol. 40, no. 1, pp. 15–24, 1997.
- [3] R. Labianca, G. D. Beretta, B. Kildani et al., "Colon cancer," *Critical Reviews in Oncology/Hematology*, vol. 74, no. 2, pp. 106–133, 2010.
 - [4] E. Budinska, V. Popovici, S. Tejpar et al., "Gene expression patterns unveil a new level of molecular heterogeneity in colorectal cancer," *The Journal of Pathology*, vol. 231, no. 1, pp. 63–76, 2013.
 - [5] S. Gurzu, Z. Szentirmay, and I. Jung, "Molecular classification of colorectal cancer: a dream that can become a reality," *Romanian Journal of Morphology and Embryology*, vol. 54, no. 2, pp. 241–245, 2013.
 - [6] E. R. Fearon, "Molecular genetics of colorectal cancer," *Annual Review of Pathology: Mechanisms of Disease*, vol. 6, no. 1, pp. 479–507, 2011.
 - [7] W. M. Grady, "Genomic instability and colon cancer," *Cancer and Metastasis Reviews*, vol. 23, no. 1/2, pp. 11–27, 2004.
 - [8] T. M. Pawlik, C. P. Raut, and M. A. Rodriguez-Bigas, "Colorectal carcinogenesis: Msi-h versus msi-l," *Disease Markers*, vol. 20, no. 4–5, p. 206, 2004.
 - [9] N. J. Llosa, M. Cruise, A. Tam et al., "The vigorous immune microenvironment of microsatellite instable colon cancer is balanced by multiple counter-inhibitory checkpoints," *Cancer Discovery*, vol. 5, no. 1, pp. 43–51, 2015.
 - [10] R. Gryfe, H. Kim, E. T. K. Hsieh et al., "Tumor microsatellite instability and clinical outcome in young patients with colorectal cancer," *New England Journal of Medicine*, vol. 342, no. 2, pp. 69–77, 2000.
 - [11] J. C. Del Paggio, "Cancer immunotherapy and the value of cure," *Nature Reviews Clinical Oncology*, vol. 15, no. 5, pp. 268–270, 2018.
 - [12] M. A. Postow, M. K. Callahan, and J. D. Wolchok, "Immune checkpoint blockade in cancer therapy," *Journal of Clinical Oncology : Official Journal of the American Society of Clinical Oncology*, vol. 33, no. 17, pp. 1974–1982, 2015.
 - [13] P. Darvin, S. M. Toor, V. Sasidharan Nair, and E. Elkord, "Immune checkpoint inhibitors: recent progress and potential biomarkers," *Experimental & Molecular Medicine*, vol. 50, no. 12, pp. 1–11, 2018.
 - [14] S. P. Patel and R. Kurzrock, "PD-L1 expression as a predictive biomarker in cancer immunotherapy," *Molecular Cancer Therapeutics*, vol. 14, no. 4, pp. 847–856, 2015.
 - [15] A. M. Goodman, S. Kato, L. Bazhenova et al., "Tumor mutational burden as an independent predictor of response to immunotherapy in diverse cancers," *Molecular Cancer Therapeutics*, vol. 16, no. 11, pp. 2598–2608, 2017.
 - [16] D. T. Le, J. N. Uram, H. Wang et al., "PD-1 blockade in tumors with mismatch-repair deficiency," *New England Journal of Medicine*, vol. 372, no. 26, pp. 2509–2520, 2015.
 - [17] S. Gurzu, Z. Szentirmay, E. Toth, and I. Jung, "Possible predictive value of maspin expression in colorectal cancer," *Recent Patents on Anti-Cancer Drug Discovery*, vol. 8, no. 2, pp. 183–190, 2013.
 - [18] L. Chang, M. Chang, H. M. Chang, and F. Chang, "Microsatellite instability: a predictive biomarker for cancer immunotherapy," *Applied Immunohistochemistry & Molecular Morphology*, vol. 26, no. 2, pp. e15–e21, 2018.
 - [19] M. Binnewies, E. W. Roberts, K. Kersten et al., "Understanding the tumor immune microenvironment (TIME) for effective therapy," *Nature Medicine*, vol. 24, no. 5, pp. 541–550, 2018.
 - [20] H.-O. Lee, Y. Hong, H. E. Etlioglu et al., "Lineage-dependent gene expression programs influence the immune landscape of colorectal cancer," *Nature Genetics*, vol. 52, no. 6, pp. 594–603, 2020.
 - [21] S. Hanzelmann, R. Castelo, and J. Guinney, "GSVA: gene set variation analysis for microarray and RNA-seq data," *BMC Bioinformatics*, vol. 14, no. 1, p. 7, 2013.
 - [22] P. Charoentong, F. Finotello, M. Angelova et al., "Pan-cancer immunogenomic analyses reveal genotype-immunophenotype relationships and predictors of response to checkpoint blockade," *Cell Reports*, vol. 18, no. 1, pp. 248–262, 2017.
 - [23] E. Frank, M. Hall, L. Trigg, G. Holmes, and I. H. Witten, "Data mining in bioinformatics using Weka," *Bioinformatics*, vol. 20, no. 15, pp. 2479–2481, 2004.
 - [24] J. M. Bland and D. G. Altman, "Survival probabilities (the Kaplan-Meier method)," *BMJ*, vol. 317, no. 7172, pp. 1572–1580, 1998.
 - [25] C. H. Mermel, S. E. Schumacher, B. Hill, M. L. Meyerson, R. Beroukhim, and G. Getz, "GISTIC2.0 facilitates sensitive and confident localization of the targets of focal somatic copy-number alteration in human cancers," *Genome Biology*, vol. 12, no. 4, p. R41, 2011.
 - [26] L. Li, C. Chen, and X. Wang, "DITHER: an algorithm for defining intratumor heterogeneity based on entropy," *Briefings in Bioinformatics*, vol. 22, no. 6, 2021.
 - [27] K. Yoshihara, M. Shahmoradgoli, E. Martínez et al., "Inferring tumour purity and stromal and immune cell admixture from expression data," *Nature Communications*, vol. 4, no. 1, p. 2612, 2013.
 - [28] A. Subramanian, P. Tamayo, V. K. Mootha et al., "Gene set enrichment analysis: a knowledge-based approach for interpreting genome-wide expression profiles," *Proceedings of the National Academy of Sciences of the United States of America*, vol. 102, no. 43, pp. 15545–15550, 2005.
 - [29] M. Kanehisa, M. Furumichi, M. Tanabe, Y. Sato, and K. Morishima, "KEGG: new perspectives on genomes, pathways, diseases and drugs," *Nucleic Acids Research*, vol. 45, no. D1, pp. D353–D361, 2017.
 - [30] P. Langfelder and S. Horvath, "WGCNA: an R package for weighted correlation network analysis," *BMC Bioinformatics*, vol. 9, no. 1, pp. 1–13, 2008.
 - [31] V. Y. Kiselev, K. Kirschner, M. T. Schaub et al., "SC3: consensus clustering of single-cell RNA-seq data," *Nature Methods*, vol. 14, no. 5, pp. 483–486, 2017.
 - [32] A. P. Patel, I. Tirosh, J. J. Trombetta et al., "Single-cell RNA-seq highlights intratumoral heterogeneity in primary glioblastoma," *Science*, vol. 344, no. 6190, pp. 1396–1401, 2014.
 - [33] Y. Benjamini and Y. Hochberg, "Controlling the false discovery rate: a practical and powerful approach to multiple testing," *Journal of the Royal Statistical Society: series B (Methodological)*, vol. 57, no. 1, pp. 289–300, 1995.
 - [34] T. Davoli, H. Uno, E. C. Wooten, and S. J. Elledge, "Tumor aneuploidy correlates with markers of immune evasion and with reduced response to immunotherapy," *Science*, vol. 355, no. 6322, 2017.
 - [35] T. A. Knijnenburg, L. Wang, M. T. Zimmermann et al., "Genomic and molecular landscape of DNA damage repair deficiency across the cancer genome atlas," *Cell Reports*, vol. 23, no. 1, pp. 239–254.e6, 2018.

- [36] C. G. A. Network, "Comprehensive molecular characterization of human colon and rectal cancer," *Nature*, vol. 487, no. 7407, pp. 330–337, 2012.
- [37] A. Tighe, V. L. Johnson, and S. S. Taylor, "Truncating APC mutations have dominant effects on proliferation, spindle checkpoint control, survival and chromosome stability," *Journal of Cell Science*, vol. 117, no. 26, pp. 6339–6353, 2004.
- [38] L. Zhang and J. W. Shay, "Multiple roles of APC and its therapeutic implications in colorectal cancer," *JNCI: Journal of the National Cancer Institute*, vol. 109, no. 8, 2017.
- [39] Y. Wu and Y. Xu, "Bioinformatics for the prognostic value and function of cubilin (CUBN) in colorectal cancer," *Medical science monitor : international medical journal of experimental and clinical research*, vol. 26, pp. e922447–e922447, 2020.
- [40] L. A. Garrett-Sinha, "Review of Ets1 structure, function, and roles in immunity," *Cellular and Molecular Life Sciences*, vol. 70, no. 18, pp. 3375–3390, 2013.
- [41] Z. Liang and X. Li, "Identification of ANXA1 as a potential prognostic biomarker and correlating with immune infiltrates in colorectal cancer," *Autoimmunity*, vol. 54, no. 2, pp. 76–87, 2021.
- [42] C. Guo, S. Liu, and M.-Z. Sun, "Potential role of Anxa1 in cancer," *Future Oncology*, vol. 9, no. 11, pp. 1773–1793, 2013.
- [43] G. Janikowska, T. Janikowski, A. Pyka-Pająk et al., "Potential biomarkers for the early diagnosis of colorectal adenocarcinoma – transcriptomic analysis of four clinical stages," *Cancer Biomarkers*, vol. 22, no. 1, pp. 89–99, 2018.
- [44] E. P. Allain, M. Rouleau, E. Lévesque, and C. Guillemette, "Emerging roles for UDP-glucuronosyltransferases in drug resistance and cancer progression," *British Journal of Cancer*, vol. 122, no. 9, pp. 1277–1287, 2020.
- [45] J. Cummings, B. T. Ethell, L. Jardine et al., "Glucuronidation as a mechanism of intrinsic drug resistance in human colon cancer: reversal of resistance by food additives," *Cancer Research*, vol. 63, no. 23, pp. 8443–8450, 2003.
- [46] A. R. P. Antunes, I. Scheyltjens, J. Duerinck, B. Neyns, K. Movahedi, and J. A. V. Ginderachter, "Understanding the glioblastoma immune microenvironment as basis for the development of new immunotherapeutic strategies," *eLife*, vol. 9, 2020.
- [47] V. Thorsson, D. L. Gibbs, S. D. Brown et al., "The immune landscape of cancer," *Immunity*, vol. 48, no. 4, pp. 812–830, 2018.
- [48] S. I. Grivnenkov, F. R. Greten, and M. Karin, "Immunity, inflammation, and cancer," *Cell*, vol. 140, no. 6, pp. 883–899, 2010.
- [49] Y. Xiong, K. Wang, H. Zhou, L. Peng, W. You, and Z. Fu, "Profiles of immune infiltration in colorectal cancer and their clinical significant: a gene expression-based study," *Cancer Medicine*, vol. 7, no. 9, pp. 4496–4508, 2018.
- [50] X. Tian, X. Zhu, W. Meng et al., "A 12-immune cell signature to predict relapse and guide chemotherapy for stage II colorectal cancer," *Aging*, vol. 12, no. 18, pp. 18363–18383, 2020.
- [51] Z. Jiang, Z. Liu, M. Li, C. Chen, and X. Wang, "Immunogenomics analysis reveals that TP53 mutations inhibit tumor immunity in gastric cancer," *Translational Oncology*, vol. 11, no. 5, pp. 1171–1187, 2018.
- [52] H. Lyu, M. Li, Z. Jiang, Z. Liu, and X. Wang, "Correlate the TP53 mutation and the HRAS mutation with immune signatures in head and neck squamous cell cancer," *Computational and Structural Biotechnology Journal*, vol. 17, pp. 1020–1030, 2019.
- [53] Z. Liu, M. Li, Z. Jiang, and X. Wang, "A comprehensive immunologic portrait of triple-negative breast cancer," *Translational Oncology*, vol. 11, no. 2, pp. 311–329, 2018.
- [54] "Comprehensive molecular characterization of gastric adenocarcinoma," *Nature*, vol. 513, no. 7517, pp. 202–209, 2014.
- [55] J. Guinney, R. Dienstmann, X. Wang et al., "The consensus molecular subtypes of colorectal cancer," *Nature Medicine*, vol. 21, no. 11, pp. 1350–1356, 2015.
- [56] L. Baniias, L. Baniias, I. Jung et al., "Immunohistochemical-based molecular subtyping of colorectal carcinoma using maspin and markers of epithelial-mesenchymal transition," *Oncology Letters*, vol. 19, no. 2, pp. 1487–1495, 2020.
- [57] S. Cousin, C. Cantarel, J. P. Guegan et al., "Regorafenib-avelumab combination in patients with microsatellite stable colorectal cancer (REGOMUNE): a single-arm, open-label, phase II trial," *Clinical Cancer Research*, vol. 27, no. 8, pp. 2139–2147, 2021.

Research Article

Creation and Validation of a Survival Nomogram Based on Immune-Nutritional Indexes for Colorectal Cancer Patients

Yulan Liu ¹, Yang Meng ², Chenliang Zhou ¹, Ya Liu,³ Shan Tian ⁴, Jiao Li ³, and Weiguo Dong ³

¹Department of Critical Care Medicine, Renmin Hospital of Wuhan University, Wuhan, China

²Department of Gastrointestinal Surgery II, Renmin Hospital of Wuhan University, Wuhan, China

³Department of Gastroenterology, Renmin Hospital of Wuhan University, Wuhan, China

⁴Department of Infectious Diseases, Union Hospital, Tongji Medical College, Huazhong University of Science and Technology, Wuhan, China

Correspondence should be addressed to Jiao Li; li.jiao@whu.edu.cn and Weiguo Dong; ddongweiguo@163.com

Yulan Liu and Yang Meng contributed equally to this work.

Received 9 February 2022; Revised 6 March 2022; Accepted 7 March 2022; Published 25 March 2022

Academic Editor: Simona Gurzu

Copyright © 2022 Yulan Liu et al. This is an open access article distributed under the Creative Commons Attribution License, which permits unrestricted use, distribution, and reproduction in any medium, provided the original work is properly cited.

Nutritional and inflammatory status was associated with prognosis in various types of malignant cancer, including colorectal cancer (CRC). This clinical research was performed to estimate the prognostic role of immune-nutritional indexes CRC in patients and to set up a survival nomogram based on the significant immune-nutritional indexes. 1024 CRC patients underwent surgical resection from Wuhan Union Hospital were enrolled and divided into the test cohort ($n=717$) and validation cohort ($n=307$). A total of 19 immune-nutritional indexes were included into our analysis. The Cox regression analysis was utilized to identify the informative immune-nutritional indexes which were closely associated with overall survival (OS) and disease-free survival (DFS). Survival nomograms were created in the test set and further verified in the validation set. Td-ROC was curved to estimate the predictive performance of survival nomograms for CRC patients. Body mass index (BMI), chemotherapy, TNM stage, T stage, lactate dehydrogenase (LDH)/prealbumin (PA), monocytes (MON)/albumin (ALB), and prognostic nutritional index (PNI) were seven potent prognostic biomarkers of CRC patients. We created an OS-nomogram based on the seven risk indexes, and the predictive accuracy expressed with area under curve (AUC) was 0.826 for 1-year, 0.809 for 3-year, and 0.80 for 5-year OS rates in the test set and 0.795 for 1-year, 0.749 for 3-year, and 0.647 for 5-year OS rates in the validation set. TNM stage, T stage, LDH/ALB, and MON/ALB were risk factors for unfavorable DFS in CRC patients. We further built a DFS-nomogram based on the four risk factors, and the predictive performance presented with AUC was 0.806 for 1-year, 0.763 for 3-year, and 0.82 for 5-year DFS rates in the test set, and 0.704 for 1-year, 0.692 for 3-year, and 0.692 for 5-year DFS rates in the validation set. Our survival nomogram based on immune-nutritional indexes is a useful and potential prognostic tool in CRC patients.

1. Introduction

Colorectal cancer (CRC) accounted for 12.7% of all newly diagnosed cancer, which is the second most frequently occurring cancer [1]. In 2020, CRC accounted for 12.4% of all deaths, being the second most common cause of cancer death based on data from 27 countries of the European Union [2].

The exact pathogenic mechanism of CRC is still uncertain, but genetic susceptibility, gut flora, dietary habit, and environmental factors are reported to play key roles in its occurrence [3]. The mainstream treatment for CRC is based on comprehensive approaches, composed of surgery, radiation, chemotherapy, and emerging immunotherapy. Although curative removal of the tumor tissues is expected to be a

curative treatment for CRC, the long-term survival outcome of CRC patients is still not promising due to the early recurrence.

Inflammation and malnutrition are proven to be involved in the progression of CRC [4]. Systemic inflammation is a marker of worse survival outcomes in approximately 20%-40% of CRC patients [5]. Several clinical studies have highlighted that serum inflammatory indexes, such as systemic immune-inflammation index (SII), pan-immune-inflammation (PII) [6], controlling nutritional status score (CONUT) [7], Gustave Roussy Immune (GRIm) Score [8], could well forecast the survival outcomes of CRC individuals. Moreover, CRC patients are the high-risk population with malnutrition, which is associated with impaired therapeutic response and higher mortality [9]. Continued malnutrition is more common in CRC patients with advanced cancer and could speed up to early death in the condition of no effective nutrition support. Hence, a better understanding of CRC patient's immune-nutritional status is critical to their survival outcomes.

Immune-nutritional indexes could not only reflect the inflammatory status of the body but also reflect the nutritional condition. Hence, early identification of inflammation and malnutrition in CRC patients is crucial. However, clinicians tend to belittle this phenomenon in the clinical practice, making it very imperative to assess the inflammatory and nutritional status of CRC patients. Among these indexes, PNI, CONUT, and GRIm scores are reported to well reflect the host immune-nutrition status in CRC patients. As immune-nutritional indexes are inexpensive to test for blood and easily accessible in the clinical practice, it is quite significant to identify novel immune-nutritional indexes for the assessment of survival outcomes in CRC patients. Hence, in this present study, our primary goal was to assess the prognostic significance of a list of novel immune-nutritional indexes. Then, our second goal was to derive and verify two survival nomograms based on immune-nutritional indexes for the precise prediction of survival outcomes in CRC patients.

2. Materials and Methods

2.1. Study Population. A total of 1474 CRC sufferers from Wuhan Union Hospital were initially analyzed, and only 1024 cases of CRC were included into the final analysis. The inclusion criteria were listed as follows: (1) the diagnosis of CRC confirmed by pathological reports, (2) surgical management performed as the first treatment, (3) CRC patients with complete preoperative laboratory examination information, and (4) CRC patients with no evidence of acute infection. The exclusion criteria were as follows: (1) systemic chemotherapy or radiotherapy before surgical resection, (2) CRC patients under the age of 18 years, (3) CRC patients who lost for follow-up, (4) CRC patients were complicated with obvious acute infection, and (5) administration of anti-inflammatory agents prior to the initiation of the surgery, such as antibiotics, nonsteroidal anti-inflammatory drugs, and glucocorticoid. All relevant materials were checked and approved by the Clinical Research Ethics

Committee (CREC) of Wuhan Union Hospital (No. 2018-S377). Written informed consents were obtained from all participants prior to the initiation of this clinical research.

2.2. Data Collection. We retrospectively collected CRC patients' baseline data and clinical information before surgical management, including demographic data, clinical information, and laboratory data. The demographic data were composed of sex, age of diagnosis, and body mass index (BMI). The clinical information was composed of tumor size, tumor site, T stage, N stage, tumor differentiation, and TNM stage. The laboratory data were composed of blood routine [lymphocyte (LYM), neutrophil (NEU), monocyte (MON), and platelet (PLT)], liver function [albumin (ALB), prealbumin (PA), lactate dehydrogenase (LDH), alkaline phosphatase (ALP), and glutamyltransferase (GGT)], and renal function [creatinine (CREA)]. Moreover, we calculated the novel immune-nutritional indexes, such as LDH/PA, LDH/ALB, GGT/ALB, GGT/PA, ALP/ALB, ALP/PA, PLT/ALB, PLT/PA, LYM/ALB, LYM/PA, NEU/ALB, NEU/PA, MON/ALB, MON/PA, ALB/CREA, and PA/CREA. The cutoff values of these immune-nutritional indexes were determined by X-tile software (version 3.4.7). We also included three established immune-nutritional indexes, PNI, CONUT, and GRIm score. The GRIm score was obtained according to a previous study [8] based on serum lactate dehydrogenase, serum albumin, and NLR.

2.3. Development and Validation of Survival Nomogram. In order to derive and verify a survival nomogram with robustness, we randomly assigned the included CRC patients into the test set ($N = 717$) and validation set ($N = 307$) according to the ratio of 7:3. In the test set, we first developed an overall survival nomogram (OS-nomogram). We initially employed a univariate Cox regression to identify the immune-nutritional variables with a close relationship to OS in CRC patients. Then, the significant immune-nutritional metrics with $P < 0.05$ were further selected into multivariate Cox regression. Only the immune-nutritional indexes determined by multivariate Cox regression ($P < 0.05$) were finally identified for the construction of OS-nomogram. The risk score equation behind the OS-nomogram was determined using the β -coefficients of the multivariate Cox regression analysis. To validate the OS-nomogram, the predicted OS rates of CRC patients in the internal validation cohort were also measured using the same regression equation derived from the test set. Similarly, the DFS nomogram was constructed based on the same method. The discrimination ability of survival nomogram for predicting survival rate was measured by time-dependent (td) receiver operating characteristic (ROC) curves. Each survival nomogram was assessed with calibration curve, which made it possible to compare the predicting survival rates with the actual survival rates. We also verified the discrimination and calibration abilities of the two survival nomograms in the validation cohort. Finally, decision curve analysis (DCA) was drawn to appraise the clinical utility of the survival nomograms. DCA is a statistical method which is widely used to evaluate prediction models. DCA

attempted to overcome the limitations of discrimination and calibration which are not very informative to full decision analytic approaches. DCA compares a clinical “net benefit” for a predictive model with default strategies of none treating or treating [10].

2.4. Statistical Analysis. All the statistical analyses were implemented with SPSS (version 20.0), MedCalc application (version 19.0.4), and R software (version 3.5.1). Categorical indexes were presented with counts (n) and percentages (%) and examined by a chi-square test or Fisher’s exact. Continuous variables were expressed as the mean differences and standard deviation or interquartile range (IQR) based on the status of data distribution. Continuous data were analyzed with Student’s t -test or nonparametric test. Spearman’s correlation analysis was adopted to measure the relationship between two immune-nutritional indexes [11]. The cumulative survival rates of CRC patients were estimated by survival analysis and analyzed using the log-rank test. Univariate combined with multivariate Cox analyses were performed to evaluate the overall effects of included variables on the survival outcomes of CRC patients. Td-ROC curves were plotted to determine the prediction accuracy of the inflammatory indexes or survival nomogram for 1-year, 3-year, and 5-year survival rates. The Akaike information criterion (AIC) was also calculated to assess the goodness of fit of the survival nomograms. AIC analysis was viewed as a good statistical system for the identification of predictive markers, which offer statistical significance for the balance between complexity and adaptation of a predictive model. AIC quantifies the relative goodness of fit for various metrics for a preferred model. The predictive model with the lowest AIC value is considered the preferred model, and the lower the AIC, the better the predictive model [12]. A P value less than 0.05 signifies that the difference is significant.

3. Results

3.1. Clinical Features of Included Participants. According to the strict inclusion criteria, a total of 1024 CRC patients who underwent surgical removal were screened into our analysis (Figure 1). Among them, the majority of participants were men (60.45%), and the median age of these included CRC patients was 58.399 ± 11.87 years. Among all, 4.21% and 63.27% of patients had a low body weight (LBW) and normal BMI, respectively. All the included patients received surgical resection, and 541 cases of CRC patients received postoperative chemotherapy.

3.2. Correlations among Immune-Inflammation Indexes. In this study, we systematically assessed all the available immune-inflammation variables in CRC patients. A total of 19 immune-inflammation indexes were included into our analysis. Based on the correlation analysis, we found these immune-inflammation indexes correlated with each other. As listed in Figure 2, we observed that LDH/PA was strongly correlated with LDH/ALB ($r = 0.77$, $P < 0.0001$), ALP/PA ($r = 0.68$, $P < 0.0001$), PLT/PA ($r = 0.62$, $P < 0.0001$), NEU/

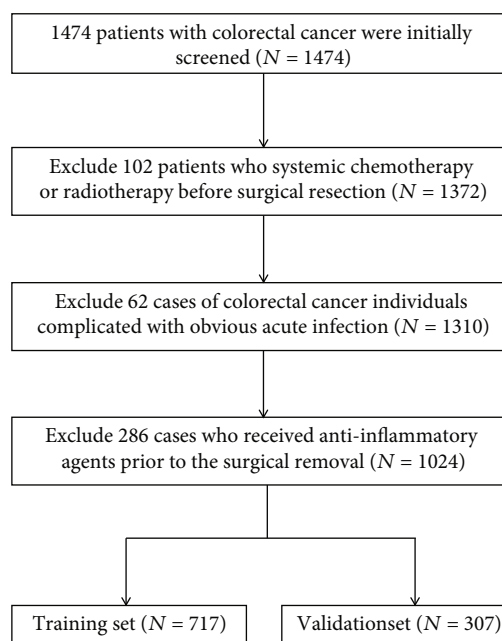


FIGURE 1: Flow chart of participant selection.

PA ($r = 0.61$, $P < 0.0001$), MON/PA ($r = 0.57$, $P < 0.0001$), and GRIm score ($r = 0.49$, $P < 0.0001$), but reversely associated with PA/CREA ($r = -0.56$, $P < 0.0001$). As for LDH/ALB, although this score was correlated with many other immune-inflammation biomarkers, the correlation was less significant than LDH/PA.

3.3. Overall Survival Nomogram Based on Immune-Nutritional Indexes. For the purpose of building survival model based on immune-nutritional indexes, we randomly assigned these CRC individuals into test set ($N = 717$) and validation set ($N = 307$) according to the ratio of 7 : 3. There were no significant differences of clinical features in the test and validation sets (Table S1). In the test set, we initially utilized univariate Cox analysis to estimate the potential risk indexes which could significantly influence the OS in CRC patients. We identified that 24 significant features, including BMI, TNM stage, T stage, N stage, tumor size, chemotherapy, LDH/PA, LDH/ALB, GGT/PA, GGT/ALB, ALP/PA, ALP/ALB, PLT/PA, PLT/ALB, LYM/PA, NEU/PA, NEU/ALB, ALB/CREA, PA/CREA, MON/PA, MON/ALB, PNI, GRIm score, and CONUT score, were all well correlated with the OS in CRC patients (Table S2). Then, these informative immune-inflammation indexes with $P < 0.05$ were further selected into the multivariable Cox model. We noticed that BMI (HR = 0.451, 95% CI: 0.022-0.924, $P = 0.0295$), chemotherapy (HR = 0.608, 95% CI: 0.403-0.917, $P = 0.0177$), T stage (HR = 3.336, 95% CI: 1.651-6.74, $P < 0.001$), TNM stage (HR = 2.419, 95% CI: 1.560-3.751, $P < 0.001$), LDH/PA (HR = 2.186, 95% CI: 1.434-3.331, $P < 0.001$), MON/ALB (HR = 1.988, 95% CI: 1.248-3.167, $P < 0.001$), and PNI (HR = 0.431, 95% CI: 0.282-0.658, $P < 0.001$) were still potent prognostic biomarkers of CRC patients after adjusting the confounding covariates (Figure 3(a)).

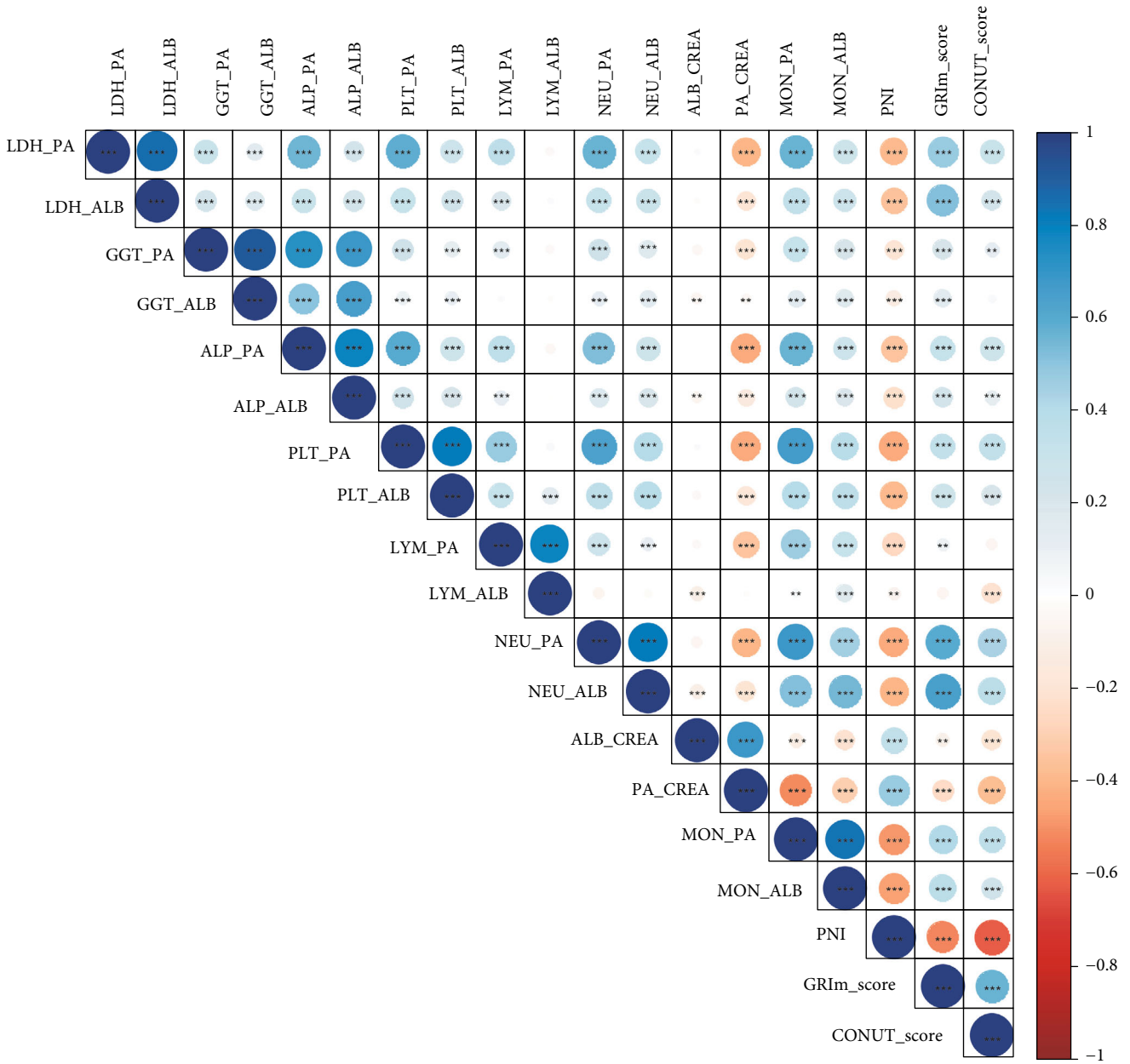


FIGURE 2: Correlations of each immune-inflammation index in CRC.

Hence, we further created an OS-nomogram based on the seven risk indexes (Figure 4(a)), and the predictive accuracy expressed with AUC was 0.826 for 1-year, 0.809 for 3-year, and 0.80 for 5-year survival rates in the test set (Figure 5(a)). This OS-nomogram exhibited the smallest AIC value of 1131. When validating the OS-nomogram in validation set, the predictive accuracy expressed with AUC was 0.795 for 1-year, 0.749 for 3-year, and 0.647 for 5-year survival rates in CRC patients (Figure 5(b)). Moreover, we divided these CRC patients into two categories (low risk and high risk) based on the median value of OS-nomogram, and the Kaplan-Meier curves exhibited the great survival difference between the two groups ($P < 0.001$), highlighting the great value of the OS-nomogram for risk stratification of CRC patients (Figure 6(a)).

3.4. Disease-Free Survival Nomogram Based on Immune-Nutritional Indexes. Similarly, univariate analysis revealed that TNM stage, T stage, N stage, chemotherapy, LDH/PA, LDH/ALB, GGT/PA, GGT/ALB, ALP/PA, ALP/ALB, PLT/PA, PLT/ALB, LYM/ALB, NEU/PA, NEU/ALB, ALB/CREA, PA/CREA, MON/PA, MON/ALB, PNI, GRIm score, and CONUT score were all well correlated with the DFS in CRC patients (Table S2). After adjusting the confounding covariates, TNM stage (HR = 3.31, HR = 2.06 – 5.30, $P < 0.001$), T stage (HR = 3.34, HR = 1.60-6.93, $P = 0.0013$), LDH/ALB (HR = 2.80, 95% CI: 1.83-4.26, $P < 0.001$), and MON/ALB (HR = 2.57, 95% CI: 1.63-4.04, $P < 0.001$) were risk factors for unfavorable DFS in CRC patients (Figure 3(b)). Hence, we further built a DFS-nomogram based on the four risk factors (Figure 4(b)), and the predictive performance

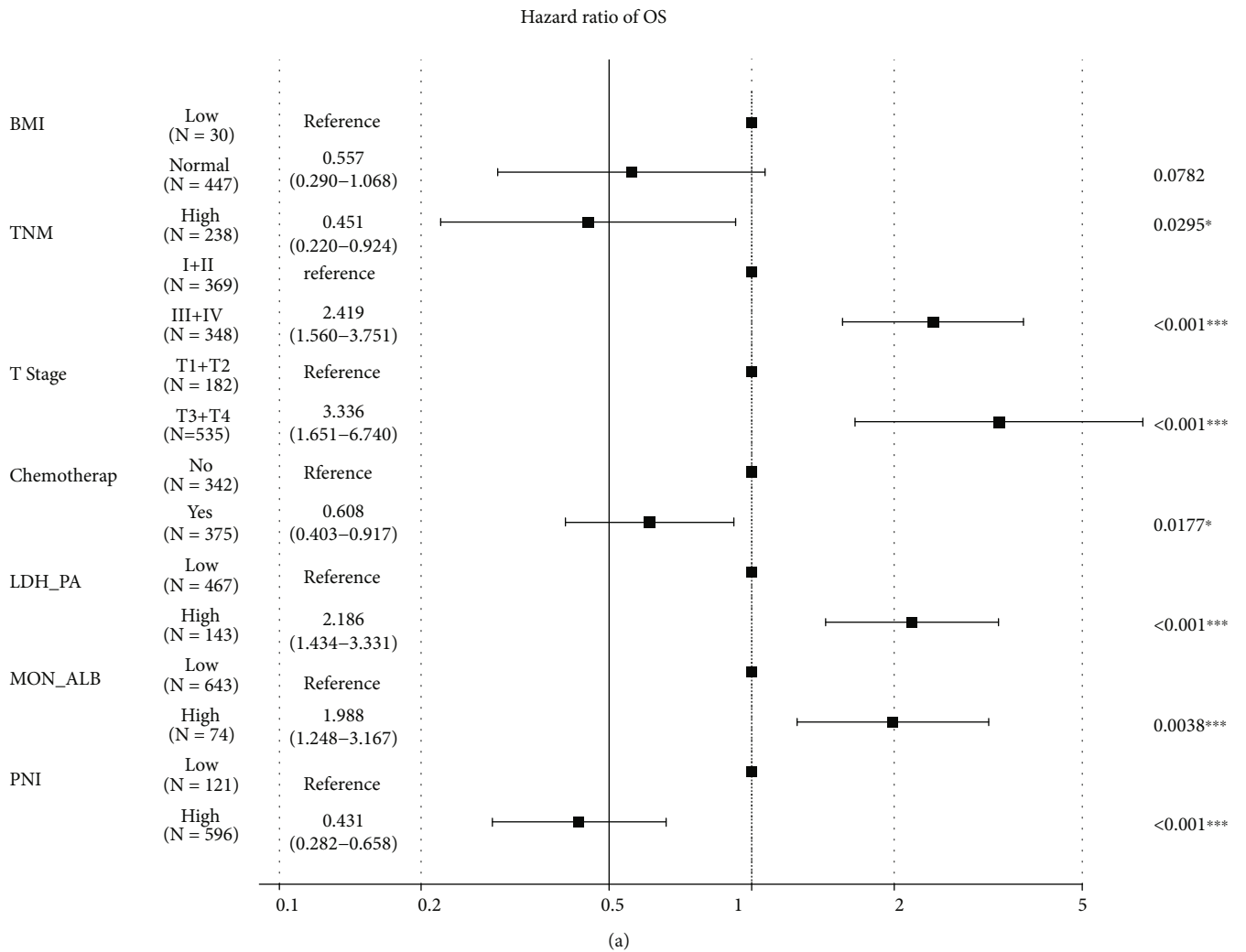


FIGURE 3: Continued.

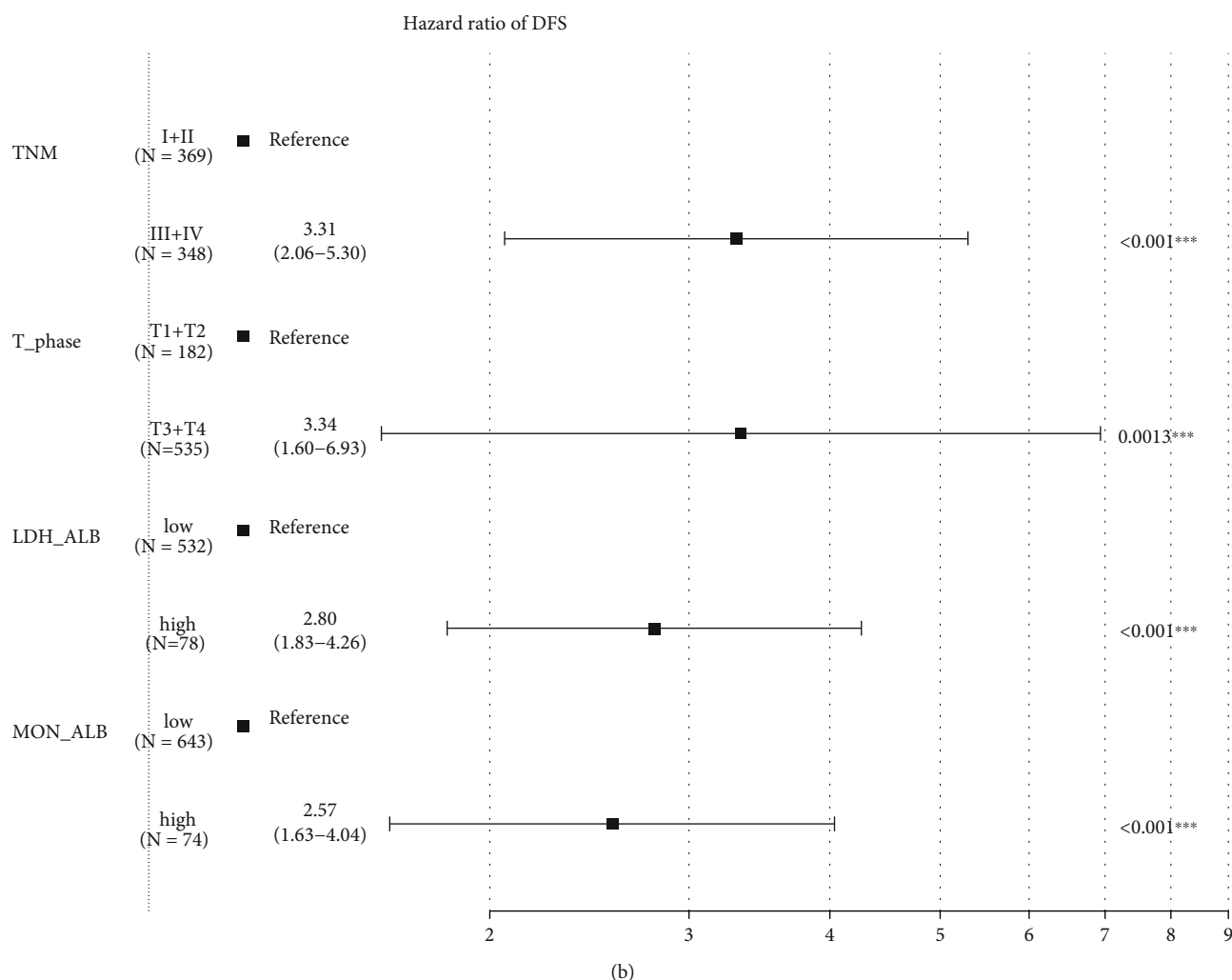


FIGURE 3: Multivariate Cox regression of survival outcomes in individuals with CRC. (a) Overall survival. (b) Disease-free survival.

expressed with AUC was 0.806 for 1-year, 0.763 for 3-year, and 0.82 for 5-year survival rates in the test set (Figure 5(c)). This DFS-nomogram exhibited the smallest AIC value of 1137.8. When verifying the DFS-nomogram in the validation set, the predictive performance presented with AUC was 0.794 for 1-year, 0.692 for 3-year, and 0.692 for 5-year survival rates in CRC patients (Figure 5(d)). Additionally, we also divided these CRC patients into two categories (low risk and high risk) based on the median value of DFS-nomogram, and the survival analysis exhibited the distinct survival difference among the two groups ($P < 0.001$), highlighting the potential value of the DFS-nomogram for risk stratification of CRC patients (Figure 6(b)).

3.5. Calibration Ability and Clinical Utility of Survival Nomograms. We applied the calibration curves to compare actual probabilities of survival rates and the predicted survival rates by survival nomograms. Figure S1A-F demonstrates good agreement for 1-year, 3-year, and 5-year predicting probabilities of OS rates and actual survival rates in both test and validation cohorts. In addition, Figure S2A-F also shows good agreement for the 1-year,

3-year, and 5-year predicting probabilities of DFS rates and actual survival rates in both test and validation sets. Moreover, we employed DCA to assess the clinical utilities of the survival nomograms for CRC patients. As presented in Figures 7(a) and 7(b), if the threshold probability of a patient was 0.25, both the OS-nomogram and DFS-nomogram added more clinical benefits than either treat-none scheme or treat-all scheme, implicating that the survival nomograms were clinically applicable for CRC patients.

4. Discussion

Systemic inflammation and malnutrition is prevailing in patients with cancer. The two factors have a significant impact on the quality of life and treatment outcomes in cancer population [13]. As malnutrition is a major element for immunodeficiency, the nutritional condition can be used to quickly evaluate the immune status of cancer patients [14]. Some clinical cohorts and meta-analyses investigated the associations between the immune-inflammation index evaluated by laboratory data and survival outcomes in malignant cancers [15–18], but few clinical researches have appraised

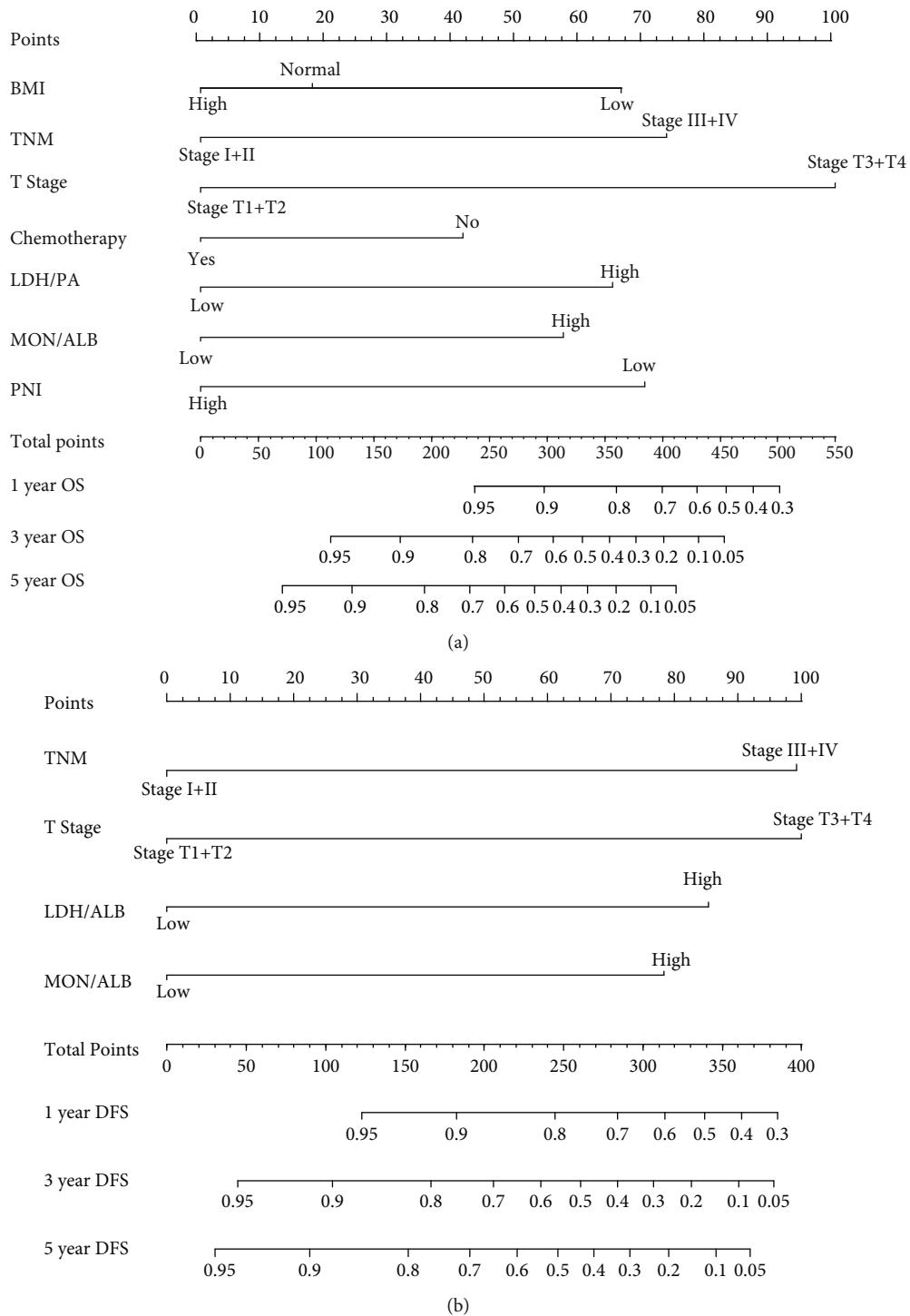


FIGURE 4: Survival nomograms based on immune-inflammation indexes for the prediction of CRC patients' survival mortality. (a) Overall survival nomogram. (b) Disease-free survival nomogram.

this correlation in CRC patients. This clinical research systematically assessed the available immune-inflammation indexes ($N = 19$) as many as possible in CRC patients. Then, we found that LDH/PA, LDH/ALB, PNI, and MON/ALB possess the most outstanding performance in the prediction of survival outcomes, and we also measured

its correlations with other immune-inflammation indexes. Finally, we screened the most informative immune-inflammation elements based on Cox regression for the construction survival nomograms. Both OS and DFS nomograms derived from immune-inflammation parameters exhibited adequate discrimination and well clinical utility.

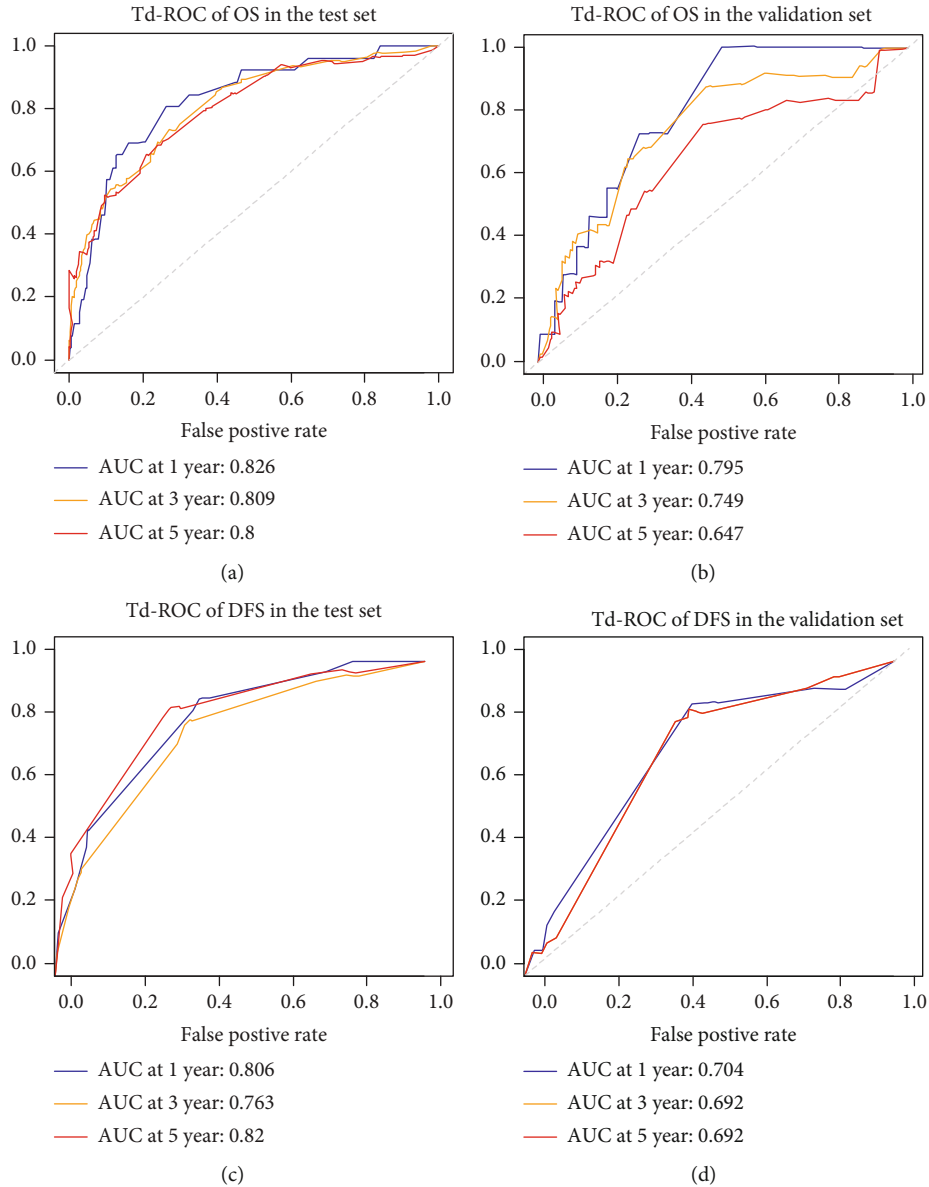
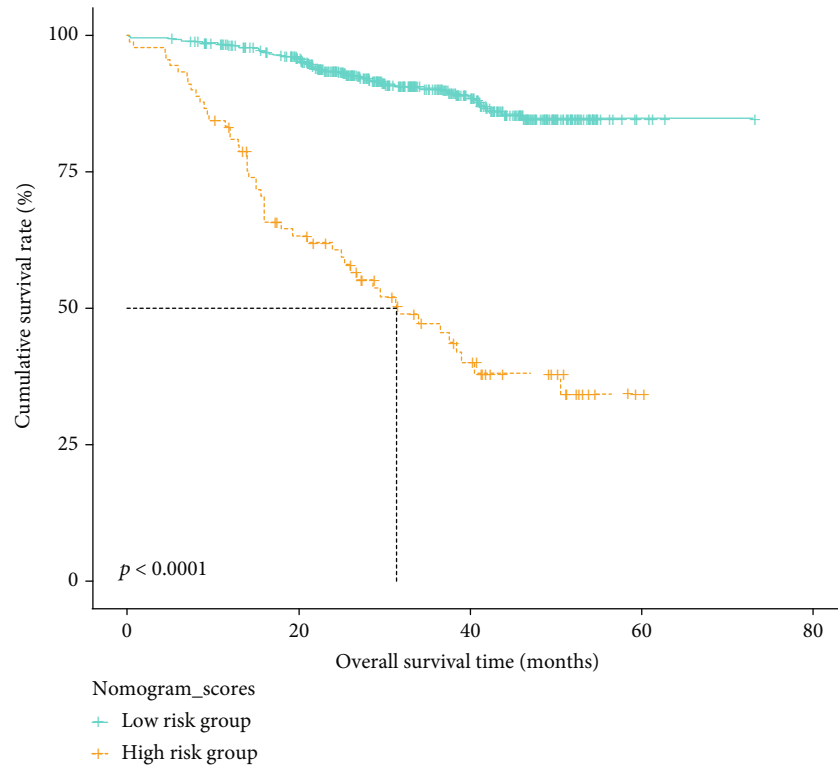


FIGURE 5: Predictive accuracy of survival nomograms presented with td-ROC curves. (a) Prediction of overall survival rate in the test set. (b) Prediction of overall survival rate in the validation set. (c) Prediction of disease-free survival rate in the test set. (d) Prediction of disease-free survival rate in the validation set.

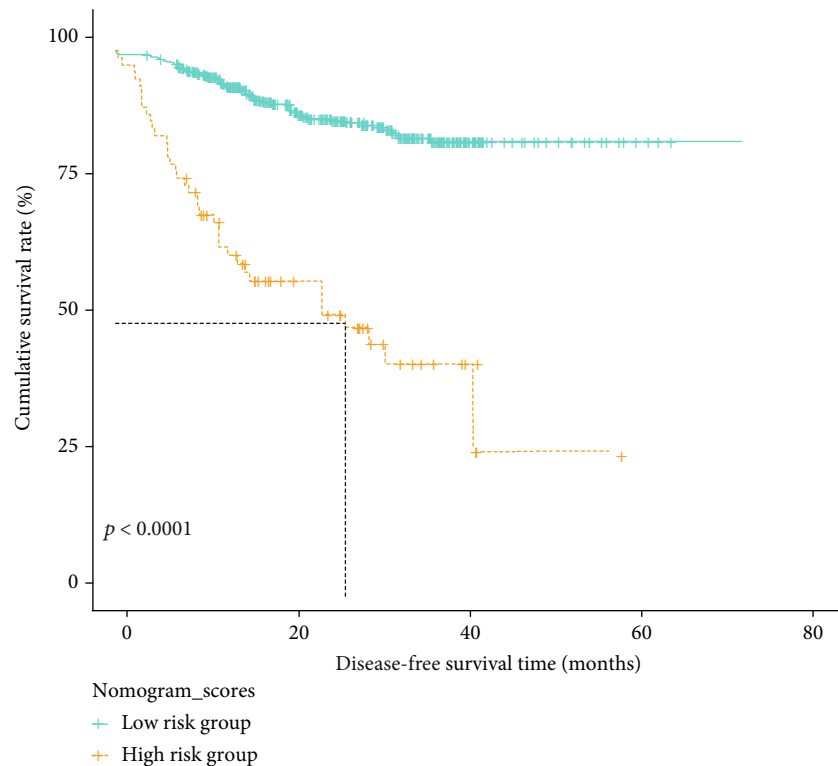
Serum LDH usually converts pyruvate to lactate in the condition of hypoxia, which occupies an important role in the metabolism of tumor cells. LDH-A is reported to be highly expressed in metastatic cancer cells and hypoxic carcinomas, whose levels closely associated with the viability of cancer cells. Levels of serum LDH are markers of immune suppression and tumor hypoxia [19–21]. Moreover, recent studies also revealed that high levels of serum LDH signify heavy tumor burden and tumor progression in cancer [22, 23]. Hence, we could conclude that high levels of serum LDH are indicative of unfavorable survival outcomes in cancer individuals. As mentioned above, serum albumin level could well reflect the nutritional status of cancer patients, and tumor-related inflammatory response may contribute to the loss of albumin. In LDH/ALB, a novel immune-

inflammation biomarker, its high level means severe inflammation and worse nutritional status. LDH/ALB is reported to be highly correlated with survival outcomes in some types of tumors, but fewer studies explored its correlation with the survival outcomes in CRC patients.

Feng et al. [24] conducted a retrospective study with a cohort of 346 resectable esophageal squamous cell carcinoma (ESCC) and concluded that LDH/ALB is a useful prognostic biomarker in patients with resectable ESCC who received surgical resection. Gan et al. [25] assessed the prognostic role of serum LDH/ALB in a cohort of 1,041 liver cancer patients who received curative resection, and they demonstrated that serum LDH/ALB was superior to other inflammatory scores in terms of predicting survival in liver cancer individuals who underwent radical surgical removal.



(a)



(b)

FIGURE 6: Kaplan-Meier curves of survival nomograms by two groups. (a) Overall survival analysis. (b) Disease-free survival analysis.

A cohort study from Turkey including 295 cases of CRC patients also reached the similar conclusion that preoperative LDH/ALB was an unfavorable prognosticator in CRC

patients receiving curative resection [26]. However, the sample size ($N = 295$) somewhat limited the persuasion of the conclusion. In our study ($N = 1024$), we also found the

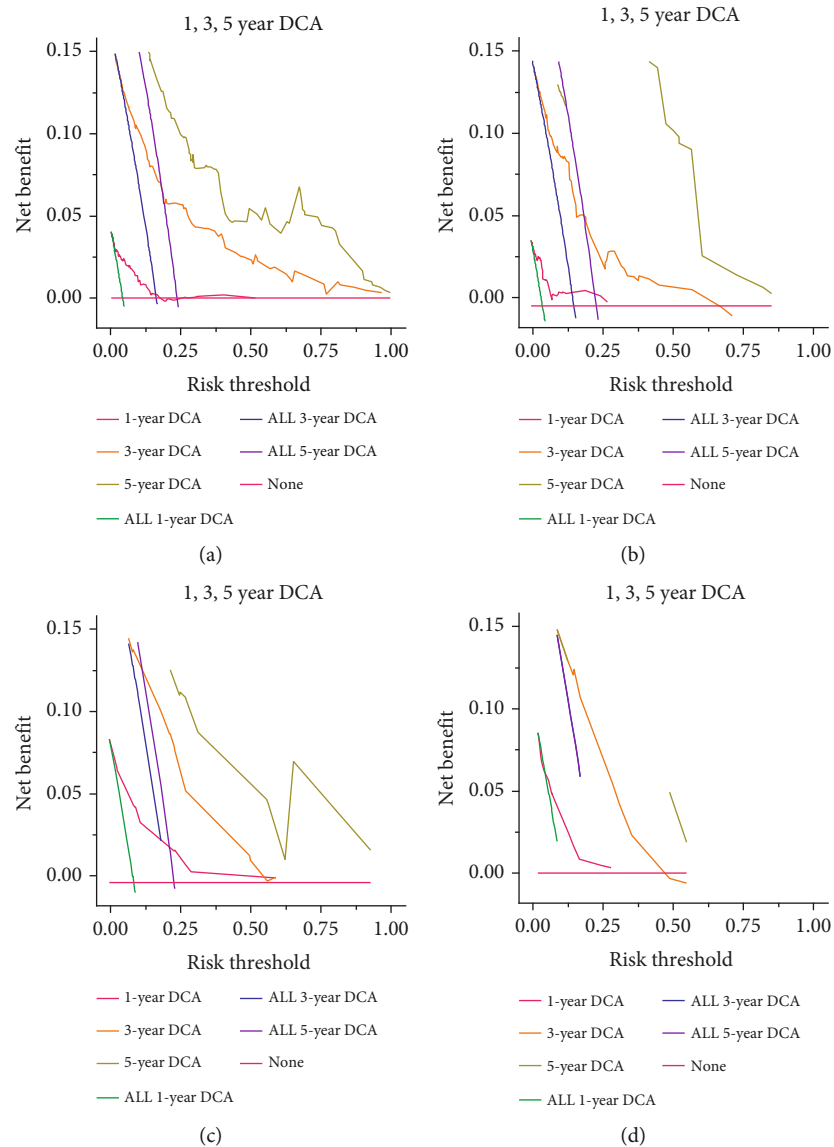


FIGURE 7: The clinical utility of survival nomograms by decision curve analysis (DCA). (a) DCA of overall survival in the test set. (b) DCA of overall survival in the validation set. (c) DCA of disease-free survival in the test set. (d) DCA of disease-free survival in the validation set.

superior predictive performance of serum LDH/ALB, and serum LDH/ALB was not only a strong prognostic biomarker for unfavorable OS but also an independent risk element for inferior DFS in CRC patients.

Protein-related malnutrition is very common in cancer patients with advanced stage and eventually leads to the damage of immune barrier. Malnutrition can seriously affect the biosynthesis of PA and ALB [27]. Compared with ALB, PA has a shorter half-life (2 days) than ALB (12 days) and could be utilized as a promising marker to monitor the nutritional status. Our study not only explored the prognostic role of serum LDH/ALB in CRC patients but also assessed the prognostic significance of serum LDH/PA in CRC patients. The multivariate Cox regression analysis revealed that serum LDH/PAB was a potent risk factor for inferior OS and DFS in patients with CRC.

The application of Mon/ALB is an objective assessment criterion of inflammatory and nutritional status, which is completely based on easily available laboratory parameters. Monocyte count, directly from blood routine, is a direct parameter of inflammatory response and also reflects the condition of immune surveillance to tumor cells. In a multicenter study with 1052 cases of rectal cancer patients, Fulop et al. [28] highlighted the clinical significance of lymphocyte-to-monocyte ratio. They clarified that the lymphocyte-to-monocyte ratio was inversely associated with neutrophil-to-lymphocyte, and the preoperative values of lymphocyte-to-monocyte can be utilized as an independent risk biomarker for less unfavorable OS in rectal cancer individuals. Serum ALB can not only effectively reflect the nutritional status of cancer patients but also be related to the severe liver function caused by inflammatory cytokines

[29]. Our results confirmed that CRC patients with high Mon/ALB were more likely to experience worse OS and DFS. Compared with some established immunonutritional indexes commonly applied in clinical practice, such as GRIm score and CONUT, MON/ALB is more accurate and convenient for immune-inflammation evaluation in patients with CRC.

Our aim was to design a precise survival model based on the independent prognostic factors for patients with CRC. Since the endpoints of this analysis were OS status, OS time, DFS status, and DFS time, so we selected the Cox proportional hazards model rather than the Kaplan-Meier marginal regression model. As the survival outcomes of CRC individuals are usually related to multiple endpoints which compete with one another to produce competitive risk data [30], the Cox proportional hazards model is a classical statistical model and widely employed in survival analysis for individuals with cancer. Accurate estimation of the cumulative incidence of survival outcomes for right-censored survival variables with multiple endpoints is the main advantage of Cox proportional hazards model. Hence, we identified seven potent factors for unfavorable OS and four risk factors for less favorable DFS in the test set based on the Cox proportional hazard model.

Three limitations still existed in this clinical analysis. First, this was a retrospective clinical research with relatively small study population. Then, we could not assess the association between dynamic changes of immune-nutritional indexes and survival outcomes in patients with CRC. In spite of the internal validation with 307 CRC patients, no external validation from another medical center was performed to evaluate the universal applicability of the survival nomograms. Hence, our conclusions should be further validated with prospective studies of more medical centers in the future.

5. Conclusion

This is the first scoring system based on immune-inflammation indexes to forecast survival outcomes in CRC sufferers. Notably, these selected immune-inflammation indexes are commonly tested among hospitalized patients in the clinical practice, which possess a practical advantage. This reliable predictive tool may play a role in risk stratification of CRC patients.

Abbreviation

CRC:	Colorectal cancer
OS:	Overall survival
DFS:	Disease-free survival
BMI:	Body mass index
LDH:	Lactate dehydrogenase (LDH)
PA:	Prealbumin
ALP:	Alkaline phosphatase
GGT:	Glutamyltransferase
CREA:	Creatinine
ALB:	Albumin
MON:	Monocytes

PLT:	Platelet
LYM:	Lymphocyte
NEU:	Neutrophil
PNI:	Prognostic nutritional index
GRIm:	Gustave Roussy Immune
CONUT:	Controlling nutritional status score
DCA:	Decision curve analysis
AIC:	Akaike information criterion
Td-ROC:	Time-dependent receiver operating characteristic.

Data Availability

The original contributions presented in the study are included in the article/Supplementary Material.

Ethical Approval

All relevant materials were checked and approved by the Clinical Research Ethics Committee (CREC) of Wuhan Union Hospital (No. 2018-S377).

Conflicts of Interest

All authors declare that they have no conflicts of interest.

Authors' Contributions

WGD and JL designed the research. ST and YL collected the clinical data. ST, YLL, and YM analyzed the data. YLL and YM wrote the manuscript. CLZ, YL, WGD, and JL revised the manuscript. All authors contributed to the article and approved the submitted version. Yulan Liu and Yang Meng contributed equally to this work and are the co-first authors.

Supplementary Materials

Table S1: the differences of basic features between test set and validation set. Table S2: univariate Cox regression of survival outcomes of CRC patients in the test cohort. Figure S1: calibration curves of OS-nomogram in the test (A-C) and validation cohorts (D-F). Figure S2: calibration curves of DFS-nomogram in the test (A-C) and validation cohorts (D-F). (*Supplementary Materials*)












References

- [1] N. A. Lakkis, O. El-Kibbi, and M. H. Osman, "Colorectal cancer in Lebanon: incidence, temporal trends, and comparison to regional and Western countries," *Cancer Control*, vol. 28, 2021.
- [2] F. Baidoun, K. Elshiwiy, Y. Elkeraiet et al., "Colorectal cancer epidemiology: recent trends and impact on outcomes," *Current Drug Targets*, vol. 22, no. 9, pp. 998–1009, 2021.
- [3] R. Percario, P. Panaccio, F. F. di Mola, T. Grottola, and P. Di Sebastiano, "The complex network between inflammation and colorectal cancer: a systematic review of the literature," *Cancers*, vol. 13, no. 24, p. 6237, 2021.
- [4] K. Thanikachalam and G. Khan, "Colorectal cancer and nutrition," *Nutrients*, vol. 11, no. 1, p. 164, 2019.

- [5] A. E. Tuomisto, M. J. Makinen, and J. P. Vayrynen, "Systemic inflammation in colorectal cancer: underlying factors, effects, and prognostic significance," *World Journal of Gastroenterology*, vol. 25, no. 31, pp. 4383–4404, 2019.
- [6] G. Fuca, V. Guarini, C. Antoniotti et al., "The pan-immune-inflammation value is a new prognostic biomarker in metastatic colorectal cancer: results from a pooled-analysis of the _Valentino_ and TRIBE first-line trials," *British Journal of Cancer*, vol. 123, no. 3, pp. 403–409, 2020.
- [7] K. Takagi, S. Buettner, and J. Ijzermans, "Prognostic significance of the controlling nutritional status (CONUT) score in patients with colorectal cancer: a systematic review and meta-analysis," *International Journal of Surgery*, vol. 78, pp. 91–96, 2020.
- [8] S. Tian, Y. Cao, Y. Duan, Q. Liu, and P. Peng, "Gustave Roussy immune score as a novel prognostic scoring system for colorectal cancer patients: a propensity score matching analysis," *Frontiers in Oncology*, vol. 11, article 737283, 2021.
- [9] C. Song, J. Cao, F. Zhang et al., "Nutritional risk assessment by scored patient-generated subjective global assessment associated with demographic characteristics in 23, 904 common malignant tumors patients," *Nutrition and Cancer-An International Journal*, vol. 71, no. 1, pp. 50–60, 2019.
- [10] A. J. Vickers, B. van Calster, and E. W. Steyerberg, "A simple, step-by-step guide to interpreting decision curve analysis," *Diagnostic and Prognostic Research*, vol. 3, no. 1, p. 18, 2019.
- [11] J. Yang, Y. Li, Q. Liu et al., "Brief introduction of medical database and data mining technology in big data era," *Journal of Evidence-Based Medicine*, vol. 13, no. 1, pp. 57–69, 2020.
- [12] T. Kogiso, Y. Moriyoshi, S. Shimizu, H. Nagahara, and K. Shiratori, "High-sensitivity C-reactive protein as a serum predictor of nonalcoholic fatty liver disease based on the Akaike Information Criterion scoring system in the general Japanese population," *Journal of Gastroenterology*, vol. 44, no. 4, pp. 313–321, 2009.
- [13] R. V. Dias, D. P. N. Barroso, E. Abdelhay, J. P. Viola, M. I. Correia, and M. R. Brum, "Nutrition and immune-modulatory intervention in surgical patients with gastric cancer," *Nutrition in Clinical Practice*, vol. 32, no. 1, pp. 122–129, 2017.
- [14] M. Veldhoen and H. Veiga-Fernandes, "Feeding immunity: skepticism, delicacies and delights," *Nature Immunology*, vol. 16, no. 3, pp. 215–219, 2015.
- [15] Y. Zhang and X. Zhang, "Controlling nutritional status score, a promising prognostic marker in patients with gastrointestinal cancers after surgery: a systematic review and meta-analysis," *International Journal of Surgery*, vol. 55, pp. 39–45, 2018.
- [16] K. Takagi, P. Domagala, W. G. Polak, S. Buettner, and J. Ijzermans, "The controlling nutritional status score and post-operative complication risk in gastrointestinal and Hepatopancreatobiliary surgical oncology: A systematic review and meta-analysis," *Annals of Nutrition and Metabolism*, vol. 74, no. 4, pp. 303–312, 2019.
- [17] Q. Zhang, K. Zhang, X. Li et al., "A novel model with nutrition-related parameters for predicting overall survival of cancer patients," *Supportive Care in Cancer*, vol. 29, no. 11, pp. 6721–6730, 2021.
- [18] K. Sugimachi, T. Iguchi, Y. Mano et al., "The impact of immunonutritional and physical status on surgical outcome after pancreaticoduodenectomy in elderly patients," *Anticancer Research*, vol. 39, no. 11, pp. 6347–6353, 2019.
- [19] O. Iglesias-Velazquez, R. M. Lopez-Pintor, J. Gonzalez-Serrano, E. Casanas, J. Torres, and G. Hernandez, "Salivary LDH in oral cancer and potentially malignant disorders: a systematic review and meta-analysis," *Oral Diseases*, vol. 28, no. 1, pp. 44–56, 2022.
- [20] C. de Jong, V. Deneer, J. C. Kelder, H. Ruven, T. Egberts, and G. Herder, "Association between serum biomarkers CEA and LDH and response in advanced non-small cell lung cancer patients treated with platinum-based chemotherapy," *Thoracic Cancer*, vol. 11, no. 7, pp. 1790–1800, 2020.
- [21] W. Wulaningsih, L. Holmberg, H. Garmo et al., "Serum lactate dehydrogenase and survival following cancer diagnosis," *British Journal of Cancer*, vol. 113, no. 9, pp. 1389–1396, 2015.
- [22] J. Ding, J. E. Karp, and A. Emadi, "Elevated lactate dehydrogenase (LDH) can be a marker of immune suppression in cancer: interplay between hematologic and solid neoplastic clones and their microenvironments," *Cancer Biomarkers*, vol. 19, no. 4, pp. 353–363, 2017.
- [23] T. Dong, Z. Liu, Q. Xuan, Z. Wang, W. Ma, and Q. Zhang, "Tumor LDH-A expression and serum LDH status are two metabolic predictors for triple negative breast cancer brain metastasis," *Scientific Reports*, vol. 7, no. 1, p. 6069, 2017.
- [24] J. F. Feng, L. Wang, X. Yang, and Y. H. Jiang, "Prognostic value of lactate dehydrogenase to albumin ratio (LAR) in patients with resectable esophageal squamous cell carcinoma," *Cancer Management and Research*, vol. 11, pp. 7243–7251, 2019.
- [25] W. Gan, M. X. Zhang, J. X. Wang et al., "Prognostic impact of lactic dehydrogenase to albumin ratio in hepatocellular carcinoma patients with Child-Pugh I who underwent curative resection: a prognostic nomogram study," *Cancer Management and Research*, vol. 10, pp. 5383–5394, 2018.
- [26] U. Aday, A. Boyuk, and H. Akkoc, "The prognostic significance of serum lactate dehydrogenase-to-albumin ratio in colorectal cancer," *Annals of Surgical Treatment and Research*, vol. 99, no. 3, pp. 161–170, 2020.
- [27] S. Delliere and L. Cynober, "Is transthyretin a good marker of nutritional status?," *Clinical Nutrition*, vol. 36, no. 2, pp. 364–370, 2017.
- [28] Z. Z. Fulop, S. Gurzu, R. L. Fulop et al., "Prognostic impact of the neutrophil-to-lymphocyte and lymphocyte-to-monocyte ratio, in patients with rectal cancer: a retrospective study of 1052 patients," *Journal of Personalized Medicine*, vol. 10, no. 4, p. 173, 2020.
- [29] J. Liu, Y. Dai, F. Zhou et al., "The prognostic role of preoperative serum albumin/globulin ratio in patients with bladder urothelial carcinoma undergoing radical cystectomy," *Urologic Oncology*, vol. 34, no. 11, pp. 481–484, 2016.
- [30] W. T. Wu, Y. J. Li, A. Z. Feng et al., "Data mining in clinical big data: the frequently used databases, steps, and methodological models," *Military Medical Research*, vol. 8, no. 1, p. 44, 2021.

Research Article

In-House Validated Map of Lymph Node Stations in a Prospective Cohort of Colorectal Cancer: A Tool for a Better Preoperative Staging

Patricia Simu ^{1,2}, Ioan Jung ², Laura Baniias ², Zsolt Zoltan Fulop ³, Tivadar Bara ³,
Iunius Simu ¹, Sebastian Andone ⁴, Raluca Ioana Stefan-van Staden ⁵,
Catalin Bogdan Satala ², Ioana Halmaciu ^{1,6} and Simona Gurzu ^{2,7}

¹Department of Radiology and Imaging, Clinical County Emergency Hospital, Targu Mures, Romania

²Department of Pathology, George Emil Palade University of Medicine, Pharmacy, Sciences and Technology, Targu Mures, Romania

³Department of Surgery, George Emil Palade University of Medicine, Pharmacy, Science and Technology, Targu Mures, Romania

⁴Department of Neurology, George Emil Palade University of Medicine, Pharmacy, Sciences and Technology, Targu Mures, Romania

⁵Laboratory of Electrochemistry and PATLAB, National Institute of Research for Electrochemistry and Condensed Matter, Bucharest, Romania

⁶Department of Anatomy, George Emil Palade University of Medicine, Pharmacy, Sciences and Technology, Targu Mures, Romania

⁷Research Center of Oncopathology and Transdisciplinary Research, George Emil Palade University of Medicine, Pharmacy, Sciences and Technology, Targu Mures, Romania

Correspondence should be addressed to Ioana Halmaciu; anca_halmaciu@yahoo.com

Received 9 January 2022; Revised 6 February 2022; Accepted 7 March 2022; Published 19 March 2022

Academic Editor: Alessandro Granito

Copyright © 2022 Patricia Simu et al. This is an open access article distributed under the Creative Commons Attribution License, which permits unrestricted use, distribution, and reproduction in any medium, provided the original work is properly cited.

Preoperative staging of colorectal cancer (CRC) based on imaging techniques such as computed tomography (CT) or magnetic resonance imaging (MRI) is crucial for identification and then removal of the positive lymph nodes (LNs). The aim of this study was to evaluate the correlation between preoperatively seen morphologic criteria (number, size, shape, structure, borders, or enhancement patterns) and histopathological features of LNs using an in-house validated map of nodal stations. A total of 112 patients with CRC that underwent surgery were preoperatively evaluated by CT scans. The locoregional, intermediate, and central LNs were CT-mapped and then removed during open laparotomy and examined under microscope. The analysis of correlations was interpreted using the suspicious-to-positive ratio (SPR) parameter. The greatest correlation was found in tumors located in the sigmoid colon, descending colon and middle rectum; SPR value was 1.12, 1.18, and 1.26, respectively. SPR proved to be 0.59 for cases of the transverse colon. Regarding the enhancement type, the dotted pattern was mostly correlated with metastatic LNs (OR: 7.84; $p < 0.0001$), while the homogenous pattern proved a reliable indicator of nonmetastatic LNs (OR: 1.99; $p < 0.05$). A total of 1809 LNs were harvested, with a median value of 15 ± 1.34 LNs/case. Transdisciplinary approach of CRC focused on pre-, intra-, and postoperatively mapping of LNs might increase the accuracy of detecting metastasized nodes for tumors of the distal colon and middle rectum but not for those of the transverse colon. In addition to morphologic criteria, the enhancement pattern of LNs can be used as a predictor of nodal involvement improving the CT-based preoperative staging.

1. Introduction

Despite individualized therapy, colorectal cancer (CRC) remains one of the most prevalent digestive malignancies

worldwide and the second leading cause of cancer-related deaths, with an increasing incidence in the last years [1–3]. Long overall survival rate (OS) is reported in patients with CRC diagnosed in early stages [2–4]. Screening programs are

developed in most of the countries but lack of optimization of policy of screening and surveillance by colonoscopy lead to diagnosis of most of the cases in advanced stages [5, 6].

Although several modern prognostic parameters were proposed, the number of harvested lymph nodes (LN) same as the number of metastatic nodes (N status) and the rate of positive vs. removed nodes (lymph node ratio—LNR) remain the most important independent prognostic parameters [7–9]. The 5-year survival rate of 75–95% was reported for patients with CRC diagnosed in stages I or II (N0) compared to 30–68% in stages III or IV [7, 8, 10]. Furthermore, 20–30% of the N0-staged recurrent cases with completely excised tumors and free resection margins (R0) could be linked to occult LN metastases [11]. An accurate imaging evaluation of the LN status is crucial for choosing extensive lymphadenectomy, pre- or postsurgery chemo- and/or radiotherapy, as well as neoadjuvant therapy.

Although LN status and identification of synchronous CRCs can be successfully done preoperatively using imaging methods such as computed tomography (CT) and magnetic resonance imaging (MRI) [9], the reported sensitivity and specificity for LN mapping via CT-scan is about 71% and 41%, respectively [12]. Several criteria have been proposed for a more accurate evaluation of LN status. LN size has been used as a predictor for positive LNs, with a threshold size of 10 mm, but the sensitivity and specificity do not exceed 71% and 67%, respectively [13–15]. In other studies, it was shown that most metastatic LNs were <5 mm whereas those beyond 10 mm were enlarged due to a good host inflammatory response [10, 11].

Japanese Society for Cancer of the Colon and Rectum, respectively, Yamamoto et al., proposed to use, as a prognostic parameter, a map of LN stations which was designed based on the localization of the LNs. They divided the LN stations into three main categories: locoregional, stations near great vessels, and stations located at the origin of great vessels [16]. Metastases in the stations located at the origin of great vessels upgrade staging at stage IV [17].

For contrasting CT-scan identification of the LN stations and suspected nodes, size, roundness, heterogeneity, and contour irregularity should be checked [18]. Based on combined features, Miao et al. proposed six patterns of internal enhancement: homogenous, striped, spotted, core, rim, and heterogenous [12]. Heterogeneity and rim pattern may correspond to the invasion of malignant cells into the subcapsular sinus via lymphatic vessels (LV), as well as a lack of blood supply which leads to necrosis of the medulla [12, 19–21]. Spotted enhancement was linked to dilated subcapsular sinuses whereas stripped pattern is considered an indicator of interlinked capillary sinus. Core and homogenous enhancements are strongly associated with negative LNs, being known as benign patterns [12].

The aim of this study was to perform an in-house validation of the map of Yamamoto et al., which reliability was previously confirmed by the team for synchronous CRCs [9, 16], and to check the correlation between CT-scan-based criteria of suspicion of LN metastases and microscopic features.

2. Materials and Methods

2.1. Criteria of Inclusion. This prospective study included 112 consecutive patients with CRC, diagnosed and surgically treated by the same surgical team, at the Emergency Clinical County Hospital of Targu Mures, Romania, between 2016 and 2020. The Approval of the Ethical Committee of the Clinical County Emergency Hospital of Targu-Mures, Romania, was obtained for the study. From each patient, signed informed consent was obtained prior surgery for both permissions to perform surgical resection and use of patient information in the scientific publications.

All patients had previous colonoscopy with a positive biopsy for carcinoma. They were referred to the Imaging Department for CRC staging before surgery. We have included all adult patients with preoperatively proved biopsy of carcinoma, in which colectomy and tumor excision was done with free proximal and distal resection margins and extensive lymphadenectomy. Criteria of exclusion: patient's refusal, preoperative oncologic therapy, inoperable cases, death before one month after surgery, associated peritoneal carcinomatosis, recurrent carcinomas, synchronous or metachronous cancers, and independently by their localization, same as diagnosis of a metastatic tumor or a rare histological variant (e.g., neuroendocrine or clear cell carcinoma).

2.2. Image Acquisition. In all patients, nonenhanced (NECT) and contrast-enhanced CT (CECT) scans, to identify the localization and characteristics of the tumor and the suspicious LNs, were done. Imagistic investigations were performed by the same team (SP, SI), same as the surgical intervention (BT) and histopathological assessment (GS, JJ, BL, and SC).

A Siemens Somatom 64 channel CT scanner was used for the acquisition of images. An abdominopelvic multiphase CT scan was performed for each patient, with nonenhanced sequence exam followed by intravenous contrast media administration and another two acquisitions: a late arterial phase, at 25 seconds after injection, and a portal-venous phase, at 70 seconds after injection of the contrasting substance. The kilovoltage ranged between 120 and 140 kV with 220 mAs. All patients have received iodinated hydro-soluble contrast media (Optiray 350, 350 mg I/ml) in a dose of 1 ml/kg of body weight with a flow rate ranging from 2 to 3 ml/sec.

2.3. Imaging Assessment. All the abdominopelvic LNs were assessed according to an in-house established protocol, based on the Japanese Classification of Colorectal, Appendiceal, and Anal Carcinoma (JCCRC) developed and updated in 2019 by the Japanese Society of Cancer of the Colon and Rectum (JSCCR). First, a map was adapted from JSCCR study “Japanese Classification of Colorectal, Appendiceal, and Anal Carcinoma: the 3rd English Edition” [16] with permission obtained from the authors, where the nodal stations were divided into three categories: locoregional—within 5 cm from tumor, intermediate-between 5 and 10 cm from tumor, alongside the great vessels, and central LNs—more than 10 cm from tumor, at the origin of great vessels

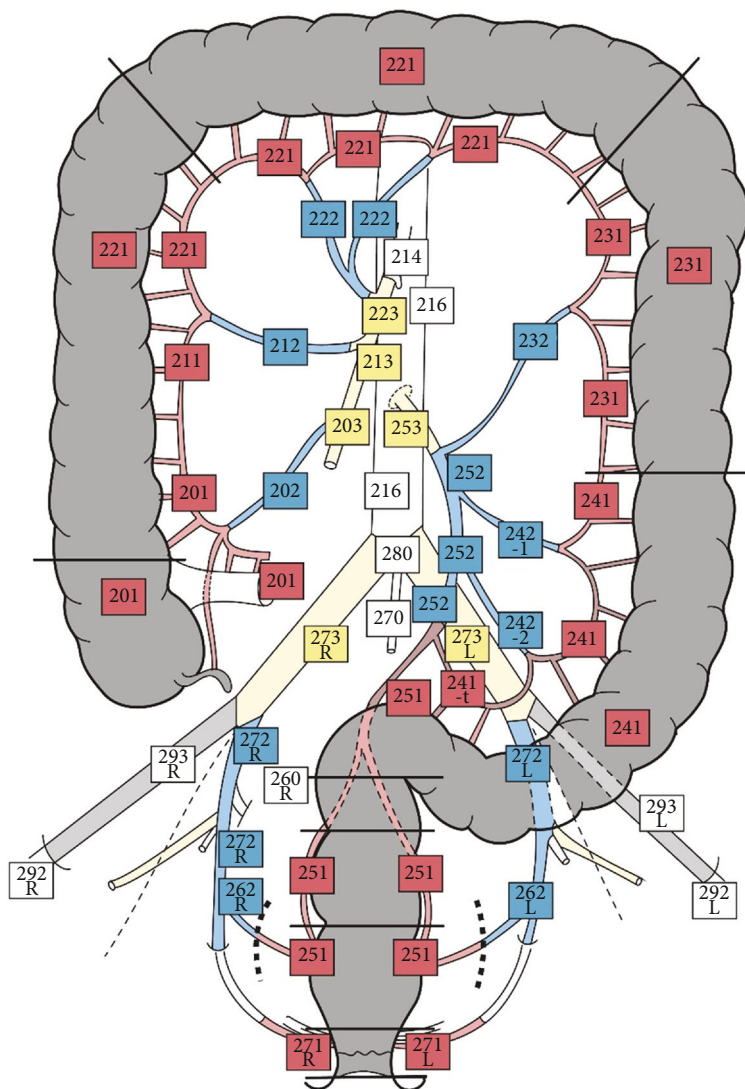


FIGURE 1: The nodal stations map, adapted with permission from the JSCCR study “Japanese Classification of Colorectal, Appendiceal, and Anal Carcinoma: the 3rd English Edition” [16]. Three categories of nodal stations are seen: locoregional (red), intermediate (blue), and central (yellow and white).

(Figure 1). The map was previously used by our team for identification and evaluation of synchronous CRCs [9]. In the present study, for any patient, an individualized map was done and the LNs suspected of metastases were ringed, to be further harvested by the surgeons.

To consider a LN as being suspected to present metastases, imaging features like short-axis diameter, shape, structure, and borders were considered. The LNs were divided into three groups according to their size: ≤ 5 mm, 5-10 mm, and ≥ 10 mm. Suspicion criteria (roundness, heterogeneous density, and irregular border) were considered depending on their size. So, if a LN was ≤ 5 mm, it needed the presence of all three criteria of suspicion; LNs between 5 and 10 mm were considered suspicious if they had two of three criteria and LNs ≥ 10 mm were always considered suspicious [12, 18]. The total number of LNs was noted in each case, with the number of suspicious LNs outlined.

For an objective evaluation, we combined the previously mentioned features with the enhancement pattern of LNs in the venous phase of CECT, using magnified images. Based on the modified criteria proposed by Miao et al. [12], five patterns of enhancement were checked: homogenous, dotted, linear, central, and peripheral. Dotted pattern was characterized by small spots (< 3 mm) of contrast enhancement within the node. Linear pattern was defined as multiple belts of low enhancement giving it a stripey appearance. Central pattern appeared as bright spot of contrast enhancement in the central region, and peripheral pattern was defined as a hypodense center with a hyperdense rim (Figures 2 and 3). The enhancement pattern of both suspicious and nonsuspicious LNs was noted to be then correlated with the pathological reports.

2.4. Surgical Interventions and Histopathological Assessment. In all patients, open laparotomy was done for colectomy and

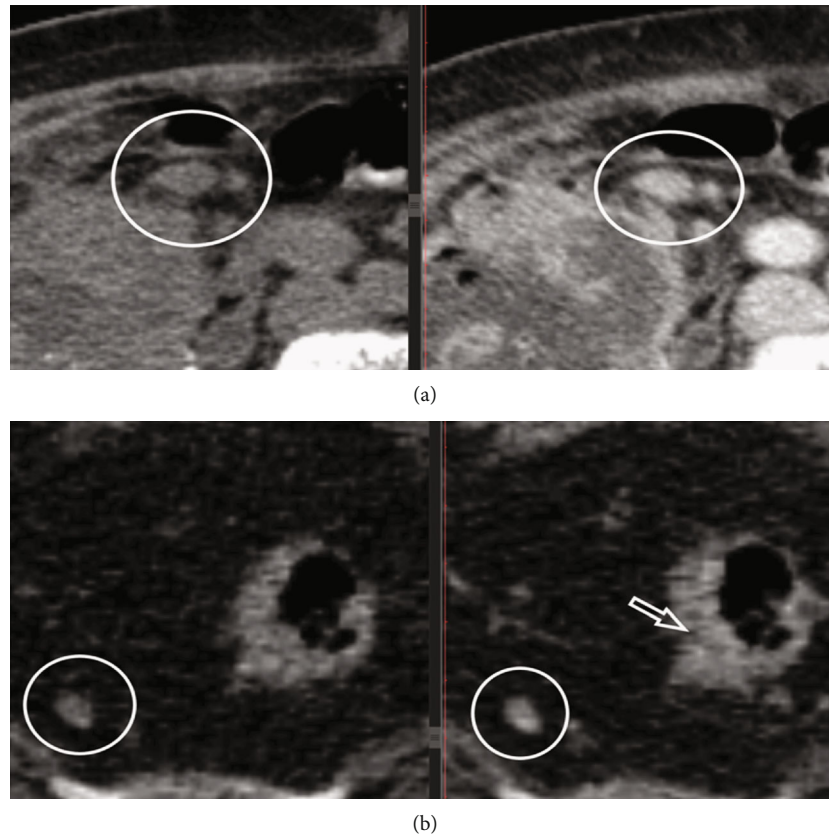


FIGURE 2: Lymph node assessment on NECT axial scan (left) and on CECT venous phase, axial view (right), with homogenous (a) and dotted enhancement pattern (b); infiltrative tumor of the rectal wall on the right side infiltrates the mesorectal fat (arrow).

surgical removal of the tumor with free proximal and distal resection margins. Based on the imaging map, the LNs which were encircled by the radiologists were harvested in individual recipients, on stations, and send for histopathological assessment [9]. In cases where the encircled nodal stations were peritumoral, the pathologist was informed to check the nodes in the resected surgical specimen.

Gross findings of the surgical specimens were done according to the current guidelines and imaging map. After formalin fixation, the palpable LNs were included for histological examination and comparison of imaging and microscopic features. The encircled suspicious LNs were included in individual histological cassettes. Then, histological slides from formalin-fixed paraffin-embedded tissue (FFPE) blocks were used for current histological assessment. When necessary, immunohistochemical stains with cytokeratin AE1/AE2 were performed for identification of occult metastases or micrometastases.

The pathological reports included the number of LNs harvested according to the nodal stations map and divided into the three groups (≤ 5 cm, between 5 and 10 cm, and ≥ 10 cm from tumor), as well as the number of positive LNs. Histological types, pTNM stage, number of LN metastases per node stations, and LNR were also mentioned in the histopathological report. The pTNM stage was established according to the American Joint Committee on Cancer staging system-8th edition (AJCC). Distant node metastases were

considered as distant metastases (pM1). Dimensions of the tumors (length and thickness), presence of vascular (V1), lymphatic (L1), and perineural invasion (n1) invasion same as the quality of the resection margins and the tumor budding degree (b) [22] were also pointed for further statistical processing.

2.5. Statistical Evaluation. The imaging assessment of the three categories of nodal stations was compared with the pathological reports and divided into four groups: positive correlation (preoperative suspicious nodes were histopathological proved metastatic), negative correlation (no suspicious nodes on imaging and no positive LNs after microscopic evaluation), false positive correlation (suspicious LNs on CT were not found positive on histology report), and false negative correlation (positive LNs under microscope were not matched by suspicious criteria on imaging assessment) [9]. The cases were then categorized based on the suspicious-to-positive ratio (SPR), which was the ratio between the number of CT-suspicious LNs and histologically positive LNs. SPR was calculated for each of the three groups of LNs (≤ 5 cm, between 5 and 10 cm, and ≥ 10 cm from tumor). Demographic (age, gender), imaging (suspicious and non-suspicious LNs), and histopathological parameters were compared between cases with positive vs. negative LNs. Sensitivity and specificity were calculated, as well as positive and negative predicted

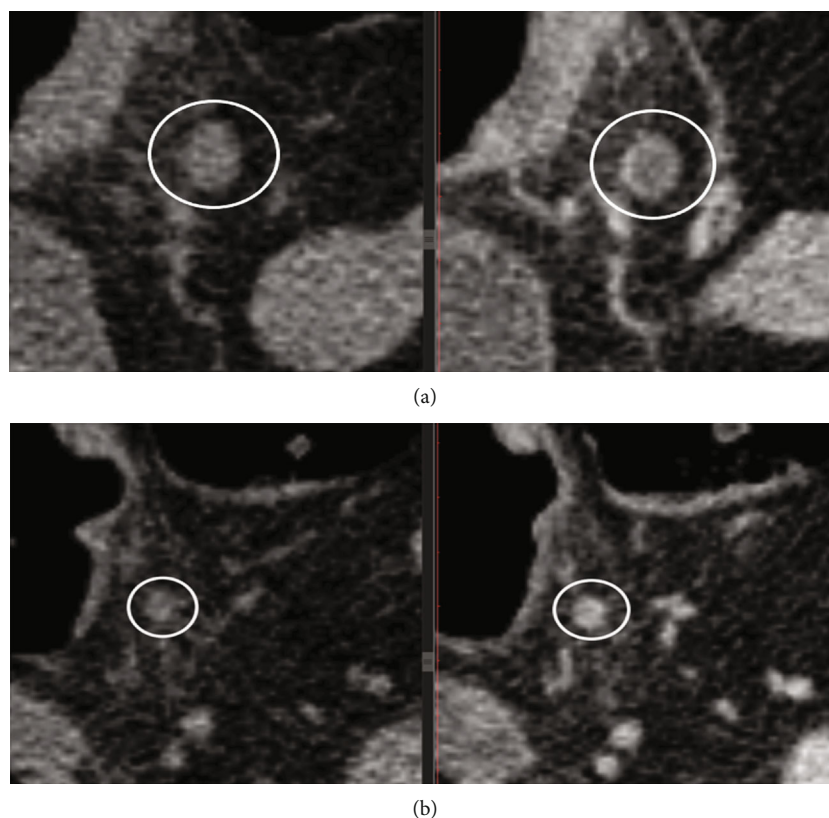


FIGURE 3: Lymph node assessment on NECT (left) axial view and on CECT scan venous phase, axial view (right), with peripheral (a) and linear enhancement pattern (b).

TABLE 1: Clinicopathological parameters of the examined colorectal cancers (G-grade of differentiation).

Variable	Number (n = 112)	Percentage (%)
Histological type		
(i) Adenocarcinoma-G1	(i) 3	(i) 2.68
(ii) Adenocarcinoma-G2	(ii) 54	(ii) 48.21
(iii) Adenocarcinoma-G3	(iii) 5	(iii) 4.47
(iv) Mucinous carcinoma	(iv) 40	(iv) 44.64
Depth of infiltration (T stage)		
(i) T1	(i) 4	(i) 3.57
(ii) T2	(ii) 13	(ii) 11.61
(iii) T3	(iii) 57	(iii) 50.89
(iv) T4	(iv) 38	(iv) 33.93
Lymph node status (N stage)		
(i) N0	(i) 73	(i) 65.18
(ii) N1	(ii) 23	(ii) 20.54
(iii) N2	(iii) 16	(iii) 14.29
Distant metastases (M stage)		
(i) M0	(i) 94	(i) 83.93
(ii) M1	(ii) 18	(ii) 16.07
AJCC staging (TNM)		
(i) I	(i) 12	(i) 10.71
(ii) II	(ii) 45	(ii) 40.18
(iii) III	(iii) 39	(iii) 34.82
(iv) IV	(iv) 16	(iv) 14.29

values (PPV, NPV). Statistically significant differences were considered for $p < 0.05$.

3. Results

3.1. Clinicopathological and Histological Aspects. From 112 patients with CRC, there were 78 males and 34 females (M : F ratio = 2.29 : 1), with a mean age of 65.60 ± 10.99 years (range 27-88 years). Most of the patients (71.42%) were diagnosed below their 60. LN metastases (LNM) were identified in one-third of the cases. Distant metastases were also seen in over one-quarter of the patients (Table 1). Mean length of the tumors was 48.14 ± 20.61 cm, whereas tumor thickness was of 20.07 ± 11.85 cm. There were 61 patients with rectal- and 51 with colon cancer. Risk of LNM was not associated with the tumor localizations but was higher in pV1L1n1b3 cases (Table 2).

3.2. Preoperative Imaging Assessment of LNs. Based on the CT-scan assessment, 1079 LNs were identified. Most LNs were seen in the first category of nodal stations—locoregional (n = 603; 33.33%), which showed a LNR of 0.10. From the 1079 nodes, 241 (22.34%) were considered “suspect of metastases,” according to the imaging protocol and were encircled on the nodal stations map. Most suspicious LNs were locoregional (n = 146; 60.58%) (Figure 4). The commonest suspicion criteria were roundness (64.56%), followed by inhomogeneity (22.75%) and irregular borders (12.67%).

TABLE 2: Distribution of lymph node metastasis (LNM) upon clinicopathological parameters.

Variable	LNM + (N1 + 2)	LNM - (N0)	p value
Gender			
Male (n = 78)	(i) 29	(i) 49	0.52
Female (n = 34)	(ii) 10	(ii) 24	
Tumor localization			
(i) Cecum (n = 13)	(i) 2	(i) 11	0.15
(ii) Ascending (n = 2)	(ii) 0	(ii) 2	
(iii) Transverse (n = 10)	(iii) 4	(iii) 6	
(iv) Descending (n = 6)	(iv) 3	(iv) 3	
(v) Sigmoid (n = 20)	(v) 11	(v) 9	
(vi) Superior rectum (n = 23)	(vi) 9	(vi) 14	
(vii) Middle rectum (n = 20)	(vii) 6	(vii) 14	
(viii) Inferior rectum (n = 18)	(viii) 3	(viii) 15	
Vascular invasion (V)			
(i) V1 (n = 29)	(i) 16	(i) 13	0.01
(ii) V0 (n = 83)	(ii) 23	(ii) 60	
Lymphatic invasion (L)			
(i) L1 (n = 46)	(i) 32	(i) 14	0.0001
(ii) L0 (n = 66)	(ii) 7	(ii) 59	
Perineural invasion (n)			
(i) n1 (n = 25)	(i) 18	(i) 7	0.0001
(ii) n0 (n = 87)	(ii) 21	(ii) 66	
Budding degree (b)			
(i) b2 + 3 - ≥ 5 buds/20 HPF (n = 67)	(i) 35	(i) 32	0.03
(ii) b1 - ≤ 5 buds/20 HPF (n = 45)	(ii) 14	(ii) 31	

The median size of the LNs was 6 ± 2.34 mm (range 2-34 mm). Almost half of them were ≤ 5 mm. LNs ≥ 10 mm were more likely to be negative (Figure 5).

3.3. Intra- and Postoperative Assessment of LNs. From the 112 cases, a total of 1809 LNs were removed during surgery and examined under microscope. The median value of the harvested nodes was 15 ± 1.34 LNs/case (range between 1 and 60 nodes); over 14 nodes were successfully retrieved in 75 cases (66.96%). From the 1809 nodes, 170 were metastatic (9.39%) (Figure 4). A percentage of 65.31% of LNs ≥ 10 mm was nonmetastatic but 70.53% of those exceeding 10 mm showed metastases at microscopic examination (Figure 5).

The NPV was 0.92 overall, with a sensitivity and specificity of 80% and 69%, respectively. The PPV was lower, being calculated at 0.42 (Table 3).

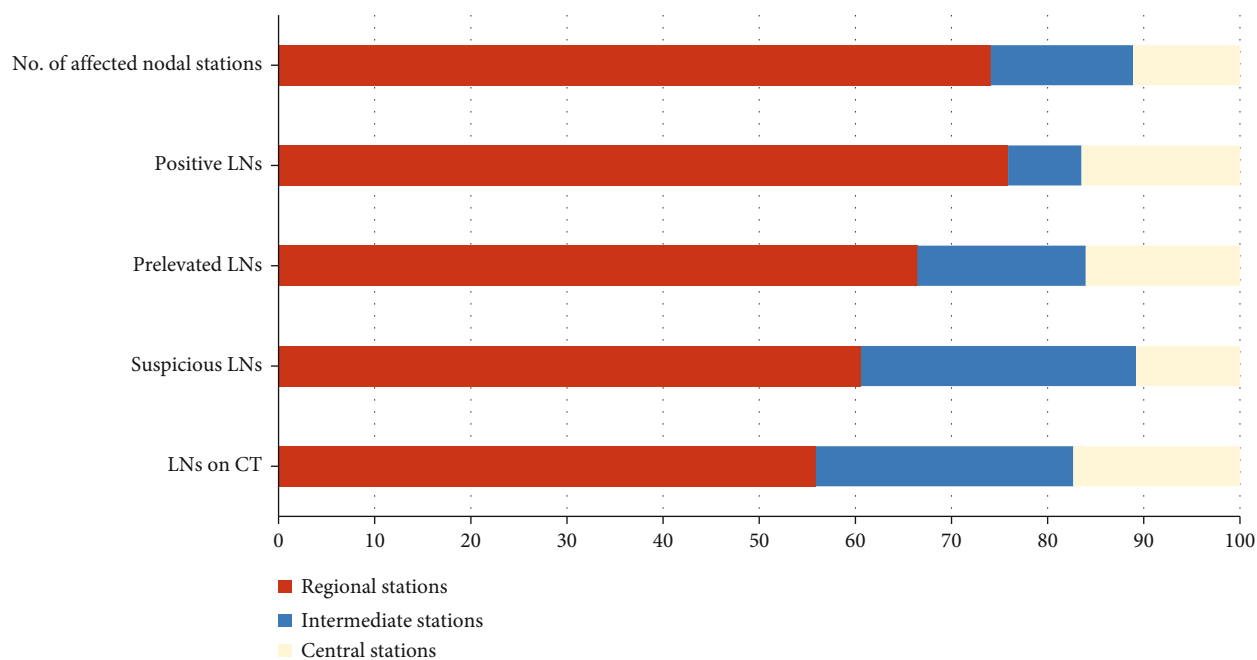
LNMs were identified in 38 of the 112 patients (33.93%). Majority of the metastatic cases involved sigma (n = 11; metastases predominantly in the station 241) and superior rectum (n = 9; nodal station 251). In most of the cases, positive LNs were seen in one nodal station, respectively, in the first category—locoregional (n = 29; 74.35%). There were 6 cases with two positive nodal stations, 3 cases with three and one case with four nodal stations with LNMs. The SPR value was 1.13 for locoregional, 5.30 for intermediate, and 0.92 for central node stations. The most accurate SPR values were obtained for the cases located on the sigmoid and descending colon same as for those of the middle rectum (1.12; 1.18; 1.26) (Figure 6).

3.4. Internal Enhancement Pattern Analysis. Both NECT and CECT examinations were used for a more objective CT-histology correlation. The homogenous (43.72%) and linear (28.83%) enhancement patterns were predominant, being more likely met in negative LNs (76.38% vs. 23.61% for homogenous pattern and 72% vs. 28% for linear pattern). Dotted, peripheral, and central patterns were rather encountered in metastatic LNs (Table 4).

3.5. Follow-Up and Survival. Follow-up of the patients was made for 21.61 ± 10.61 months. From the total of 112 patients, 79 (70.53%) survived over 20 months. No gender predilection was observed. Looking at the age distribution, a statistical difference was seen between patients younger or older than 60 years ($p < 0.05$, $p: 0.024$, CI 95%). At 20 months after surgery, the highest OS was seen for stages I (75%) and II (86.66%), followed by stages III (64%) and IV (37.5%). LN status proved to have independent prognostic value.

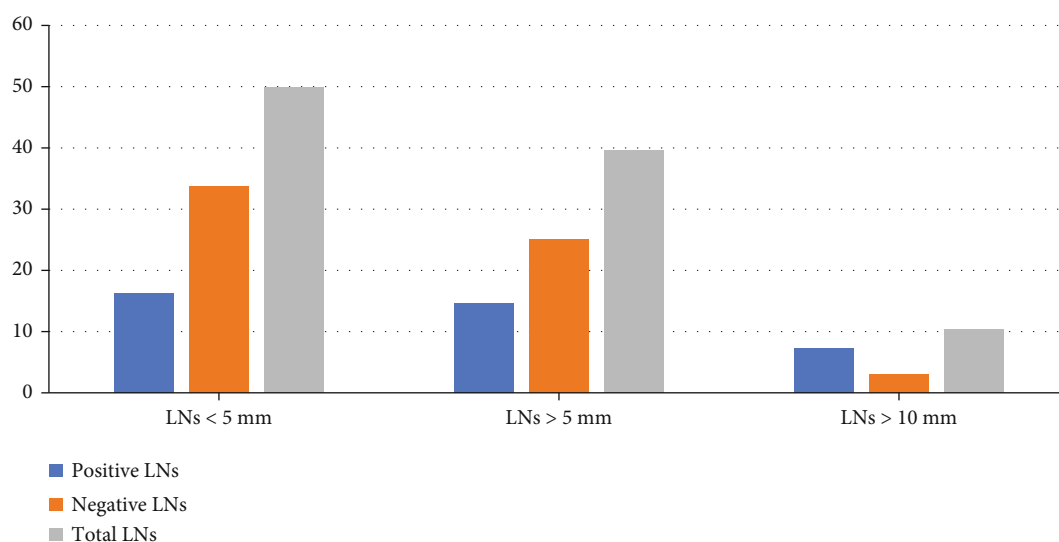
4. Discussion

This study confirmed the fact that a transdisciplinary approach of CRC diagnosis and therapeutic management can successfully improve the staging accuracy. It also confirmed the independent prognostic value of LN status and the role of vascular, lymphatic, and perineural invasion, and same as tumor budding degree for predicting the risk of LNMs [22–25]. Although the diagnostic techniques have been improved and certain pathological and molecular markers have been found to have an impact on prognosis,



	Total no. of LNs on CT	Total no. suspicious LN	Total no. of harvested LNs	Total no. positive LNs	Nodal stations affected	LNR	SPR
Locoregional	603	146	1202	129	40	0.10	1.13
Intermediate	289	69	317	13	8	0.04	5.30
Central	187	26	290	28	6	0.08	0.92
TOTAL	1079	241	1809	170	54	0.09	1.41

FIGURE 4: Distribution of LNs, identified on CT scan, per stations, based on the imaging map, and their correlation with the histopathological findings (LNR: lymph node ratio; SPR: suspicious-to-positive ratio).



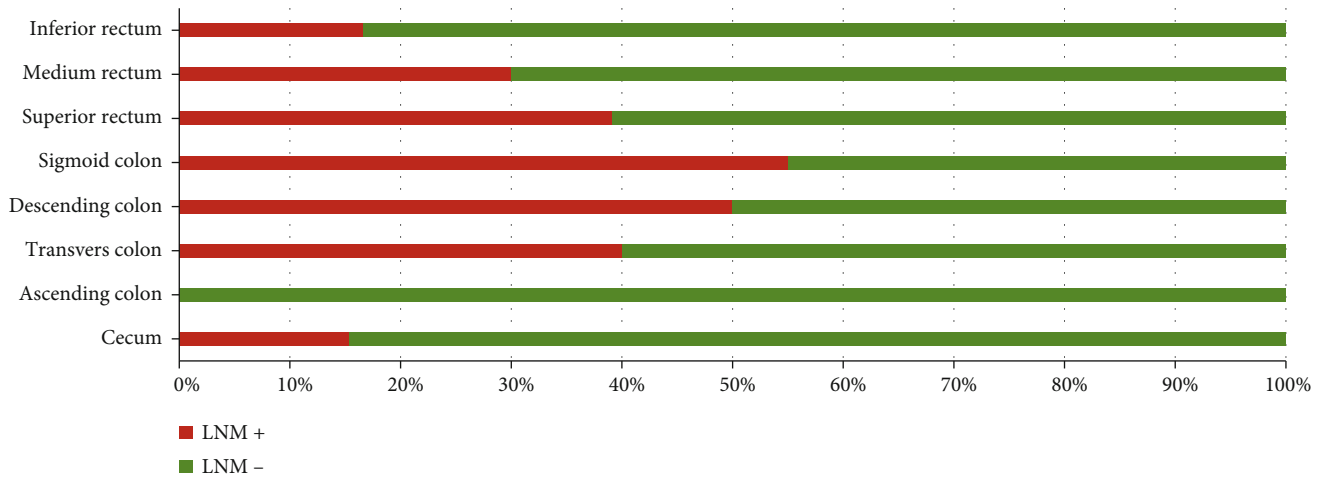
	Positive LNs	Negative LNs	Total LNs
LN < 5 mm	16,21%	33,73%	49,95%
LN > 5 mm	14,64%	25,02%	39,66%
LN > 10 mm	7,32%	3,05%	10,37%

FIGURE 5: Distribution of metastatic and non-metastatic LNs based on their size.

TABLE 3: Chi-square test showing association between CT-scan suspected node rate and histologic examination (LNM: lymph node metastases).

	LNM +	LNM -	Marginal row totals
Suspicious LNs	156 (92.02) [44.48]	85 (148.98) [27.47]	241
Nonsuspicious LNs	256 (319.98) [12.79]	582 (518.02) [7.9]	838
Marginal column totals	412	667	1079 (grand total)

The chi-square statistic is 92.6485. The p value is < 0.00001. Significant at p < .05.



Tumor location	No. of cases	No. of cases with LNM	No. of positive LN	No. of nodal stations affected	No. of LNs on CT	No. of suspicious LNs	No. of LNs prelevated	SPR (no. of suspicious/positive LNs)
Cecum	13	2	6	2	113	23	256	3,83
Ascending colon	2	0	0	0	20	4	22	-
Transvers colon	10	4	41	6	120	24	275	0,59
Descending colon	6	3	11	3	37	13	72	1,18
Sigmoid colon	20	11	34	13	175	38	350	1,12
Superior rectum	23	9	46	16	257	77	335	1,67
Medium rectum	20	6	23	9	198	29	328	1,26
Inferior rectum	18	3	7	4	156	30	169	4,29

FIGURE 6: Distribution of lymph nodes (LNs) based on the location of the primary tumor, the number of prelevated/harvested LNs, and suspicious-to-positive ratio (SPR) value.

TABLE 4: Distribution of enhancement patterns in metastatic vs. non-metastatic nodes (OR: odds ratio, CI 95%).

Enhancement pattern	OR	Lower	Upper	p value
Homogenous	1.99	1.09	3.62	0.02
Dotted	7.84	3.17	19.38	<0.0001
Linear	0.48	0.20	1.14	0.09
Central	2.85	0.40	20.14	0.29
Peripheral	3.25	0.23	44.69	0.37

the 5-year OS does not exceed 68% for patients with LNMs [10]. Since the main therapeutic approach remains surgery, one of the most crucial points in staging of CRC is preoper-

atively identification of the suspicious LNs and removal of the suspect nodes.

In our study, the preoperative imaging assessment was done according to the JCCRC, developed and updated in 2019 by JSCCR guidelines [16]. Each case was evaluated by a team of radiologists, surgeons, and pathologists, with an in-house protocol and a map of LN stations that helped making the correlations between imaging and pathological features.

An important and recognized independent prognostic factor, for patients with CRC, is also the number of harvested LNs [7, 26]. At least 12 LNs are indicated to be evaluated but LNR needs to be also counted [7, 27]. The method

proposed in this study was successfully proved to enhance the number of identified LNs per case till 15, with a LNR of 0.10 for regional nodes.

On the other hand, although several studies showed that size of the LNs is not an adequate parameter to predict nodal involvement [18, 26], a cut-off value of 10 mm showed a sensitivity and specificity of 71% and 67%, respectively [13]. Size alone fails to be an accurate predictor for node metastasis. It can be an indicator of suspicion only if it is combined with the other parameters such inhomogeneity, irregular borders, heterogeneous density same as presence of dotted, peripheral, or central enhancement pattern. We noticed that, since almost half of the LNs were under 5 mms, the size makes difficult distinguishing spots of enhancement under or over 3 mm. Comparing our findings with those previously reported by Miao et al. [12], our dotted pattern was similar to the previously called spotted pattern, it being correlated with positive LNs (OR: 7.84 and $p < 0.000100$). Homogeneous pattern was associated with nonmetastatic LNs (OR: 1.99, $p < 0.05$, $p: 0.02$).

In this cohort, the sensitivity and specificity of CT-scan evaluation were 80% and 69%, respectively. A similar sensitivity but a better specificity (97%) was previously reported [28, 29]. It can be explained but the fact that MRI was used by Brown et al., which has a greater accuracy in depicting differences of signal in nodes [29]. Despite using a more convenient method, our NPV was quite high (0.92), meaning that nonsuspicious LNs were more likely to be negative.

The SPR is a parameter which was introduced by the authors' team to evaluate the correlation between suspicious LNs on CT-scan and positive LNs confirmed under microscope. We noticed the most accurate SPR values for tumors located in the sigmoid colon, descending colon, and middle rectum (1.12, 1.18, and 1.26, respectively). For these cases, the majority of LNs with suspicious criteria on CT were confirmed as positive by pathologist, notwithstanding the fact that the number of cases in the descending colon category was significantly lower than the other two groups. At the opposite pole, tumors localized at the level of transverse colon had SPR value below 1 (0.59), meaning that CT failed to identify all the positive LNs, using only the classic criteria of suspicion. It highlights the limitations of CT scan in some cases. This observation was first time highlighted in literature.

There were some limitations of the study. For more statistically significant results, further research for longer periods on larger cohorts of patients using a standardized preoperative evaluation protocol is necessary. It should include CT acquisition and examination of nodal stations based on the enhancing pattern. MRI confirmation of the data would increase the significance of the proposed method. All the imaging data must be correlated with histological reports to also highlight the morphological changes which might interfere with the enhancement pattern.

5. Conclusions

In-house validation of the mapping of the nodal stations affected by CRC might be an important tool of raising the

accuracy of detecting the number of suspected LNs. Assessment of the SPR values could be a key in prognosis of these patients, especially for those with tumors of the distal colon and middle rectum.

Data Availability

The clinicopathological data used to support the findings of this study are available from the corresponding author upon request.

Conflicts of Interest

None of the authors have any conflicts of interests.

Authors' Contributions

SP drafted the paper, performed the imagistic examination, and contributed to the study design; JI supervised the histological interpretation and contributed to the study design; BL and SCB contributed to the gross findings and histological examination of the surgical specimens; FZZ and BT performed the surgical interventions and contributed to the collection of clinical data; SI and HI participated at imagistic investigations and clinical follow-up; AS participated at collection of clinical data and statistical assessment; SVSRI provided the financial support of the study and participated at the samples collections; GS contributed to the histological assessment, supervised the experiment and interpretation of the data, and give the final consent for publication. Patricia Simu and Laura Baniias equally contributed to this work.

Acknowledgments

This work was supported by a grant of the Romanian National Authority for Scientific Research, CNCS—UE-FISCDI, project number 20 PCCF/2018, code: PN-III-P4-ID-PCCF-2016-0006.

References

- [1] F. Bray, J. Ferlay, I. Soerjomataram, R. L. Siegel, L. A. Torre, and A. Jemal, "Global cancer statistics 2018: GLOBOCAN estimates of incidence and mortality worldwide for 36 cancers in 185 countries," *CA: a Cancer Journal for Clinicians*, vol. 68, no. 6, pp. 394–424, 2018.
- [2] J. L. Agnew, B. Abbadessa, and I. M. Leitman, "Strategies to evaluate synchronous carcinomas of the colon and rectum in patients that present for emergent surgery," *International Journal of Surgical Oncology*, vol. 2013, Article ID 309439, 7 pages, 2013.
- [3] S. Gurzu, Z. Szentirmay, and I. Jung, "Molecular classification of colorectal cancer: a dream that can become a reality," *Romanian Journal of Morphology and Embryology*, vol. 54, no. 2, pp. 241–245, 2013.
- [4] J. Choi, S. N. Oh, D. M. Yeo et al., "Computed tomography and magnetic resonance imaging evaluation of lymph node metastasis in early colorectal cancer," *World Journal of Gastroenterology*, vol. 21, no. 2, pp. 556–562, 2015.

- [5] E. Ray-Offor and F. B. Abdulkareem, "Screening colonoscopy in Port Harcourt, Nigeria," *Gastroenterology Insights*, vol. 10, no. 1, pp. 1–4, 2019.
- [6] B. A. Suci, S. Gurzu, L. Marginean et al., "Significant shrinkage of multifocal liver metastases and long-term survival in a patient with rectal cancer, after trans-arterial chemoembolization (TACE): a case report," *Medicine (Baltimore)*, vol. 94, no. 42, article e1848, 2015.
- [7] Z. Z. Fulop, S. Gurzu, T. Bara et al., "Lymph node ratio, an independent prognostic factor for patients with stage II-III rectal carcinoma," *Pathology, Research and Practice*, vol. 215, no. 6, p. 152384, 2019.
- [8] C. Fortea-Sanchis, D. Martínez-Ramos, and J. Escrig-Sos, "The lymph node status as a prognostic factor in colon cancer: comparative population study of classifications using the logarithm of the ratio between metastatic and nonmetastatic nodes (LODDS) versus the pN-TNM classification and ganglion ratio systems," *BMC Cancer*, vol. 18, no. 1, p. 1208, 2018.
- [9] P. Simu, I. Jung, L. Baniyas et al., "Synchronous colorectal cancer: improving accuracy of detection and analyzing molecular heterogeneity—the main keys for optimal approach," *Diagnostics*, vol. 11, no. 2, p. 314, 2021.
- [10] L. Zhou, J. Z. Wang, J. T. Wang et al., "Correlation analysis of MR/CT on colorectal cancer lymph node metastasis characteristics and prognosis," *European Review for Medical and Pharmacological Sciences*, vol. 21, no. 6, pp. 1219–1225, 2017.
- [11] M. L. Ong and J. B. Schofield, "Assessment of lymph node involvement in colorectal cancer," *World Journal of Gastrointestinal Surgery*, vol. 8, no. 3, pp. 179–192, 2016.
- [12] S. S. Miao, Y. F. Lu, H. Y. Chen et al., "Contrast-enhanced CT imaging for the assessment of lymph node status in patients with colorectal cancer," *Oncology Letters*, vol. 19, no. 5, pp. 3451–3458, 2020.
- [13] F. E. de Vries, D. W. da Costa, K. van der Mooren, T. A. van Dorp, and B. C. Vrouenraets, "The value of pre-operative computed tomography scanning for the assessment of lymph node status in patients with colon cancer," *European Journal of Surgical Oncology*, vol. 40, no. 12, pp. 1777–1781, 2014.
- [14] A. M. Leufkens, M. A. van den Bosch, M. S. van Leeuwen, and P. D. Siersema, "Diagnostic accuracy of computed tomography for colon cancer staging: a systematic review," *Scandinavian Journal of Gastroenterology*, vol. 46, no. 7-8, pp. 887–894, 2011.
- [15] S. Burton, G. Brown, N. Bees et al., "Accuracy of CT prediction of poor prognostic features in colonic cancer," *The British Journal of Radiology*, vol. 81, no. 961, pp. 10–19, 2008.
- [16] Japanese Society for Cancer of the Colon and Rectum, "Japanese classification of colorectal, appendiceal, and anal carcinoma: the 3d English edition secondary publication," *Journal of the Anus, Rectum and Colon*, vol. 3, no. 4, pp. 175–195, 2019.
- [17] J. W. Huh, Y. J. Kim, and H. R. Kim, "Distribution of lymph node metastases is an independent predictor of survival for sigmoid colon and rectal cancer," *Annals of Surgery*, vol. 255, no. 1, pp. 70–78, 2012.
- [18] B. Markl, J. Roflsle, H. M. Arnholdt et al., "The clinical significance of lymph node size in colon cancer," *Modern Pathology*, vol. 25, no. 10, pp. 1413–1422, 2012.
- [19] C. J. McMahan, N. M. Rofsky, and I. Pedrosa, "Lymphatic metastases from pelvic tumors: anatomic classification, characterization, and staging," *Radiology*, vol. 254, no. 1, pp. 31–46, 2010.
- [20] E. L. Servais, C. Colovos, A. J. Bograd, J. White, M. Sadelain, and P. S. Adusumilli, "Animal models and molecular imaging tools to investigate lymph node metastases," *Journal of Molecular Medicine (Berlin, Germany)*, vol. 89, no. 8, pp. 753–769, 2011.
- [21] L. Li, S. Mori, M. Sakamoto, S. Takahashi, and T. Kodama, "Mouse model of lymph node metastasis via afferent lymphatic vessels for development of imaging modalities," *PLoS One*, vol. 8, no. 2, article e55797, 2013.
- [22] L. Baniyas, S. Gurzu, Z. Kovacs, T. Bara, T. Bara Jr., and I. Jung, "Nuclear maspin expression: a biomarker for budding assessment in colorectal cancer specimens," *Pathology, Research and Practice*, vol. 213, no. 9, pp. 1227–1230, 2017.
- [23] E. Al-Sukhni, K. Attwood, E. M. Gabriel, C. M. LeVea, K. Kanehira, and S. J. Nurkin, "Lymphovascular and perineural invasion are associated with poor prognostic features and outcomes in colorectal cancer: a retrospective cohort study," *International Journal of Surgery*, vol. 37, pp. 42–49, 2017.
- [24] R. C. Lopes, S. Silveira Junior, and K. De Souza Koch, "Incidence of angiolymphatic invasion in colorectal cancer," *Journal of Coloproctology (Rio de Janeiro)*, vol. 32, no. 3, pp. 240–245, 2012.
- [25] J. Ferlay, M. Colombet, I. Soerjomataram et al., "Cancer incidence and mortality patterns in Europe: estimates for 40 countries and 25 major cancers in 2018," *European Journal of Cancer*, vol. 103, pp. 356–387, 2018.
- [26] P. Schrembs, B. Martin, M. Anthuber, G. Schenkirsch, and B. Märkl, "The prognostic significance of lymph node size in node-positive colon cancer," *PLoS One*, vol. 13, no. 8, article e0201072, 2018.
- [27] B. Markl, "Stage migration vs immunology: the lymph node count story in colon cancer," *World Journal of Gastroenterology*, vol. 21, no. 43, pp. 12218–12233, 2015.
- [28] B. Markl, T. Schaller, Y. Kokot et al., "Lymph node size as a simple prognostic factor in node negative colon cancer and an alternative thesis to stage migration," *American Journal of Surgery*, vol. 212, no. 4, pp. 775–780, 2016.
- [29] G. Brown, C. J. Richards, M. W. Bourne et al., "Morphologic predictors of lymph node status in rectal cancer with use of high-spatial-resolution MR imaging with histopathologic comparison," *Radiology*, vol. 227, no. 2, pp. 371–377, 2003.

Research Article

Application of Prognostic Models Based on Psoas Muscle Index, Stage, Pathological Grade, and Preoperative Carcinoembryonic Antigen Level in Stage II-III Colorectal Cancer Patients Undergoing Adjuvant Chemotherapy

Li Shan,¹ Tian Li ,² Wenhao Gu,³ Yuting Gao,³ Erdong Zuo,¹ Huizhu Qiu,¹ Rong Li,¹ and Xu Cheng ¹

¹Department of Hematology and Oncology, Taicang Hospital Affiliated to (Taicang No. 1 People's Hospital), Taicang, Suzhou 215400, China

²School of Basic Medicine, Fourth Military Medical University, No. 169 Changle West Rd, Xi'an 710032, China

³Department of Radiology, Taicang Hospital Affiliated to Soochow University (Taicang No. 1 People's Hospital), Taicang, Suzhou 215400, China

Correspondence should be addressed to Tian Li; fmmult@foxmail.com and Xu Cheng; chx1029@163.com

Received 4 November 2021; Accepted 3 January 2022; Published 2 February 2022

Academic Editor: Simona Gurzu

Copyright © 2022 Li Shan et al. This is an open access article distributed under the Creative Commons Attribution License, which permits unrestricted use, distribution, and reproduction in any medium, provided the original work is properly cited.

Objective. To investigate the effect of sarcopenia on the prognosis of stage II-III colorectal cancer patients undergoing adjuvant chemotherapy. **Methods.** A total of 196 stage II-III colorectal cancer patients who received 8 cycles of postoperative chemotherapy were retrospectively analyzed. An abdominal CT acquired at 3-4 weeks after surgery was used to calculate the psoas muscle index. Subsequently, once gender-specific receiver operating characteristic curves were plotted and cut-off values of psoas muscle index were defined, the clinicopathological characteristics and the prognosis of patients with high and low values were compared. Lastly, prognostic models were established based on the independent prognostic factors of relapse-free survival and overall survival identified by COX analysis. **Results.** Based on the psoas muscle index, the prevalence of sarcopenia was 37.5% among 196 patients. This prevalence has significant correlation with patients' age and gender. However, it was not related to the AJCC stage, T stage, lymph node metastasis, pathological grade, grade III-IV myelosuppression, or preoperative carcinoembryonic antigen level. In addition, both the relapse-free and the overall survival of patients with low and high psoas muscle indexes were significantly different. COX analysis indicated that the psoas muscle index was an independent prognostic factor. Both the overall survival prognostic model based on patients' psoas muscle index, stage, pathological grade, and preoperative carcinoembryonic antigen level and the relapse-free survival prognostic model based on patients' psoas muscle index, pathological grade, and preoperative carcinoembryonic antigen level could accurately predict the prognosis of patients. **Conclusion.** For stage II-III colorectal cancer patients, the presence of sarcopenia before adjuvant chemotherapy would adversely affect their recurrence-free and overall survival. Prognostic models based on psoas muscle index, stage, pathological grade, and preoperative carcinoembryonic antigen level could accurately predict the prognosis in these patients.

1. Introduction

Colorectal cancer is one of the most common malignant digestive tract tumors in Europe and North America [1]. In China, colorectal cancer is the third most common cancer, ranking the third among all causes of cancer-related deaths

in women and the fifth in men [2, 3]. Despite continuous progresses in treatment strategies, the survival rate of colorectal cancer remains poor due to late diagnosis, fast progression, and easy metastasis [4, 5]. The TNM (tumor, lymph node, and metastasis) staging system, which is widely used in the staging and prognostic prediction of patients

with cancers including colorectal cancer, categorizes colorectal cancer patients into four different stages according to their TNM staging. Although theoretically, the prognosis of patients at the same stage should be similar, in clinical practice, vast differences are often observed. Therefore, it is necessary to identify new biological indicators to improve the accuracy of prognostic prediction [6, 7].

Sarcopenia is a syndrome characterized by the progressive and extensive loss of skeletal muscle mass and strength [8, 9]. According to the literature, sarcopenia has an effect on the postoperative complications and the long-term survival of patients with different cancers including gastric [10] esophageal [11] and colorectal cancer [12]. However, for stage II-III colorectal cancer patients receiving adjuvant chemotherapy, no studies have so far utilized CT before chemotherapy to determine the presence of sarcopenia as well as investigating the effect of sarcopenia on the prognosis.

Therefore, this study retrospectively analyzed the correlation between the incidence of sarcopenia and the clinicopathological characteristics, and the relapse-free survival (RFS), as well as the overall survival (OS) of 196 stage II-III colorectal cancer patients undergoing adjuvant chemotherapy. It was found that the psoas muscle index (PMI) was not only an effective indicator of the incidence of sarcopenia, but also one of the independent prognostic factors. Subsequently, for the first time, prognostic models based on patients' PMI after surgery were established for the prognostic prediction of these patients. Furthermore, because the parameters we utilized were from routine examinations during the baseline evaluation of colorectal cancer patients, these two models were economic, convenient, and accurate, making them suitable for further implementation.

2. Materials and Methods

Patients who were admitted to our institution between January 2011 and December 2018 were included in the study. This study was approved by the Ethics Committee of our institution (approval number: 2021-KY-155). All patients' diagnoses were confirmed by histopathology. In addition, enrolled patients underwent postoperative 8 cycles of 5-fluorouracil-based adjuvant chemotherapy in the Department of Oncology and were subsequently followed up. Prior written comprehensive informed consent for routine CT scan studies and treatment had been obtained from all patients. The TNM staging was performed according to the eighth edition of the American Joint Committee on Cancer (AJCC) colorectal cancer staging system (8th edition). Alternatively, the diagnosis of grade III-IV myelosuppression was based on WHO acute and subacute toxic effect grading criteria for anticancer drugs; that is, the patient was diagnosed to have grade III-IV myelosuppression if one of the following criteria was met: white blood cell count $\leq 1.9 \times 10^9/L$, neutrophil count $\leq 0.9 \times 10^9/L$, hemoglobin value ≤ 79 g/L, or platelet count $\leq 49 \times 10^9/L$.

A routine and an enhanced abdominal scan was performed using Revolution CT scanner (GE Healthcare, Chicago, Illinois, United States) for all enrolled patients. The

scan was acquired 3-4 weeks after surgery but before the start of systemic chemotherapy. Fasting for solids and liquids was required 8 h prior to the scan. Once the scan was completed, the cross-sectional area of bilateral psoas major muscles on the transverse plane of the lower edge of the third lumbar vertebral body on abdominal CT was measured by the same radiologist (Supplementary Figure 1). Next, the PMI was calculated as the sum of the area divided by the square of the patient's height, the unit of which was mm^2/m^2 . The PMI is affected by patient gender owing to different body shapes of males and females. Consequently, gender-specific receiver operating characteristic (ROC) curves were plotted according to the recurrence status. Subsequently, once PMI cut-off values were defined based on Youden's index, corresponding indicators of patients in the high-PMI group and those in the low-PMI group were compared.

Observation indicators used in this study included patient age, gender, AJCC stage, T stage, N stage, pathological grade, presence of myelosuppression after chemotherapy, preoperative CEA level, RFS, OS, and PMI.

RFS and OS prognostic models were established based on the independent prognostic factors identified from multifactor COX analysis. Specific calculation formula is shown as follows:

$$\text{risk factor} = \sum_{i=1}^n \text{Coef}_i * x_i, \quad (1)$$

where Coef_i is the risk factor and x_i is either the patient's stage (stage II = 0, stage III = 1), pathological grade (grade 1 = 1, grade 2 = 2, and grade 3 = 3), CEA value, or PMI (PMI high = 0, PMI low = 1). A prognostic nomogram model for patients' RFS and OS was then constructed according to the risk factors.

Patients were divided into a high-risk group and a low-risk group depending on whether their PMI was higher than the median of risk factors. Subsequently, the RFS and the OS of the two groups were compared by the Kaplan-Meier (KM) survival analysis, whereas the accuracy of the prognostic model in predicting patients' 1-year, 3-year, and 5-year RFS and OS was evaluated by the area under the ROC curve (AUC). Last, heatmap, risk score distribution map, and recurrence and survival state distribution map were adopted to determine whether the prognostic model could distinguish between high- and low-risk patients.

Statistical analysis: Other than the gender-specific ROC curves and the cut-off values, which were plotted in SPSS 23.0 software, all statistical analyses were conducted in R software (version 3.6.2). $P < 0.05$ was considered statistically significant. Correlations between the PMI and patients' clinical characteristics were assessed by logistic regression, whereas correlations between the PMI and other clinical parameters including RFS and OS were explored by univariate and multivariate COX regression analyses. The prognostic nomogram model was constructed using the RMS plugin of R software. Alternatively, correlations between the PMI and risk factors as well as RFS and OS were investigated using the KM estimator. The ROC analysis of risk factors was conducted using the survival ROC plugin of

R software. Heatmap analysis was completed via the pheatmap plugin, data visualization was achieved via the Ggplot2 plugin of R software.

3. Results

Gender-specific ROC curves were first plotted according to the patient's recurrence state after surgery, so that the cut-off value could be determined. It was found that for male patients, the AUC and the cut-off value were 0.655 and 585.93 mm²/m², respectively. Alternatively, for female patients, these values were 0.634 and 456.21 mm²/m², respectively. Detailed results are shown in Supplementary Figure 2.

Of the 196 included patients, 109 were male and 87 were female. The median age was 64 years, and the average age was 62.2 ± 10.2 years (range 27–83). Seventy-five patients had stage II colorectal cancer, and the remaining 121 patients had stage III colorectal cancer. One patient's tumor was staged as T1, 10 as T2, 40 as T3, and 145 as T4. There were 121 patients with positive lymph nodes and 75 patients with negative ones. Based on differentiation, 9 cases were identified as well differentiated, 154 as moderately differentiated, and 33 as poorly differentiated. Forty-three cases developed grade II–IV myelosuppression. According to PMI measurements, 74 patients were divided into the low-PMI group, and the remaining 122 into the high-PMI group. Details are listed in Table 1.

Logistic analysis indicated that the PMI was correlated only with the patients' age and gender, but not with stage, T stage, lymph node metastasis, pathological grade, presence of grade III–IV myelosuppression, or preoperative CEA level. Detailed results are listed in Table 1.

KM analysis suggested that both the RFS and the OS of patients with a low PMI were significantly poorer than those of patients with a high PMI ($P = 0.003$ and 0.001 , respectively). More specifically, the 5-year RFS and OS of low-PMI patients were merely 60.2% and 63.4%, whereas for high-PMI patients, these were 78.5% and 80.7%, respectively, as shown in Figures 1(a) and 1(b).

Univariate COX regression analysis showed that patients' RFS and OS were related to multiple clinicopathological characteristics, including the patient's stage, lymph node metastasis, pathological grade, presence of grade III–IV myelosuppression after chemotherapy, preoperative CEA level, and PMI. In contrast, multivariate COX regression analysis indicated that the RFS was correlated with the patient's stage, pathological grade, preoperative CEA level, and PMI, whereas the OS was correlated with the pathological grade, preoperative CEA level, and PMI. In addition, PMI was identified as an independent prognostic factor of patients' RFS and OS. Detailed results are shown in Tables 2 and 3 and Figures 2(a) and 2(b).

An RFS prognostic model was established based on patients' PMI, stage, pathological grade, and preoperative CEA level. The risk score = PMI * 0.868 + stage * 0.843 + pathological grade * 1.623 + preoperative CEA level * 0.009. Similarly, an OS prognostic model was constructed based on patients' PMI, pathological grade, and

preoperative CEA level. The risk score = PMI * 0.812 + pathological grade * 1.747 + preoperative CEA level * 0.013. As shown in Figures 3(a) and 3(b), a prognostic nomogram model for patients' RFS and OS was then constructed according to the above risk factors.

It was found that the RFS of high-risk patients was substantially lower than that of low-risk patients ($P = 1.1E - 11$). The 5-year RFS of the two groups was 49.4% and 93.7%. The AUC of the 1-year, 3-year, and 5-year ROC curves was 0.840, 0.806, and 0.854, respectively as shown in Figures 4(a)–4(d). Heatmap, risk score, and recurrence state distribution map all indicated that the prognostic model could accurately distinguish the RFS status of high-risk patients from that of low-risk patients, as shown in Figures 4(e)–4(g).

It was found that the OS of high-risk patients was substantially lower than that of low-risk patients ($P = 1.1E - 11$). The 5-year OS of the two groups of patients was 63.4% and 95.0%. The AUC of the 1-year, 3-year, and 5-year ROC curves was 0.744, 0.741, and 0.803, respectively, as shown in Figures 5(a)–5(d). Heatmap, risk score, and survival state distribution map all indicated that the prognostic model could accurately distinguish the OS status of high-risk patients from that of low-risk patients, as shown in Figures 5(e)–5(g).

4. Discussion

According to the consensus of the European Working Group on Sarcopenia in Older People in 2010, sarcopenia can be categorized as primary or secondary depending on the cause [13]. Primary sarcopenia is defined as muscle loss that is only related to age and does not have any obvious cause. In contrast, secondary sarcopenia is often caused by one or more obvious reasons such as inflammatory diseases, malignant tumors, and malnutrition [14–16].

Accurate diagnosis of sarcopenia currently requires the determination of three parameters: muscle strength, muscle mass, and physical fitness [17, 18], although it remains controversial how these three indicators should be applied to the diagnosis of the disease. At present, the most used indicator is the muscle mass. The European Working Group on Sarcopenia in Older People has described CT and MRI as the gold standards for estimating muscle mass [19]. CT scan has now been adopted as a routine examination during the diagnosis, staging, and monitoring of cancer patients, making it a suitable method of assessing muscle mass. However, the measurement of systemic skeletal muscle is not only extremely complicated, but also inconvenient for clinical practice. Although the study has suggested that the amount of skeletal muscle in the third lumbar vertebral plane is directly proportional to the amount of skeletal muscle in the entire body [19], the measurement of the former is equally complicated and prone to error. Recently, another study has indicated that the PMI is significantly related to the amount of skeletal muscle among the Asian population [20]. Therefore, in our study, the PMI was adopted as the indicator of muscle mass, which was subsequently utilized to plot gender-specific ROC curves. In

TABLE 1: Correlation between patients' clinicopathological characteristics and PMI.

Clinical characteristics	Total no.	PMI		Ratio of low PMI (%)	Odds ratio in PMI	P	
		High	Low				
Age	>60 years old	119	64	55	42.01	1.031 (1.001–1.063)	0.045
	≤60 years old	77	58	19	24.68		
Gender	Male	109	79	30	27.78	0.225 (0.225–0.735)	0.003
	Female	87	43	44	50.57		
Stage	II	75	51	24	32.00	1.361 (0.746–2.485)	0.315
	III	121	71	50	41.32		
T stage	T1	1	0	1	100.00	0.823 (0.509–1.329)	0.425
	T2	10	3	7	70.00		
	T3	40	30	10	25.00		
	T4	145	89	56	38.62		
Lymph node	N0	75	51	24	32.00	1.395 (0.980–1.986)	0.064
	N1	64	43	21	32.81		
	N2	57	28	29	50.88		
Pathological grade	G1	9	7	2	22.22	0.797 (0.414–1.534)	0.497
	G2	154	91	63	40.91		
	G3	33	24	9	27.27		
CEA	High	73	46	27	36.99	0.998 (0.985–1.101)	0.751
	Normal	123	76	47	38.21		
Myelosuppression	Grade III-IV	43	25	18	41.86	1.247 (0.626–2.485)	0.530

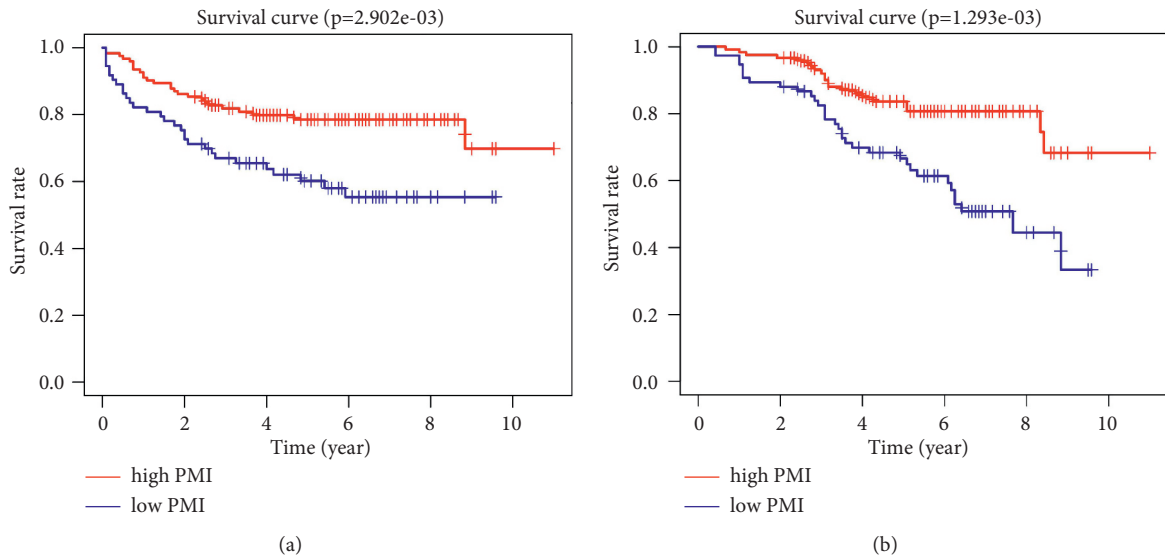


FIGURE 1: Low-PMI colorectal cancer patients is associated with poor RFS and OS. (a) RFS; (b) OS.

TABLE 2: COX regression analysis results on correlations between patients' PMI, clinicopathological characteristics, and RFS.

Parameter	Univariate COX analysis			Coef	Multivariate COX analysis		
	HR	95% CI	P		HR	95% CI	P
Age	1.020	0.992–1.048	0.162	—	0.997	0.969–1.025	0.828
Gender	0.794	0.470–1.342	0.389	—	0.969	0.543–1.726	0.914
Stage	3.395	1.712–6.734	0.001	0.843	2.324	1.143–4.727	0.020
T	1.071	0.676–1.697	0.769	—	0.994	0.636–1.554	0.981
N	2.046	1.478–2.832	1.60E–05	—	1.054	0.571–1.947	0.866
Pathological grade	5.082	3.012–8.575	1.11E–09	1.623	5.066	2.909–8.821	9.81E–09
Grade III-IV myelosuppression	2.859	1.675–4.880	1.17E–04	—	1.403	0.772–2.548	0.267
CEA	1.009	1.000–1.016	0.041	0.009	1.009	1.000–1.017	0.038
PMI	2.315	1.366–3.923	0.002	0.868	2.382	1.398–4.058	0.001

TABLE 3: COX regression analysis results on correlations between patients' PMI, clinicopathological characteristics, and OS.

Parameter	Univariate COX analysis			Multivariate COX analysis			
	HR	95% CI	P	Coef	HR	95% CI	P
Age	1.041	1.005–1.078	0.026	—	1.023	0.984–1.063	0.253
Gender	1.003	0.529–1.902	0.993	—	1.289	0.641–2.590	0.476
Stage	3.279	1.442–7.455	0.005	—	1.163	0.257–5.262	0.845
T	1.221	0.669–2.230	0.516	—	1.001	0.559–1.795	0.996
N	2.043	1.374–3.036	4.14E-04	—	1.297	0.591–2.846	0.516
Pathological grade	4.607	2.461–8.623	1.79E-06	1.747	5.737	2.956–11.135	2.42E-07
Grade III-IV myelosuppression	3.229	1.703–6.123	3.29E-04	—	1.885	0.921–3.859	0.083
CEA	1.011	1.003–1.020	0.010	0.013	1.013	1.005–1.022	0.002
PMI	2.110	1.113–4.000	0.022	0.812	2.252	1.179–4.302	0.014

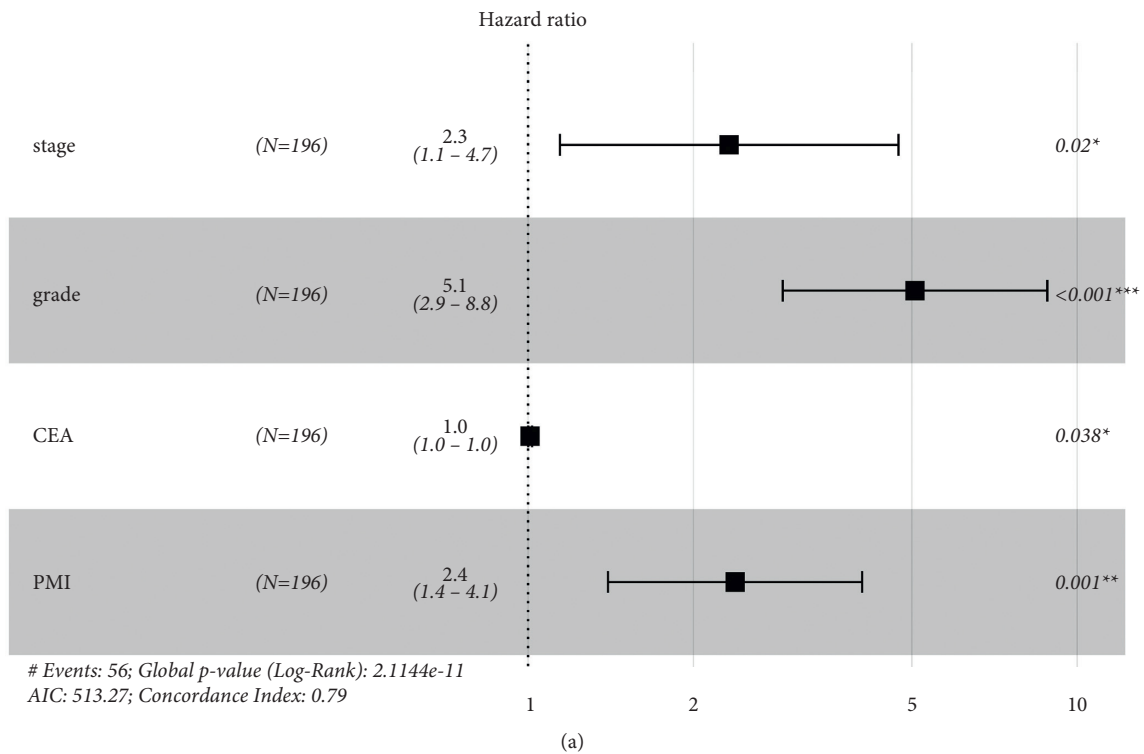


FIGURE 2: Continued.

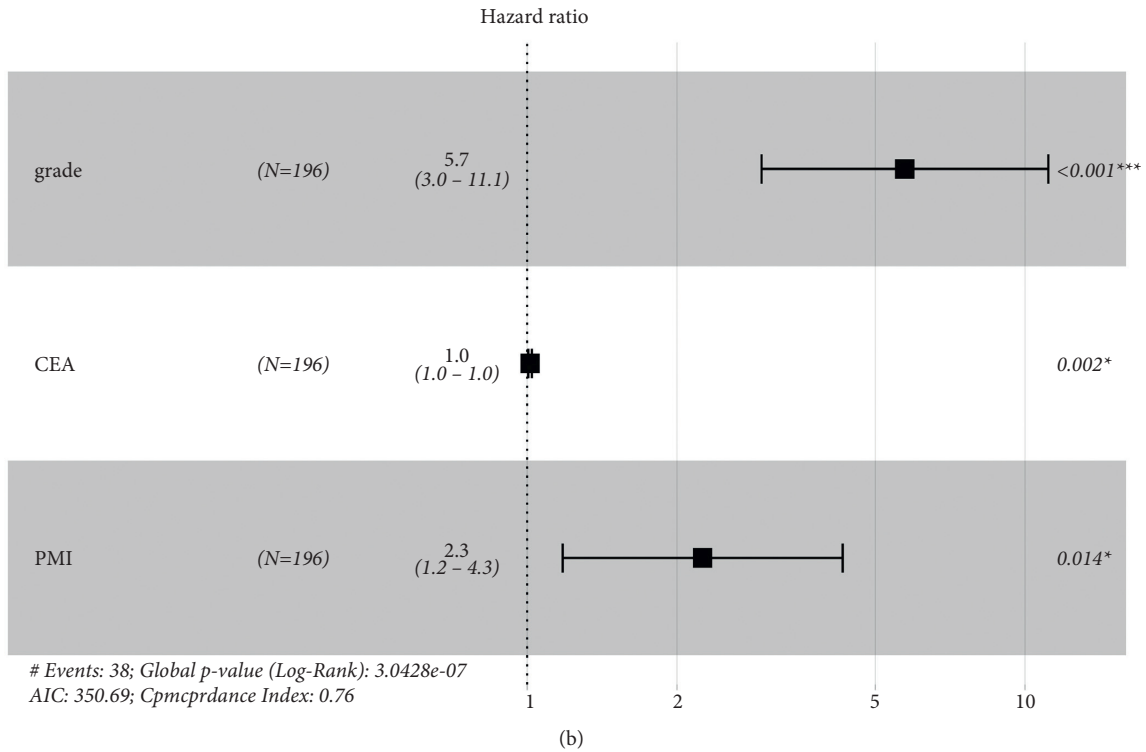


FIGURE 2: Forest plot of patients' RFS and OS from multivariate COX regression analysis. (a) RFS; (b) OS.

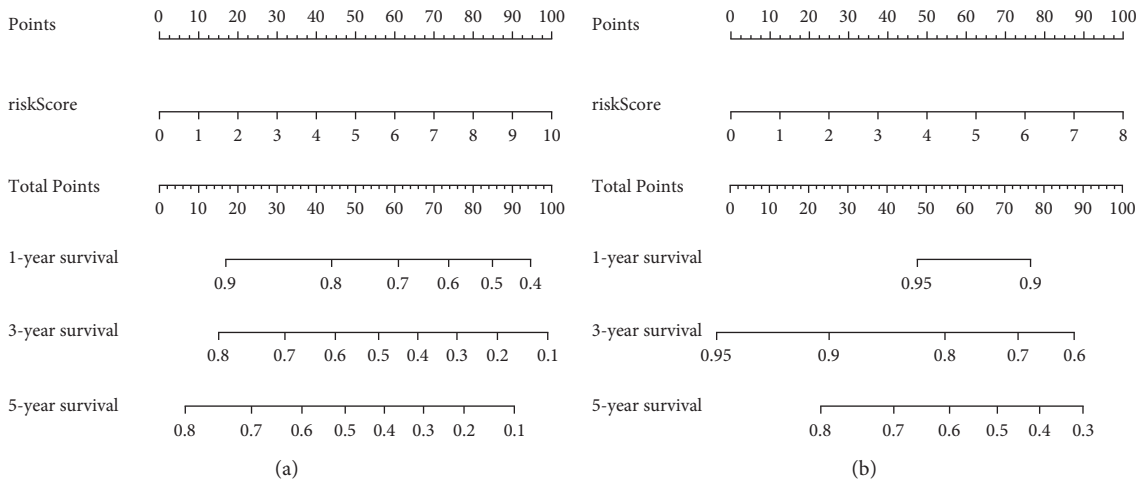


FIGURE 3: Prognostic model nomograms. (a) RFS; (b) OS.

addition, PMI cut-off values were determined according to Youden's index as the standard to diagnose sarcopenia, and correlations between the incidence of sarcopenia and the clinicopathological characteristics as well as the prognosis of stage II-III colorectal cancer patients undergoing adjuvant chemotherapy were investigated.

Research by Lieffers et al. [21] found that the overall prevalence of sarcopenia in 234 stage II-IV colorectal cancer patients was 38.9%. Alternatively, Miyamoto et al. [22] reported that the incidence of sarcopenia in 220 stage I-III

colorectal cancer patients was 25%. Similarly, our study discovered that the prevalence of sarcopenia in 196 stage II-III colorectal cancer patients undergoing adjuvant chemotherapy was 37.5%, a ratio that is of significance. In addition, we found that the incidence of a low PMI in patients aged over 60 years and in patients aged less than 60 years was 42.01% and 24.68%, respectively, whereas the incidence of a low PMI in female and male patients was 50.57% and 20.78%, respectively. In both comparisons, the difference was statistically significant, which was consistent with the

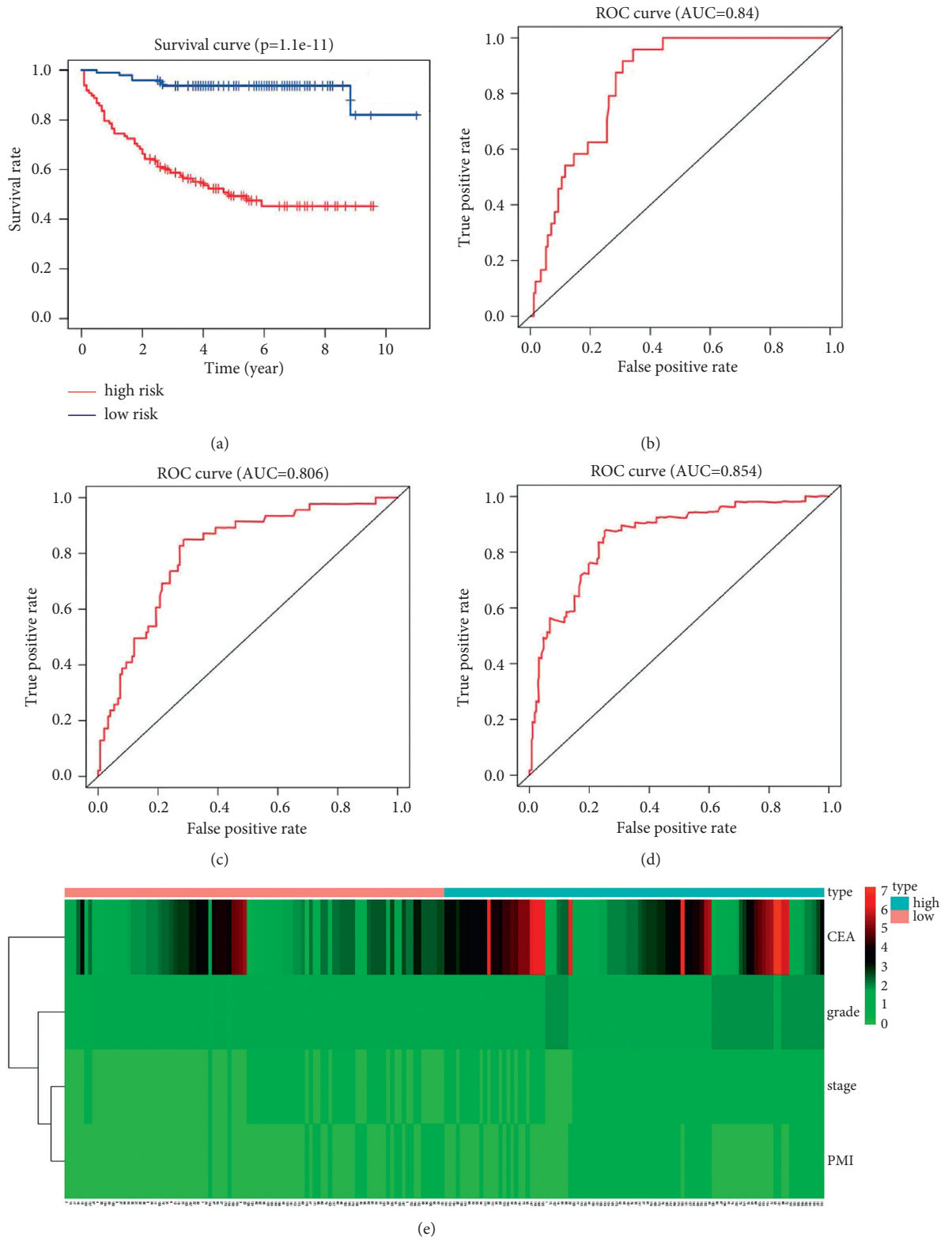


FIGURE 4: Continued.

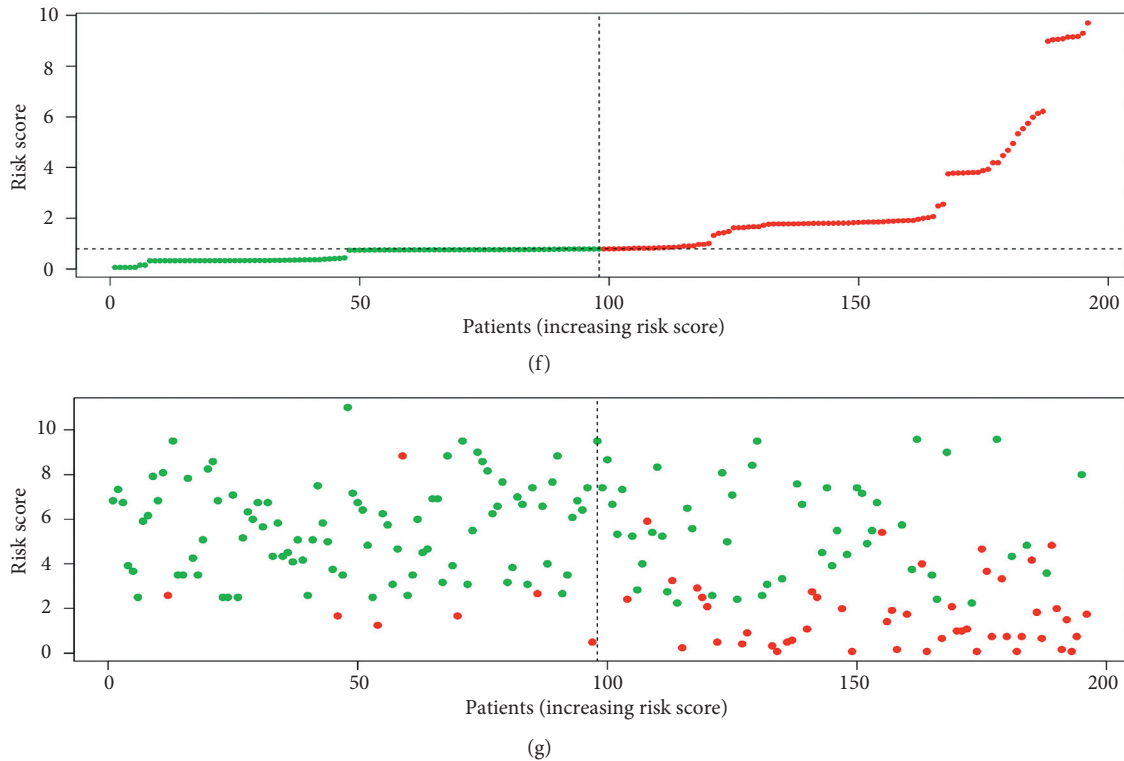


FIGURE 4: Evaluation of the prognostic in predicting patients' RFS. (a) KM analysis; (b) 1-year ROC; (c) 3-year ROC; (d) 5-year ROC; (e): heatmap; (f) risk score distribution map; (g) recurrence state distribution map.

results from relevant research on the correlation between the prevalence of sarcopenia and the patient's age and gender [23].

As was previously mentioned, an important cause of sarcopenia is cancer. Therefore, theoretically, it is expected that patients' tumor stage should be related to the incidence of sarcopenia. A study by Zhuang et al. revealed the relationship between sarcopenia and the stage, T stage, and lymph node metastasis of gastric cancer patients [24]. In contrast, another study by McSorley et al. [25] reported that there was no correlation between the incidence of sarcopenia and the TNM stage of colorectal cancer patients. This is consistent with our findings that the incidence of low PMI is irrelevant to the patient's stage, T stage, N stage, or pathological grade. This result suggested that the correlation between sarcopenia and the clinical characteristics of stage II-III colorectal cancer patients required further investigation. Even though no correlation between patients' T stage and sarcopenia was found, the decline in the PMI showed a clear upward trend with increasing N stage, especially between N0, N1, and N2 (N0 vs. N1 vs. N2: 32.00% vs. 32.81% vs. 50.88%, $P = 0.064$). Therefore, it was concluded that compared with the local size and local invasion of the tumor, the lymph node metastasis status could exhibit a greater impact on the incidence of sarcopenia. Alternatively, while the action mechanism of sarcopenia on the side effects of chemotherapy has not been clarified, multiple studies have reported that sarcopenia increased the risk of chemotherapy-related grade III-IV toxicity among colon cancer

patients [12, 26]. However, in our study, no correlation between sarcopenia and grade III-IV myelosuppression was observed. This was likely because most stage II and a small number of stage III patients included in this study only received capecitabine single-agent chemotherapy. Therefore, the fact that only 43 patients developed grade III-IV myelosuppression was likely a result of the weak intensity of chemotherapy. In addition, the small sample size could also contribute to a possible bias, and no grade III-IV side effects other than myelosuppression were considered, which could also contribute to a possible bias.

Sarcopenia is a response to increased tumor biological activity and metabolism, the latter of which first causes a severe systemic inflammatory response and ultimately leads to muscle loss [27]. Several recent studies have indicated that a systemic inflammatory response is directly related to the prognosis of multiple malignant tumors [28]. For example, overall survival was significantly associated with increased neutrophil-to-lymphocyte and decreased lymphocyte-to-monocyte ratio in patients with rectal cancer. [29] This result suggested that the infiltration of inflammatory cells into the tumor is a factor of poor prognosis for patients with rectal cancer. Furthermore, since it has been reported that the actin secreted by muscle cells can inhibit the growth of tumor cells [29], sarcopenia can increase the risk of tumor recurrence and compromise the patient's OS by incurring actin damage. In a retrospective analysis of 220 stage I-III colorectal cancer patients who received radical resection, Miyamoto et al. found that patients with sarcopenia had considerably less

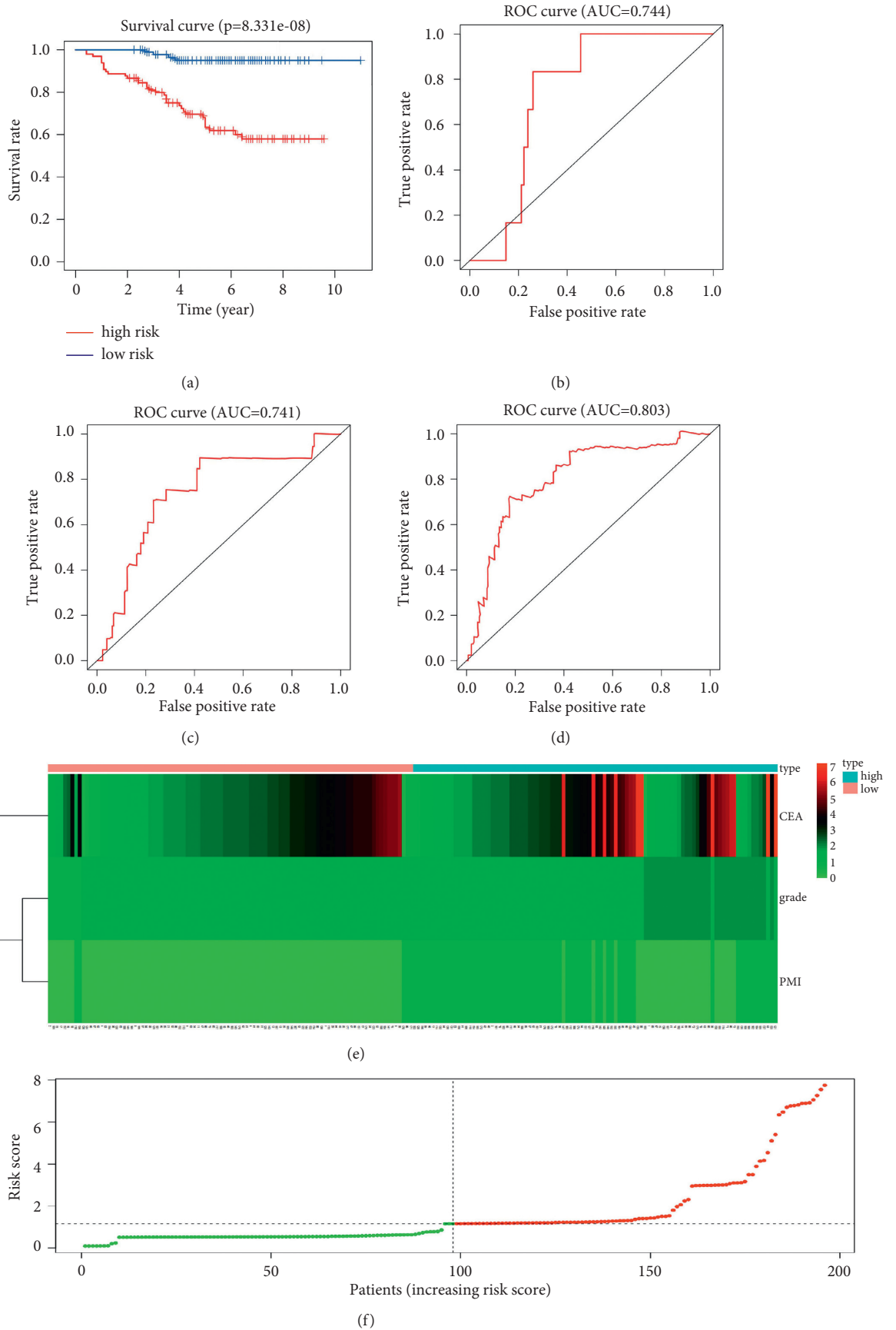


FIGURE 5: Continued.

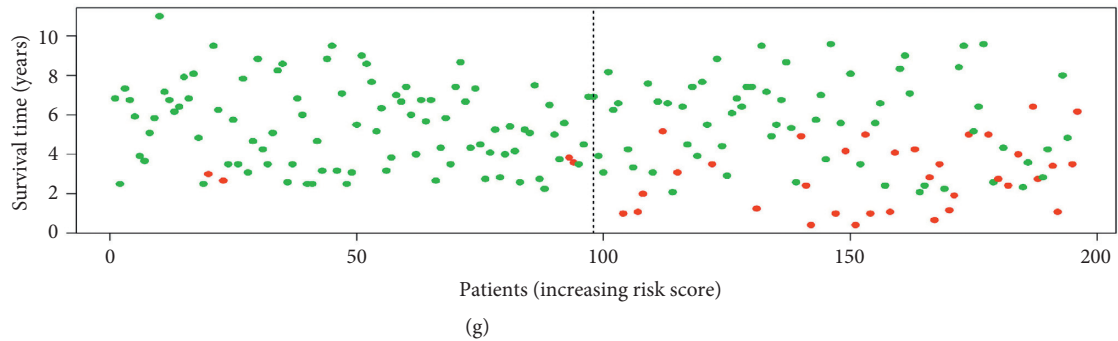


FIGURE 5: Evaluation of the prognostic in predicting patients' OS. (a) KM analysis; (b) 1-year ROC; (c) 3-year ROC; (d) 5-year ROC; (e) heatmap; (f) risk score distribution map; (g) survival state distribution map.

RFS and OS. Another meta-analysis of 12 studies including 5,337 nonmetastatic colorectal cancer patients also reported that sarcopenia was a negative factor for patient's survival outcome. However, up until now, there have been no studies that either utilized CT to determine the presence of sarcopenia before chemotherapy among stage II-III colorectal cancer patients receiving adjuvant chemotherapy or investigated the effect of sarcopenia on the prognosis of the same patient group. Therefore, this study retrospectively analyzed the relationship between the incidence of sarcopenia and the RFS as well as the OS of 196 patients. The results showed that the 5-year RFS and OS for patients with a low PMI were merely 60.2% and 63.4%, respectively. However, for patients with a high PMI, these were 78.5% and 80.7%, which were significantly higher ($P = 0.003$ and 0.001 , respectively). This finding suggested that sarcopenia affected the RFS and OS of stage II-III colorectal cancer patients receiving postoperative adjuvant chemotherapy. In addition, Wang et al. discovered that the incidence of sarcopenia before surgery is an independent prognostic factor for colorectal cancer patients [30]. Similarly, in this study, univariate COX regression analysis found that patients' RFS and OS were related to their tumor stage, lymph node metastasis, pathological grade, presence of grade III-IV myelosuppression, preoperative CEA level, and PMI. Alternatively, multivariate COX regression analysis suggested that patients' RFS was correlated with their stage, pathological grade, preoperative CEA level, and PMI, whereas their OS was correlated with their pathological grade, preoperative CEA level, and PMI. Based on these results, it was concluded that the PMI was an independent prognostic factor for the RS and the OS of stage II-III colorectal cancer patients undergoing adjuvant chemotherapy.

The study also established an RFS prognostic model based on patients' PMI, stage, pathological grade, and preoperative CEA level, as well as an OS prognostic model based on patients' PMI, pathological grade, and preoperative CEA level. Both models were subsequently verified by KM analysis, ROC analysis, heatmap, risk score distribution map, and recurrence status distribution map. The results indicated that the prognostic models could accurately predict patients' 1-, 3-, and 5-year RFS and OS as well as distinguishing between low- and high-risk patients.

In conclusion, approximately one-third of stage II-III colorectal cancer patients undergoing postoperative adjuvant chemotherapy could develop sarcopenia, the incidence of which was an independent prognostic factor of patients' RFS and OS. The use of the PMI in determining the presence of sarcopenia is both convenient and economic. Therefore, for colorectal cancer patients who have undergone radical surgery, their PMIs should be measured prior to the start of adjuvant chemotherapy to predict prognosis. For patients with a low PMI, individualized interventions such as nutritional support can be considered to increase muscle quantity and quality and consequently improve prognosis. Prognostic models established in this study based on the PMI, stage, pathological grade, and preoperative CEA level can accurately predict the prognosis of stage II-III colorectal cancer patients undergoing postoperative adjuvant chemotherapy and therefore should be implemented in the future.

This study had several limitations. First, it was a retrospective study conducted in a single center. Second, some prognostic factors for colon cancer patients, such as budings and lymph node ratio, were not included in our COX regression analysis [31, 32]. Third, there are other techniques widely used to assess muscle mass, such as magnetic resonance imaging and bioelectric impedance analysis [18], which we were unable to perform because this study was a retrospective analysis and it was possible to compare the prevalence of muscle loss between those techniques and PMI. Hence, comprehensive studies with multicenters and multitechniques are warranted in the future.

Abbreviations

TNM:	Staging, tumor, lymph node, and metastasis staging
RFS:	Relapse-free survival
OS:	Overall survival
PMI:	Psoas muscle index
CEA:	Carcinoembryonic antigen
AJCC:	American Joint Committee on Cancer
ROC:	Receiver operating characteristic
KM:	Kaplan–Meier.

Data Availability

The raw data are available in Supplementary Materials. More information can be accessed from the corresponding author.

Ethical Approval

This study was approved by the Ethics Committee of the First People's Hospital of Taicang (2021-KY-155).

Consent

Written informed consent was obtained from the participants.

Conflicts of Interest

The authors declare that they have no conflicts of interest.

Authors' Contributions

W. H. G. participated in data visualization, conceptualization, writing of the original draft, and formal analysis. T. L. participated in formal analysis and data curation. S. L. participated in conceptualization, providing resources, review and editing, supervision, project administration, and funding acquisition. Y. T. G., E. D. Z., H. Z. Q., and L. R. helped with methodology and software. X. C. participated in writing, review, and editing. Li Shan and Wenhao Gu contributed equally to this work.

Acknowledgments

The authors would like to thank Editage (<https://www.editage.com>) for English language editing. This study was supported by the Science and Technology Development Plan of Taicang in Jiangsu Province, PRC (Grant no. TC2020JCYL20).

Supplementary Materials

Supplementary Figure 1. Assessment of the psoas muscle index (PMI). PMI was calculated as the sum of cross-sectional area of bilateral psoas major muscles in the lower edge of the third lumbar vertebral body (L3) and divided by the square of the patient's height. (A) Right sectional area of psoas major muscles; (B) left sectional area of psoas major muscles. *Supplementary Figure 2.* Gender-specific ROC curves. (A) Male patients; (B) female patients. (*Supplementary Materials*)

References

- [1] M. M. Center, A. Jemal, R. A. Smith, and E. Ward, "Worldwide variations in colorectal cancer," *CA: A Cancer Journal for Clinicians*, vol. 59, no. 6, pp. 366–378, 2009.
- [2] R. M. Feng, Y. N. Zong, S. M. Cao, and R. H. Xu, "Current cancer situation in China: good or bad news from the 2018 Global Cancer Statistics?" *Cancer Communications*, vol. 39, no. 1, Article ID 22, 2019.
- [3] J. Chen, Z. Wang, X. Shen, X. Cui, and Y. Guo, "Identification of novel biomarkers and small molecule drugs in human colorectal cancer by microarray and bioinformatics analysis," *Molecular Genetics & Genomic Medicine*, vol. 7, no. 7, Article ID e00713, 2019.
- [4] C. C. Compton, "Colorectal carcinoma: diagnostic, prognostic, and molecular features," *Modern Pathology*, vol. 16, no. 4, pp. 376–388, 2003.
- [5] Y. Sun, B. Yang, M. Lin, H. Yu, H. Chen, and Z. Zhang, "Identification of serum miR-30a-5p as a diagnostic and prognostic biomarker in colorectal cancer," *Cancer Biomarkers*, vol. 24, no. 3, pp. 299–305, 2019.
- [6] S. Ren, W. Wang, H. Shen et al., "Development and validation of a clinical prognostic model based on immune-related genes expressed in clear cell renal cell carcinoma," *Frontiers Oncology*, vol. 10, Article ID 1496, 2020.
- [7] W. Wang, Q. Wu, Z. Wang et al., "Development of a prognostic model for ovarian cancer patients based on novel immune microenvironment related genes," *Frontiers Oncology*, vol. 11, Article ID 647273, 2021.
- [8] A. Gostyńska, M. Stawny, K. Dettlaff, and A. Jelińska, "Clinical nutrition of critically ill patients in the context of the latest ESPEN guidelines," *Medicina*, vol. 5512 pages, 2019.
- [9] A. J. Cruz-Jentoft, G. Bahat, J. Bauer et al., "Sarcopenia: revised European consensus on definition and diagnosis," *Age and Ageing*, vol. 48, no. 1, pp. 16–31, 2019.
- [10] K. Kuwada, S. Kuroda, S. Kikuchi et al., "Clinical impact of sarcopenia on gastric cancer," *Anticancer Research*, vol. 39, no. 5, pp. 2241–2249, 2019.
- [11] P. R. Boshier, R. Heneghan, S. R. Markar, V. E. Baracos, and D. E. Low, "Assessment of body composition and sarcopenia in patients with esophageal cancer: a systematic review and meta-analysis," *Diseases of the Esophagus*, vol. 318 pages, 2018.
- [12] O. Vergara-Fernandez, M. Trejo-Avila, and N. Salgado-Nesme, "Sarcopenia in patients with colorectal cancer: a comprehensive review," *World Journal of Clinical Cases*, vol. 8, no. 7, pp. 1188–1202, 2020.
- [13] A. J. Cruz-Jentoft, J. P. Baeyens, J. M. Bauer et al., "Sarcopenia: European consensus on definition and diagnosis: report of the European working group on sarcopenia in older People," *Age and Ageing*, vol. 39, no. 4, pp. 412–423, 2010.
- [14] G. Bano, C. Trevisan, S. Carraro et al., "Inflammation and sarcopenia: a systematic review and meta-analysis," *Maturitas*, vol. 96, pp. 10–15, 2017.
- [15] G. R. Williams, H. N. Rier, A. McDonald, and S. S. Shachar, "Sarcopenia & aging in cancer," *Journal of Geriatric Oncology*, vol. 10, no. 3, pp. 374–377, 2019.
- [16] F. Meyer and L. Valentini, "Disease-related malnutrition and sarcopenia as determinants of clinical outcome," *Visual Medicine*, vol. 35, no. 5, pp. 282–291, 2019.
- [17] T. S. Bowen, G. Schuler, and V. Adams, "Skeletal muscle wasting in cachexia and sarcopenia: molecular pathophysiology and impact of exercise training," *Journal of Cachexia Sarcopenia Muscle*, vol. 6, no. 3, pp. 197–207, 2015.
- [18] M. Tosato, E. Marzetti, M. Cesari et al., "Measurement of muscle mass in sarcopenia: from imaging to biochemical markers," *Aging Clinical and Experimental Research*, vol. 29, no. 1, pp. 19–27, 2017.
- [19] A. M. Ryan, D. G. Power, L. Daly, S. J. Cushen, E. N. í Bhuachalla, and C. M. Prado, "Cancer-associated malnutrition, cachexia and sarcopenia: the skeleton in the hospital closet 40 years later," *Proceedings of the Nutrition Society*, vol. 75, no. 2, pp. 199–211, 2016.

- [20] Y. Hamaguchi, T. Kaido, S. Okumura et al., "Proposal for new diagnostic criteria for low skeletal muscle mass based on computed tomography imaging in Asian adults," *Nutrition*, vol. 32, no. 11-12, pp. 1200–1205, 2016.
- [21] J. R. Lieffers, O. F. Bathe, K. Fassbender, M. Winget, and V. E. Baracos, "Sarcopenia is associated with postoperative infection and delayed recovery from colorectal cancer resection surgery," *British Journal of Cancer*, vol. 107, no. 6, pp. 931–936, 2012.
- [22] Y. Miyamoto, Y. Baba, Y. Sakamoto et al., "Sarcopenia is a negative prognostic factor After curative resection of colorectal cancer," *Annals of Surgical Oncology*, vol. 22, no. 8, pp. 2663–2668, 2015.
- [23] K. M. Kim, H. C. Jang, and S. Lim, "Differences among skeletal muscle mass indices derived from height-, weight-, and body mass index-adjusted models in assessing sarcopenia," *Korean Journal of Internal Medicine (Korean Edition)*, vol. 31, no. 4, pp. 643–650, 2016.
- [24] C. L. Zhuang, D. D. Huang, W. Y. Pang et al., "Sarcopenia is an independent predictor of severe postoperative complications and long-term survival after radical gastrectomy for gastric cancer: analysis from a large-scale cohort," *Medicine (Baltimore)*, vol. 95, no. 13, Article ID e3164, 2016.
- [25] S. T. McSorley, D. H. Black, P. G. Horgan, and D. C. McMillan, "The relationship between tumour stage, systemic inflammation, body composition and survival in patients with colorectal cancer," *Clinical Nutrition*, vol. 37, no. 4, pp. 1279–1285, 2018.
- [26] H. W. Jung, J. W. Kim, J. Y. Kim et al., "Effect of muscle mass on toxicity and survival in patients with colon cancer undergoing adjuvant chemotherapy," *Supportive Care in Cancer*, vol. 23, no. 3, pp. 687–694, 2015.
- [27] S. Dodson, V. E. Baracos, A. Jatoi et al., "Muscle wasting in cancer cachexia: clinical implications, diagnosis, and emerging treatment strategies," *Annual Review of Medicine*, vol. 62, pp. 265–279, 2011.
- [28] G. Malietzis, N. Johns, H. O. Al-Hassi et al., "Low muscularity and myosteatosis is related to the host systemic inflammatory response in patients undergoing surgery for colorectal cancer," *Annals of Surgery*, vol. 263, no. 2, pp. 320–325, 2016.
- [29] B. K. Pedersen and M. A. Febbraio, "Muscles, exercise and obesity: skeletal muscle as a secretory organ," *Nature Reviews Endocrinology*, vol. 8, no. 8, pp. 457–465, 2012.
- [30] S. Wang, H. Xie, Y. Gong et al., "The value of L3 skeletal muscle index in evaluating preoperative nutritional risk and long-term prognosis in colorectal cancer patients," *Scientific Reports*, vol. 10, no. 1, Article ID 8153, 2020.
- [31] L. Baniias, S. Gurzu, Z. Kovacs, T. Bara, T. Bara Jr., and I. Jung, "Nuclear maspin expression: a biomarker for budding assessment in colorectal cancer specimens," *Pathology, Research & Practice*, vol. 213, no. 9, pp. 1227–1230, 2017.
- [32] Z. Z. Fulop, S. Gurzu, T. Bara et al., "Lymph node ratio, an independent prognostic factor for patients with stage II-III rectal carcinoma," *Pathology, Research & Practice*, vol. 215, no. 6, Article ID 152384, 2019.